SKRIFTER NR. 172

Geological and geophysical research in Svalbard and on Jan Mayen

NORSK POLARINSTITUTT
OSLO 1980

DET KONGELIGE MILJØVERNDEPARTEMENT

NORSK POLARINSTITUTT

Rolfstangveien 12, Snarøya, 1330 Oslo Lufthavn, *Norway*

SALG

Bøkene selges gjennom bokhandlere eller bestilles direkte fra:

Universitetsforlaget
Boks 2977, Tøyen
Oslo 6
Norway

Global Book Resources Ltd.
109 Great Russell Street
London WC 1B 3NA
England

ORDERS

may be placed at your bookstore or you may order direct from:

Columbia University Press
136 South Broadway
Irvington-on-Hudson
NY 10533, U.S.A.

SKRIFTER NR. 172

Geological and geophysical research in Svalbard and on Jan Mayen

NORSK POLARINSTITUTT
OSLO 1980

Printed November 1980
ISBN 82–90307–12–8

Contents

On the zero-point deviation of Eppley pyranometers

By Vidar Hisdal

Introduction

In connection with studies of the spectral composition of radiation from sun and sky in Ny-Ålesund (78°55′N, 11°56′E), some measurements were also made of the relation between the total shortwave irradiance and the part of this irradiance that is contained in the wavelength interval above 700 nm. The measurements were carried out during the months of May and June 1976–77 by means of an Eppley precision pyranometer equipped with WG-295 Schott glass hemispheres for measuring irradiance within the whole shortwave spectrum (i.e. global radiation or sky radiation) and a RG-695 outer glass hemisphere for wavelengths exceeding 700 nm.

One type of the outer filter-glass hemispheres was mounted on the pyranometer for a few minutes, and then quickly replaced by the other type. This procedure was repeated several times in the course of most observation series, and the output voltage of the thermopile was measured continuously by a potentiometric stripchart recorder.

Problem

Fig. 1 shows, as an example, two sections of a recording of the thermopile voltage made at noon with clear sky. (Note that the recorder sensitivity used for sky radiation is twice as great as that used for global radiation.) A prominent feature of the figure is the more or less marked difference between the line representing zero voltage and the registration curve when the shortwave radiation is cut off by placing a box over the glass hemispheres. This zero-point deviation is of special importance when making comparative measurements with different types of cut-off filters. However, general measurements of global radiation and, particularly, of sky radiation made with Eppley pyranometers, or instruments of similar types, may be significantly influenced as well. In spite of this fact the effect has been given surprisingly little attention. The problem has been discussed by Drummond and Roche (1965), and recently, from a more general point of view, by Gulbrandsen (1978), where further references may be found. The present discussion contains some supplementary results, based on the radiation conditions at an Arctic station.

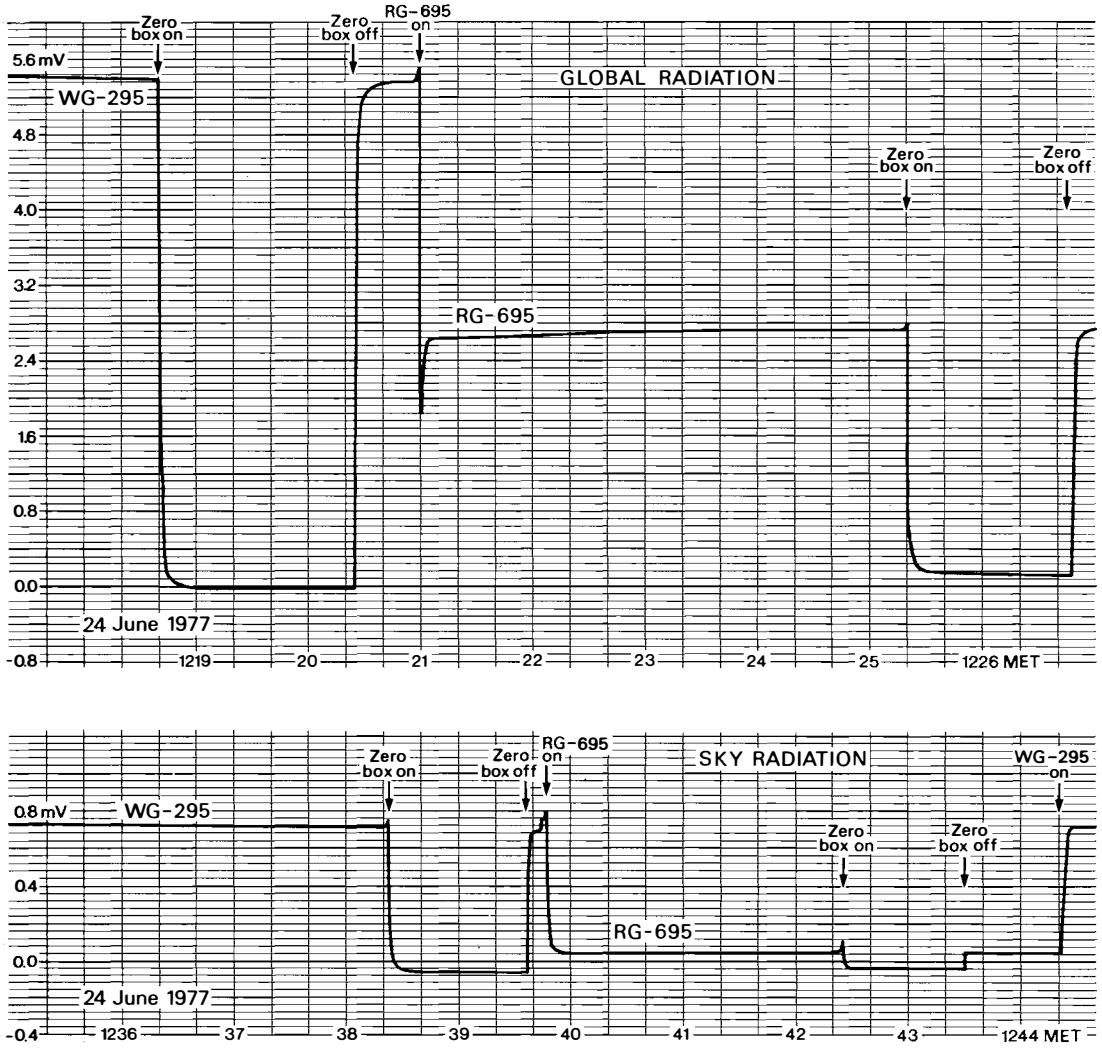

Fig. 1. *Two sections of a recording of the thermopile voltage made at noon with clear sky. The recorder sensitivity for sky radiation is twice that used for global radiation.*

Generally, radiative heating (net gain) or cooling (net loss) of the glass hemispheres results in glass temperatures that are more or less different from that of the surrounding air, which ideally should equal the inner instrument temperature. This involves an "extra" longwave radiative exchange between the inner glass hemisphere and the sensitive part of the thermopile. When the shortwave radiation is screened totally off from the glass hemispheres, therefore, the thermopile will usually not give a zero voltage output, but show negative (cooled hemisphere) or positive (heated hemisphere) deviation from the electrical zero point. To correct for this effect, the zero-point deviation has to be substracted from the deflection obtained before the shortwave radiation is screened off.

Measurements

The pyranometer was mounted on a thin, light, wooden plate, which was freely exposed to the air on both sides, to minimize the heating effects of the instrument from below. The glass hemispheres were shaded by covering them with a double-walled aluminium box (diameter 15 cm). A small bimetal thermometer was attached to the inner wall of the box, and care was taken that the box temperature did not deviate much (less than 2°C) from that of the surrounding air, although this point does not seem to be very critical. The air temperature during the observation periods stayed generally between — 5° and + 5°C, and the winds were mostly light to moderate. No special investigations of the influence of wind speed or of artificial ventilation of the instrument were carried out. It may be mentioned, however, that in accordance with results of previous experiments, our data did not indicate that even strong ventilation was sufficient to give a satisfactory reduction of the zero-point deviation.

The magnitude of the zero-point deviation was estimated by a slight "extrapolation backwards" from the point where the recorder curve after a nearly vertical drop had flattened out, which according to our observations occurred about 10 to 20 seconds after the box had been put on the instrument. (A more detailed discussion of the procedure is given by GULBRANDSEN op. cit.) When taking off the zero-point box, or changing the outer glass hemisphere, or screening off direct solar radiation (to measure sky radiation), the pyranometer naturally had to be left undisturbed for a few minutes to make sure that the temperature conditions in the glass thermopile system had stabilized. It was normally easy to follow this stabilization process by examining the course of the recorder curve.

Results

It appears from Fig. 1 that in the case of global radiation (WG-295 filter) only a slight negative zero-point deviation is present. With the RG-695 filter, on the other hand, which absorbs considerably more shortwave radiation, there is a fairly marked positive deviation, amounting to about 5% of the total deflection. In the case of sky radiation, the deviation is negative for both filters, but is smallest for RG-695, due to its greater shortwave absorption. In relative units, however, the deviation for RG-695 is much greater than for WG-295, about 80% against 9% of the uncorrected voltage deflection. It should be added that if the box was placed on the pyranometer for a sufficiently long time, the recorder curve soon started to approach the zero line. However, it might take up to ten minutes, in some cases even more, before the zero-point deviation had completely disappeared.

The examples given in Fig. 1 are typical for observations taken in the middle of the day. Some main results of the "day measurements" (solar altitude between 28° and 35°) as well as evening/night-measurements (solar altitude between 14° and 19°) are given in Table 1. In the day, we find that for global radiation,

Table 1. *Sign and percentage values of the zero-point deviation. Percentages refer to thermopile voltages not corrected for the zero-point deviation. Means are calculated without regard to the sign of the deviations. Solar altitude for day measurements: 28° to 35°, for evening/night measurements (in parentheses): 14° to 19°.*

Type of radiation	Filter	Number of days	Number of obs.	Sign of deviation	Percentage deviations Range	Mean
Clear sky						
Global	WG–295	10 (4)	30 (9)	All neg.(All neg.)	0.0–2.6	1.0 (3.0)
radiation	RG–695	10 (4)	25 (6)	All pos. (5 pos. 1 neg.)	2.5–7.5	4.8 (2.5)
Sky	WG–295	4 (3)	16 (9)	All neg. (All neg.)	6.0–15.8	10.7 (16.7)
radiation	RG–695	4 (3)	12 (5)	All neg. (All neg.)	13.6–133	70.7(>100)
Overcast						
Global	WG–295	3 (2)	15 (5)	5 pos. 10 neg. (All neg.)	0.0–1.8	0.7 (0.7)
radiation	RG–695	3 (2)	15 (4)	All pos. (All pos.)	3.5–8.7	6.2 (5.2)

clear sky, the zero-point deviations are small, only 1 % on an average, and they are all negative. With an overcast sky, the percentage deviations are still smaller, and one-third of them (all from the same day) are positive. As might be expected, the corresponding measurements with the RG filter show positive deviations only, both for an overcast and a clear sky, meaning that for all cases this filter has a net gain of radiant heat. Also, the relative magnitude of the deviations is notably larger, averaging 5–6 % of the total deflection. When measuring sky radiation, on the other hand, there is a net heat loss, even for the RG filter. It may be noted that for this latter group the percentage deviation is large and very variable, the average amounting to as much as 70 % of the uncorrected deflection.

As the sun sinks, the heat gain of the glass hemispheres should tend to decrease, while the heat loss should tend to increase. A comparison between the results of the day- and evening/night-measurements in Table 1 gives clear evidence of such a tendency. Relative to the energy measured by the thermopile, a positive zero-point deviation is considerably smaller in the evening/night and a negative deviation is larger (equality in the case of global radiation, overcast). It should be added that generally this also applies to deviations given in absolute measure (in mV or W m^{-2}, data not given), although naturally the difference day-night is not so conspicuous in this case as when relative values are compared.

Judging from the measurements made in Ny-Ålesund, global radiation is not much influenced by the zero-point deviation, at least if the sun is not too low in the sky. It should be remembered, however, that the effect is of a systematic character. Neglect of the effect in the case of sky radiation, on the other hand, would mean an error of about 10 % for solar altitudes around 30°. For lower solar altitudes the percentage error is apt to be considerably greater. When corresponding measurements are made with the RG-695 filter the conditions are still worse. Thus, measurements of sky radiation with this filter would be quite pointless if the zero-point deviation is not observed simultaneously.

To the extent that comparable data are published by GULBRANDSEN (1978),

his results agree well with those outlined above. This applies both to the sign and to the order of magnitude of the zero-point deviation. Evidently, some dissimilarities have to be expected, not only because of the limited size of the observation materials, but also because of differences in the radiation climates of the two stations considered (Bergen and Ny-Ålesund).

Concluding remarks

The zero-point deviation may have a certain influence on the determination or checking of the pyranometer calibration factor. This check is usually conducted by comparing the difference between global radiation and sky radiation with simultaneous pyrheliometer measurements of direct solar radiation. Our daytime observations show negative zero-point deviations that, on an average, are somewhat smaller for global than for sky radiation (—0.048 mV against —0.079 mV). This would increase the calibration factor (multiplication factor) by no more than about 0.6%. A corresponding calculation for the RG-695 filter on the other hand, would give an average factor about 7% too high. It should be remembered, however, that when checking the calibration factor, successive readings of the shaded and the unshaded pyranometer are no doubt often carried out more rapidly than in our case. This means that the glass hemispheres may not have sufficient time to reach thermal equilibrium. The zero-point deviations are then apt to be practically equal in the two cases, and the influence on the instrument check should be negligible. A good agreement with the manufacturer's calibration factor needs not mean, therefore, that the zero-point deviation is insignificant.

It is difficult to say to what extent it is possible to work out average corrections for the zero-point deviation, in order to adjust for instance monthly radiation values. It seems at any rate a complicated task, as it probably has to be done for individual regions and seasons separately. A simple adjustment of the pyranometer calibration factor (multiplication factor), e.g. by reducing it by 2% when using the RG-695 filter, as recommended by the Eppley Laboratory (in the calibration certificates), or by 9%, as proposed by DRUMMOND and ROCHE (1965), cannot give a general solution to the problem. The best solution, perhaps the only one, would probably be to redesign the pyranometer with a view to obtaining a decisive reduction of the zero-point deviation.

Acknowledgement

I should like to thank Mr. A. GULBRANDSEN and Mr. T. VINJE for valuable discussions and criticisms.

References

DRUMMOND, A.J. and J.J. ROCHE, 1965: Corrections to be applied to measurements made with Eppley (and other) spectral radiometers when used with Schott colored glass filters. *J. Appl. Meteor.* **4**:741–744.

GULBRANDSEN, A., 1978: On the use of pyranometers in the study of spectral solar radiation and atmospheric aerosols. *J. Appl. Meteor.* **17**:899–904.

Locating ability of the tripartite seismic station on Jan Mayen

By Andrzej Kijko[1] and Anders Sørnes[2]

Abstract

This paper reports calculated locating accuracy for the Jan Mayen tripartite station. The standard error of epicenter location close to the station is 3 km. At 60 km from the center of the island the standard error varies between 4 km and 7 km due to the highly unsymmetrical tripartite station. The theoretical results are compared with the accuracy obtained in locating known explosions. The recording during a crustal survey rendered suitable data for comparison purposes.

Introduction

Jan Mayen is the northernmost volcanic island on the mid-Atlantic ridge system. The large Beerenberg volcano which is the northernmost active volcano in the world above sea level, dominates the 380 km² island (Fig. 1). The island is 54 km long and its width varies between 2.5 km in the middle and 15 km across Beerenberg. The height of Beerenberg is 2,277 m above sea level.

Beerenberg had a major flank eruption in September 1970, which initially produced a 6 km long northeast trending fissure on the northeastern flank. The south-west end of the fissure was 600 m above sea level, while the northeast end nearly reached sea level. Dominantly alkaline lava from the fissure formed about 4 km² of new land, which, however, has later been partially eroded by strong wave action and drift ice. Sylvester (1975) has given a survey of the 1970 eruption and the historic activity and concluded that the eruption frequency is 150 years $\pm$ 75 years.

A tripartite seismic array was installed in the second half of 1971, prompted by the 1970 eruption. It was intended as the main part of a surveillance system which hopefully could predict future eruptions. Both the 1970 Beerenberg eruption and the 1973 Heimaey eruption in Iceland were preceded by a few earthquakes which were deeper than normal for the respective areas. This may be an important prediction criterion (Bjørnsson and Einarsson 1975). The general level of seismic activity and any change in the geographical pattern are alternative criteria that might be used.

[1] Institute of Geophysics, Polish Academy of Sciences, Warsaw, Poland.
[2] Seismological Observatory, University of Bergen, Norway.

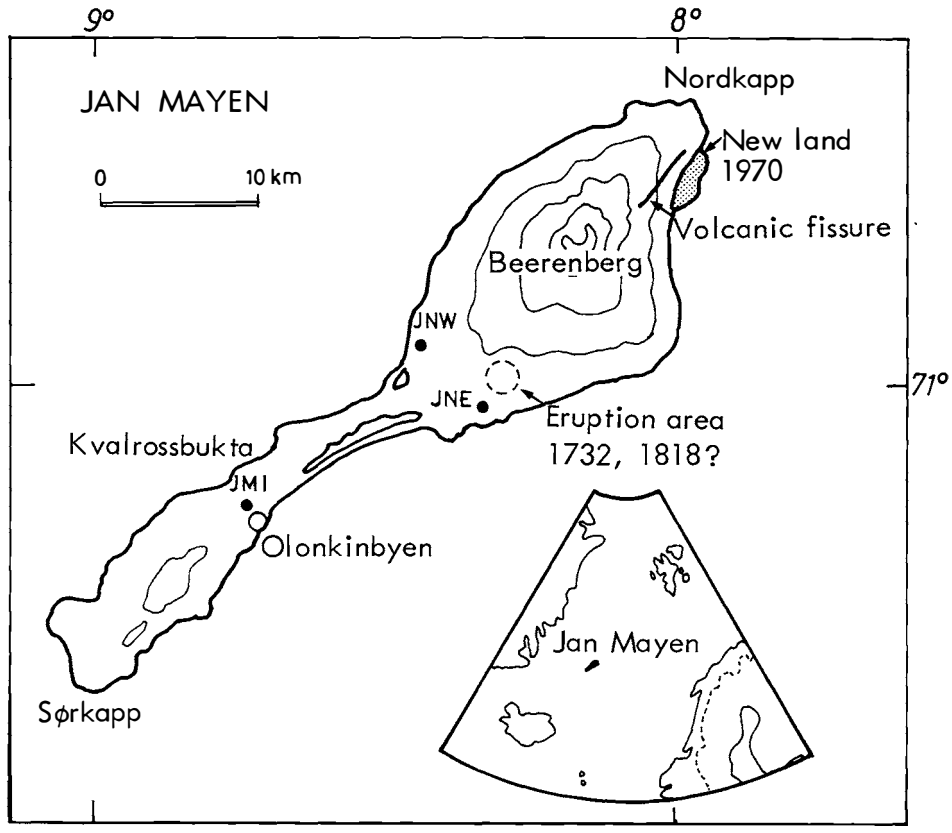

Fig. 1. *An outline map of Jan Mayen with some relevant features drawn in.*

There are several other geophysical problems. The tectonic setting of Jan Mayen is not yet clear. The intersection of the southern end of Mohn's Ridge and the central part of the Jan Mayen fracture zone have still not been located with accuracy. Different models for the location and persistence of Beerenberg as a central volcano have been proposed (SYLVESTER 1975). One model, for example, assumes that Jan Mayen was created by eruptions from a short segment of a spreading ridge caught between en échelon segments of the Jan Mayen fracture zone.

These gephysical problems may to some extent be solved by the seismic data from the tripartite station on Jan Mayen if the location accuracy is good enough. This paper will present the expected locating accuracy of earthquakes near Jan Mayen based on data from the tripartite station.

Recording and play-back equipment

Most of the instrumentation of the tripartite station has been supplied by Teledyne Geotech. The seismometers are of the S-13 type operated at a resonance frequency of 1 Hz and represent the high-pass filter of the system.

The two northernmost elements of the array, JNE and JNW, have only a vertical component. The outputs of these sensors are frequency modulated

(680 ± 125 Hz) and transmitted about 25 km by surface cables to the recording camp. The JMI element of the array has a three-component set of seismometers, one vertical and two horizontal (one parallel and one transverse to the long axis of the island). The outputs of these three seismometers are amplified and transmitted about 3 km by surface cables in analogue mode. At the recording camp all five components are recorded on a Teledyne-Geotech Flexicorder RM-100 in FM-mode at a tape speed of 15/160 inches per second. The recorder employs one inch wide tape and a 14 inch spool lasting 10.6 days. Since only seven tracks are used (five seismic plus timing and flutter) the tapes can be turned and another 10.6 days be recorded on each. The recording part represents the low-pass filter of the system and is 3dB down at 31 Hz.

The timing system receives signals from an external high precision oscillator (Hewlett-Packard Model 5065A Rubidium Vaper Frequency Standard), with a long-term stability of better than 2×10^{-11} per month and a short-term stability conservatively rated at less than 7×10^{-12} rms averaged over a one-second period. This signal is made into an IRIG-C time code and also recorded in FM-mode. The time-coding instrument has been supplied by Labteknikk.

In the event of an earthquake, a threshold trigger on a seismic channel starts a six-channel visual recorder, a Gulton TR-666. This recorder first has a chart speed of 1 cm/s for ten seconds, and then a chart speed of 0.1 cm/s for 55 seconds. Because it is repeated every minute, the timing code can be read in all cases. All five seismic channels and the coded timing signals are transcribed from the magnetic tape with a delay time of 18 seconds. The differences in arrival times of the P-wave, transcribed when the chart speed is 1 cm/s, can be determined with a precision better than ± 0.1 second. The S-P time differences at the three array points can be read with a precision of ± 0.2 second. The Flexicorder has fast forward and rewind capabilities and events can later be played back on site with a manually set chart speed of maximum 10 cm/s on the TR-666, giving a much better precision.

The data are analyzed in detail at the Seismological Observatory in Bergen. The standard procedure is to play back the tapes with a speed-up of 40x and to write the data on a 16 channel Siemens Oscillomink jet-pen recorder with a maximum chart speed of 100 cm/s. This gives a second length of 2.5 cm. The high-pass end of the seismic channel band-width is to some extent limited by the jet-pen galvanometers which have a typical upper frequency response of 3 dB down at 800 Hz. This corresponds to 20 Hz signal frequency. Different continuous adjustable filter settings can be employed by the use of Krohn-Hite band-pass filters, Model 330 N. A typical standard error in Bergen is 0.01 second for P-differences and 0.1 second for S-P readings.

Earth structure beneath Jan Mayen

A seismic refraction survey was carried out at Jan Mayen in August 1973 in order to obtain a crustal velocity model (Sørnes and Navrestad 1976) needed for locating local earthquakes recorded by the permanent seismic

station. Twenty-five depth charges (135 kg TNT each) were detonated around the island and recorded by both the permanent station and three temporary field stations. The following average P-wave velocity structure has been calculated based on the recorded data, assuming layering with constant velocities in each layer.

Layer 1 has a thickness of 0.5 km at the island, assuming a velocity of 2.5 km/s. Layer 2, with a velocity of 3.14 km/s ($\sigma = 0.09$ km/s), reached a depth of about 3 km. Layer 3, with a velocity of 6.33 km/s ($\sigma = 0.07$ km/s), reached a depth of 18 km. Layer 4, below 18 km, may have a velocity as great as 8.27 km/s and $\sigma = 0.086$ km/s.

Computer procedure for locating earthquakes

A computer program has been developed to locate earthquakes by the method of least squares, using the differences of first arrival times between the three stations $t_{p1i} = t_{p1} - t_{pi}$ ($i = 2,3$) and the differences of arrival times of S- and P-waves at the three stations $t_{spi} = t_{si} - t_{pi}$ ($i = 1,2,3$). P and S arrival times for each station are given by an equation of refracted waves:

$$\begin{aligned} t_{pi} &= t_0 + \Delta_i/V_i + a_i + \varepsilon_{pi} \\ t_{si} &= t_0 + (\varrho + 1) \cdot (\Delta_i/V_i + a_i) + \varepsilon_{si} \quad . \end{aligned} \tag{1}$$

where:

t_0 – origin time

Δ_i – epicentral distance

V_i – velocity of the first arrival. It is known that the velocities V_i are random variables with the two first moments known as:

$E(V_i) = < V_i > \; ; \; E(V_i - < V_i >)^2 = \sigma_{vi}^2$.

E – expectation operator

a_i – intercept time

$E(a_i) = < a_i > \; ; \; E(a_i - < a_s >)^2 = \sigma_{ai}^2$.

$\varrho + 1 = <V_p>/<V_s>$ – the ratio of P to S wave velocity

ε_{pi}, ε_{si} – the reading error of P and S arrival time. We assume that

$E(\varepsilon_{pi}) = 0$; $E(\varepsilon_{pi}^2) = \sigma_{pi}^2$

$E(\varepsilon_{si}) = 0$; $E(\varepsilon_{si}^2) = \sigma_{si}^2$

The velocities, intercept times and their variances depend on different functions of distance in different distance ranges. These functions are obtained from deep seismic sounding (SØRNES and NAVRESTAD 1976). We assume that $\varrho = 0.73$. The problem of locating an earthquake is reduced to a minimization of a non-linear function

$$F(<\theta>) = \min_{\theta \varepsilon \Omega_\theta} F(\theta) \tag{2}$$

where

$$F(\theta) = [t - t(\theta)]^T \Sigma_t^{-1} [t - t(\theta)] \tag{3}$$

$\theta = (x, y,)^T$ – coordinates of epicenter within the domain Ω_θ.
t – vector of observations $= (t_1, \ldots, t_5)^T = (t_{sp1}, t_{sp2}, t_{sp3}, t_{p12}, t_{p13})$

Σ_t – covariance matrix of vector t,

$$\Sigma_t = E[t - t(<\theta>)] [t - t(<\theta>)]T \tag{4}$$

T – denotes matrix transposition.

It is easy to prove that the matrix Σ_t has the form

$$\Sigma_t = \left\| \begin{matrix} \Sigma_t^{11}, & \Sigma_t^{12} \\ \Sigma_t^{21}, & \Sigma_t^{22} \end{matrix} \right\| \tag{5}$$

where

$$\{\Sigma_t^{11}\}_{\alpha,\beta} = \begin{cases} \sigma_{tp\alpha}^2 + \sigma_{ts\alpha}^2 + \varrho^2 \sigma_{m\alpha}^2 & \alpha = \beta \\ 0 & \alpha \neq \beta \end{cases}$$
$$\alpha,\beta = 1,2$$

$$\{\Sigma_t^{22}\}_{\alpha,\beta} = \begin{cases} \sigma_{tp\alpha}^2 + \sigma_{m\alpha}^2 + \sigma_{tp\beta}^2 + \sigma_{m\beta}^2 & \alpha = \beta \\ 0 & \alpha \neq \beta \end{cases}$$
$$\alpha,\beta = 1,2$$

$$\{\Sigma_t^{21}\}_{\alpha,\beta} = \begin{cases} -\sigma_{tp\alpha}^2 + \varrho \sigma_{m\alpha}^2 & \alpha = 1,2;\ \beta = 1 \\ \sigma_{tp\alpha+1}^2 + \varrho \sigma_{m\alpha+1}^2 & \alpha = 1,2;\ \beta = \alpha + 1 \\ 0 & \alpha = 1;\ \beta = 3 \\ 0 & \alpha = 2;\ \beta = 2 \end{cases}$$

$$\sigma_{m\alpha}^2 = \sigma_{v\alpha}^2 \Delta_\alpha^2 / <V_\alpha>^4 + \upsilon_{a\alpha}^2$$

and

$$\Sigma_t^{12} = (\Sigma_t^{21})^T$$

The elements of the matrix Σ_t contain information about the deviation of the theoretical model of the process from the true process. An exhaustive analysis of the effect of errors of model parameters in the regression analysis has been performed as recently as in the sixties (Klepikov and Sokolov 1962; Wolberg 1967; Fedorov 1972, 1974). In seismology, an analysis of this kind has been applied by Peters and Crosson (1972) and Kijko (1975, 1976, 1977).

The computer program is described in detail by Kijko (1978 a and b). None of the shots of the 1973 crustal survey offered enough S data to locate the epicenter by using the permanent array. By including the three temporary field stations we were able to compose three-point arrays which could be used for a few shots. We selected the three shots with three readings for both P and S (shot Nos. 7, 10, and 11), and one with one S-reading missing but only one e-reading (shot No. 9). The distances between real and calculated epicenter for shot Nos. 7, 9, 10, and 11 were 1.6, 3.1, 5.2, and 4.1 km, respectively. All

four shots are very close to, or within, the 3-value isoline in Fig. 2. The larger mislocation for the last three shots is due to the fact that the sites we had to choose were nearly in line (JMI, the middle of the island, and Nordkapp), while the sites were better distributed for shot No. 7 (JNE, JNW, and Nordkapp). We thus see that the mislocations found when using the computer programs are of the order expected from independently calculated and observed standard errors as shown in Figs. 2 and 3.

Procedure for estimating the standard errors of epicenter location

In the general case of a non-linear least squares estimation of parameters θ, the covariance matrix Σ_θ is built by linearizing the model in the nearest vicinity of the true value $<\theta>$ and may be expressed by formula (6):

$$\Sigma_\theta = (A^T \Sigma_t^{-1} A)^{-1} \tag{6}$$

where

$$\{A\}_{i,j} = \left.\frac{\delta t_i(\theta)}{\delta \theta_j}\right| \theta = <\theta> \tag{7}$$

$$i = 1, \ldots, 5, \quad j = 1,2.$$

Considering (1) and (7), it is easy to verify that the elements of the matrix A have the form:

$$\{A\}_{\alpha,\beta} \begin{cases} \varrho \cos Az_\alpha / <V_\alpha> , & \alpha = 1, 2, 3;\ \beta = 1 \\ \varrho \sin Az_\alpha / <V_\alpha> , & \alpha = 1, 2, 3;\ \beta = 2 \\ \cos Az_1 / <V_1> - \cos Az_{\alpha-2} / <V_{\alpha-2}>, & \alpha = 4, 5;\ \beta = 1 \\ \sin Az_1 / <V_1> - \sin Az_{\alpha-2} / <V_{\alpha-2}>, & \alpha = 4, 5;\ \beta = 2 \end{cases} \tag{8}$$

where Az_i is the azimuth for the epicenter relative to the station with number i.

The equation (6) together with (5) and (8) form the basis for the solution of the problem. The elements on the diagonal of the covariance matrix (6) are the variances of the estimated parameters $<x>$, $<y>$ of the epicenter. We also determine the variance of the epicenter position. We take the standard error of the epicenter position to be the radius of the circle, the area of which is equal to that of the ellipsoid of the standard error of the coordinates x, y. It is easy to show that the standard error of the epicenter position so defined is described by the formula

$$\sigma_{xy} = [\Sigma_{\theta 1,1}\ \Sigma_{\theta 2,2} - (\Sigma_{\theta 2,1})^2]^{\frac{1}{4}}$$

Fig. 2 shows the standard error of epicenter position as isoline curves calculated by the formulae given above. The standard error of the P-arrival readings has been assumed to be 0.01 s and the standard error of the S-arrival readings twice that value. The earth structure parameters are assumed to be the exact values calculated from the 1973 survey, except for the 0.5 km thin uppermost layer, which is ignored:

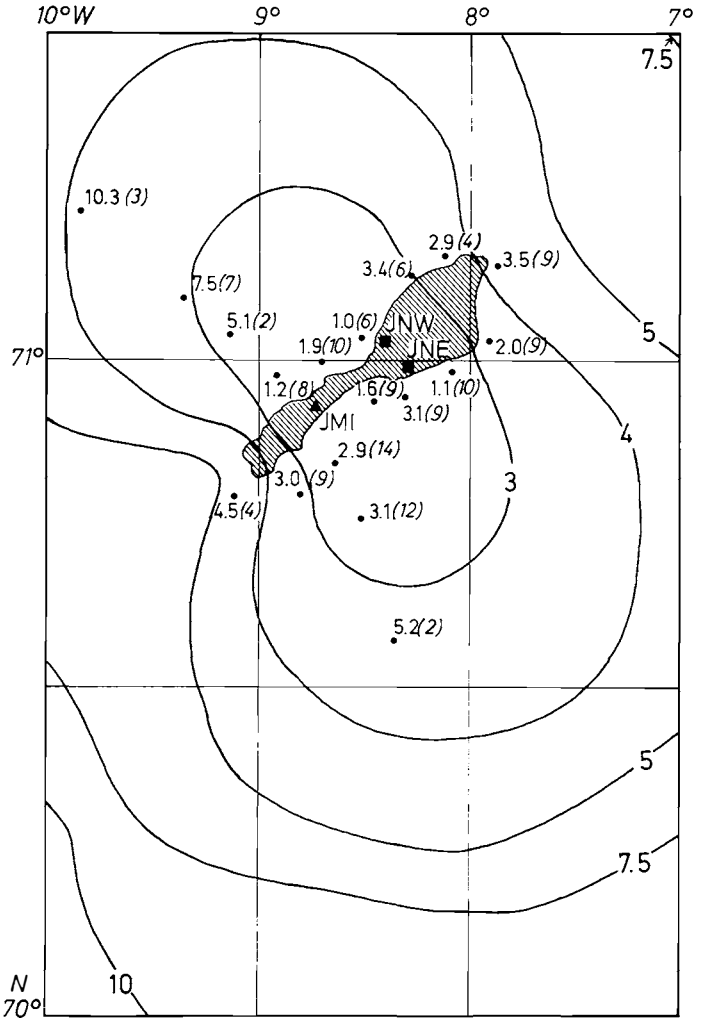

Fig. 2. *Calculated and observed standard errors of epicenter location shown as isoline and discrete values respectively. Numbers in parentheses are the sum of the weights for the observations included.*

Depth (km)	v = P-velocity (km/s)	σ_v (km/s)	a = intercept time (s)	σ_a (s)
0–3	3.136	0.085	0.24	0.14
3–18	6.332	0.065	1.83	0.36
>18	8.271	0.086	4.93	0.43

Also shown in Fig. 2 are the standard errors of the epicenter positions obtained by a graphical method for the shots detonated during the 1973 crustal survey. The numbers in parentheses are the sums of weights for the observations included. The weights were allotted subjectively as 3, 2, or 1 according to whether the input data had been given the quality prefix i, (none) or e, respectively. The graphical location method is described in detail by

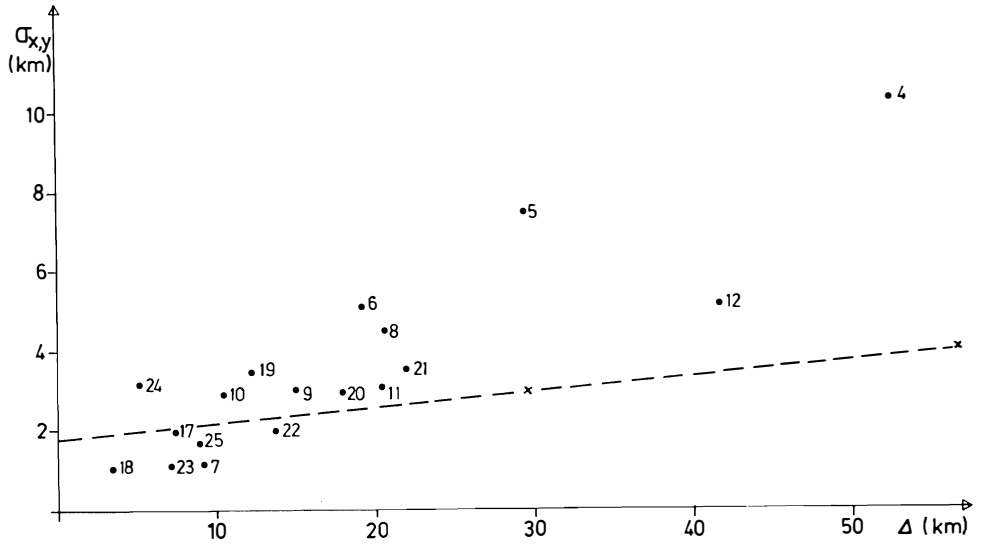

Fig. 3. *Calculated (dotted line) and observed standard errors of epicenter location versus distance to the nearest station. The numbers give the numbering of the shots included, following* SØRNES *and* NAVRESTAD *(1976).*

FJELDSKAAR and SØRNES (1978). In order to estimate a standard error value to be a measure of accuracy which could be compared with theoretically calculated standard errors, a distance residual was measured graphically against the true epicenter for each isoline observation. In this way an observed standard error became available even if the sum of the weights was as low as 2 (two e-observations).

Discussion

Fig. 2 shows that the calculated and the observed standard errors of locating are of the same order of magnitude for epicenters close to the island. For epicenters at increasing distances from the island, the observed standard errors increase more rapidly than the calculated values. This feature is more clearly seen in Fig. 3 where the standard errors are plotted as a function of the distance to the nearest station. The observed data are the readings obtained from some charges detonated during a crustal survey in 1973 (SØRNES and NAVRESTAD 1976). The numbering of the shots in that survey is retained in Fig. 3. The more rapid increase of the errors relative to distance for the observed data is due to the size of the shots (135 kg TNT). It is seen in Fig. 2 that the more distant shots have been located by little and poor data (low sum of weight). Since the calculated and observed standard errors for well-recorded near events are of the same order of magnitude, it might be inferred that well-recorded, more distant, events can be located with the standard errors of the same order of magnitude as the corresponding calculated standard errors.

The above conclusion is also consistent with the data shown in Fig. 4. In this

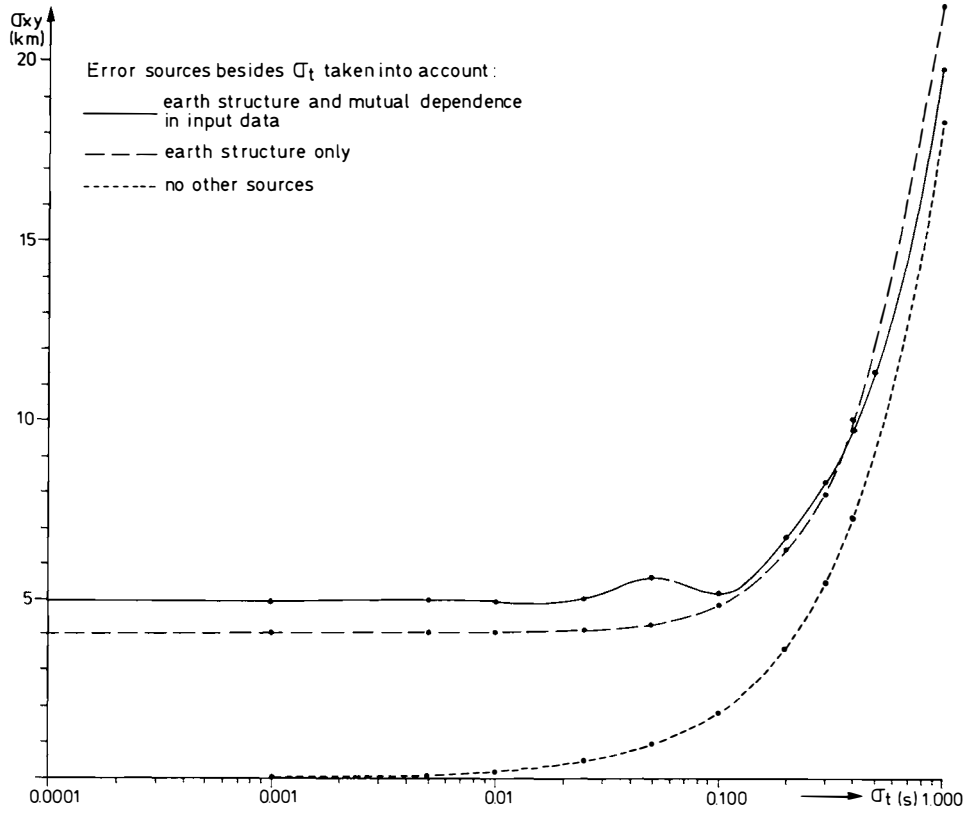

Fig. 4. *Standard error of location versus standard error of the time readings with and without other sources of error taken into account. The standard error values are averaged over the area: 70°–71°30' N, 7°–10° W.*

figure the standard error of epicenter location is shown as a function of the standard error of the arrival time readings for different cases of other error sources being taken into account. It is seen that the location error caused by the low precision of the parameters of the crustal structure, averaged over the whole area, is so large that the standard error of the arrival time data can be as large as 0.1 s before this causes any increase in location error. No higher locating errors than those calculated are therefore anticipated, since such a high reading error as 0.1 s is only expected beyond the distance where complete lack of some data is likely.

Acknowledgement

One of the authors (A. K.) is grateful for holding an exchange scholarship granted by the Norwegian Ministry of Foreign Affairs, while this paper was prepared at the Seismological Observatory, University of Bergen. He is also grateful for all the facilities placed at his disposal at the University of Bergen.

This study is part of a project "Seismic Surveillance" supported by a grant from the Norwegian Research Council for Science and the Humanities. Cand. real. Willy Fjeldskaar has been scientific assistant paid for by this grant and

has given valuable assistance during the preparation of this paper. The seismic station on Jan Mayen is run by the Norwegian Defence Communications Administration which has generously put all data about it and all recordings at our disposal.

References

BJØRNSSON, S. and P. EINARSSON, 1975: Seismicity of Iceland. Pp. 225–239. In: KRISTIANSSON, L. (Ed.): *Geodynamics of Iceland and the North Atlantic Area.* Proc. NATO Advanced Study Institute, Reykjavik, Iceland, 1–7 July, 1974. D. Reidel Publishing Co., Dortrecht.

FEDOROV, V. V., 1972: *Theory of optimal experiments.* Academic Press, New York.

— 1974: Regression problems with controllable variables subject the error. *Biometrica* **61** (1): 49–55.

FJELDSKAAR, W. and A. SØRNES, 1978: *Hyposenterbestemmelse ved hjelp av den seismiske trepunktstasjonen på Jan Mayen.* Institute Report, Seismological Observatory, Bergen.

KIJKO, A., 1975: On optimal extension of regional networks of seismic stations. *Publs. Inst. Geoph. Pol. Ac. Sci.* **96**: 57–119.

— 1976: An analysis of the extension of the regional seismic network in Upper Silesia. *Acta. Geoph. Pol.* XXIV: 205–215.

— 1977: An algorithm for the optimum distribution of a regional seismic network. II. An analysis of the accuracy of location of local earthquakes depending on the number of seismic stations. *Pageoph.* **115**: 1011–1021.

— 1978 a: *Short distance location program for a tripartite seismic array.* Institute Report, Seismological Observatory, University of Bergen.

— 1978 b: *Short distance location program for a tripartite seismic array. Version II. Incomplete set of input data, determination of the depth.* Institute Report, Seismological Observatory, University of Bergen.

KLEPILOV, N. P. and S. N. SOKOLOV, 1972: *Analysis and planning of experiments by the method of maximum likelyhood.* Pergamon Press, London.

PETERS, D. C. and R. S. CROSSON, 1972: Application of prediction analysis to hypocenter determination using a local array. *Bull. Seism. Soc. Am.* **62**: 775–788.

SYLVESTER, A. G., 1975: History and surveillance of volcanic activity on Jan Mayen island. *Bull. Volcanol.* **34** (2): 1–23.

SØRNES, A. and T. NAVRESTAD, 1976: Seismic survey of Jan Mayen. *Norsk Polarinstitutt Årbok* 1975: 37–52.

WOLBERG, J. R., 1967: *Prediction analysis.* D. van Nostrand Co., Inc., Princetion.

The local seismicity in the Jan Mayen area

By A. Sørnes[1] and W. Fjeldskaar[1]

Abstract

The local seismicity in the Jan Mayen area during the last two decades is described in time and space. The data are presented in a way that will ease evaluation of future data with regard to forecasting any new volcanic eruption of Beerenberg. The intersection between the fracture zone and the Mohns ridge is shown to be east of Jan Mayen. It is also shown that the seismicity of the fracture zone has no sidestep near Beerenberg. This rules out the possibility that this volcanism is caused by a small segment of a spreading ridge caught between en échelon fault segments. Evidence is now accumulating that the Mohns ridge is offset right laterally by a small fracture zone at 71 ½°N.

Introduction

A detailed study of the local seismicity in the Jan Mayen area has not been possible earlier because precise information about the crustal and sub-crustal velocities has been lacking. This was the case until the results of the regional seismic shooting survey in 1973 were worked out (Sørnes and Navrestad 1976). A regional seismicity study using data recorded by a single station on Jan Mayen in the time period 1962–1973 has been published (Navrestad and Sørnes 1974). That paper will in the following be referred to as Paper 1. In 1971 a tripartite station was installed by the Norwegian Defense Communication Administration. This station greatly improved the locating accuracy (Kijko and Sørnes 1980). The present paper is a study of the data collected by the tripartite station. One objective is to continue and extend the study of the seismicity pattern and recurrence rates initiated in Paper 1, quoted above. Such studies provide the background data on which future seismic activity must be compared. This may provide warnings of any new volcanic eruption for the small isolated community on this Arctic island. Another objective of this study is to use the seismic data to investigate the tectonic setting of the Beerenberg volcano in relation to the Jan Mayen Fracture Zone (JMFZ) and the Mohns ridge.

Distribution of the larger seismic events

Epicenter maps of seismic events large enough to have been located by stations at teleseismic distances provide a coarse view of the tectonic setting of an area. A series of epicenter maps were presented in Paper 1. In practice, the

[1] Seismological Observatory, University of Bergen, 5014 Bergen, Norway.

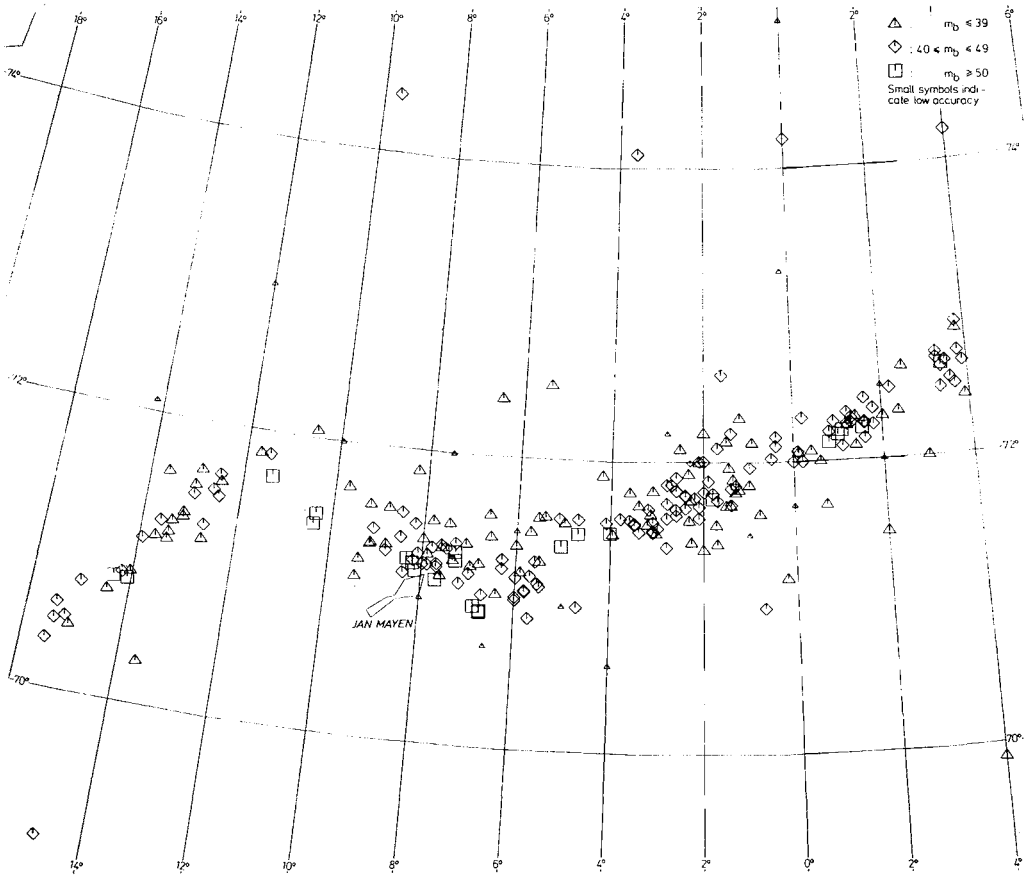

Fig. 1. *Epicenter map 1955–1977.*

lowest magnitude turned out to be $m_b = 3.9$. Data prior to 1955 were not used because of the low hypocenter accuracy of the available data. One of the regional epicenter maps in Paper 1 included data for eighteen years, 1955–1972. A similar regional epicenter map is shown in Fig. 1 in the present paper. This figure includes data for 23 years, 1955–1977. The last available determinations by the International Seismological Center (ISC) were from December 1976. The Preliminary Determination of Epicenters (PDE) by the US Geological Survey was completed with chronological monthly listings for Desember 1977. The PDE data in our file are replaced by the ISC determinations as soon as they become available. The PDE data are so comprehensive that the data for 1977 included in Fig. 1 give a sufficiently correct picture of the seismicity for events located by stations at teleseismic distances. If more than one determination is available, the most accurate ones chosen for the various time periods are the following:

1955–1963 SYKES (1965)
1964–1976 ISC, Newbury
1977 PDE of US Geological Survey, Boulder.

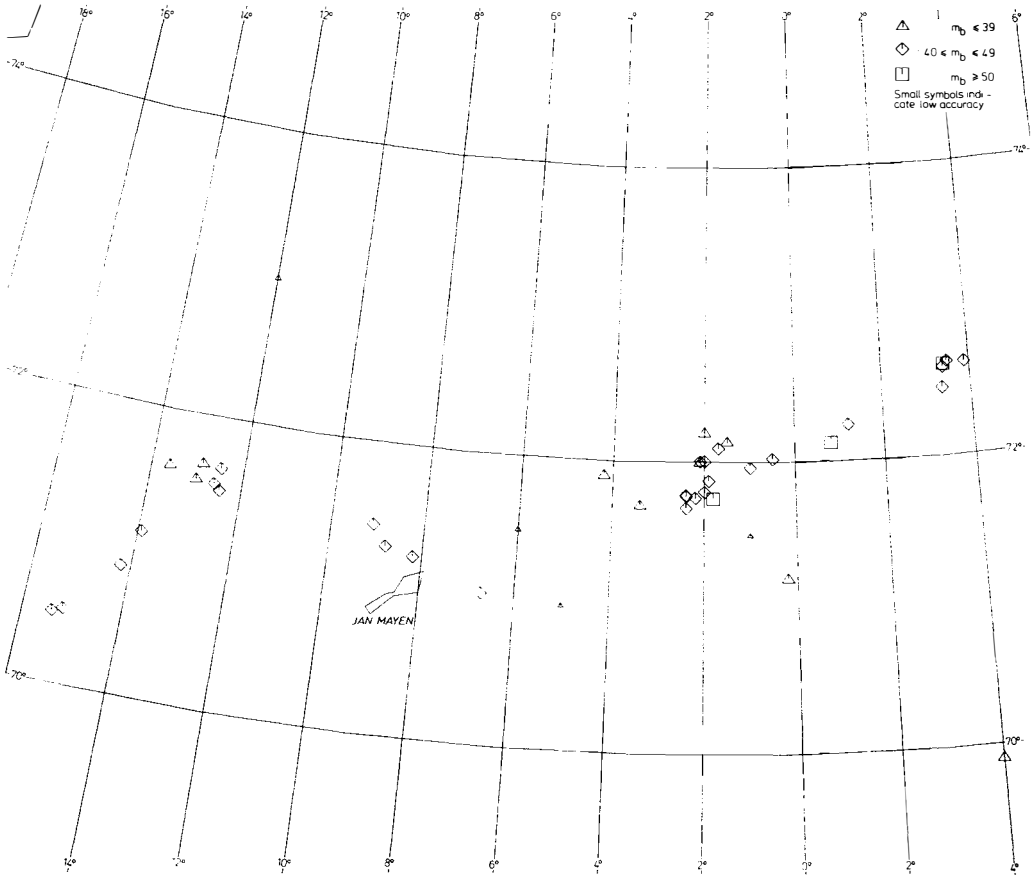

Fig. 2. *Epicenter map June 1975 — December 1977.*

Determinations of other events by other researchers or institutions are indicated by small symbols in Fig. 1.

In Paper 1 some epicenter maps for 31-month intervals were given to find out if there were any variations of the seismicity in time and space. The first of these maps covered the 31-month period starting in January 1955. The two other maps covered similar time periods, shortly before and shortly after the September 1970 Beerenberg eruption. The present paper includes a corresponding map in Fig. 2 for the last 31-month period for which a complete data set is available, June 1975 to December 1977.

Earthquake swarms of larger events

It was shown inPaper 1 that the earthquakes along the plate boundary from Svalbard to Iceland have the same tendency to cluster into swarms. An earthquake swarm in this context was defined as three or more events during 48 hours within an area less than 1° longitude and less than 2° latitude. Only events large enough to be located by distant stations were examined in Paper 1. In the present paper the corresponding data collected in the time period following the

time period included in Paper 1 are analysed. The data covered by Paper 1 have also been reexamined.

Fig. 3 shows the distribution of earthquake swarms in the Norwegian Sea during the time interval August 1954 to December 1977. No event with $m_b < 3.9$ has been included. The notation 08/59(6) means that the swarm occurred in August 1959 and comprised six events. Fig. 4 shows the number of events occurring in each month as a function of time.

A closer look at the six swarms closest to Jan Mayen between 6°W and 10°W (Fig. 3) does not associate the JMFZ with earthquake swarms if the sequences are subdivided in the three traditional types (Mogi 1963): 1) mainshock-aftershocks, 2) foreshocks-mainshock-aftershocks, and 3) a swarm sequence. We take the three swarms closest to Jan Mayen to be volcanic swarms related to Beerenberg which is known to be a central volcano in the area. Two of these swarms, 01/73(3) and 01/73(6) in fact were much closer to Beerenberg (Fig. 9), and were also associated with the highest monthly total number of local events recorded (Fig. 5). The third swarm, 08/67(4), was associated with the second highest total monthly number of events (Fig. 5). The JMI records indicate that these local events most probably are volcanic events related to the Beerenberg

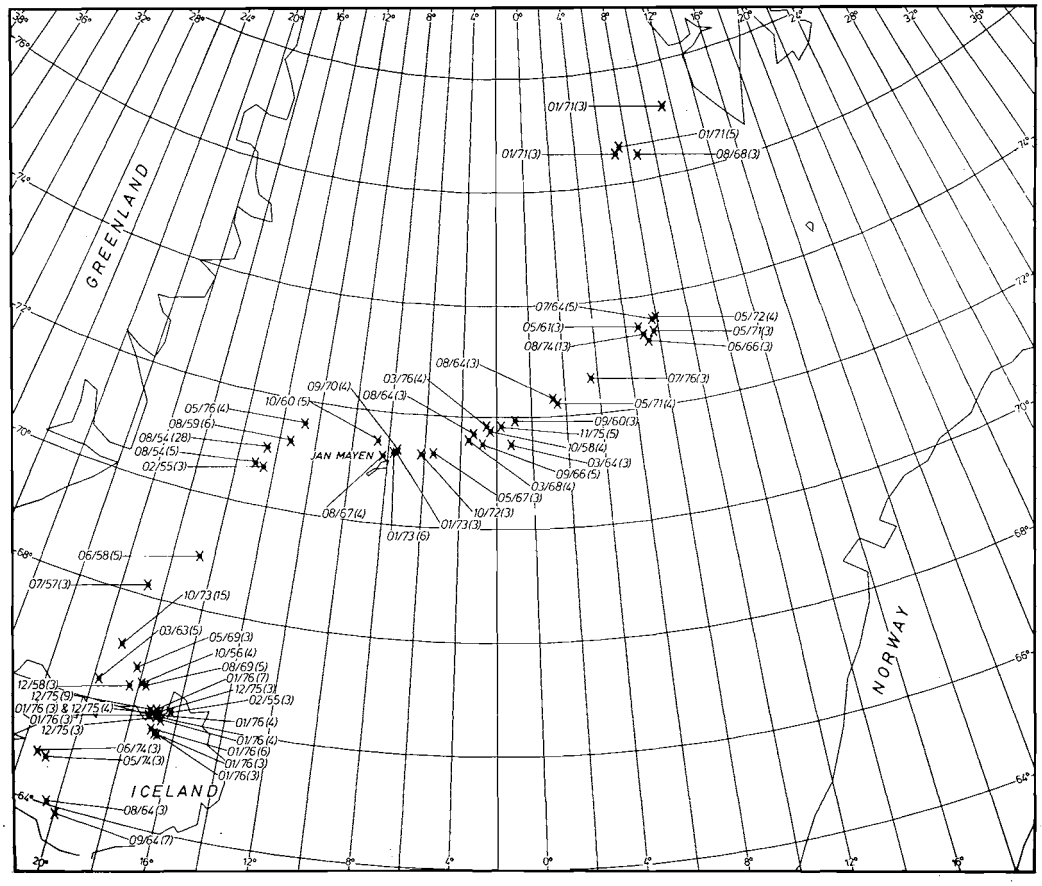

Fig. 3. *Earthquake swarms in the Norwegian Sea.*

volcano: typical distance to JMI is only 23 kilometres. The three swarms close to Jan Mayen in Fig. 3, 10/60(5), 09/70(4), and 10/72(3) all have a mainshock which is more than 0.6 m_b units larger than the second largest shock. These sequences are therefore not swarms in the restrictive sense (BÅTH 1979). The 09/70(4) events were preceding or directly associated with the 1970 Beerenberg eruption. Fig. 9 shows that the swarm 10/72(3) also occurred more to the south and closer to Jan Mayen.

The northernmost swarm on the Kolbeinsey ridge, 05/76(4), and the southernmost on Mohns ridge, 05/67(3), are true swarms by any definition.

One must bear in mind that the time window used in Fig. 3 is as short as 48 hours. This window was arbitrarily chosen in Paper 1 in order to find out if short term clustering patterns of the seismic activity in the area could be of help in evaluating teleseismic data for predicting any new eruption of the Beerenberg volcano.

Recent frequency of local earthquakes

The simplest parameter for the description of the local seismic activity within 100 kilometres of the main seismic station on Jan Mayen is the number of events (Fig. 5). In Paper 1 a figure which gave the monthly number of local events was shown. An extended version of that figure, including also the last years, is here shown in Fig. 5.

By a glance on the visual records in Fig. 5 one can easily see if the seismic activity is above average. In order to check if this frequency gives reason to suspect an imminent volcanic eruption one has to study the geographical distribution of the events as described in the next paragraph. This procedure constitutes at present the volcanic surveillance system.

Distribution of local activity

The tripartite seismic station which came into full operation on Jan Mayen during the second half of 1972, permits location of local events also (FJELDSKAAR and SØRNES 1978; KIJKO 1978a, b). The accuracy of the determinations by the tripartite station has been investigated by KIJKO and SØRNES (1979).

Fig. 6 shows the epicenters of two local concentrated earthquake swarms which occurred soon after the station came into operation. The first of these

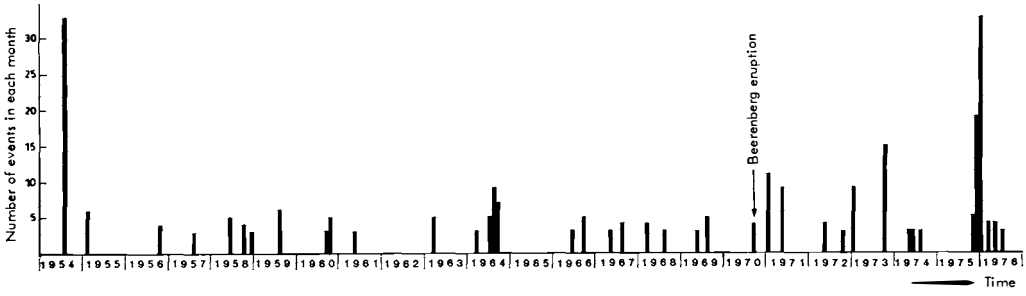

Fig. 4. *Number of earthquakes in swarm versus tine.*

corresponds to the teleseismic swarm 10/72(3) east of Beerenberg. The other corresponds to the teleseismic swarms 01/73(3) and 01/73(6) on the northern flank of Beerenberg. The short time window (48 hours) used for the teleseismically defined swarms is not applied for the corresponding larger swarms located by the tripartite station. The activity in January 1973 brought the monthly number of local events up to 371, the highest number recorded (104 events occurred in one day). All these events had depths less or equal to 18 km. Fig. 7 shows all local events located during the time period February 1973 to December 1978 which have depths less than 18 km. Fig. 8 shows all events located in the same time interval with depths equal to or greater than 18 km.

The distribution of the epicenters in Figs. 6–8 is believed to give a fair picture of the real local seismicity even though malfunctioning of one or more of the array elements has made it impossible to locate a number of events in several time periods. The data sampling imposed by the technical functioning or malfunctioning of the station might be significant in a seismicity study, particularly because a clustering effect is shown to be present in this area. In nearly all of the time period at least one element of the array has been recording continuously on some device, usually a visual recorder. The study of these records does not indicate that any repetitive source has been missed.

Accuracy of epicenter determinations near Jan Mayen

Fig. 9 shows a comparison between thirteen epicenters determined by the local station and by the International Seismological Centre. The events chosen belong to the 10/72(3), 01/73(3), and 01/73(6) swarms. It appears that the international network locations are biased to the north of the real positions.

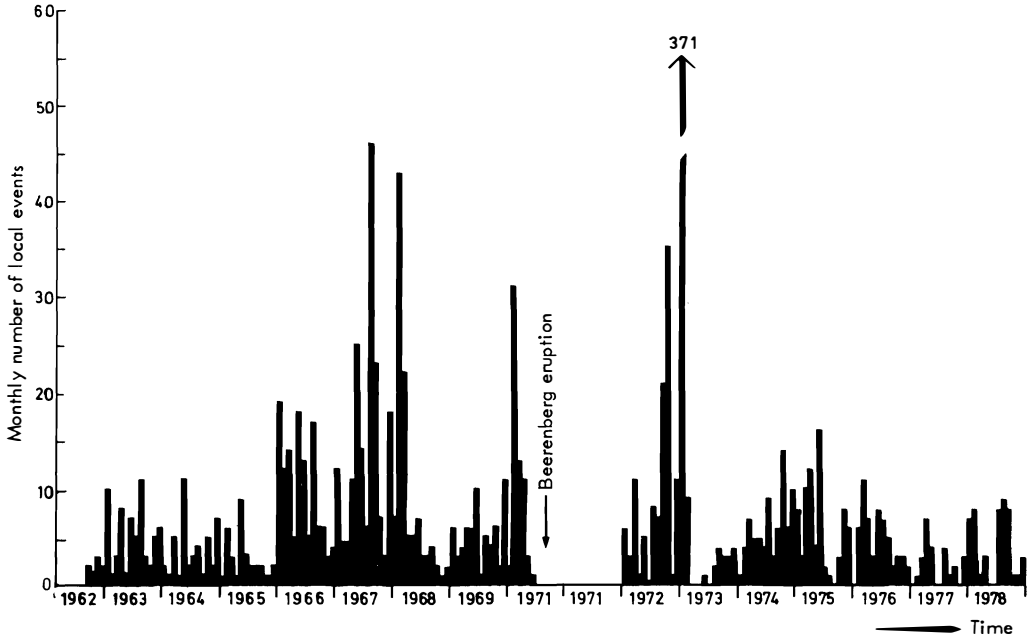

Fig. 5. *Local earthquake frequency versus time.*

This bias may be caused by the uneven distribution of the international network or travel time anomalies due to the earth structure in the area. The ISC location error depends strongly on the number of teleseismic recordings as shown in Fig. 10. The true epicenters are here assumed to be the position determined from the data recorded at the tripartite station on Jan Mayen. The standard error of epicenter location by the tripartite station is 3 km close to the network. At 60 km from the network the standard error varies between 4 and 7 km due to the highly unsymmetrical array (KIJKO and SØRNES 1980).

Discussion

The teleseismic data available suggest that the seismic activity in the Jan Mayen area has increased during the last two decades, noticeably after the volcanic eruption in September 1970 (Figs. 1 and 2)compared with the figures in Paper 1. The same comparisons also show that the activity has come closer to Jan Mayen. The increase is larger than one should expect as a result of the better detection capabilities of the expanding international network. SYLVESTER (1975) found that the eruption frequency of the Beerenberg volcano is 150 $\pm$ 75 years. The variation in the local seismicity may be associated with such a periodicity.

It was concluded in Paper 1 that the larger events recorded at distant stations are not useful for the prediction of volcanic eruptions at Jan Mayen. The reason for this is that the location accuracy by the distant stations is very low for the

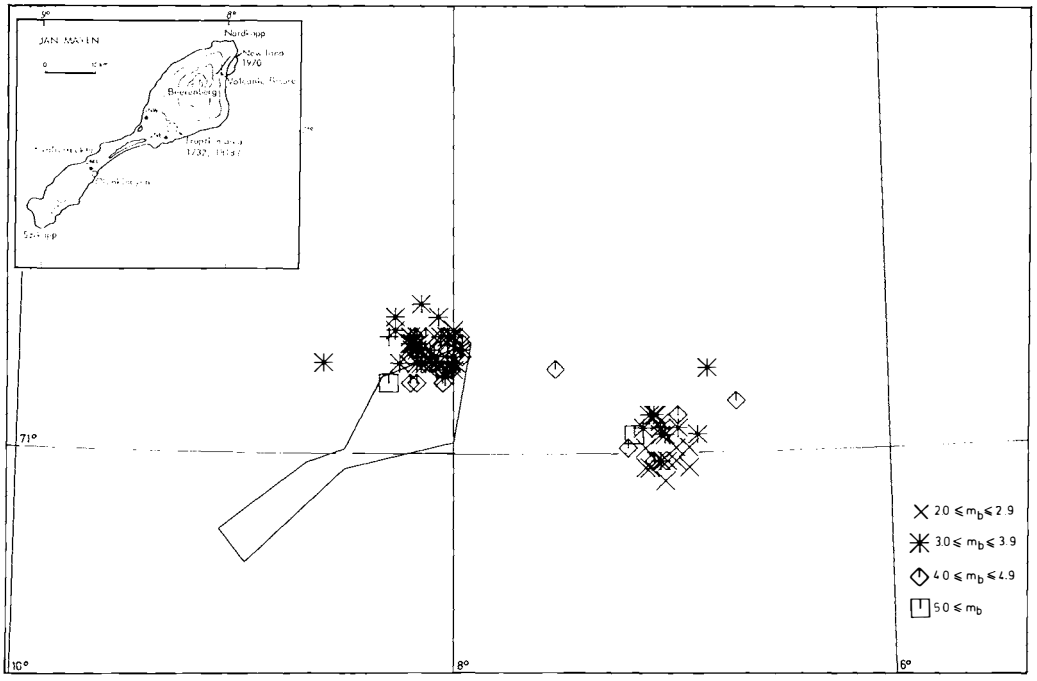

Fig. 6. *Epicenters of two local swarms, $h \leq 18$km. An outline map of Jan Mayen showing the station sites is also inserted.*

magnitude window which most events belong to in this area. Teleseismic data also become available too late for prediction purposes. The events along the whole seismic zone also show approximately the same trend to cluster into swarms when a short-term window (48 hours) is applied on the events with magnitudes above the teleseismic location threshold.

Earthquake swarms generally occur along the crest of the ridge systems contrary to the larger single events which concentrate along fracture zones. Such a rough criterion is of course not suited to delineate precisely the presently active JMFZ. (An older, now inactive, eastern branch of the JMFZ will not be considered in the present paper.) An interesting point is firstly whether the earthquake swarms near to Jan Mayen line up with the Mohns ridge activity or are associated with the Beerenberg volcano which is a central volcano on or close to the JMFZ. Secondly, a short segment of a spreading ridge might be caugt between en échelon segments of the JMFZ. The data in Figs. 2 and 3 indicate that the Beerenberg volcano might be located at the ridge crest-fracture zone intersection, but the following discussion of the local earthquakes gives evidence to the contrary.

In the present paper the clustering trend is studied by reexamining and extending the data base (Figs. 2 and 3). The six swarms along the JMFZ closest to Jan Mayen were also subdivided into the three Mogi types. The conclusion is that none of these appear to be swarm sequences in the restricted sense. The earthquakes along the JMFZ are either associated with a mainshock or are associated with volcanic activity of Beerenberg.

The frequency of local earthquakes as recorded by the tripartite station on

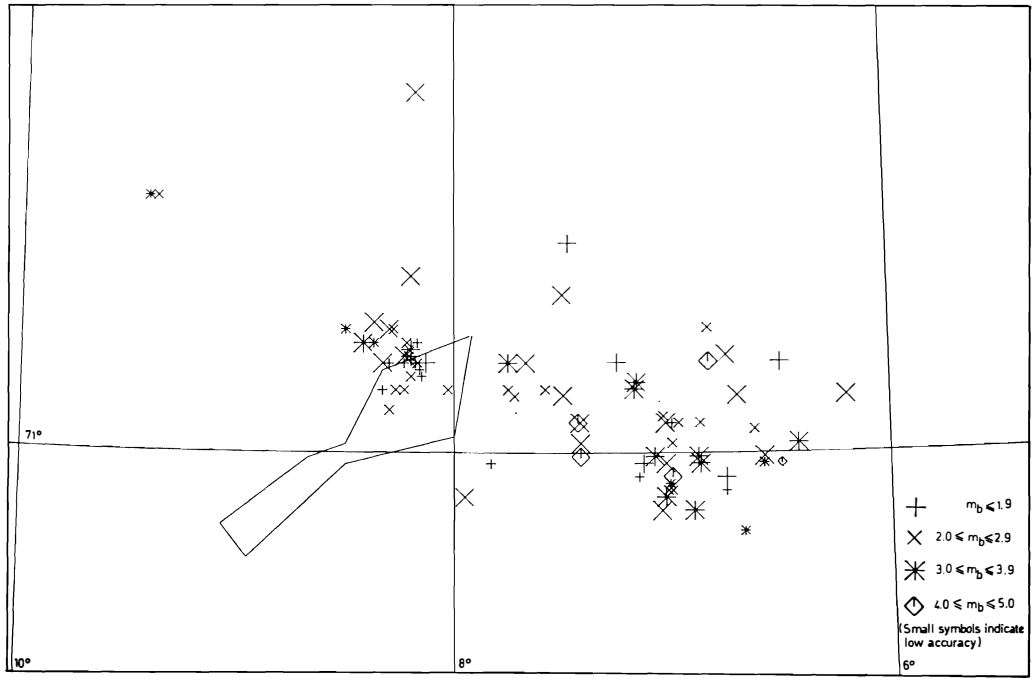

Fig. 7. *Locations of shallow local events February 1973 — December 1978, h < 18km.*

Jan Mayen is of course the most direct and quickest way to use the local seismicity for volcanic prediction (Fig. 5). When this frequency gives rise to concern one should use the locating ability of the local station. The operators of the station can use graphical aids and locate the events immediately (FJELDSKAAR and SØRNES 1978). At present this is the only practical prediction procedure available for volcanic eruptions on Jan Mayen.

Figs. 6–8 show that the seismicity zone has an average strike of approximately 117° on crossing Jan Mayen. The seismic zone coincides with the northern termination escarpment of the Jan Mayen ridge. This indicates that the JMFZ for some length is very close to the northern boundary of a possible micro-continent. Several studies have shown that the middle part of the Jan Mayen ridge may be a micro-continent (ELDHOLM and THIEDE 1979). For the very northern part of the ridge only one study has given estimates of crustal thickness and P_n velocity (SØRNES and NAVRESTAD 1976). That study indicated a crustal thickness of 18 km and a P_n velocity as high as 8.27 km/sec., not only beneath the seismic station but also to the south and to the west of the island.

Fig. 8 shows that the deeper events occur in a narrower zone than the shallower events in Fig. 7. Fig. 6 shows the positions of two local swarms. One is associated with the central volcano at Jan Mayen and the other might indicate the intersection between Mohns ridge and the JMFZ. Such intersections are often accompanied by a bathymetric depression. The two most recent bathymetric maps published have one pronounced depression at about the position of the eastern swarm in Fig. 6, even though they disagree as to the exact bathymetry in that area (PERRY et al. 1977; GRØNLIE and TALWANI 1977). SYLVESTER

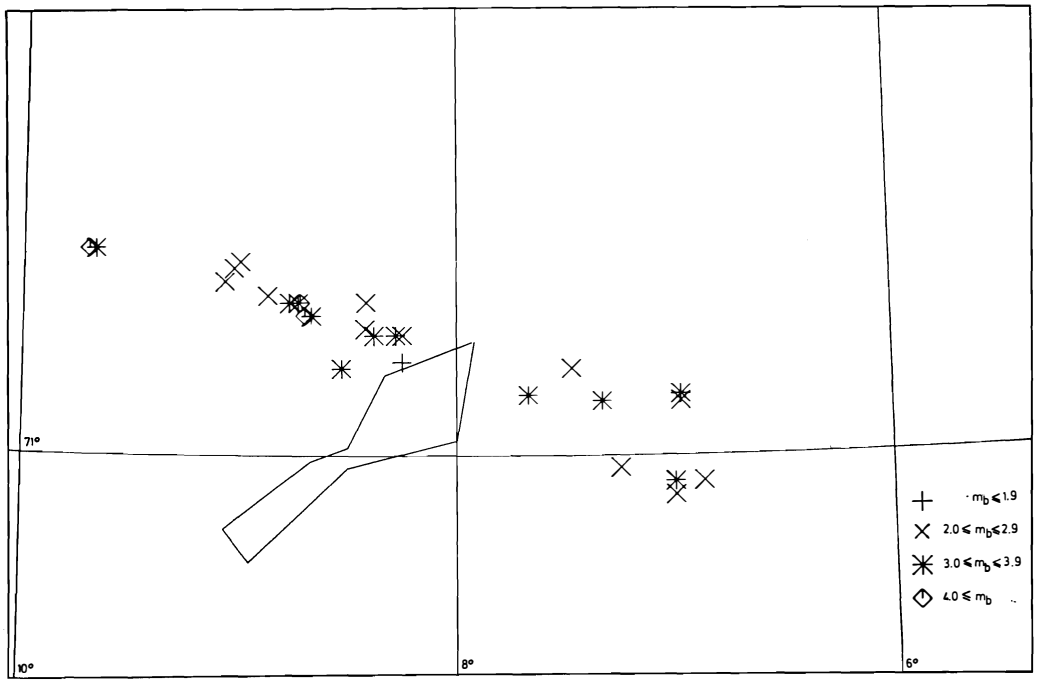

Fig. 8. *Locations of deeper local events February 1973 — December 1978, h≥18km. Depth range 18–45 km.*

(1975) has discussed the position of the central volcanoes in relation to the intersection of fracture zones and the mid-Atlantic ridges. Some of these volcanoes are located at the intersections, but the present study shows clear evidence that this is not the case for Beerenberg.

Fig. 9 shows that the teleseismic network is biased to mislocate events near Jan Mayen to the north. This blurs seismicity maps like the one in Fig. 1. The seismicity pattern in Fig. 1 along with recent bathymetric and particularly recent aeromagnetic data indicate that another minor fracture zone at about 71½°N may offset the Mohns ridge right laterally just north of the Jan Mayen fracture zone (PERRY et al. 1977). This may be the reason why the bathymetry does not give the necessary evidence to locate the Mohns ridge JMFZ intersection. The above points may also offer the explanation of the seismicity area immediately northeast of Jan Mayen which appears in the seismicity map of BUNGUM and HUSEBYE (1977).

The local seismicity pattern presented in this study rules out the possibility that Beerenberg as a central volcano can be explained by a short segment of a spreading ridge caught between en échelon segments of the JMFZ. This was one of the possibilities discussed by SYLVESTER (1975). JOHNSON and HEEZEN (1977) found that the JMFZ was a broad band of en échelon topographic escarpments and ridges. BUNGUM and HUSEBYE (1977) discussed three reliable fault plane solutions along the JMFZ. One event east of Jan Mayen had a strike-slip solution with a nodal plane parallel with the average strike of the JMFZ itself, i.e. 120°. Two events west of Jan Mayen had, however, strike directions of 100° and 104° (BUNGUM 1978). BUNGUM and HUSEBYE (1977)

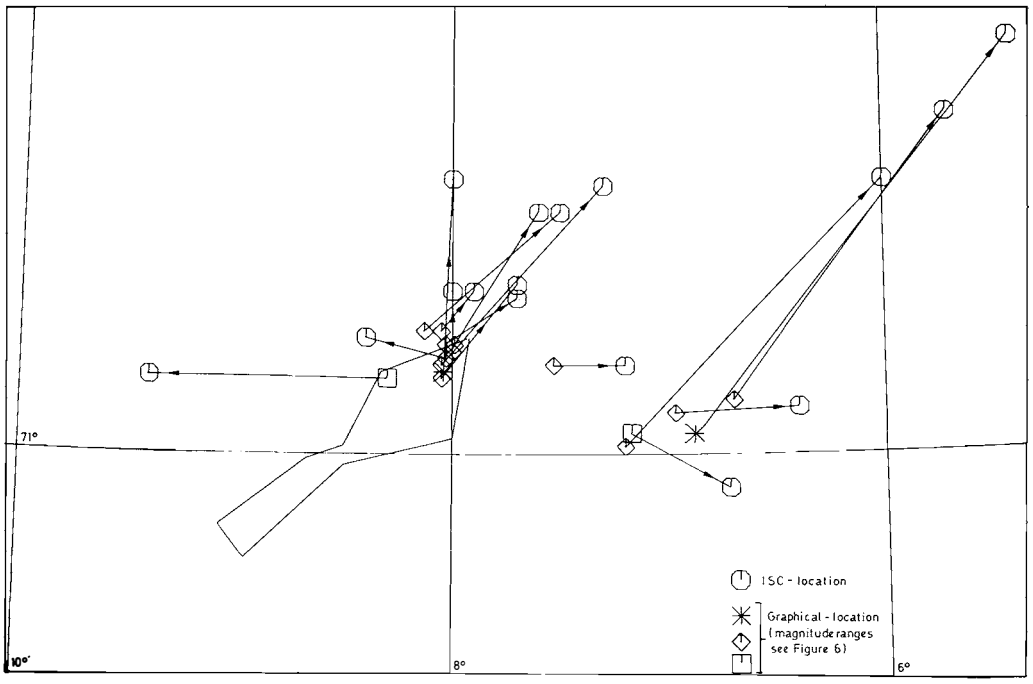

Fig. 9 *Comparison between 13 epicenters determined by the local tripartite station and by ISC.*

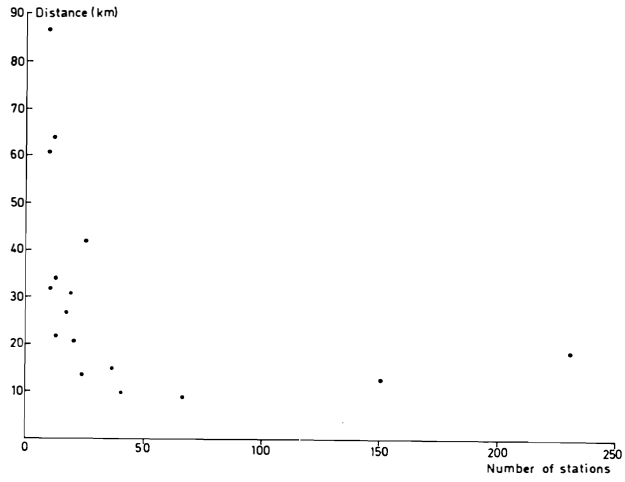

Fig. 10. *The distance between epicenters determined by the local tripartite station and by ISC versus the number of stations used by ISC.*

found these strikes to coincide with the strike of the northeasterly facing escarpment. They found support for the hypothesis that the transform portion of the JMFZ consists of en échelon faults in the above fault plane data along with their seismicity map and with a spreading model for the Norwegian Sea with poles of rotation north of the JMFZ. The present study shows that the seismic activity zone near Jan Mayen strikes at the same angle as the fracture zone without any sign of en échelon fault system. It is, however, only the eastern part of the active section of the fracture zone which is covered with the local data recorded at Jan Mayen. The latest bathymetric maps available (GRØNLIE and TALWANI 1977; PERRY et al. 1977) show a more smoothly varying escarpment than those available one decade ago (e.g. JOHNSON and HEEZEN 1967). The possibility that the JMFZ consists of a large scale system of en échelon faults still remains, but no such step has been definitely located to date.

Acknowledgements

The seismic data from the tripartite station on Jan Mayen were put to our disposal by the Norwegian Defense Communications Administration. The Norwegian Research Council for Science and Humanities has granted the salary for one of the authors (W.F.) under the project D.41.13–12: Seismic surveillance. The above mentioned support and cooperation are greatly appreciated.

References

BUNGUM, H., 1978: Reanalyzation of three focal-mechanism solutions for earthquakes from Jan Mayen, Iceland and Svalbard. *Tectonophysics* **51**: T15–T16. (Letter Section).

BUNGUM, H. and E. HUSEBY, 1977: Seismicity of the Norwegian Sea: the Jan Mayen fracture zone. *Tectonophysics* **40**: 351–360.

BÅTH, M., 1979: Teleseismic magnitude relations. *Institute Report* No. 2–79, *Seismological Institute, Uppsala.*

ELDHOLM, O. and J. THIEDE, 1980: Cenozoic continental separation between Europe and Greenland. *Palaeogeogr., Palaeoclimatol, Palaeoecol.* **30**: 243–259.

FJELDSKAAR, W. and A. SØRNES, 1978: Hyposenterbestemmelse ved hjelp av den seismiske trepunktstasjonen på Jan Mayen. *Institute Report, Seismological Observatory, Bergen.*

GRØNLIE, G. and M. TALWANI, 1977: Geophysical Atlas Norwegian-Greenland Sea. *WEMA Research Series* **4**. Lamont-Doherty Geological Observatory, New York.

JOHNSON, G. L. and B. C. HEEZEN, 1967: Morphology and evolution of the Norwegian-Greenland Sea. *Deep-Sea Research* **14**(6): 755–772.

KIJKO, A., 1978a: Short distance location program for a tripartite seismic array. *Institute Report, Seismological Observatory, Bergen.*

— 1978b: Short distance location program for a tripartite seismic array. Version II. Incomplete set of input data, determination of the depth. *Institute Report, Seismological Observatory, Bergen.*

KIJKO, A. and A. SØRNES, 1980: Locating ability of the tripartite seismic station on Jan Mayen. *Norsk Polarinstitutt Skrifter* Nr. 172: 11–20 (this volume).

MOGI, K., 1963: Some discussions on aftershocks, foreshocks and earthquake swarms — the fracture of a semi-infinite body caused by an inner stress origin and its relation to the Earthquake phenomena (third paper). *Bull. Earthq.Res.Inst.* **41**: 615–658.

NAVRESTAD, T. and A. SØRNES, 1974: The seismicity around Jan Mayen. *Norsk Polarinstitutt Årbok* 1972: 29–40.

PERRY, R. K., H. S. FLEMING, N. Z. CHERKIS, R. H. FEDEN, and J. V. MASSINGILL, 1977: Bathymetry of the Norwegian-Greenland and Western Barents Sea: *Geol. Soc. Am.* MC-210.

SØRNES, A. and T. NAVRESTAD, 1976: Seismic survey of Jan Mayen. *Norsk Polarinstitutt Årbok* 1975: 37–52.

SYLVESTER, A. G., 1975: History and surveillance of volcanic activity on Jan Mayen Island. *Bull. Volcanol.* **39**(2): 1–23.

SYKES, L. R., 1965: The seismicity of the Arctic. *Bull. Seism. Soc. Am.* **55**(2): 519–536.

Glacial erosion, sedimentation and microfauna in the inner part of Kongsfjorden, Spitsbergen

By A. Elverhøi, O. Liestøl, and J. Nagy[1]

Abstract

Kongsvegen is a subpolar, grounding glacier (area 800 km²) calving into the inner basin of Kongsfjorden. An annual sedimentation rate of 10 cm in this basin is estimated from organic varves formed due to the time-lag between organic sedimention in the spring and clastic in the summer. An annual erosion rate of c. 1 mm is calculated for Kongsvegen.

This high erosion rate is partly due to the vulnerability of the low-metamorphic sedimentary rocks to glacial comminution, producing fine-grained tills. Subglacial meltwater discharge transports substantial debris masses into the fjord.

The meltwater enters the fjord through a tunnel at sea level, flowing at >50 cm/s with 500 mg/l in suspension. The glaciomarine deposits are characterized by homogenous mud with slightly decreasing grain size seawards and scattered ice-rafted pebbles. Beneath the meltwater stream, the sediments are laminated due to variation in meltwater/sediment discharge.

During the retreat of the glacier a transgressive mud sequence is deposited, above the basal till. During glacial surges (every 50–200 years), the glaciomarine sediments are overrun and reworked.

The foraminiferal distribution in the basin in front of Kongsvegen is presented together with the sedimentological data, a combination which might be useful in the interpretation of certain Quaternary glaciomarine environments. The fauna is of arctic type but contains a few species whose main distribution is boreal. The low faunal diversity is attributed to the combined effect of high turbidity and extremely soft substrate. Presence of planktonic species is explained by influx of North Atlantic water. Postmortem destruction of agglutinated shells seems to have taken place.

The sedimentary environment in the area studied may be comparable to that during Pleistocene deglaciations in high latitude regions. Thick Quaternary sequences on Arctic shelf areas may therefore consist of originally glaciomarine deposits.

1. Introduction

1.1 The investigated area.

Around 50% of Spitsbergen is covered by ice, and Kongsfjorden is located in the strongly glaciated northwestern part of the island (Fig. 1). The mouth of Kongsfjorden has no sill so the main (outer) fjord basin communicates with the North Atlantic through Kongsfjordrenna, a depression which crosses the continental shelf and terminates on the slope.

[1] Institutt for geologi, Universitetet i Oslo, Blindem, Oslo 3.

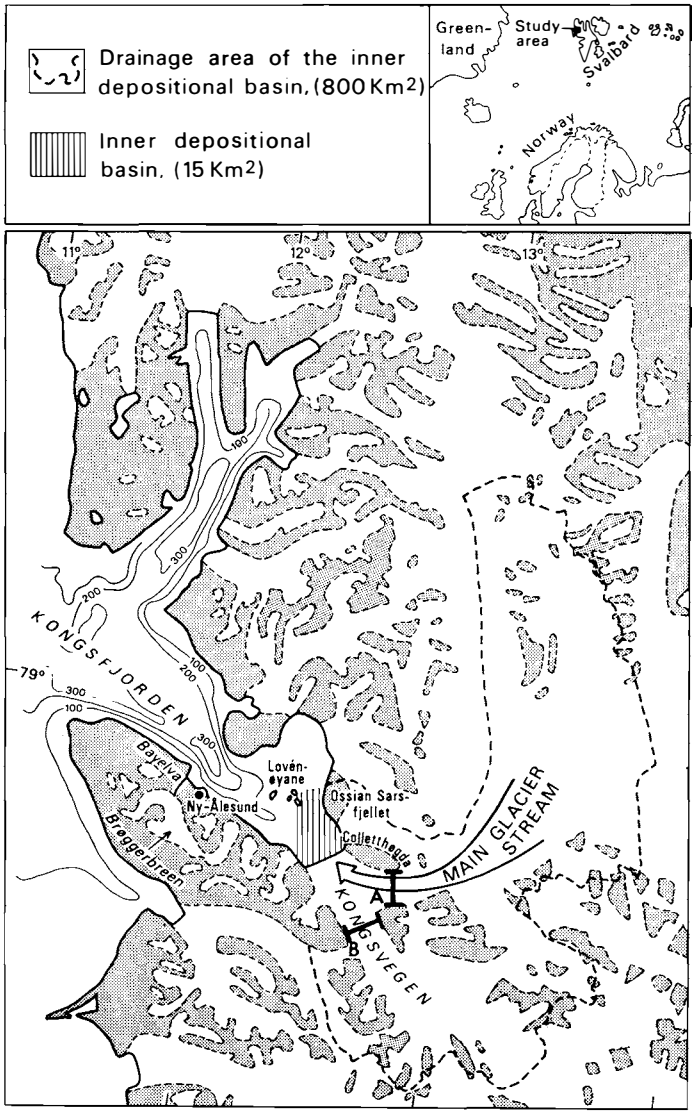

Fig. 1. *Map of Kongsfjorden with surrounding areas. Study area shaded. Note location of Brøggerbreen with Bayelva. White areas on land are ice covered. Section A and B refer to the investigated profiles during the German (DDR) Expedition in 1964–65.*

The present study is concentrated in the inner part of Kongsfjorden, which is separated from the main basin by a sill formed by Lovénøyane and the shallow ridge extending north and south of these islands. The sill lies at depths less than 50 m while the basin on the inside has a maximum depth of 94 m. The southern and eastern coasts of the inner basin are mainly formed by the fronts of Kongsvegen and Kronebreen. The main glacier stream flows from Holtedahlsfonna just south of Colletthøgda (Fig. 1).

1.2. Purpose of the study.

Large parts of the marine Quaternary sequence both on land and shelf areas around the North Atlantic are considered to have been deposited under the direct influence of ice sheets or glaciers. Sedimentological parameters and foraminiferal faunas are often used for interpreting these glaciomarine deposits both with regard to palaeoclimate and more local environmental conditions. One important purpose of the present study is thus to present sedimentological and faunal data in close combination, to enable such Quaternary environments to be interpreted in more detail.

For some years glaciohydrological investigations have been carried out by Norsk Polarinstitutt in Bayelva on the southern side of Kongsfjorden (Fig. 1). This small river system drains Brøggerbreen, a minor glacier below pressure melting point, which terminates on land. Preliminary calculations based on sediment load measurements in Bayelva indicate 1 mm annual erosion (Repp 1979). As the main part of the Kongsfjorden area is drained by larger and much more active glaciers, this runoff is probably not representative for the region. For a more comprehensive picture, measurements from these larger glaciers are also needed.

In the major glaciers calving into the fjords, meltwater rivers are not accessible for direct sampling. In this case an estimate of the sedimentation rate in the fjord, and the sediment transport through the fjord can be made. These data enable the probable amount of glacial erosion to be calculated, which is the second main scope of the study.

2. Glaciological and geological background

2.1. Glacier movement.

At present the fronts of most Spitsbergen glaciers are generally retreating (Liestøl 1975). However, part of this retreat is counterbalanced by periodical (40–200 years) surging episodes. During surges the ice fronts advance from between a few hundred metres and more than 10 kilometres within a few months or years. Previous mapping and observation show that Kongsvegen advanced 2 km between 1936 and 1948, and the front lay a further 2 km out during its most extensive surge in 1869 (Fig. 2). In contrast to some of the minor glaciers, which are cold based, the sole of Kongsvegen is at pressure melting point over large areas. The glacier tongue of Kongsvegen has a very high velocity, much faster than most other Svalbard glaciers. In the summer, its maximum measured speed exceeds 4 m/day (Voigt 1967). However, due to intensive calving, the front retreats 50–100 m during the summer. During the winter with no calving, the velocity drops to below 1 m/day, while the front progresses 30–100 m.

2.2 Erosion

Kongsvegen and its minor branches are underlain by lithified but unmetamorphic shales, siltstones, and fine-grained sandstones of mostly reddish colour (Orvin 1940). Glacial comminution of such fine-grained sediments produces a

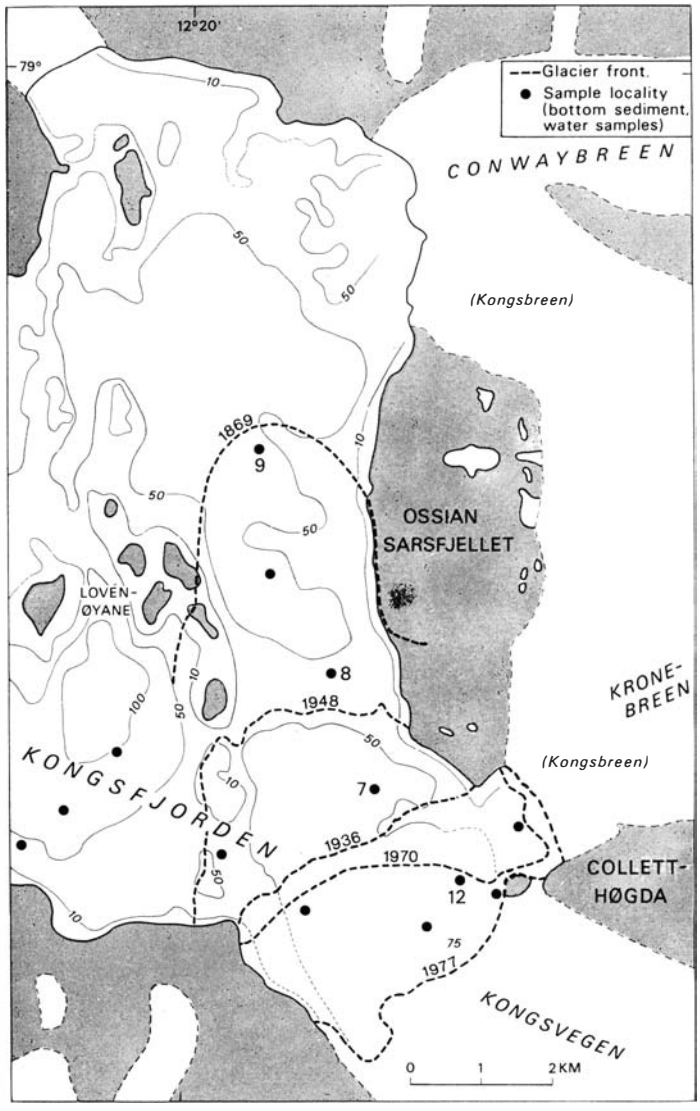

Fig. 2. *Bathymetric map of inner part of Kongsfjorden showing position of the front of Kongsvegen during the last hundred years. Sediment cores from numbered stations were studied in detail, while material from unnumbered stations served as a control.*

fine-grained till (Jørgensen 1977). Around 50 % clay and silt is common in basal tills from Kongsvegen and Brøggerbreen.

During the summer, even in the cold minor glaciers, meltwater rivers are observed running subglacially. Sand and gravel are transported as bed load while the finer material is carried in suspension. Part of the latter is transported through the fjords onto the shelf (Fig. 3).

In the first part of September, mean air temperature generally falls below 0° C, and glacial runoff drops to almost nil. An exception is Kongsvegen, where meltwater is produced all year round. Normally, the inner part of Kongsfjorden is ice covered from November/December to the middle of June.

3. Material and methods

3.1. Field work.

In the middle of May 1978 and 1979, bottom samples were recovered from the inner part of the fjord using a 45 mm gravity corer and a box corer (Fig. 2). The lengths of the cores were up to 1 m. Both in May and July 1979 water samples were taken by Nansen bottle and Tabb bottle. At the same time currents were measured at selected stations by an instrument made by A/S SENSORDATA.

3.2. Laboratory treatment.

After being radio-photographed, the cores were split with an osmotic knife. The grain size analyses were made by dividing the samples at 63 μm. The coarser fractions, sand (0.063–2 mm) and gravel (0.2–1.6 cm), were separated by wet sieving. Grades finer than 63 μm were measured by pipette analyses. Calculation of suspended matter concentration in water samples was based on weighing the filtrates on Nuclepore filters. Grain size and composition of the suspended matter samples were estimated from binocular and scanning electron microscope analyses of the filtrates.

For the foraminiferal analyses the >63 μm fraction have been used. The foraminifera were concentrated by means of carbon tetrachloride (CCl_4). The number of foraminiferal species is given per 1 cm³ wet sediment, having a dry weight of about 0.8 g.

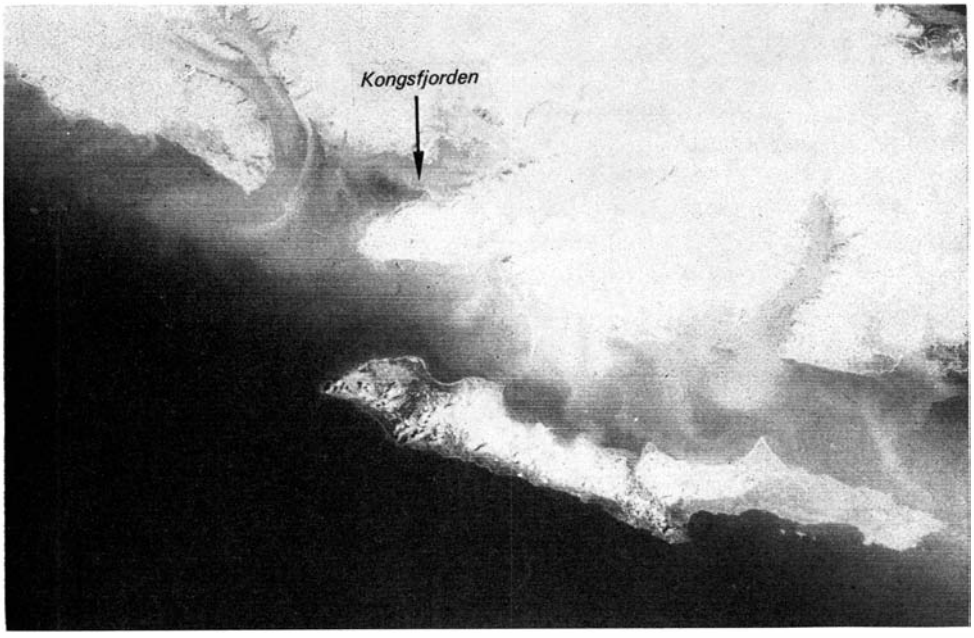

Fig. 3. *Satellite photo showing sediment transport from Kongsfjorden onto the shelf.* (LANDSAT, *9th July 1976.*)

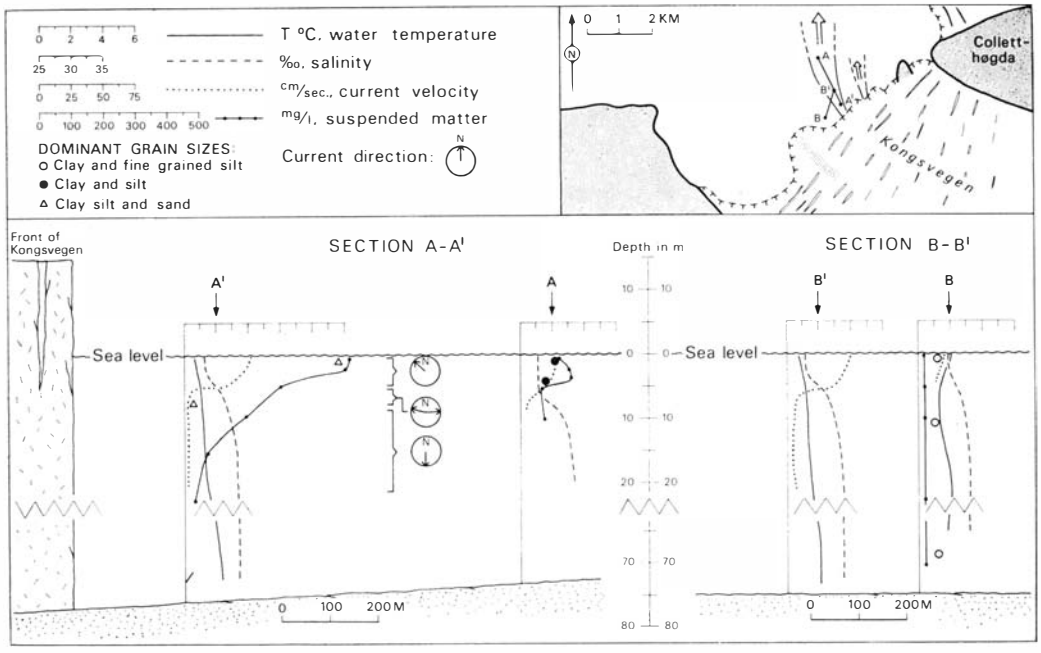

Fig. 4. *Inset map showing meltwater streams marked by arrows flowing out of Kongsvegen. The sections show the distribution of different hydrographical parameters, suspended matter and dominant grain sizes (for location see inset map). Dominant grain sizes are estimated from scanning electron microscopy.*

4. Depositional environment

4.1. Meltwater discharge.

At the front of Kongsvegen meltwater of brackish composition emerges from the ice at two restricted localities at the sea level (Fig. 4). It is assumed that the meltwater flows out of a tunnel into which sea water seems to penetrate far up, to be gradually mixed with the sediment-laden fresh water (Fig. 5).

Sedimentation of the coarser material therefore starts far into the tunnel itself where the meltwater current velocity decreases on meeting the fjord water. After reaching the glacier front the meltwater flows seawards as a fan-like stream on top of the salt water (Figs. 4 and 5). Its thickness and salinity increase slightly seawards as additional sea water is mixed with it. Current velocity as well as suspended matter concentration and maximum grain size diminish and c. 2 km away from the front mostly clay and silt are left in suspension.

Aside from the meltwater stream, brackish surface water with considerably lower concentrations of suspended matter was found. In this upper layer the flow direction was observed to be rather irregular and the current velocity low (<10 cm/s).

Below the brackish surface layer (including the stream), oceanic water flows into the fjord at a velocity of 5–10 cm/s. [The water exchange processes in the fjord are under investigation and will be published later by B. Wiseman.]

The amount and flow pattern of the outflowing meltwater are variable. During a cold period, with air temperatures close to 0° C, the meltwater dis-

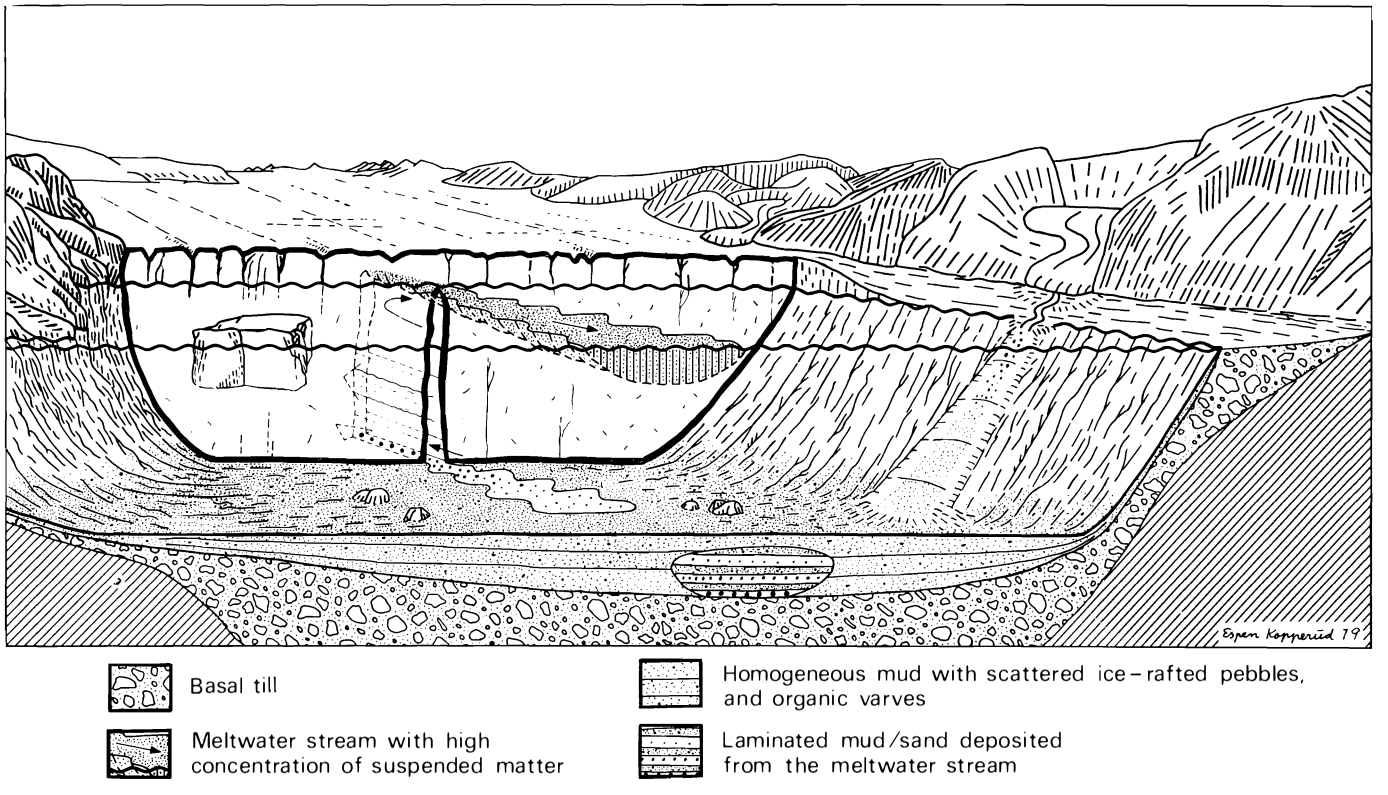

Fig. 5. *Diagrammatic section of the inner part of Kongsfjorden showing the front of Kongsvegen in the background. Meltwater is transported through the tunnel and deposits coarser grained, laminated sediment near the glacier front. Sea water flows into the glacier through the lower part of the tunnel and is gradually mixed with the outflowing meltwater.*

charge decreased. At that time a NW wind was blowing into the fjord, forcing the meltwater into a 10 m broad stream along the ice front. Calved ice was also pushed up to the front, hampering the surface meltwater stream. The data presented here are from a rather warm period with a katabatic wind blowing seawards, and are perhaps not fully representative for average conditions.

4.2. Sediment supply from Kongsvegen.

Salinity, together with sediment load, was measured in a vertical profile just outside the tunnel. As we know the salinity of the oceanic water (S_o) entering the tunnel, the salinity of the brackish water (S_b) flowing from the tunnel, and the sediment load of the same brackish water (P_b), the original meltwater sediment load (P_m) can be calculated by means of the formula:

$$P_m = \frac{P_b \cdot S_o}{S_o - S_b}$$

The sediment load of the ocean water and the salinity of the meltwater are extremely small in relation to the other figures and are therefore ignored in this estimate.

The sediment load in the subglacial river before mixing with sea water was thus calculated to be c. 2500 mg/l, which is about twice the amount found in Bayelva at the same time.

Owing to the sampling difficulty near the front of Kongsvegen, measurements were carried out only once. Calculation of total sediment discharge in a meltwater stream has to be based on a long observation period with frequent sampling because runoff and sediment load exhibit dramatic changes both diurnally and seasonally. However, as the concentration values calculated for the "fresh" subglacial river of Kongsvegen are of the same order of magnitude as measured in Bayelva, the values observed at the glacier front (Fig. 4) may be applied to estimate the sediment supply.

Assuming a 100 m broad and 4 m deep stream flowing for 24 hours with a velocity of 50 cm/s, and loaded with 500 mg/l sediment, $1 \cdot 10^4$ ton or approximately $0.4 \cdot 10^4$ m^3 material is carried to the fjord. Even hypothetically, application of this estimated value to a 60-day ablation season results in $2.6 \cdot 10^5$ m^3 sediment carried out, an amount which corresponds to 0.3 mm erosion on the 800 km^2 large drainage area of Kongsvegen and surrounding areas (Fig. 1). Additional sediments are brought out from the minor outlet (Fig. 4). However, no measurements were undertaken at this site.

4.3. Sediment flux.

A quantitative estimate of the sediment transport through the inner basin of Kongsfjorden was attempted, but due to the observed variability in flow pattern and problems with the ice, the calculation was not successful.

The brackish surface layer was usually flowing out of the inner basin through the northern outlet between Lovénøyane and Ossian Sarsfjellet (Fig. 1). However, in periods with NW blowing winds, the surface water was inhibited to

flow seawards, and the brackish water masses were confined to the inner basin. Sometimes the meltwater also was observed to flow seawards through the southern outlet (Fig. 2). As an average for the melt season (60 days), the meltwater may flow through the northern outlet two-thirds of the period.

Water sampling in the summer of 1978 during a period with outflowing water showed 20–30 mg/l sediment in the brackish surface layer (Repp 1978). Application of 20 mg/l and 10 cm/s for the outflowing water of 6 m depth in the 2 km broad cross section between Ossian Sars and Lovénøyane (Fig. 2) during a 40 day season, shows a sediment flux of 10^5 ton or 0.5 10^5 m^3. The listed values are based on field reports of Repp (1978) and Wiseman (1979) in addition to own observations. The obtained value must be treated as approximate.

Density stratification has been observed in Kongsfjorden (B. Wiseman pers. comm.) and sediment transport of flocculated particles may take part along different strata (Relling & Nordseth 1979). However, compared to the mass transport in the surface layer, this transport must be of minor importance.

Even though the amount of sediment flux is unknown, field observations and satellite photographs show extensive mass transport out of the fjord (Fig. 3). This is in contrast to a typical Norwegian fjord where sediments (including material from glaciers, e.g. Hardangerjøkulen) are effectively trapped within the fjord itself (Holtedahl 1975). The situation at Kongsfjorden may partly be caused by the high input of fine-grained sediments easily carried in suspen-

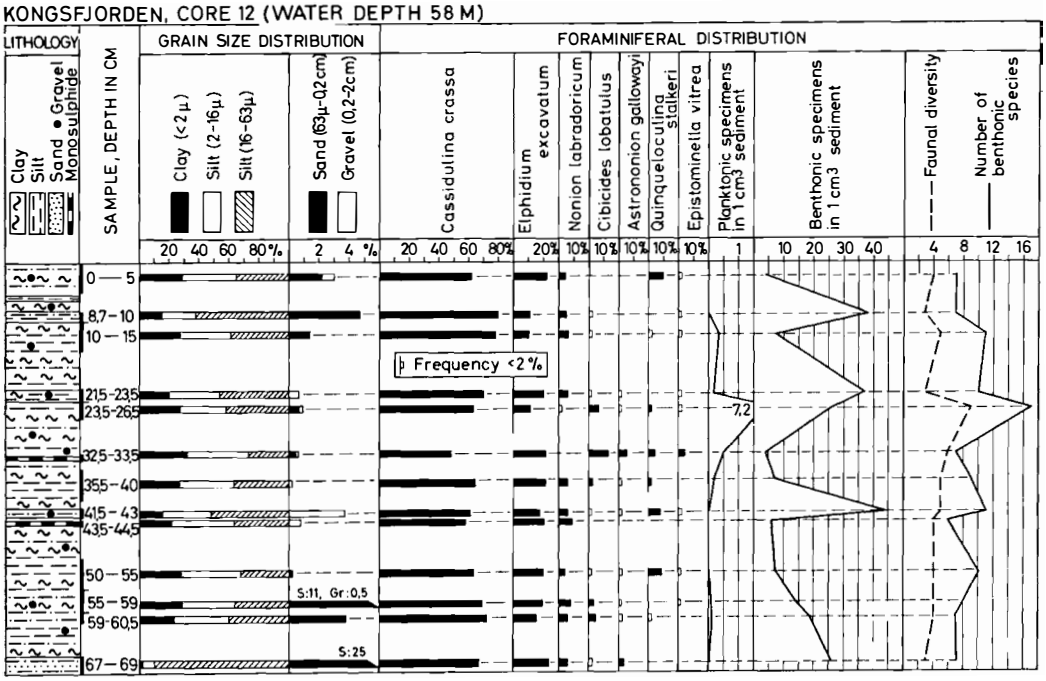

Fig. 6. *Stratigraphy of core 12 including lithology, grain size distribution, percentage frequency of selected foraminiferal species, and main faunal parameters.*

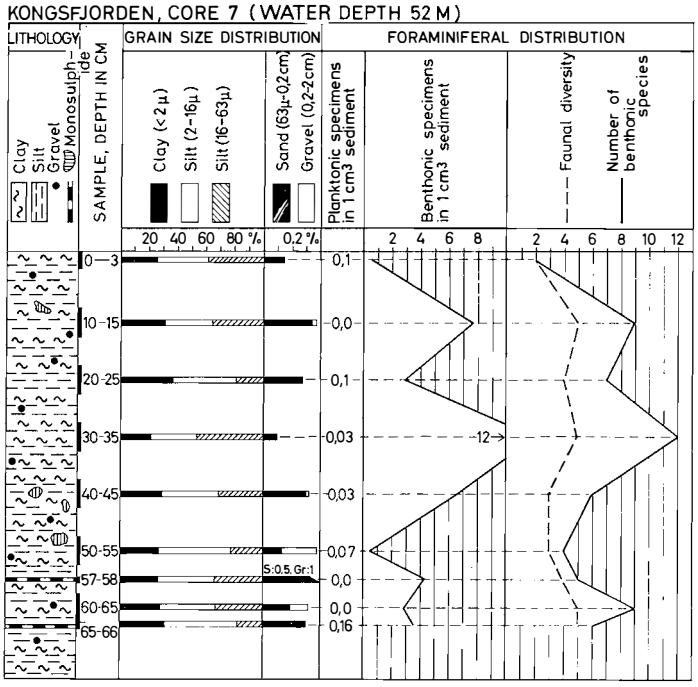

Fig. 7. *Stratigraphy of core 7 including lithology, grain size distribution and main faunal parameters.*

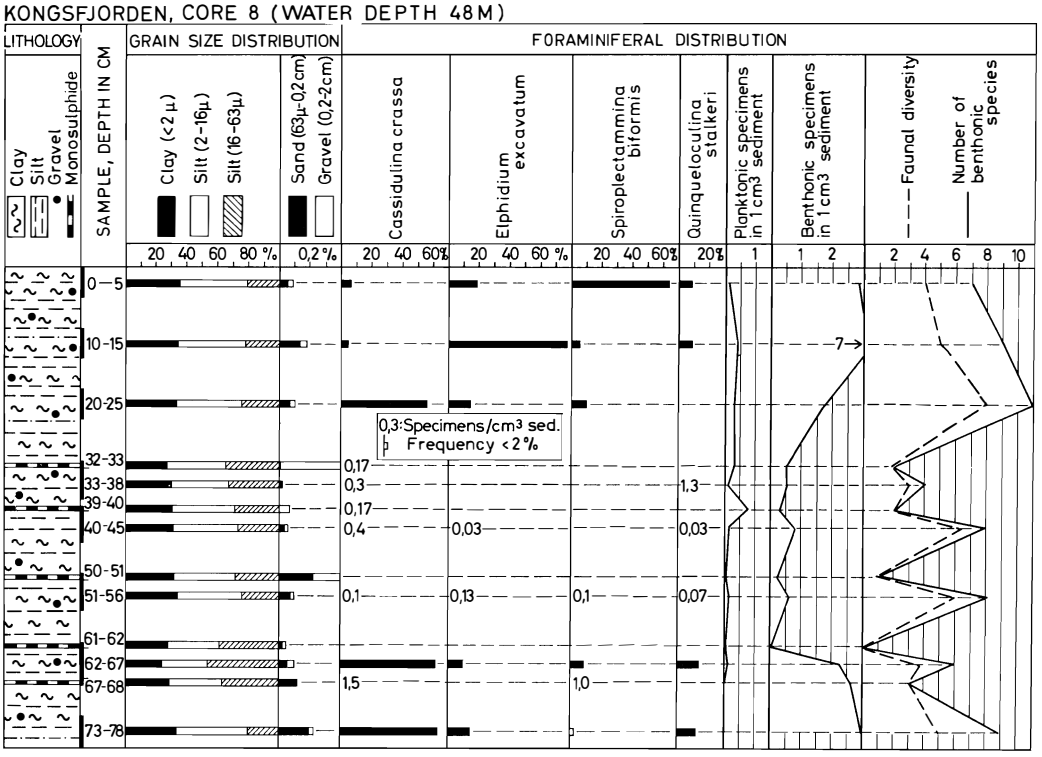

Fig. 8. *Stratigraphy of Core 8 including lithology, grain size distribution, percentage frequency of selected foraminiferal species, and main faunal parameters.*

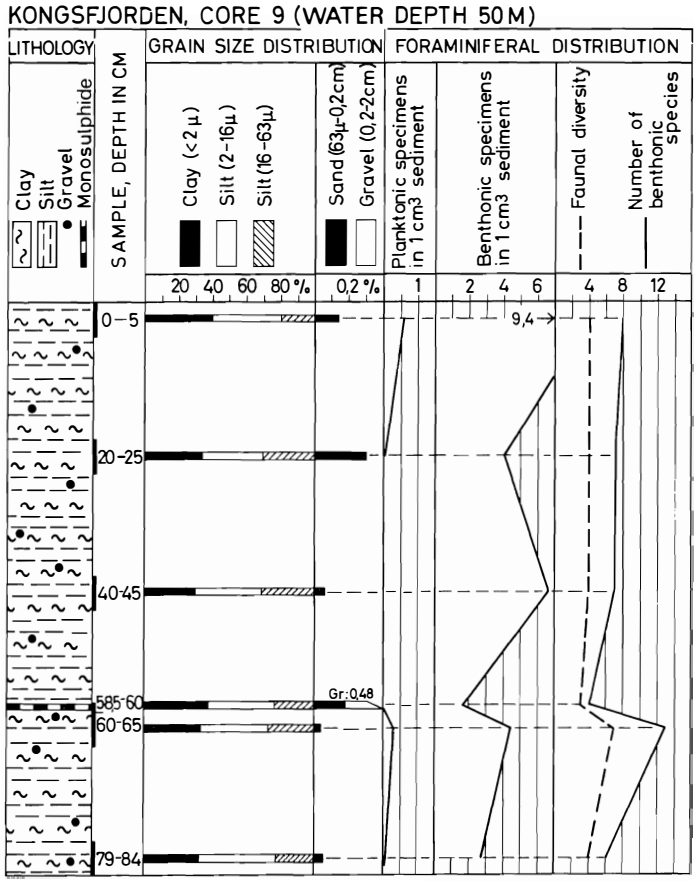

Fig. 9. *Stratigraphy of core 9 including lithology, grain size distribution, and main faunal parameters.*

sion by the outflowing surface water. Additionally, Kongsfjorden is much shorter than a typical Norwegian fjord, impelling the surface water seawards.

Due to the high sediment transport out of the fjord, the NW Spitsbergen shelf differs from the Norwegian, and also from many other present shelves (except near deltas) which are characterized by low clastic supply (Swift et al. 1971; Elverhøi 1979).

4.4 Bottom sediments.

Sandy sediments are confined to the glacier front near the meltwater outflow where muddy and sandy layers alternate (Fig. 6). Current velocities observed in the meltwater stream indicate that sand-sized particles can be transported to at least 200–300 m in front of the glacier. However, the current velocities decrease downwards and outwards in the stream (Fig. 4), causing settling of sandy sediments through the underlying slowly moving oceanic water. The observed variability in flow direction and sediment supply further explains the alternation of sandy and muddy layers.

The position of the outflow is probably not fixed over a longer period of time,

and therefore an alternating sand-mud sequence may be deposited also at other places near the ice front as the position of the meltwater tunnel shifts laterally, and as the front retreats.

500–600 m ahead of the front, soft, red-coloured, muddy sediment (with 95% <32 μm) floors the fjord bottom (Figs. 7, 8, 9, 10). The red colour of this sediment originates from the reddish Devonian deposits underlying the glacier. The bottom sediments show no sign of stratification other than the monosulphidic layers which occur rhythmically (Fig. 11). The distance between these black layers is 12–15 cm near the front, decreasing to 6–8 cm further out (Figs. 6, 7, 8, 9). The lack of clastic lamination is attributed to the fact that clays flocculate in marine water, forming particles behaving hydrodynamically like silt (SAURAMO 1923). Thus, only "silt-sized" particles are settling, without any mechanical separation, and form a homogenous mud.

In the bottom sediments a reducing environment seems to exist below 15–20 cm as monosulphidic layers are observed only below this level (Fig. 11). Bioturbation was seen in some cores, in which cases the monosulphidic layer was not so well developed.

Coarser grains and pebbles, interpreted as ice-rafted material, were observed in the majority of the cores, but this ice-dropped material constitutes only a small part of the total sediment input, in spite of frequent calving. Coarse-grained sediments are generally confined to near-shore regions, particularly to delta-like areas at the outlets of rivers draining minor glaciers which terminate on land.

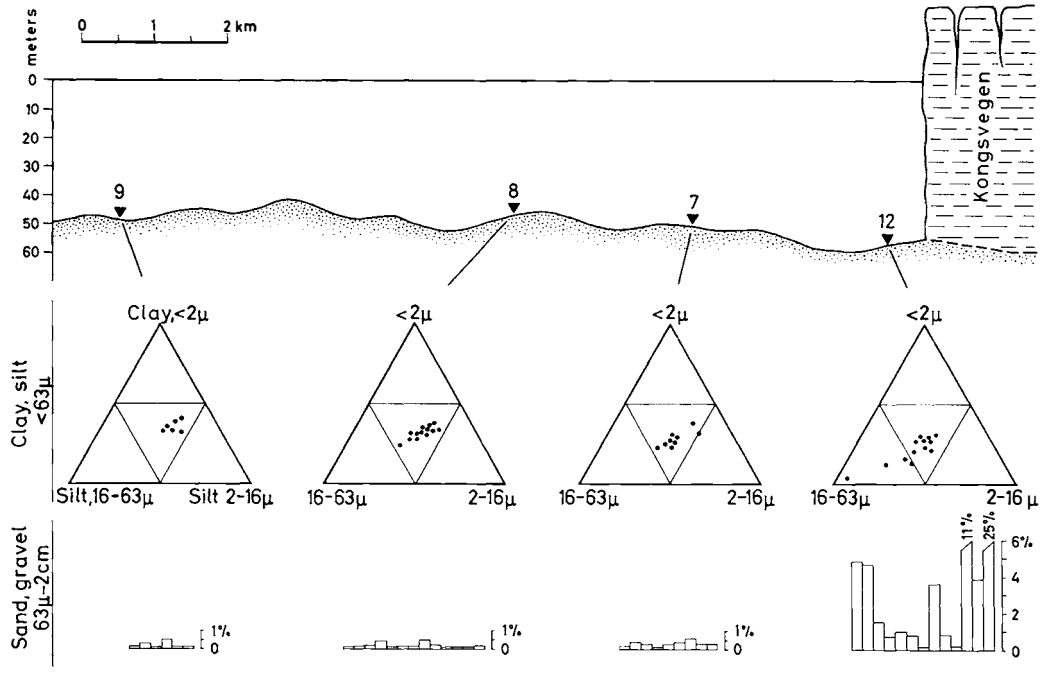

Fig. 10. *Section of the inner basin of Kongsfjorden summarizing the grain size distribution of the cores.*

4.5. Typical depositional features.

In a model for wet-based tidewater glaciers – such as Kongsvegen – presented by EDWARDS (1978), the meltwater runs subglacially. This is not the case in Kongsvegen where the meltwater flows out through a tunnel at the sea surface, a situation which have commonly been found (field observations and aerial photographs) for the Spitsbergen glaciers. We thus suggest that the model presented in Figs. 4 and 5 is more valid for a wet-based glacier grounding into the sea. EDWARDS (1978) further proposed randomly laminated mud with dropstones as diagnostic for a glaciomarine environment. Locally, beneath the meltwater stream, such sediments are found in Kongsfjorden, while for the fjord as a whole, homogenous mud with organic varves and subordinate amounts of coarser clasts are characteristic. In less active glaciers than Kongsvegen, sandy sediments may be deposited subglacially (Fig. 5) with only clay- and silt-sized particles reaching the front.

We therefore conclude that this kind of Arctic glaciomarine environment is best characterized by homogenous mud with scattered pebbles, deposited from suspension and from icebergs, respectively. Coarse-grained laminae indicate a position close to the meltwater outflow near the glacier front.

If the glacier is retreating, the homogenous mud progrades up the fjord above the frontal sediment with its sandy laminae. In this manner a transgressive sequence is deposited above the basal till.

4.6. Organic varve formation.

During the spring, but while the fjord is still covered by ice (c. ½ m thick), organic matter is produced in abundance in the water masses (Fig. 12a). The filtrates from this period contained diatoms, larval shells of bivalves and gastropods, copepods, and considerable amounts of amorphous organic matter which probably represent algal tissue. At 1 m water depth a suspended matter concentration of 10–15 mg/l was obtained (REPP 1978) and microscope analyses (binocular and scanning) show very low content of clastics (Fig. 12a). Water samples from greater depths showed decreasing concentrations, but still a relatively great abundance of organic matter. The samples obtained during the

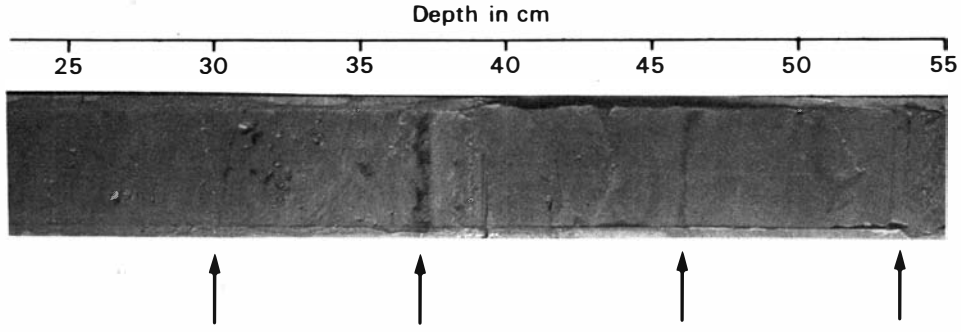

Fig. 11. *Photo of Core 8 showing four monosulphidic layers (marked by arrows). Patches of monosulphide due to bioturbation.*

summer (Fig. 4) were also studied by microscope, but biogenic matter was less often found (Fig. 12b). As shown earlier monosulphide layers occur rhythmically in the bottom sediment (Fig. 11).

Iron sulphides in the sediments are generally believed to form by reaction of H_2S and Fe^{2+} in solution.

H_2S forms during the decay of organic matter by bacterial reduction of SO^{2-}, while Fe^{2+} is produced by reduction of Fe^{3+} in clastic minerals (BERNER 1971). Data presented by BERNER also show that the iron sulphide content is positively correlated with the content of organic matter in a sediment.

The black colour of the monosulphide layers indicates a primary high organic content at those horizons compared to the surrounding sediment. The spring and early summer, with high organic production and low clastic content in the water masses, may be the most favourable time for accumulation of these organic-rich layers.

Normally iron monosulphide converts to pyrite by reaction with S^0 (BERNER 1971). However, FeS_2 was not observed in the black layers. Black-coloured sediments without pyrite are reported from other regions, i.e. the Black Sea, where the lack of pyrite formation is explained by the paucity of H_2S and elemental sulphur (VOLKOV 1961).

Organic varves have previously been described by FLINT (1971) who has related their origin to the cyclicity of organic production. The observations from Kongsfjorden indicate that organic varve formation in this area is strongly influenced by the time-lag between the blooming period of plankton (May–June) and the ablation season (July–August). If these seasons had coincided, the concentration of organics to certain horizons would probably have been too low for formation of visible monosulphide layers.

4.7. Sedimentation rate.

In core 7, 8, 9 and 12 (Fig. 2), 100% water content was measured below a depth of 20 cm. By application of 10 cm as an average for the annual sedimentation in the inner basin with an area of 15 km², and reduction for the

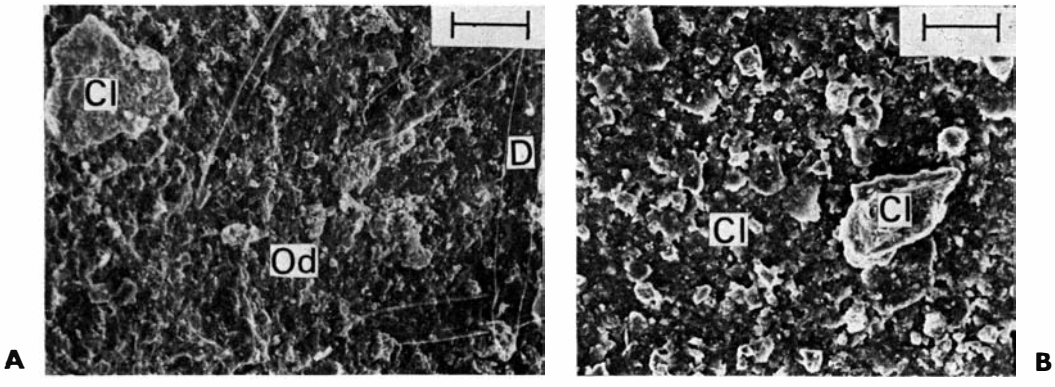

Fig. 12. *SEM photos of suspended matter on Millipore filters from water samples taken in the inner basin of Kongsfjorden. A: Sample from May. B: Sample from the middle of June. Cl: Clastic grains. D: Diatoms. Od: Organic debris. Scale bar = 20 μm.*

water content, $5 \cdot 10^5$ m^3 or 10^6 tons annual deposition is calculated. It corresponds to 0.6 mm erosion in the drainage area of Kongsvegen (see also section 4.2.).

This value is of the same order of magnitude as that obtained from the meltwater stream. In addition, however, the minor meltwater outlets of Kongsvegen and Kronebreen (Figs. 2 and 4) also contribute to the sediment input in the inner basin of Kongsfjorden. These glaciers cover only a minor part of the total drainage area, but as they are less active than Kongsvegen, they also produce less sediment (see section 6). Kongsvegen is thus proposed as the main sediment contributor, an idea supported by the correspondence in annual deposition calculated from sedimentation and from runoff. With this sedimentation rate, it will take about 500 years for the inner basin of Kongsfjorden (average water depth 50 m) to be filled up. It seems probable, however, that the present degree of ice coverage has existed only since the 18th century (the little ice age). During most of the Holocene period the ice cover of the area was of considerably smaller extent.

4.8. Glaciomarine sedimentation, surging and pseudo-till formation.

As stated earlier, Kongsvegen is now retreating, but periodically advances rapidly during a surge. Similar conditions are well known from nearly all Spitsbergen glaciers, and may also have been common during the Quaternary in the Arctic and other glaciated regions. This pattern of glacier movement, with the corresponding sedimentation, leads to some general remarks on glacial deposition.

At Kongsvegen during an intersurge period (50–200 years) 5–20 m of sediment would be deposited in the inner basin. During a surging episode these glaciomarine sediments would be reworked, resulting in a till or pseudo-till with a composition approaching that of a true basal till. Solely from textural observation, the glaciomarine phase of the sediment cycle may not be recognized, leading to the false conclusion that the sediments had been deposited directly from the glacier. However, the microfauna in the glaciomarine sediments (discussed in next chapter) may be expected to be preserved also in the reworked deposits, thereby enabling a recognition of the original environment.

At present most Spitsbergen glaciers terminate in the inner part of the fjords, but with a climatically induced regional advance, thick "till" deposits may be formed farther out in the fjords or on the shelf during a relatively short period.

Based on seismic data thick (>600 m) Quaternary sediments are found on the shelf and shelf edge west of Spitsbergen and in the Barents Sea (Kristoffersen & Elverhøi in prep.). The fact that rather thick glaciomarine deposits may form rapidly proximally to a partly ice covered area, lead to the view that thick Quaternary shelf sequences may contain considerable amounts of originally glaciomarine sediments. Quaternary glaciomarine sediments laid down during periods with reduced ice cover, may have been reworked to form pseudo-till during periods with increased ice cover.

Thus, if the high sedimentation rate observed in Kongsfjorden is typical of

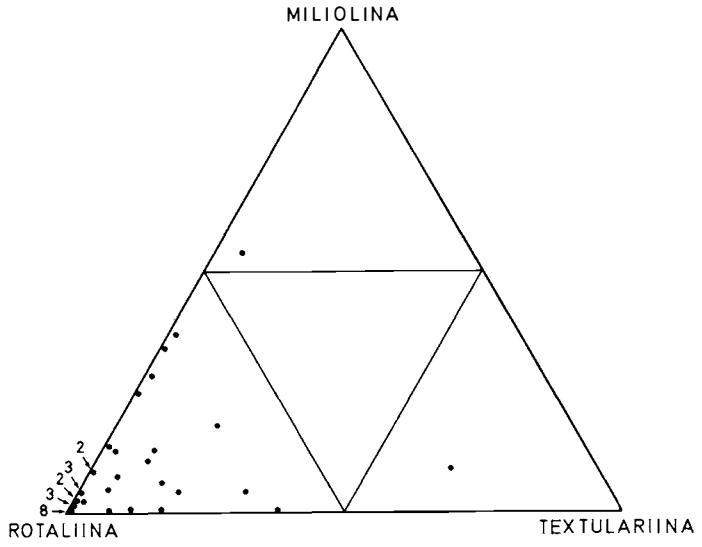

Fig. 13. *Triangular plot of the samples from inner basin of Kongsfjorden showing ratio of three foraminiferal suborders.*

such environments, glaciomarine sedimentation must play a more important role in the sedimentary cycle than generally assumed. Reworking of glaciomarine sediments is also reported from the North Sea Quaternary sequence (LØKEN 1976; JANSEN 1976), where the depositional history is difficult to interpret, particularly because of this reworking. For a better understanding of the build-up of glacial shelf deposits, more data on the subjects of glaciomarine sedimentation, glacial onset, and reworking are obviously needed.

5. Foraminifera

5.1. Main features of benthonic assemblages.

The faunal diversities given in this paper are calculated in accordance with WALTON's (1964) definition. The Fisher α-indices were obtained by the graphic method described by MURRAY (1973).

The triangular plot (Fig. 13) shows that the assemblages are dominated by the suborder Rotaliina in nearly all samples. Textulariina and Miliolina are common in a large number of samples, but are dominant only in two. It must be noted, however, that the distribution of Textulariina seems to be increasingly affected downwards in the cores by diagenetic solution of the wall cement of *Spiroplectammina biformis*. Corroded calcareous shells are also found. Average faunal diversity has been calculated individually for each core. The values vary from 4.3 to 4.9 and are shown graphically in Fig. 15. Fisher α-indices plotted on Fig. 14 are lower than 5, and mostly between 1 and 3. The number of specimens per cubic centimetre is strongly variable; average values calculated for the cores vary from 1.7 to 18.

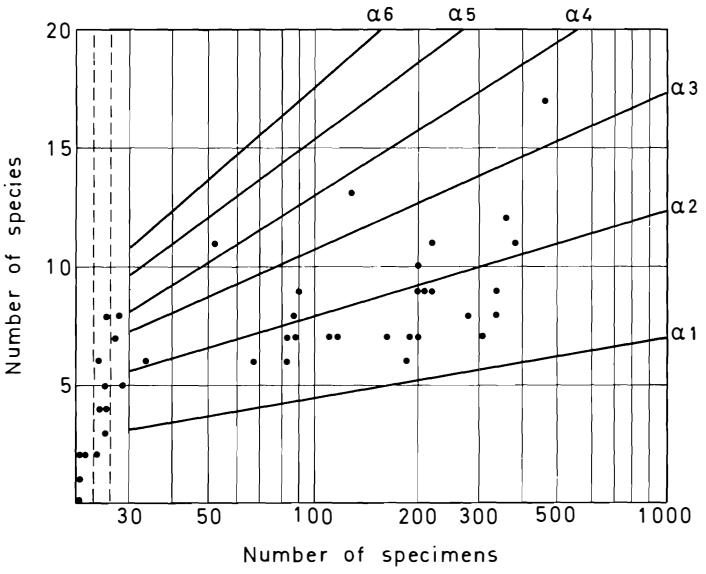

Fig. 14. *Plot of the α-diversity values for samples from the inner basin of Kongsfjorden.*

5.2. Distribution of benthonic species.

In the examined cores a total of 38 benthonic species have been observed and their distribution is shown in detail in Fig. 16. The samples are, with a few exceptions, dominated by *Cassidulina crassa* which accounts for up to 84% of the assemblages. The average frequency of this species ranges from 38 to 66%. (Averages are calculated for the individual cores.) Abundant species are *Elphidium excavatum* (average 8–27%), *Quinqueloculina stalkeri* (average 2.7–20%), and *Spiroplectammina biformis* (average up to 18%). Common species are *Nonion labradoricum* (average 0.7–4.9%) and *Cibicides lobatulus* (average 0.5–2.8%). The six species mentioned above represent in average 94–96.5% of the assemblages, consequently the remaining 32 species occur very sporadically. The specimens of *Elphidium excavatum* belong to the arctic forma *clavata*.

Cassidulina laevigata and *Trifarina angulosa* are represented by a few specimens in nine and five samples, respectively. The distribution of both species is regarded generally as boreal with well known occurrences in the North Sea area (Höglund 1947; Risdal 1964; Nagy & Ofstad 1980). Both species have been found recently in Storfjordrenna (western Barents Sea) where *Cassidulina laevigata* occurs with frequencies of up to 36% (Østby & Nagy in prep.). It seems probable that the occurrences in Kongsfjorden are near the northern limit of the distribution of this species.

Nonion labradoricum and *Cibicides lobatulus* occur in 26 and 21 samples, respectively. In the majority of these samples both species are markedly smaller than the sizes found in the Barents Sea.

5.3. Planktonic species.

Planktonic foraminifera occur in small quantities in a total of 25 samples distributed in the four cores. The number of specimens per cubic centimetre

sediment is 0.6 or less except for two samples which have 0.83 and 7.2, respectively.

The planktonic/benthonic ratio is less than 0.1 excepting seven samples where the values vary from 0.1 to 0.6. The richest planktonic assemblage is found in core No. 12 at a depth of 23.5–26.5 cm.

The planktonic assemblages found in Kongsfjorden are composed of arctic and subarctic elements if compared with the main distribution pattern compiled by Bé (1977). The dominant species in Kongsfjorden is *Globoquadrina pachyderma* which is mainly confined to arctic (and antarctic) regions but is common also in subpolar areas. *Globigerinita bradyi* and *Globigerina quinqueloba* are less frequent in Kongsfjorden. Both species occur mainly in subarctic (and subantarctic) waters, but are present in reduced amounts also in polar areas.

5.4. Environmental interpretation.

The occurrence of planktonic species, although in minor quantities, indicates a direct influence of North Atlantic waters in the inner basin of Kongsfjorden. It is in agreement with the measured current direction in the lower water masses, and with the salinities which reached 33‰ below a depth of c.10 m (Fig. 4). The open nature of the fjord and its short length are important in this connection. The benthonic assemblages are characterized by low diversities, indicating unfavourable or changing ecological conditions. This is illustrated in Fig. 15 where it appears that the average number of species in the cores varies between 7.7 and 8.5. These low values are probably only to a minor

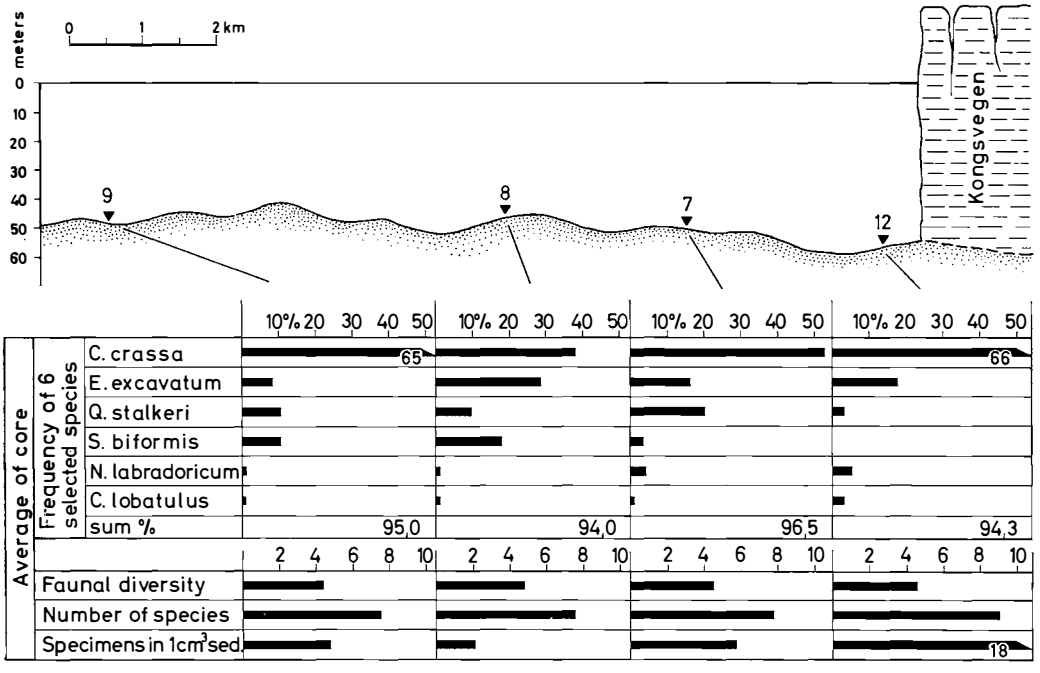

Fig. 15. *Section of inner basin of Kongsfjorden to show frequency of selected foraminiferal species and main faunal parameters calculated as averages for the cores.*

degree caused by the salinity which is not particularly low in the bottom waters. A more important limiting factor seems to be high turbidity during the summer, resulting in a very soft substrate. In this connection it must be mentioned that turbidities of 20 and 15 mg/l are measured in the bottom waters.

Among the cores, No. 12 is located closest to the front of Kongsvegen and contains the highest average number of benthonic specimens per cubic centimetre sediment and most species per sample. These comparatively rich assemblages are probably related to the more coarse-grained bottom sediment at this locality where the amount of silt and coarser grain sizes reach their maximum values (Fig. 10).

5.5. Foraminifera in the monosulphide layers.

The samples used for studying the lithology and foraminifera of the monosulphide layers had thicknesses around 1 cm. Consequently, they included not only the few millimetres thick black layer, but also a varying amount of the mud above and below.

As shown in Figs. 6 to 9, most of the samples containing monosulphide layers have a smaller content of foraminiferal shells per cubic centimetre sediment and less species than most of the samples taken from the "usual" mud in the same core, although the latter show also strong variation in these faunal parameters. The reduced assemblages associated with the monosulphide layers are most probably related to decreased supply of empty shells to the sediment in winter and spring time. A decrease in number of shells will also reduce the apparent number of species because of the small size of the samples. Diagenetic solution of shells may have further accentuated this picture in the middle and lower parts of core 8.

5.6. Diagenetic changes in the assemblages.

The agglutinated species *Spiroplectammina biformis* is present in cores 7, 8, and 9 where it attains maximum frequencies in the uppermost samples and decreases irregularly downwards. An example is core 9 where *S. biformis* is represented with 28% at a depth of 0–5 cm, 18% at 20–25 cm, 9% at 40–45 cm, 0% at 58.5–60 cm, 0.7% at 60–65 cm, and 5% at 79–84 cm.

There is no sign of the marine environment having become less favourable for the foraminifera downwards in the cores. The decreasing frequency of *S. biformis* must, therefore, be explained by solution of the wall cement combined probably with increased pressure in the sediment. This interpretation is supported by the observation of some partially destroyed specimens in the lower part of cores 7, 8, and 9.

A rapid postmortem destruction of *S. biformis* would explain the fact that this species is missing or very sparsely represented in Pleistocene and early Holocene sediments, e.g. in southern Norway, Denmark, and the North Sea even though parts of these sequences are supposed to have been deposited in glacially influenced environments more or less comparable to those prevailing in Kongsfjorden. Partial solution of calcareous foraminifera has been observed in core 7 at a depth of 40–66 cm and in core 9 at a depth of 58.5–60 cm.

BENTHONIC FORAMINIFERA — Percentage distribution of species; **PL. FORAM.** — % distr.

CORE NUMBER 12 (58m)

SAMPLE, DEPTH IN CM	0–5	8,7–10	10–15	21,5–23,5	23,5–26,5	32,5–33,5	35,5–40	41,5–43	43,5–44,5	50–55	55–59	59–60,5	67–69
Ammodiscus catinus													
Ammodiscus gullmarensis													
Astrononion gallowayi				0,9	0,4	4,3	0,9	1,5		1,4	1,2	1,8	2,6
Bolivina pseudopunctata	0,8	1,3	1,3										
Buccella calida			0,4										
Buccella frigida				0,9			1,4	0,5					
Cassidulina crassa	61,7	79,8	76,3	69,9	63,5	47,8	64,4	61,2	55,8	63,2	68,8	73,0	67,3
Cassidulina laevigata			0,4		0,6								
Cibicides bertheloti					3,2				2,9				
Cibicides lobatulus		1,6	0,9	0,6	6,4	13,0	2,7	1,8		1,0	2,9	4,2	1,6
Cribrost. crassimargo													
Dentalina ittai													
Eggerella scabra													
Elphidium excavatum	21,7	10,4	11,3	20,6	11,3	21,2	21,3	18,1	20,6	19,6	19,1	15,0	22,8
Elphidium frigidum					0,4			0,6		0,5			0,5
Elphidium incertum									2,9				
Epistominella nipponica					3,6		0,9		8,8	0,5	0,3		
Epistominella vitrea	1,7	1,3	1,8	0,6	1,3	4,3		0,5		1,0	0,6		
Fissurina furcillifera					0,4								
Islandiella helenae								0,5					
Lagena distoma													
Lagena gracillima	0,8												
Lagena mollis													
Miliolinella subrotunda													
Nonion labradoricum	3,5	4,9	4,5	5,9	1,7		5,6	5,9	8,8	3,4	6,8	4,8	4,7
Nonionella auricula					2,1		0,5						
Oolina melo						4,3							
Patellina corrugata					0,2								
Protelphidium orbiculare													0,5
Pullenia osloensis			0,9		0,2								
Quinqueloculina stalkeri	9,6		0,9		2,1	4,3	2,3	9,2		8,8		0,6	
Spiroplectamm. biformis													
Stainforthia loeblichi				0,3	0,4					0,5	0,3	0,6	
Stainforthia schreibersiana		0,65	0,9										
Textuloria torquata													
Trifarina angulosa					1,9								
Trifarina fluens								0,5					
Triloculina trihedra				0,3									
Specimens in 1 cm³ sediment	3,8	38	7,3	37	26	3,8	7,2	43,5	5,6	6,8	14	18,5	25,7
Species per sample	7	7	11	9	17	7	9	11	6	10	8	7	7
Faunal diversity	4	3	5	3	9	6	5	5	4	4	4	4	3
PL. FORAM. % distr.: Globigerina quinqueloba					5,6								
Globigerinita bradyi			90,0	100	68,9		83,4			100	100	100	
Globoquadr. pachyderma			10,0		25,5	100	16,6						
Specimens in 1 cm³ sediment			0,33	0,11	7,2	0,5	0,2			0,03	0,04	0,11	

CORE NUMBER 7 (52m)

SAMPLE, DEPTH IN CM	0–3	10–15	20–25	30–35	40–45	50–55	57–58	60–65	65–66
Ammodiscus catinus									
Ammodiscus gullmarensis									
Astrononion gallowayi				1,1			4,0		
Bolivina pseudopunctata		2,3		1,4				1,1	
Buccella calida									
Buccella frigida			1,1	0,6					
Cassidulina crassa	83,4	65,7	73,9	74,1	55,3	58,8	50,0	34,5	18,2
Cassidulina laevigata						5,9			
Cibicides bertheloti									
Cibicides lobatulus				0,8			4,0	1,1	
Cribrost. crassimargo									
Dentalina ittai				0,3					
Eggerella scabra									
Elphidium excavatum		9,8	15,9	10,7	6,5	23,6	31,0	25,3	9,1
Elphidium frigidum									
Elphidium incertum									
Epistominella nipponica			3,4	0,3	2,0				
Epistominella vitrea		2,8		3,3	0,5	5,9		1,1	
Fissurina furcillifera									
Islandiella helenae									4,5
Lagena distoma									
Lagena gracillima									
Lagena mollis		0,5							
Miliolinella subrotunda									
Nonion labradoricum		3,8	2,3	2,8	2,0	5,9		6,9	9,1
Nonionella auricula									
Oolina melo									
Patellina corrugata									
Protelphidium orbiculare									
Pullenia osloensis									
Quinqueloculina stalkeri		14,1	2,3	4,4	33,7			28,7	54,5
Spiroplectamm. biformis	16,6	0,5	1,1				11,5	1,1	4,5
Stainforthia loeblichi									
Stainforthia schreibersiana		0,5		0,3					
Textuloria torquata									
Trifarina angulosa									
Trifarina fluens									
Triloculina trihedra									
Specimens in 1 cm³ sediment	0,66	7,7	2,9	12,1	6,6	0,5	4,3	2,9	3,6
Species per sample	2	9	7	12	6	5	5	8	6
Faunal diversity	2	5	4	5	3	3	4	5	5
PL. FORAM. % distr.: Globigerina quinqueloba									
Globigerinita bradyi			66,6		100	100			100
Globoquadr. pachyderma	100		33,4	100					
Specimens in 1 cm³ sediment	0,1		0,1	0,03	0,03	0,07			0,16

CORE NUMBER 8 (48m)

SAMPLE, DEPTH IN CM	0–5	10–15	20–25	32–33	33–38	39,5–40,5	40,5–45	50,5–51,5	51,5–56,5	61–62	62–67	67–68	73–78
Ammodiscus catinus													
Ammodiscus gullmarensis			1,9										
Astrononion gallowayi		0,5											
Bolivina pseudopunctata											1,5		2,2
Buccella calida													
Buccella frigida													
Cassidulina crassa	6,0	4,3	55,8	33,0	56,2	50,0	50,0		17,6		61,8	56,2	63,3
Cassidulina laevigata		2,4		67,0		50,0	8,3						
Cibicides bertheloti		0,5					4,1	100					
Cibicides lobatulus	1,2		1,9		12,5		16,7		11,8				1,1
Cribrost. crassimargo													
Dentalina ittai													
Eggerella scabra			1,9										
Elphidium excavatum	18,1	76,7	13,5		6,2		4,1		23,5		10,3		13,3
Elphidium frigidum													1,1
Elphidium incertum													
Epistominella nipponica		2,8	3,8										
Epistominella vitrea			1,9								4,4		1,1
Fissurina furcillifera													
Islandiella helenae									5,9				
Lagena distoma												6,3	
Lagena gracillima													
Lagena mollis													
Miliolinella subrotunda									5,9				
Nonion labradoricum	1,2		1,9				4,1						3,3
Nonionella auricula													
Oolina melo													
Patellina corrugata													
Protelphidium orbiculare													
Pullenia osloensis													
Quinqueloculina stalkeri	8,4	7,6	5,8		25,0		4,1		11,8		13,2		12,2
Spiroplectamm. biformis	63,8	4,8	9,6						17,6		8,8	37,5	2,2
Stainforthia loeblichi													
Stainforthia schreibersiana													
Textuloria torquata	1,2												
Trifarina angulosa		0,5	1,9				8,3		5,9				
Trifarina fluens													
Triloculina trihedra													
Specimens in 1 cm³ sediment	2,8	7,0	1,7	0,5	0,5	0,3	0,8	0,2	0,6		2,3	2,6	3,0
Species per sample	7	9	11	2	4	2	8	1	8		6	3	9
Faunal diversity	4	5	8	2	3	2	7	1	7		4	3	5
PL. FORAM. % distr.: Globigerina quinqueloba	25,0	16,6											
Globigerinita bradyi	50,0	16,6	33,4		50,0	60							
Globoquadr. pachyderma	25,0	66,6	66,6	100	50,0	40	100		100		100		
Specimens in 1 cm³ sediment	0,13	0,4	0,3	0,3	0,13	0,83	0,07		0,03		0,03		

CORE NUMBER 9 (50m)

SAMPLE, DEPTH IN CM	0–5	20–25	40–45	58,5–60	60–65	79–84
Ammodiscus catinus				6,6		
Ammodiscus gullmarensis						
Astrononion gallowayi					1,5	
Bolivina pseudopunctata					0,7	
Buccella calida						
Buccella frigida						
Cassidulina crassa	50,1	60,5	71,5	80,0	46,3	84,0
Cassidulina laevigata	0,4				0,7	
Cibicides bertheloti					2,2	
Cibicides lobatulus					3,0	
Cribrost. crassimargo	1,8					
Dentalina ittai						
Eggerella scabra						
Elphidium excavatum	13,5	14,3	8,0	6,6	2,2	3,6
Elphidium frigidum						
Elphidium incertum				6,6		
Epistominella nipponica					1,5	1,2
Epistominella vitrea	0,4		0,5		0,7	
Fissurina furcillifera						
Islandiella helenae						
Lagena distoma						
Lagena gracillima						
Lagena mollis						
Miliolinella subrotunda		1,7				
Nonion labradoricum			0,5		2,2	1,2
Nonionella auricula						
Oolina melo						
Patellina corrugata						
Protelphidium orbiculare						
Pullenia osloensis						
Quinqueloculina stalkeri	4,2	3,4	10,5		37,3	4,8
Spiroplectamm. biformis	28,4	18,5	8,5		0,7	4,9
Stainforthia loeblichi						
Stainforthia schreibersiana	0,7	1,7	0,5			
Textuloria torquata						
Trifarina angulosa						
Trifarina fluens					0,7	
Triloculina trihedra						
Specimens in 1 cm³ sediment	9,4	4,0	6,7	1,7	4,5	2,7
Species per sample	8	6	7	4	13	6
Faunal diversity	4	4	4	3	7	4
PL. FORAM. % distr.: Globigerina quinqueloba	50,0				33,4	
Globigerinita bradyi	50,0				66,6	
Globoquadr. pachyderma						
Specimens in 1 cm³ sediment	0,6				0,3	

Fig. 16. *Distribution chart of formainifera found in inner basin of Kongsfjorden.*

5.7. Reference list of foraminifera.

In the cores from Kongsfjorden totally 41 foraminiferal species are recognized (Fig. 16). For taxonomic references concerning 22 of these species, see FEYLING-HANSSEN & al. (1971). The remaining 19 species are not treated in that publication or deviate in nomenclature. An alphabetic reference list of these is given below.

Sixteen of the observed species are illustrated on Pl. 1. The specimens shown will be preserved in the collection of the Paleontological Museum of the University of Oslo (Nos. A37918-A37940).

Ammodiscus catinus HÖGLUND 1947, p. 11, Pl. 8, Figs. 1, 7; Pl. 28, Figs. 19–23; Text-figs. 82–84, 105–107, 109.
Ammodiscus gullmarensis Höglund 1948. NAGY 1965, p. 117, Pl. 1, Fig. 9.
Buccella calida (CUSHMAN & COLE 1930). *Eponides frigida* var. *calida* CUSHMAN & COLE 1930, p. 98, Pl. 13, Fig. 13. *Buccella frigida* var. *calida* (CUSHMAN & COLE); FEYLING-HANSSEN 1976, p. 353, Pl. 1, Figs. 6–7, Pl. 2, Figs. 7–9.
Cibicides bertheloti (D'ORBIGNY 1839). FEYLING-HANSSEN 1964, p. 338, Pl. 18, Figs. 21–24.
Cribrostomoides crassimargo (NORMAN 1892). *Alveolophragmium crassimargo* (NORMAN); LOEBLICH & TAPPAN 1953, p. 29, Pl. 3, Figs. 1–3.
Eggerella advena (CUSHMAN 1922). LOEBLICH & TAPPAN 1953, p. 36, Pl. 3, Figs. 8–10.
Elphidium excavatum (TERQUEM) forma *clavata* CUSHMAN 1930. FEYLING-HANSSEN 1972, p. 339, Pl. 1, Figs. 1–9, Pl. 2, Figs. 1–9.
Elphidium frigidum CUSHMAN 1933, p. 5, Pl. 1, Fig. 8.
Epistominella nipponica KUWANO 1962, p. 58, Pl. 47, Fig. 7.
Epistominella vitrea PARKER in PARKER & al. 1953, p. 9, Pl. 4, Figs. 34–36, 40–41.
Fissurina furcillifera (BUCHNER 1940), p. 489, Pl. 47, Figs. 318–326.
Globigerina quinqueloba NATLAND 1938. BÉ 1977, Pl. 9, Fig. 15.
Globigerinita bradyi (WIESNER 1931). BÉ 1977, Pl. 9, Fig. 19.
Globoquadrina pachyderma (EHRENBERG 1861). BÉ 1977, Pl. 10, Fig. 22.
Islandiella helenae FEYLING-HANSSEN 1976, p. 155, Figs. 1–4.
Lagena distoma PARKER & JONES 1864. FEYLING-HANSSEN 1964, p. 286, Pl. 11, Figs. 6–8.
Stainforthia loeblichi (FEYLING-HANSSEN 1954). KIHLE&LØFALDLI 1973.
Stainforthia schreibersiana (CZJZEK 1848). KIHLE & LØFALDLI 1973.
Textularia torquata PARKER 1952. LOEBLICH & TAPPAN 1953, p. 35, Pl. 2, Figs. 12–21.

6. Glacial erosion

6.1. Annual erosion (average value).

Part of the project described in this paper is an attempt to quantify the glacial erosion rate in an area covered with subpolar valley glaciers and ice streams. As a first order approximation of glacial erosion, the estimated values of annual sedimentation (10^6 ton) and sediment flux ($0.5\ 10^5$ ton) may be applied. Additional, coarse-grained sediments, mainly bed load, are deposited within the meltwater tunnel (Fig. 5). With reference to measurements in Bayelva representing Brøggerbreen's (Fig. 1) erosion of similar rocks, 30% of the total transport is represented by bedload (REPP 1979).

Applying the value 2500 mg/l in the meltwater stream of Kongsvegen (section 4.2), 10^5 ton coarse-grained sediment may potentially be deposited annually beneath the glacier front. Additional coarse-grained deposition at the fronts of the other glaciers in the vicinity seems likely. Using the total amount of

annual sedimentation in the inner basin, 0.4 10^6 ton may be deposited in the close vicinity of the glacier front and within the inner basin. Summarizing the annual sedimentation, sediment flux and coarse-grained deposition, 1.5 10^6 ton appears to be annually eroded beneath the 800 km^2 ice covered area of Kongsvegen, corresponding to 1 mm annual erosion. Even though the applied values are somewhat speculative, the derived estimate accords reasonably well with the annual sediment-transport and erosion rate at Brøggerbreen. Accordingly, the value of 1 mm may be used as a working approximation for the average erosion below the Kongsvegen glacier complex.

6.2. Glacial erosion, ice movement and bedrock.

The erosive capability of glaciers is dependent on a number of factors: basal thermal regime, sliding velocity, pressure, the amount of debris within the sole, the efficiency of removal of rock debris, the quality of the bedrock (resistance to quarrying, permeability) (see also SUGDEN & JOHN 1976 and SUGDEN 1978).

In areas like the Kongsfjorden region the erosion rate has a markedly uneven distribution already, with much more intensive abrasion under temperate ice streams than under the thin polar ice caps. Theoretically, ice erosion should be most intensive where the ice mass transport is largest. This follows from the fact that both erosion rate and ice mass transport are roughly proportional to the thickness (pressure) and velocity (mean and sliding). In a regular valley glacier the erosion should be most intensive below the equilibrium line where transport is largest. In the complex glacier system in the investigated area, containing both polar ice caps and fast flowing temperate ice streams, conditions are much more complicated. During the last German Expedition 1964–65, both depth and velocity measurements were made along cross sections on the two main ice streams which after confluence, form the Kongsvegen ice front (Fig. 1). Depth, width, and surface inclination are nearly the same for both ice streams, but the velocity and hence the ice transport are very different. The southern stream (section B, Fig. 1) is almost stagnant with a maximum surface velocity of only 4 cm a day, whereas the flow rate of the northern one (section A) is 110 cm a day. If the velocity drops with the same percentage to the bottom, then the erosion rate should be theoretically almost 30 times greater below the northern one. It is therefore reasonable to believe that the lower part of the fast-flowing northern stream draining the ice fields of Isachsen- and Holtedahl-fonna is responsible for a large part of the eroded material reaching the head of Kongsfjorden. It is of course difficult to estimate the erosion here, but there is reason to believe that it amounts to many times the average value, perhaps a couple of centimetres a year.

The high erosion rate in the Kongsfjorden area may also be due to the low consolidation of the bedrock (mainly Devonian sandstones) beneath the main glacial stream. The glacial comminution of these fine-grained clastic rocks produce similarly fine-grained tills. The stratification of the bedrock below Kongsvegen strikes the main ice stream to almost a right angle. Increased erosion may therefore occur in more "soft" layers by hard pieces broken away from the resistant layers upstream.

In Spitsbergen the larger glaciers are all of the subpolar type, but some of the minor ones are polar, with their entire mass below pressure melting point. The latter type reveal themselves by the total absence of discharge during the winter. In front of the subpolar ones large ice masses formed by refrozen meltwater accumulate. This water which amounts to only a very small fraction of the summer discharge, is exceptionally clear with no sign of suspended material. At both types of glacier, the runoff is confined to a couple of months. The discharge is therefore very high in relation to the yearly precipitation, which in this area amounts to c. 800 mm. Contraction of sediment load increases with increasing runoff. It is therefore the large discharges, and especially the peak floods, that account for the major part of the total sediment transport. Short sampling intervals are therefore needed especially during the floods, to get a true total value.

The intensive subglacial meltwater discharge may also favour the glacial erosion by transporting the more fine-grained till components away from the sole. The glacial abrasion may thus be more intensive.

6.3. Comments on subpolar glacial erosion.

The estimated value for glacial erosion represents the subglacial meltwater erosion during an intersurging period. The glacial comminution is not possible to measure. However, if the glacial comminution exceeds the subglacial meltwater erosion, till sediments are piling up below the glacier. On the other hand, if the meltwater is able to carry out more rock debris than the glacier may produce, only the biggest boulders may be left behind in the ice covered areas. Further, the glacial erosion may also vary strongly in response to surging/intersurging periods. In surging periods with high glacier velocities, the erosion rate may increase and correspondingly, the production of till sediments increases. It is therefore possible that the subglacial meltwater below Kongsvegen now erodes into masses deposited during the 1948 surge.

The processes of glacial erosion are summarized by SUGDEN & JOHN (1976). However, the role of surging/intersurging periods and the effect of meltwater erosion are not treated in that publication. An attempt is made in the present paper, but it is obvious that more observations are needed to really understand the processes going on under the polar glaciers.

Conclusions

The main glacial, sedimentological and faunal characteristics of the Kongsfjorden and Kongsvegen area are summarized in the following list:

The glacier.

1. Type of glacier: grounding glacier calving into the sea. Mostly at pressure melting point at the sole. Retreating 50–100 m per year. Retreat interrupted by periodic surging involving 1–2 km advance during few years.
2. Rate of movement at the front: 1–4 m/day, maximum in summer.

3. Glacial comminution of the underlying shales, siltstones, and sandstones, produce fine-grained till.
4. Annual erosion rate: 1 mm.

The basin.

1. An open fjord without sill in the mouth area with influx of oceanic water.
2. Katabatic winds blow out the fjord.

Sedimentary features and processes.

1. Meltwater enters the basin from a glacial tunnel at sea level.
2. Oceanic water penetrates into the glacier and is gradually mixed with the outflowing meltwater.
3. Brackish surface water flows seawards through the basin and disperses: sand and mud deposited as laminae below the meltwater stream near the glacier front, homogenous mud further out and to the side.
4. The annual sedimentation rate is 10 cm wet mud or 3 cm dry sediment.
5. Ice-rafted pebbles are few in number.
6. Glacial surge will rework glaciomarine deposits.
7. Organic varves are present. Their formation is probably due to a time-lag between high organic production and clastic sedimentation (spring and summer, respectively).
8. The brackish surface water transports suspended sediment out to the shelf.

The foraminifera.

1. The general aspect of the benthonic assemblages is arctic, but a few species with boreal main distribution are also present.
2. The benthonic assemblages show low diversities, and there is a correlation between increased grain size and increased diversity.
3. Planktonic foraminifera occur, although in small quantities.
4. Postmortem destruction of an agglutinated species (*S. biformis*) seems to have taken place below the sea bed surface.

The most marked features of the investigated area are the high erosional and sedimentation rates. Comparable values might be expected from glaciated areas during the Quaternary. The main reasons for the rather high erosional and depositional rates in the Kongsfjorden area seem to be: 1. The weakly lithified and fine-grained nature of the rocks underlying the glacier. 2. The glacial comminution of these rocks into an argillaceous basal till. 3. The intensive subglacial water discharge during the summer, transporting the material into the basin.

The benthonic foraminiferal assemblages in the inner basin of Kongsfjorden show low diversities, a phenomenon which seems to be mainly attributed to the high turbidity of the bottom water and to the very soft substrate. Salinities of 33‰ are measured near the bottom suggesting that this factor has a minor limiting effect in the area. Scattered occurrences of planktonic foraminifera, indicate influx of North Atlantic water.

Acknowledgement

We are grateful to PER JØRGENSEN and HARALD MAJOR for discussion and critical comments on the manuscript, and to GUNNBJØRG QUALE for discussion of the planktonic foraminifera.

The present research was financed by Norsk Polarinstitutt.

References

BÉ, A. W. H., 1977: An Ecological, Zoogeographic and Taxonomic Review of Recent Planktonic Foraminifera. **In:** RAMSAY, S. T. S. (ed.) *Oceanic Micropaleontology* **1:** 1–100. Acad. Press, London.

BERNER, R. A., 1971: *Principles of chemical sedimentology*. McGraw Hill, New York. 240 pp. (Inter. series in the Earth and Planary Sciences.)

BUCHNER, P., 1940: Die Lagenen des Golfes von Neapel und der marinen Ablagerungen auf Ischia. *Novo Acta Leopoldina, Neue Folge* **9:** 363–560.

CUSHMAN, J. A., 1933: New arctic foraminifera collected by Capt. R. A. Barlett from Fox Basin and off the northeast coast of Greenland. *Smithsonian Misc. Coll.* **89**(9). 8 pp.

CUSHMAN J. A. and W. S. COLE, 1930: Pleistocene foraminifera from Maryland. *Cushman Lab. foram. Res., Contr.* **6**(4): 94–100.

EDWARDS, M. B., 1978: Glacial environments. **In:** H. G. READING (ed.) *Sedimentary Environments and Facies*. 557 pp. Blackwell Scientific Publ., London.

ELVERHØI, A., 1979: Sedimentological and mineralogical investigations of Quaternary bottom sediments off the Norwegian west coast. *Norsk Geologisk Tidsskrift* **59:** 273–284.

FEYLING-HANSSEN, R. W., 1964: Foraminifera in Late Quaternary deposits from the Oslofjord area. *Norges geol. Unders.* **225.** 383 pp.

— 1972: The foraminifer Elphidium excavatum (Terquem) and its variant forms. *Micropaleontology* **8**(3): 337–354.

— 1976: A mid-Wisconsinian Interstadial on Broughton Island, Arctic Canada, and its foraminifera. *Arctic and Alpine Res.* **8**(2): 161–182.

FEYLING-HANSSEN R. W. et al., 1971: Late Quaternary Foraminifera from Vendsyssel, Denmark and Sandnes, Norway. *Bull. geol. Soc. Denmark* **21,** pt. 2–3: 67–317.

FLINT, R. F., 1971: *Glacial and Quaternary geology*. John Wiley and Sons, Inc., New York. 892 pp.

HOLTEDAHL, H., 1975: The geology of the Hardangerfjord, West Norway. *Norges geol. unders.* **323:** 1–87.

HÖGLUND, H., 1947: Foraminifera in the Gullmar Fjord and the Skagerak. *Zool. Bidr. från Uppsala* **26.** 328 pp.

JANSEN, J. H. F., 1976: Late Pleistocene-Holocene history of the northern North Sea, based on acoustic reflections records. *Neth. J. Sea Res.* **10**(1): 1–43.

JØRGENSEN, P., 1977: Some properties of Norwegian tills. *Boreas* **6:** 149–157.

KIHLE, R. and M. LØFALDLI, 1973: Stratigraphic Atlas. *NTNF's Continental Shelf Project* **35.**

KRISTOFFERSEN, Y. and A. ELVERHØI (in prep): The distribution of unconsolidated sediments in the northwestern part of the Barents Sea.

KUWANO, Y., 1962: Foraminiferal Biocoenoses of the seas around Japan, a survey of Pacific-side biocoenoses. *Res. Inst. Nat. Resour., Misc. Rep.* No. 58–59.

LIESTØL, O., 1975: Glaciological work in 1975. *Norsk Polarinstitutt Årbok* 1975: 147–158.

LOEBLICH, A. R. and H. TAPPAN, 1953: Studies of Arctic Foraminifera. *Smithsonian Misc. Coll.* **121**(7). 150 pp.

LØKEN, T., 1976: Geology of the superficial sediments in the northern North Sea. *Norwegian Geotechnical Institute Publ.* Nr. 114.

MURRAY, J. W., 1973: *Distribution and Ecology of Living Benthic Foraminiferids*. London. Heinemann Education Books. 274 pp.

NAGY, J., 1965: Foraminifera in some bottom samples from shallow waters in Vestspitsbergen. *Norsk Polarinstitutt Årbok* 1963: 109–125.

NAGY, J. and K. OFSTAD, 1980: Quaternary foraminifera and sediments in the Norwegian Channel. *Boreas*. **9**: 39–52.

ORVIN, A. K., 1940: Outline of the geological history of Spitsbergen. *Skr. Svalbard og Ishavet* Nr. 78.

ØSTBY, K. L. and J. NAGY, in prep.: Foraminiferal distribution in Quaternary sediments in the western Barents Sea.

PARKER, F. L., F. B. PHLEGER and J. F. PEIRSON, 1953: Ecology of foraminifera from San Antonio Bay and environs, Southwest Texas. *Cushman Found. Foram. Res., Spec. Publ.* **2:** 1–75.

RELLING, O. and K. NORDSETH, 1979: Sedimentation of a river suspension into a fjord basin. Gaupnefjord in Western Norway. *Norsk geogr. Tidsskr.* **33:** 187–203.

REPP, K., 1978: *Field work in the Ny-Ålesund area 1978.* Unpub. field report, Norsk Polarinstitutt 1978. 10 pp.

— 1979: Breerosjon, glasio-hydrologi og materialtransport i et høyarktisk miljø Brøggerbreene, Vest-Spitsbergen. *Unpub. cand. real. thesis, University of Oslo.* 136 pp.

RISDAL, D., 1964: Foraminiferenes relasjon til dybdeforholdene i Oslofjorden, med en diskusjon av de senkvartære foraminifersoner. *Norges geol. Unders.* **226.** 142 pp.

SAURAMO, M., 1923: Studies on the Quaternary varve sediments in southern Finland. *Bull. Comm. Geol. de Finlande* **60.** 164 pp.

SUGDEN, D. E., 1978: Glacial erosion by the Laurentide ice sheet. *Jour. of Glaciology* **20**(83): 367–391.

SUGDEN, D. E. and B. S. JOHN, 1976: *Glaciers and Landscape. A Geomorphological Approach.* Arnold, London. 376 pp.

SWIFT, D. J. P., D. P. STANLEY, and J. R. CURRAY, 1971: Relict sediments on continental shelves: a reconsideration. *Jour. Geol.* **79:** 322–346.

VOIGT U., 1967: Direkte Beobachtungen der Unterseite des Kongsvegens. **In:** Die Wissenschaftlichen Ergebnisse der Deutschen Spitzbergenexpedition 1964–1965. Teil 1: Die geodätischen und glaziologischen Arbeiten. *Nationalkomitee für Geodäsie und Geophysik der Deutschen Demokratischen Republik bei der Deutschen Akademie der Wissenschaften zu Berlin* Nr. III/9.

VOLKOV, I. I., 1961: Iron sulphides, their interdependence and transformation in the Black Sea bottom sediments. *Akad. Nauk. SSSR. Okeanologii Trudy.* **50:** 68–92.

WALTON, W. R., 1964: Recent foraminiferal ecology and paleo-ecology. **In**: IMBRIE J. and N. D. NEWELL (eds.). *Approaches to Paleoecology*: 151–237. Wiley & Sons, New York.

WISEMAN, J. M., Jr., 1979: *Arctic coastal processes Spitsbergen Report.* Coastal Studies Institute, Louisiana State University 1979. 26 pp.

Plates 1

PLATE 1

Fig. 1. *Ammodiscus catinus* HØGLUND, from core 9, sediment depth 58.5–60 cm, × 107.

Figs. 2–3. *Spiroplectammina biformis* PARKER & JONES. 2: from core 9, sediment depth 0–5 cm, × 105. 3: partially destructed specimen from core 7, sediment depth 65–66 cm, × 116.

Fig. 4. *Quinqueloculina stalkeri* LOEBLICH & TAPPAN, from core 8, sediment depth 0–5 cm, × 106.

Fig. 5. *Bolivina pseudopunctata* HØGLUND, from core 7, sediment depth 30–35 cm, × 100.

Figs. 6–7. *Trifarina angulosa* (TODD), two specimens from core 12, sediment depth 23.5–26.5 cm, × 105.

Figs. 8–9. *Stainforthia schreibersiana* (CZJZEK). 8: from core 7, sediment depth 10–15 cm, × 100. 9: from core 9, sediment depth 40–45 cm, × 103.

Figs. 10–11. *Epistominella nipponica* KUWANO. Spiral (10) and umbilical (11) side of a specimen from core 12, sediment depth 23.5–26.5 cm, × 93.

Figs. 12–13. *Epistominella vitrea* PARKER. Spiral (12) and umbilical (13) side of a specimen from core 7, sediment depth 30–35 cm, × 103.

Figs. 14–17. *Elphidium excavatum* (TERQUEM) forma *clavata* CUSHMAN. Three specimens showing different development of the umbilical knob; from core 9, sediment depth 0–5 cm, × 108. (14–15: same specimen).

Figs. 18–19. *Cassidulina crassa* D'ORBIGNY. Side and edge view of a specimen from core 9, sediment depth 20–25 cm, × 97.

Figs. 20–22. *Cassidulina laevigata* D'ORBIGNY. 20–21: side and edge view of a specimen from core 8, sediment depth 10–15 cm, × 101. 22: side view of a specimen from core 8, sediment depth 39.5–40.5 cm, × 101.

Figs. 23–24. *Cibicides bertheloti* (D'ORBIGNY). Umbilical (23) and spiral (24) side of a specimen from core 12, sediment depth 23.5–26.5 cm, × 106.

Figs. 25–26. *Globigerina quinqueloba* NATLAND. Spiral (25) and umbilical (26) side of a specimen from core 12, sediment depth 23.5–26.5 cm, × 120.

Figs. 27–28. *Globoquadrina pachyderma* (EHRENBERG). Umbilical (27) and spiral (28) side of a specimen from core 12, sediment depth 23.5–26.5 cm, × 120.

Figs. 29–30. *Globigerina quinqueloba* NATLAND. Umbilical (29) and spiral (30) side of a specimen from core 9, sediment depth 0–5 cm, × 125.

Figs. 31–32. *Globigerinita bradyi* WIESNER. Two specimens from core 12, sediment depth 23.5–26.5 cm × 123.

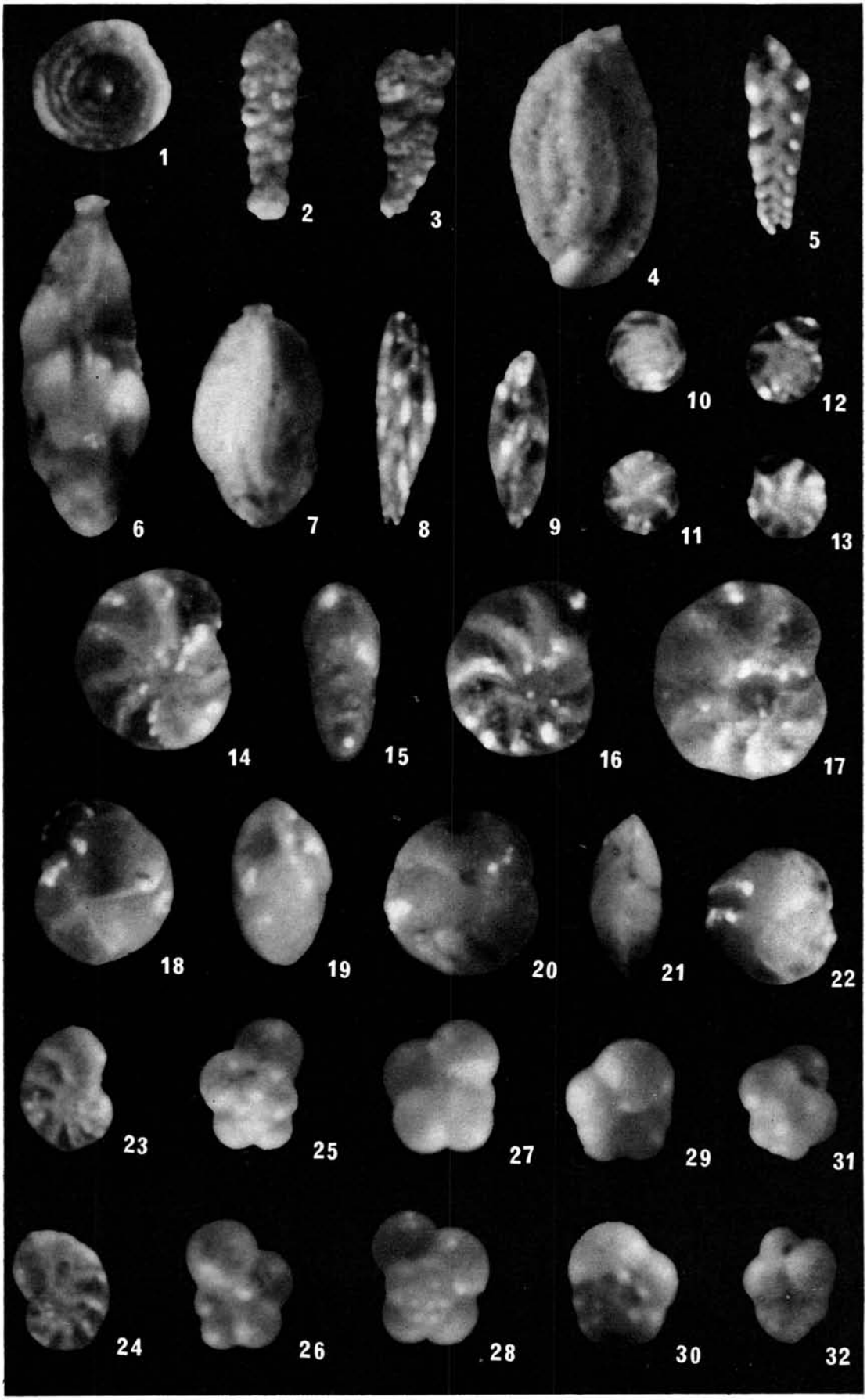
1
2
3
4
5
6
7
8
9
10
11
12
13
14
15
16
17
18
19
20
21
22
23
25
27
29
31
24
26
28
30
32

Foraminiferal stratigraphy of Jurassic deposits on Kongsøya, Svalbard

By Magne Løfaldli[1] and Jenö Nagy[2]

Abstract

From a 95 m thick Jurassic section, 53 samples were analysed for foraminifera. The faunal sequence consists of arenaceous species except for one horizon with calcareous forms in addition. Of the recognized species, 38 are identified as, and 8 are compared to known species. *Haplophragmoides barentsi* is new. Most of the species are illustrated.

The lower part of the section (upper Wilhelmøy Formation) is referred to the Lower Jurassic; its depositional environment is interpreted as brackish and, to a lesser extent, fresh water lagoonal. The upper part of the section (part of the Janusfjellet Formation) mainly belongs to the Callovian and Oxfordian. It seems to have been deposited in inner shelf waters with slightly stagnant bottom conditions except for one horizon with more open circulation.

1. Introduction

Kongsøya is the central, and largest island of Kong Karls Land which is a group of three main, and many smaller islands, located in the eastern part of the Svalbard Archipelago (Fig. 1). Kong Karls Land is composed of Rhaetian, Jurassic and Lower Cretaceous sediments capped by basaltic lavas.

The sedimentary sequence of Kong Karls Land forms part of the Mesozoic platform deposits which cover the eastern part of the Svalbard Archipelago and continue into the Spitsbergen Trough. This structural depression is the main outcrop area of Jurassic and Cretaceous sediments in Svalbard, but deposits of the same age are believed to have a large regional extent also in offshore areas of the Barents Shelf (Nagy 1973; Bjærke & Thusu 1976; Edwards 1976).

The Mesozoic of Kong Karls Land generally consists of clays, shales, siltstones, and sandstones. These lithologies are poorly consolidated and, therefore, particularly suitable for micropaleontological studies. They contrast markedly with corresponding sediments in the Spitsbergen Trough which show a considerably higher grade of diagenesis.

The first comprehensive description of the geology of Kong Karls Land was published by Nathorst (1901). Detailed information on the sedimentary

[1] Institutt for Kontinentalsokkelundersøkelser, Håkon Magnussons gt. 1B, Postboks 1883, 7001 Trondheim.

[2] Institutt for geologi, Universitetet i Oslo, Postboks 1047, Oslo 3.

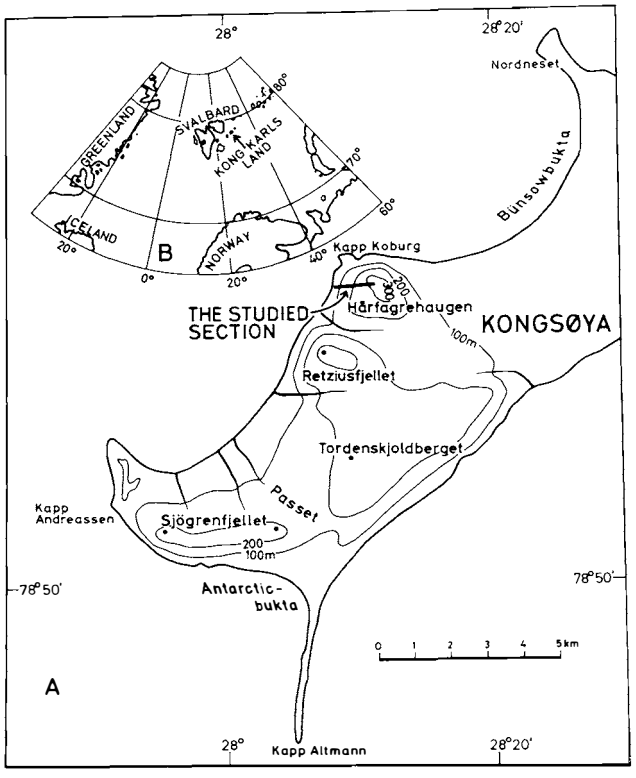

Fig. 1. (*A*) *Location of the studied section on Kongsøya, Kong Karls Land.* (*B*) *Setting of Kong Karls Land within the Arctic.*

sequence and an extensive revision of the stratigraphic nomenclature was presented by SMITH et al. (1976). A modified nomenclature published by EDWARDS et al. (1979) is principally followed in the present paper.

This paper is based on material collected by the Norwegian Polar Research Institute and the Continental Shelf Institute during the summer of 1976. The field work was conducted by DR. M. B. EDWARDS, and the section on Fig. 2 is based on his observations.

2. Lithostratigraphy

The examined samples were collected from a section measured on the western slope of Hårfagrehaugen, a c. 300 m high mountain located in the western part of Kongsøya. Four members (belonging to three formations) are recognized within the section. These units are briefly described below and illustrated in Fig. 2.

2.1. Sjøgrenfjellet Member of the Wilhelmøya Formation.

Only the upper 12.3 m of this member is present in the measured section. It consists of poorly consolidated sand with some silt and clay. The upper 10 m of the member forms a coarsening upwards sequence.

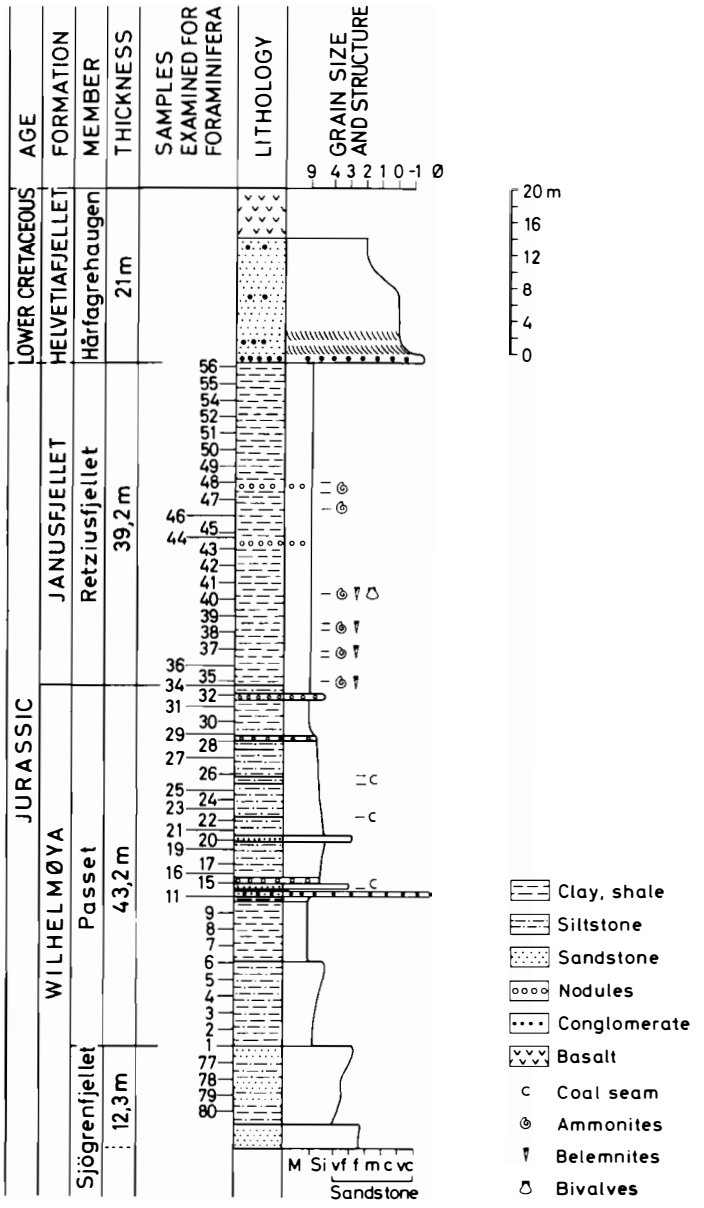

Fig. 2. *Section from the western slope of Hårfagrehaugen showing lithostratigraphy and the position of samples examined for foraminifera.*

2.2. Passet Member of the Wilhelmøya Formation.

This member is 43.2 m thick in the investigated section where it consists of silt and clay with subordinate amounts of sand. Four thin beds of coal are found within the member and a conglomeratic bed is present 18 m above its base. Clay–ironstone nodules occur at three horizons. The lower 10 m of the member show a slight coarsening upwards tendency. The top of the member is apparently cut by a disconformity marked by an 80 cm thick, hard ledge-forming nodule horizon overlain by a sandy bed.

2.3. Retziusfjellet Member of the Janusfjellet Formation.

The Retziusfjellet Member consists of shales which are mainly black, dark grey, brownish, and to a lesser extent olive in colour. The shale contains calcareous, and occasionally pyritic nodules. The macrofauna consists mainly of ammonites, belemnites, and some bivalves. The best preserved specimens are found in the concretions. The thickness of the member is 39.2 m in Hårfagrehaugen where both its base and top boundary is formed by a disconformity.

2.4. Hårfagrehaugen Member of the Helvetiafjellet Formation.

This is a non-marine unit consisting of sandstones with some siltstones, shales and conglomeratic horizons. Coal, carbonaceous beds and plant fossils are characteristic. Flows of basaltic lava are included in the formation. The depositional environment of the unit is regarded as fluvio-deltaic.

3. Material and methods

From the Hårfagrehaugen section a series of 53 samples were examined for foraminifera. Specimens in varying states of preservation were found in two samples from the Sjøgrenfjellet Member, 16 samples from the Passet Member, and 19 from the Retziusfjellet Member. Altogether 16 samples were barren.

Most of the samples were only slightly consolidated, and these were disintegrated by soaking in water. A few harder samples were soaked for about ten minutes in 10% hydrogen peroxide. The samples were washed through a sieve of 0,1 mm mesh, and the material remaining on the screen was analysed for foraminifera.

In addition to the foraminifera, ammonites from nine horizons of the Hårfagrehaugen section are included in the present paper. Many of the ammonites occurred in the calcareous concretions and were found loose on the mountain slope.

The samples used in the study are preserved at the Continental Shelf Institute, Trondheim.

4. General notes on paleoenvironment

4.1. The foraminiferal sequence.

The foraminiferal faunas found in the investigated section have very low diversities, and consist entirely of arenaceous species. An exception is sample 48 which contains quite a large number of species including both arenaceous and calcareous forms.

The faunal succession (Fig. 3) is subdivided into four assemblages named from below: *Ammodiscus rugosus*, *Ammodiscus asper*, *Ammobaculites suprajurassicum*, and *Recurvoides disputabilis*. The introduction of formal biostratigraphical zones is avoided at the present stage of study of the area.

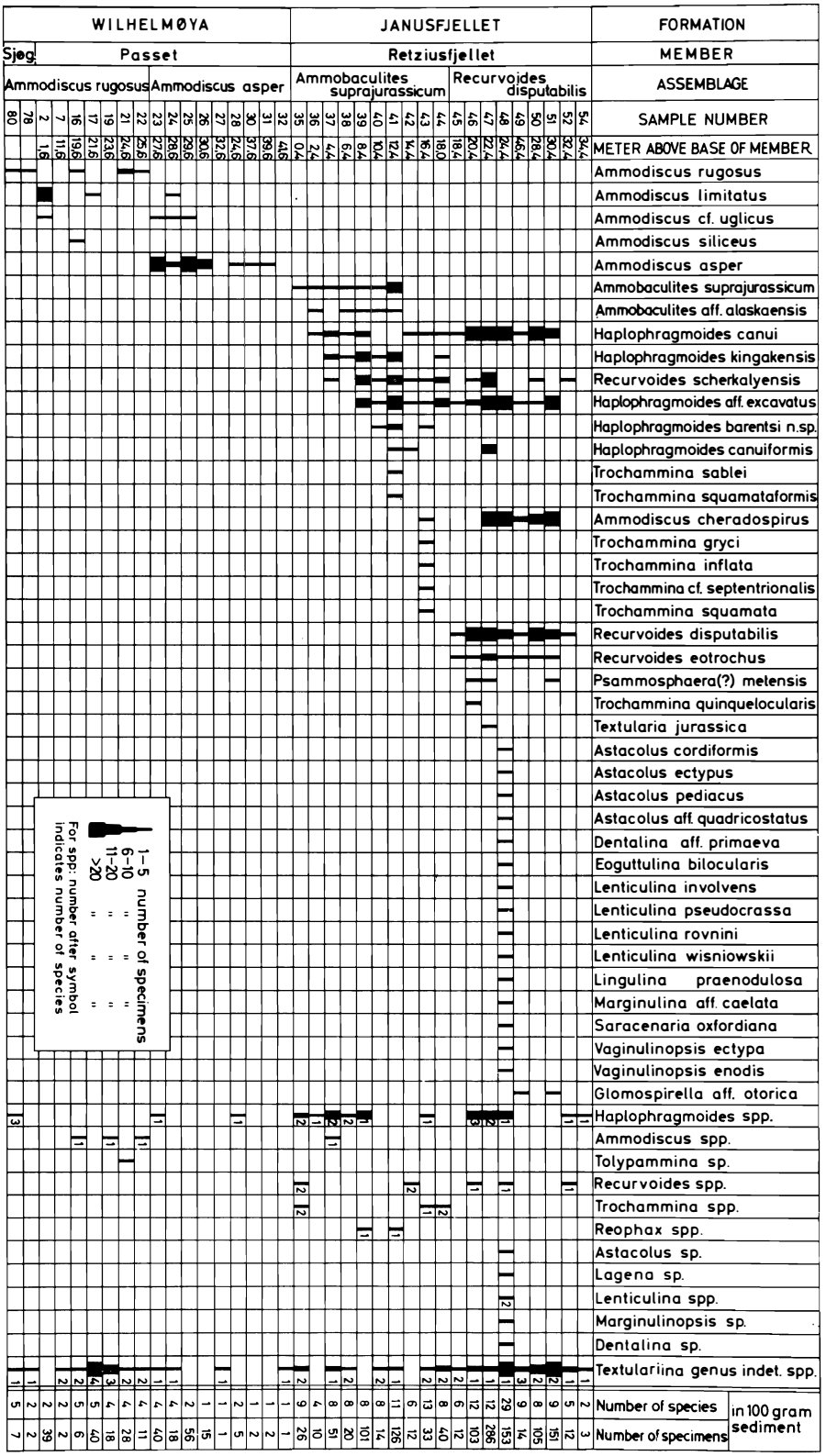

Fig. 3. *Distribution chart of foraminifera in the Hårfagrehaugen section. Symbols indicate specimens in 100 gram sediment.*

4.2. Comparison with other Jurassic assemblages.

The assemblages found in the Hårfagrehaugen section differ clearly from most Lower, Middle and early Upper Jurassic faunas described. European faunas north of the Tethys consist predominantly of Nodosariidae as shown in many papers, among the most recent are: NØRVANG (1957), CIFELLI (1959), CORDEY (1962), LUTZE (1960), BROUWER (1969), and NORLING (1972). Subordinate calcareous groups include species of Ceratobuliminidae and Ophthalmidiidae which are mainly found in the Lower Jurassic, and Epistominidae, Spirillinidae and Involutinidae which most frequently occur in the Middle Jurassic. Polymorphinids and simple arenaceous species are sometimes common. Lower and Middle Jurassic faunas from Alaska also show a great expansion of Nodosariidae (TAPPAN 1955).

The Hårfagrehaugen assemblages show greatest affinity to the faunas described by SOUAYA (1976) from the Lower Jurassic part of a well drilled on Linckens Island (Arctic Canada), to a Callovian assemblage recorded by DIBNER (1961) from Frans Josef Land, and to assumed Lower and Middle Jurassic faunas reported by KLUBOV (1972) from Wilhelmøya (Svalbard). In the Linckens Island sequence, arenaceous genera are dominant, and *Ammodiscus* is quite common. The Frans Josef Land assemblage contains *Ammodiscus*, *Ammobaculites*, *Haplophragmoides*, and *Verneuilina*. The Wilhelmøya faunas consist entirely of arenaceous genera including species of *Ammodiscus*, *Textularia*, *Saccammina*, *Trochammina*, *Glomospira*, *Ammobaculites*, and *Recurvoides*.

4.3. Arenaceous faunas and low diversity.

In addition to the localities mentioned above, partly or wholly arenaceous faunas are reported from many Mesozoic and Caenozoic sequences. Important publications include: TAPPAN (1955), MELLO (1971), BROOKE & BROWN (1972), MOORKENS (1976), and CHAMNEY (1977). Arenaceous assemblages have been interpreted as indicating at least five types of marine conditions: 1) Shallow water and reduced salinity. 2) High latitude cool conditions. 3) Great depth. 4) Increased turbidity. 5) Poorly circulated bottom water.

The following environmental discussion is mainly based on faunal comparisons down to generic level, species diversity (= number of species), and species dominance (= percentage frequency of the most common species). The use of these, or similar parameters on foraminiferal assemblages is discussed by WALTON (1964), GIBSON (1966), and MURRAY (1973).

Low diversity and high dominance are associated with extreme or changing conditions such as strong current activity, high turbidity, reduced salinity, low temperature, and reduced oxygen content. Slightly stagnant waters seem to have lower dominance than brackish areas, probably because of the more stable character of the former.

4.4. Preservation of foraminifera.

It is clear that paleoenvironmental interpretations will potentially be influenced by postmortem changes in the fossil assemblages. In our material the most important source of error is the possibility of diagenetic destruction of

calcareous foraminifera and agglutinated forms with calcareous or organic cement.

The nature of the wall cement has been examined in specimens of *Ammodiscus*, *Haplophragmoides*, *Recurvoides*, *Ammobaculites*, *Trochammina* and *Glomospirella* from the Retziusfjellet Member; and in *Ammodiscus* from the Passet and Sjøgrenfjellet Members. The specimens were placed in 4% hydrochloric acid for 15 minutes and none of them showed dissolution effects.

In the marine Retziusfjellet Member calcareous ammonite shells and belemnite rostra are preserved (Fig. 2) not only in concretions, but also in the shales. Some of the ammonites show the inner nacreous layer. Furthermore, calcareous foraminifera are present in sample 48 taken from shale. These observations suggest that calcareous fossils are generally not dissolved in the Retziusfjellet Member.

In the marginal marine to nonmarine Passet and Sjøgrenfjellet Members no calcareous fossils were found. It is therefore difficult to decide from this study whether diagenetic dissolution of carbonate has occurred.

5. Environment of Sjøgrenfjellet and Passet Member

5.1. Foraminiferal assemblages.

This part of the Hårfagrehaugen section is characterized by the *Ammodiscus rugosus* and *Ammodiscus asper* assemblages, both of which consist wholly of arenaceous foraminifera. Nearly all specimens belong to the genus *Ammodiscus*, with a few representatives of *Haplophragmoides* and *Tolypammina*. The number of species per sample is extremely low and reaches a maximum of 5. Of 32 analysed samples, 14 were barren of foraminifera.

5.2. Distribution trends of Ammodiscus.

As shown by Phleger & Walton (1950), *Ammodiscus* occur in relatively small amounts in recent bay environments. On the other hand, Chamney (1977), in a study of Albian foraminifera from Canada, found representatives of *Ammodiscus* to occur in assemblages interpreted to be from the shallow normal marine shelf to the deeper slope. In general, the thicker and coarser forms occur in nearshore waters, while thinner and more siliceous forms indicate deeper conditions and low energy.

5.3. Interpretation.

The top of the Sjøgrenfjellet Member and base of the Passet Member must have been deposited under brackish conditions, probably in a lagoon or a bay (Fig. 4). Such conditions are indicated by the entirely arenaceous fauna with low diversity, high dominance, and the presence of coarsely agglutinated representatives of *Ammodiscus*. The lithology of the sequence supports this interpretation. The coarsening upwards sequences at the top of the Sjøgrenfjellet Member and base of the Passet Member probably represent barrier sand bodies.

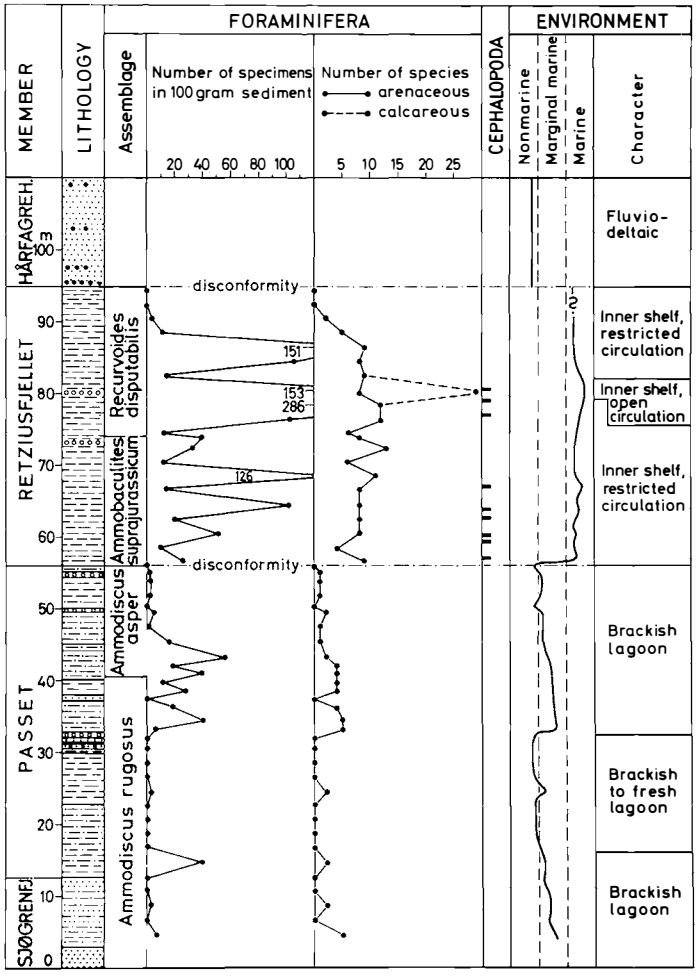

Fig. 4. *Distribution of main faunal parameters within the Hårfagrehaugen section and paleoenvironmental interpretation.*

Higher up in the section the conditions changed from brackish to partially fresh water as indicated by several samples barren of foraminifera. In the middle of the Passet Member the environment again became more brackish, and these conditions prevailed until the top of the member. The generally clayey and silty lithology of the sequence also suggests deposition in a sheltered lagoonal environment. The occurrence of coal seams in the upper half of the member indicates some kind of coastal vegetation.

6. Environment of Retziusfjellet Member

6.1. Foraminiferal assemblages.

The faunal sequence of this member is divided into the *Ammobaculites suprajurassicum* and *Recurvoides disputabilis* assemblages. Both consist mainly of arenaceous species, and the most common genera are *Haplophragmoides*, *Re-*

curvoides, *Ammobaculites*, *Trochammina*, and *Ammodiscus*. In addition to arenaceous genera, sample 48 contains many nodosariid forms belonging to *Astacolus*, *Lenticulina*, *Vaginulinopsis*, *Dentalina*, *Marginulina*, *Saracenaria*, and *Marginulinopsis*. The diversity is higher than in the underlying assemblages but still low when compared to many Jurassic assemblages from other areas. An exception is sample 48 as it contains 29 species. In addition to the foraminifera, cephalopods are quite common within the member and were found loose at nine horizons. Bivalves were observed only at one horizon.

6.2. Distribution trends of arenaceous genera.

Recent marginal marine assemblages frequently include large numbers of *Haplophragmoides*, *Trochammina*, and *Ammobaculites*, as shown by LOWMAN (1949) and PHLEGER & WALTON (1950), but these genera do also occur together in recent open sea environments (ELLISON 1951). The distribution of the same genera is discussed by CHAMNEY (1977) in Albian deposits in Arctic Canada. He considered *Haplophragmoides* to be fairly tolerant to fresh-water, but to reach its maximum in the marine environment of the outer shelf at an approximate depth of 130 m. *Ammobaculites* was found to be common in several marine environments from near-shore waters to the outer shelf. The primary environment of *Trochammina* was considered to be the marginal marine waters, but evolute forms of the genus appear to indicate depth with lower energy levels.

WALTON (1955) found a bimodal distribution of living *Recurvoides* in Todos Santos Bay (California) with one maximum lying shallower than 180 m and the second at approximately 500 m. A bimodal distribution appears also from the data presented by CHAMNEY (1977) from the Albian of Canada. The concentration of *Recurvoides* is here highest at depths 40–80 m and again at depths exceeding 200 m.

6.3. Distribution trends of Nodosariidae.

In the Jurassic, this group occupied ecological niches somewhat different from those of the present day. At that time, nodosariids characterized the middle and inner neritic region (BARNARD 1950; POKORNY 1958). GORDON (1970) pointed out that this group preferred shelf areas covered by terrigenous sediments containing some carbonate, whereas in extremely shallow waters, nodosariids and nodosariid-mixed assemblages seemed to disappear.

Since the Jurassic, Nodosariidae have retreated to deeper waters and decreased in relative abundance; thus today they populate more open waters attaining maximum frequency in the outer neritic and upper bathyal region.

6.4. Interpretation.

The faunal sequence of the Retziusfjellet Member indicates deposition in an inner shelf environment (Fig. 4). For the whole unit (except sample 48) we assume the presence of more or less stagnant conditions in the benthic boundary layer caused by restricted circulation of the bottom water coupled with a considerable supply of organic matter. This interpretation is based on: 1) the entirely arenaceous foraminiferal faunas with low diversities and only a slight

tendency to high dominance, 2) the generally fine-grained nature and dark colours of the sediment, 3) observations of pyritized nodules and ammonites, and 4) the occurrences of belemnites and ammonites which indicate normal salinity in the upper water layer.

The affinity of arenaceous foraminifera to more or less stagnant conditions has been suggested by several authors. TAPPAN (1955) reported that low diversity assemblages containing mostly arenaceous species are characteristic of black shale facies independent of age and area. MOORKENS (1976) discussed stagnant marine environments in different Early Tertiary sedimentary basins or North Western Europe. He assumed that arenaceous assemblages will be produced by the following factors: muddy sediment relatively rich in organic matter; weakly alkaline or slightly acidic pH-values; and negative or low positive Eh-values.

Sample 48 is of particular interest because of its mixed fauna. By its content of several nodosariid genera the fauna shows a principal similarity to typical Jurassic shelf assemblages described for instance from Europe north of Tethys. The presence of nodosariids in this part of the Retziusfjellet Member indicates that normal marine bottom conditions had replaced the stagnant environment for a short period. Supporting evidence for this interpretation is the lighter colour of the sediment.

7. Age and Correlation

The following discussion is based on foraminifera and (for the Retziusfjellet Member) also on ammonites. The age relations are summarized in Fig. 5. Information on the stratigraphical distribution of foraminifera are taken chiefly from the following papers: LOEBLICH & TAPPAN (1950), TAPPAN (1955), BROUWER (1969), BULYNNIKOVA et al. (1972), NORLING (1972), and SOUAYA (1976).

7.1. Sjøgrenfjellet and Passet Member — foraminifera.

The two assemblages recognized in these members show Lower Jurassic aspects. *Ammodiscus siliceus* and related forms are recorded mainly from the Lower Jurassic. The most abundant species in the upper part of the Passet Member, *Ammodiscus asper*, is commonly recorded from the Lower Jurassic. *Ammodiscus limitatus* is described from that series, with similar forms known from the Rhaetian and Middle Jurassic. Forms related to *Ammodiscus rugosus* occur in the Pliensbachian and Toarcian.

7.2. Retziusfjellet Member — foraminifera.

The assemblages occurring in this unit are characterized by Middle and Upper Jurassic species in addition to more long-ranging forms. The *Ammobaculites suprajurassicum* assemblage, which is present in the lower part of the member, contains the following species with occurrences concentrated to the Bathonian–Kimmeridgian interval of the Jurassic: *Ammobaculites suprajurassicum*, *Haplophragmoides canui*, *Recurvoides scherkalyensis*, *Textularia jurassica*, and *Trochammina gryci*.

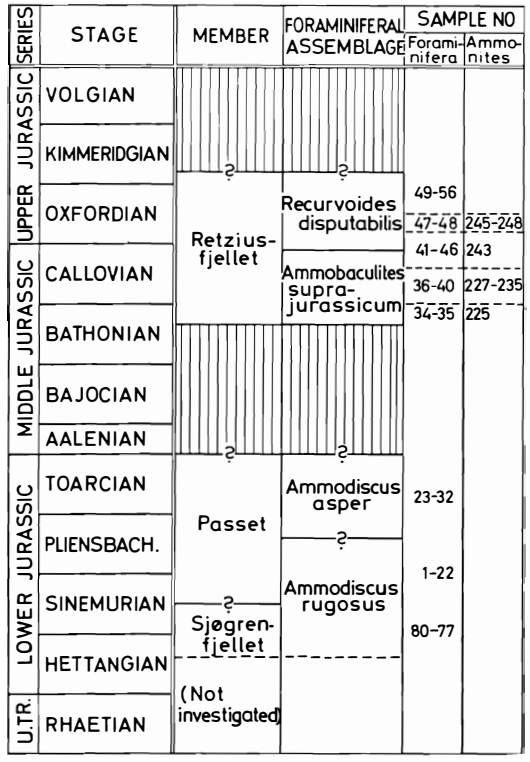

Fig. 5. *Age relationships in the Hårfagrehaugen section based on foraminifera and ammonites.*

The upper part of the Retziusfjellet member is characterized by the *Recurvoides disputabilis* assemblage. It contains the following species, which are mainly concentrated into the interval Callovian–Kimmeridgian: *Recurvoides disputabilis*, *Recurvoides eotrochus*, *Trochammina quinquelocularis*, *Ammodiscus cheradospirus*, *Haplophragmoides canuiformis*, *Lenticulina involvens*, *Lingulina praenodulosa*, *Lenticulina wisniowski*, *Saracenaria oxfordiana*, *Lenticulina pseudocrassa*, *Lenticulina rovnini*, *Vaginulinopsis ectypa*, and *Vaginulinopsis exodis*. The last three species are mainly recorded from the Oxfordian.

7.3. Retziusfjellet Member — ammonites.

The lowermost ammonite locality lies at the base of the member (Table 1) and contains *Arcticoceras* cf. *kochi* and *Cadoceras* sp. A closer determination is impossible because of the fragmentary nature of the material. In East Greenland the genus *Arcticoceras* occurs in the Upper Bathonian *Arcticoceras kochi* and *Cadoceras variable* Zones, while the first true *Cadoceras* appears in the latter unit (Callomon 1959).

Higher up in the sequence a *Pseudocadoceras* fauna occurs at six localities containing forms identical with or related to species described from Alaska. The most common species are *Pseudocadoceras chinitnense* and *Pseudocadoceras grewingki*, but in addition *Cadoceras* (*Stenocadoceras*) *multicostatum* is also found. In East Greenland *Pseudocadoceras* spp. appears in the Lower Callovian *Sigaloceras*

Table 1

LOCALITY NO.	METRES ABOVE BASE OF MEMBER	DETERMINATIONS	AGE
248	26,2	Cardioceras (C.) aff.cordatum (Sowerby 1813).	Lover Oxfordian
245	23,2	Cardioceras (C.) aff.cordatum (Sowerby 1813). Cardioceras (C.) excavatum (Sowerby 1815)	
243	21,4	Pseudocadoceras (?) sp.	Callovian?
235	11,4	Cadoceras (Stenocadoceras) multicostatum Imlay 1953. Pseudocadoceras chinitnense Imlay 1953.	Lower to Middle Callovian
231	7,6	Pseudocadoceras chinitnense Imlay 1953.	
230	6,4	Pseudocadoceras cf. grewingki (Pompeckj 1900).	
228	4,2	Pseudocadoceras grewingki (Pompeckj 1900).	
227	?	Pseudocadoceras chinitnense Imlay 1953.	
225	0.4	Arcticoceras cf. kochi Spath 1932 Cadoceras (C.) sp.	Upper Bathonian

List of ammonites identified from the Hårfagrehaugen section and the ages provided by this group.

calloviense Zone. The rich faunas which contain *Pseudocadoceras* and *Cadoceras* (*Stenocadoceras*) in Alaska are referred to the Lower and Middle Callovian by Imlay (1953).

The upper two ammonite localities contain *Cardioceras* aff. *cordatum* and *Cardioceras excavatum*. Both species are well known from Lower Oxfordian deposits (*cordatum* Zone) of England, Scotland and the Hebrides (Arkell 1933). The latter form is also recorded from Novaja Zemlja from sediments referred to the Lower Oxfordian (Dibner 1961).

7.4. Conclusions.

The foraminiferal assemblages indicate that the Passet Member and the upper part of the Sjøgrenfjellet Member should be referred to the Lower Jurassic. It must be noted in this connection that a Rhaetian-early Lower Jurassic age has been suggested for the Sjøgrenfjellet Member by Smith et al. (1976) and Bjærke (1977) on palynological evidences. Their investigation included, however, also older parts of the member.

The disconformity defining the upper boundary of the Passet Member is marked both by a lithological and a faunal break. The corresponding hiatus seems to include the Middle Jurassic probably up to the upper Bathonian.

Known occurrences of the foraminiferal species found in the Retziusfjellet Member are mainly concentrated in the Callovian–Kimmeridgian which is in

general accordance with the ages indicated by the ammonites. The base of the member belongs to the Upper Bathonian. The lower and middle parts of the member are referred to the Callovian and Lower Oxfordian. The upper part of the unit may contain Upper Oxfordian and somewhat younger strata but conclusive evidence is lacking in the studied section.

Systematic part

In this paper, some forty species of foraminifera are recorded. Most of these species are arenaceous. In certain determinations, open nomenclature "cf." and "aff." are used. In the synonymy lists, the original descriptions and one or two newer publications are mentioned. Illustrations of the various species are presented on Plates 1 to 6. Open nomenclature "sp." are omitted from the following account but are recorded in Fig. 3.

The foraminiferal classification employed in the paper follows the "Treatise on Invertebrate Paleontology", Part C (LOEBLICH & TAPPAN 1964).

The specimens figured on the plates will be deposited in the Paleontological Museum of the University of Oslo. The registration numbers of the specimens (e.g. A37831) refer to the collections of this museum.

Family SACCAMMINIDAE Brady 1884.

Psammosphaera? metensis (TERQUEM)
(Pl. 1, Fig. 13)

1862: *Annulina metensis* TERQUEM, p. 433, Pl. 5, Figs. 6a, b.
1969: *?Psammosphaera metensis* (TERQUEM)–BROUWER, p. 24, Pl. 1, Figs. 12–13.

Remarks: This species seems to be a flattened *Psammosphaera*.

Family AMMODISCIDAE REUSS 1862.

Ammodiscus asper (TERQUEM)
(Pl. 1, Figs. 6–7)

1864: *Involutina aspera* TERQUEM, p. 431, Pl. 10, Figs. 21a, b.
1955: *Involutina aspera* TERQUEM–TAPPAN, p. 38, Pl. 8, Figs. 10–13.
1969: *Ammodiscus asper* (TERQUEM)–BROUWER, p. 24, Pl. 1, Figs. 6–9.

Remarks: This species is rough and granular in appearance, with regular coiling.

Ammodiscus cheradospirus LOEBLICH & TAPPAN
(Pl. 1, Figs. 1–3)

1950: *Ammodiscus cheradospirus* LOEBLICH & TAPPAN, p. 6, Pl. 1, Figs. 1–2.
1960: *Involutina cheradospira* (LOEBLICH & TAPPAN) – WALL, p. 44, Pl. 2, Figs. 1–3.

Remarks: The individuals seem to be somewhat larger and more flattened than those described by LOEBLICH & TAPPAN (1950).

Ammodiscus limitatus (TERQUEM)
(Pl. 1, Figs. 8–10)

1864: *Involutina limitata* TERQUEM, p. 433, Pl. 10, Figs. 24a–b.
1976: *Ammodiscus* sp. cf. *A. limitatus* (TERQUEM)–SOUAYA, p. 264, Pl. 9, Fig. 13.

Ammodiscus rugosus TERQUEM
(Pl. 1, Figs. 11–12)

1886: *Ammodiscus rugosus* TERQUEM, p. 9, Pl. 1, Figs. 15a–b.
1976: *Ammodiscus* sp. cf. *A. rugosus* TERQUEM–SOUAYA, p. 264, Pl. 9, Fig. 22.

Remarks: The individuals have strongly granular wall, especially in the central part of the tests. The tests are concave and have an oval shape.

Ammodiscus siliceus (TERQUEM)

1862: *Involutina silicea* TERQUEM, p. 450, Pl. 6, Figs. 11a–b.
1960: *Involutina silicea* TERQUEM–BIZON, p. 4, Pl. 1, Figs. 2a, b; Pl. 4, Fig. 1.

Ammodiscus cf. *uglicus* EHREMEEVA

1972: cf. *Ammodiscus uglicus* EHREMEEVA–BULYNNIKOVA et. al. p. 35, Pl. 2, Figs. 1–4; Pl. 5, Figs. 1–8, 10, 11.

Remarks: Our specimens are larger in size than EHREMEEVA's species, mature individuals reaching a diameter of 0.4–0.5 mm.

Glomospirella aff. *otorica* ROMANOVA
(Pl. 6, Fig. 16)

1972: aff. *Glomospirella otorica* ROMANOVA–BULYNNIKOVA et al. p. 33, Pl. 1, Figs. 7–8.

Remarks: The specimens from Kong Karls Land have more flattened tests and are less regularly coiled than ROMANOVA's species.

Family LITUOLIDAE DE BLAINVILLE 1825.

Haplophragmoides barentsi n.sp.
(Pl. 3, Figs. 8–14)

Description: Test small, planispiral, periphery broadly rounded; chambers distinct, 10–15 in the last coil; sutures almost flush or very slightly depressed, weakly curved; a fairly deep umbilical depression in the central part occupies about one-third the diameter of the test; aperture a low arched slit at base of apertural face; wall finely arenaceous; colour yellowish gray.

Dimensions: The holotype has maximum diameter 0.55 mm, minimum diameter 0.48 mm, thickness 0.2 mm. Other specimens range from 0.45 to 0.55 mm in maximum diameter, 0.36 to 0.44 mm in minimum diameter, 0.17 to 0.22 mm in thickness.

Remarks: This species resembles *Haplophragmoides fistulosus*, BYKOVA 1953, but has a larger size and more chambers.

Occurrences and types: The species is found in sample 40, 41 and 43. The holotype is A37832 from sample 41.

Haplophragmoides canui CUSHMAN
(Pl. 1, Figs. 4–5)

1930: *Haplophragmoides canui* CUSHMAN, p. 133, Pl. 4, Figs. 1a–b.
1955: *Haplophragmoides canui* CUSHMAN–TAPPAN, p. 42, Pl. 9, Figs. 11–15.

Remarks: This species shows a great variability in thickness and general appearances, which is probably due to postmortem distortion in various planes. A similar situation is also reported by TAPPAN (1955). Our individuals are most similar to the more compressed specimens figured by TAPPAN (Pl. 9, Figs. 15a–b).

Haplophragmoides canuiformis DAIN
(Pl. 2, Figs. 1–2)

1972: *Haplophragmoides* (?) *canuiformis* DAIN–BULYNNIKOVA et al., p. 48, Pl. 8, Figs. 2, 3; Pl. 19, Fig. 2.

Haplophragmoides aff. *excavatus* CUSHMAN & WATERS
(Pl. 2, Figs. 3–6)

1927: aff. *Haplophragmoides excavatus* CUSHMAN & WATERS, p. 82, Pl. 10, Figs. 3a, b.
1976: aff. *Haplophragmoides excavatus* CUSHMAN & WATERS–SOUAYA, p. 267, Pl. 3, Fig. 13.

Remarks: Our individuals show a large degree of variation in size but most of them are slightly smaller and thinner than CUSHMAN & WATER's figured specimens.

Haplophragmoides kingakensis TAPPAN
(Pl. 6, Figs. 24–27)

1955: *Haplophragmoides kingakensis* TAPPAN, p. 43, Pl. 10, Figs. 1–6.
1972: *Haplophragmoides kingakensis* TAPPAN–NORLING, p. 43, Fig. 13B.

Remarks: According to TAPPAN (1955), this species shows a great variability. Our individuals are most similar to the smaller forms figured by TAPPAN on Pl. 10, Figs. 5a–b and Figs. 6a–b.

Recurvoides disputabilis DAIN
(Pl. 2, Figs. 10–11)

1972: *Recurvoides disputabilis* DAIN–BULYNNIKOVA et al., p. 55, Pl. 10, Figs. 6, 7; Pl. 11, Figs. 1–4; Pl. 19, Fig. 1.

Recurvoides eotrochus DAIN
(Pl. 2, Figs. 7–9)

1972: ?*Recurvoides eotrochus* DAIN–BULYNNIKOVA et al., p. 53, Pl. 9, Fig. 9; Pl. 10, Figs. 3–5.

Recurvoides scherkalyensis LEVINA
(Pl. 3, Figs. 5–7)

1972: *Recurvoides scherkalyensis* LEVINA–BULYNNIKOVA et. al. Pl. 9, Fig. 8; Pl. 10, Fig. 1.

Ammobaculites aff. *alaskaensis* TAPPAN
(Pl. 4, Figs. 13–14)

1955: aff. *Ammobaculites alaskaensis* TAPPAN, p. 43, Pl. 12, Figs. 1–10.
1976: aff. *Ammobaculites alaskaensis* TAPPAN–SOUAYA, p. 268, Pl. 5, Fig. 3.

Remarks: The chambers in the coil are slightly off-centre in some individuals and these appear almost trochoid instead of planispiral.

Ammobaculites suprajurassicum (SCHWAGER)
(Pl. 2, Figs. 12–13; Pl. 3, Figs. 3–4)

1865: *Haplophragmium suprajurassicum* SCHWAGER, p. 92, Pl. 2, Figs. 1a–b.
1960: *Ammobaculites suprajurassicum* (SCHWAGER)–LUTZE, p. 442, Pl. 26, Figs. 10–12; Pl. 27, Figs. 4–5.

Family TEXTULARIIDAE EHRENBERG 1838

Textularia jurassica (GÜMBEL)
(Pl. 6, Fig. 8)

1862: *Textilaria jurassica* GÜMBEL, p. 228, Pl. 5, Figs. 17a–b.
1960: *Textularia jurassica* (GÜMBEL)–BIELECKA, p. 115, Pl. 1, Fig. 6.

Family TROCHAMMINIDAE SCHWAGER 1877

Trochammina gryci TAPPAN
(Pl. 4, Figs. 1–2)

1955: *Trochammina gryci* TAPPAN, p. 50, Pl. 14, Figs. 12–14.
1969: *Trochammina gryci* TAPPAN–BROUWER, p. 26, Pl. 1, Figs. 24, 25.

Trochammina inflata (MONTAGU)
(Pl. 3, Figs. 1–2)

1808: *Nautilus inflatus* MONTAGU, p. 81, Pl. 18, Fig. 3.
1960: *Trochammina inflata* (MONTAGU)–LUTZE, p. 447, Pl. 28, Figs. 1–3.

*Trochammina quinqueloculari*s DAIN
(Pl. 6, Figs. 12–13)

1972: *Trochammina quinqueloculari*s DAIN–BULYNNIKOVA et al., p. 87, Pl. 24, Figs. 6, 8–10.

Trochammina sablei TAPPAN
(Pl. 6, Fig. 7)

1955: *Trochammina sablei* TAPPAN, p. 50, Pl. 14, Figs. 6–9.
1969: *Trochammina sablei* TAPPAN–BROUWER, p. 26, Pl. 1, Figs. 26, 27.

Trochammina cf. *septentrionalis* SCHAROVSKAJA
(Pl. 4, Figs. 3–4)

1972: cf. *Trochammina septentrionalis* SCHAROVSKAJA–BULYNNIKOVA *et al.*, Pl. 27, Fig. 5.

Remarks: Our individuals have less chambers in the last coil than SCHAROVSKAJA's species.

Trochammina squamata JONES & PARKER

1860: *Trochammina squamata* JONES & PARKER, p. 304.
1976: *Trochammina squamata* JONES & PARKER–SOUAYA, p. 275, Pl. 3, Fig. 17.

Trochammina squamataformis KAPTARENKO–CHERNOUSOVA
(Pl. 4, Figs. 5–6)

1959: *Trochammina squamataformis* KAPTARENKO–CHERNOUSOVA, p. 51, Pl. 8, Figs. 1–2.
1976: *Trochammina* sp. cf. *T. squamataformis* KAPTARENKO–CHERNOUSOVA–SOUAYA, p. 275, Pl. 11, Fig. 16.

Family NODOSARIIDAE EHRENBERG 1838

Astacolus cordiformis (TERQUEM)
(Pl. 4, Figs. 15–16)

1864: *Cristellaria cordiformis* TERQUEM, p. 413, Pl. 9, Fig. 14.
1972: *Astacolus* ex. gr. *cordiformis* (TERQUEM)–NORLING, p. 51, Fig. 22.

Astacolus ectypus LOEBLICH & TAPPAN
(Pl. 6, Figs. 21–23)

1950: *Astacolus ectypus* LOEBLICH & TAPPAN, p. 8, Pl. 1, Figs. 14–18.

Astacolus pediacus TAPPAN
(Pl. 5, Figs. 9–12)

1955: *Astacolus pediacus* TAPPAN, p. 56, Pl. 17, Figs. 1–10.
1969: *Astacolus pediacus* TAPPAN–SOUAYA, p. 277, Pl. 8, Fig. 20.

Astacolus aff. *quadricostatus* (TERQUEM)
(Pl. 6, Figs. 14–15)

1863: aff. *Marginulina quadricostata* Terquem, p. 190, Pl. 8, Fig. 12.
Remarks: TERQUEM's figured specimen is more slender than our species.

Dentalina aff. *primaeva* D'ORBIGNY
(Pl. 4, Figs. 7–8)

1850: aff. *Dentalina primaeva* D'ORBIGNY, p. 242.
1936: aff. *Dentalina primaeva* D'ORBIGNY–MACFADYEN, p. 150, Pl. 1, Fig. 260.
Remarks: Our individuals have less chambers and are also less inflated than D'ORBIGNY's species.

Lenticulina involvens (WISNIOWSKI)
(Pl. 6, Figs. 17–20)

1890: *Cristellaria involvens* WISNIOWSKI, p. 224, Pl. 9, Fig. 32.
1976: *Lenticulina involvens* (WISNIOWSKI)–SOUAYA, p. 278, Pl. 8, Fig. 23.

Lenticulina pseudocrassa (MYATLYUK)
(Pl. 5, Figs. 13–16)

1954: *Cristellaria pseudocrassa* MYATLYUK, p. 104, Pl. 26, Figs. 8a–b.
1976: *Lenticulina pseudocrassa* (MYATLYUK)–SOUAYA, p. 278, Pl. 8, Fig. 14.

Lenticulina rovnini (DAIN)
(Pl. 6, Figs. 10–11)

1972: *Astacolus rovnini* DAIN–BULYNNIKOVA et al., Pl. 38, Figs. 7–8.

Lenticulina wisniowskii (MYATLYUK)
(Pl. 4, Figs. 17–19)

1939: *Cristellaria wisniowskii* MYATLYUK, pp. 57, 73, Pl. 4, Fig. 43.
1976: *Lenticulina* sp. cf. *L. wisniowskii* (MYATLYUK)–SOUAYA, Pl. 6, Fig. 20.

Marginulina aff. *caelata* LOEBLICH & TAPPAN
(Pl. 4, Figs. 9–12)

1950: aff. *Marginulina caelata* LOEBLICH & TAPPAN, p. 46, Pl. 12, Figs. 10a–b

Remarks: The specimens from Kong Karls Land show a more central aperture and a larger coil than those figured by LOEBLICH & TAPPAN (1955).

Saracenaria oxfordiana TAPPAN
(Pl. 5, Figs. 1–4)

1955: *Saracenaria oxfordiana* TAPPAN, p. 64, Pl. 26, Fig. 27.
1976: *Saracenaria oxfordiana* TAPPAN–SOUAYA, p. 280, Pl. 8, Fig. 15.

Vaginulinopsis ectypa LOEBLICH & TAPPAN
(Pl. 5, Figs. 5–8)

1950: *Vaginulinopsis ectypa* LOEBLICH & TAPPAN, p. 46, Pl. 12, Figs. 17–20.

Vaginulinopsis enodis LOEBLICH & TAPPAN

1950: *Vaginulinopsis enodis* LOEBLICH & TAPPAN, p. 46, Pl. 12, Figs. 11–16.

Lingulina praenodulosa (DAIN)
(Pl. 6, Figs. 1–6)

1972: *Geinitzinita praenodulosa* DAIN–BULYNNIKOVA et al., p. 108, Pl. 33, Figs. 1–5.

Family POLYMORPHINIDAE D'ORBIGNY 1839
Eoguttulina bilocularis (TERQUEM)
(Pl. 6, Fig. 9)

1864: *Polymorphina bilocularis* TERQUEM, p. 293, Pl. 11, Figs. 9–32.
1960: *Eoguttulina bilocularis* (TERQUEM)–BIELECKA, p. 143, Pl. 7, Fig. 60.

Acknowledgements

The authors wish to thank the following persons for critical reading and improvement of the manuscript: Dr. JACOB G. VERDENIUS, Continental Shelf Institute, Trondheim; Dr. DAVID WORSLEY, Paleontological Museum, University of Oslo; BARRIE DALE and ADRIAN READ, Institute of Geology, University of Oslo.

References

ARKELL, W. J., 1933: *The Jurassic system in Great Britain.* Oxford University Press. 681 pp.

BARNARD, T., 1950a: The uses of foraminifera in Lower Jurassic stratigraphy. *Intern. Geol. Congr., 18th, London, 1948. Rept.* **15:** 34–41.

— 1950b: Foraminifera from the Upper Lias of Byfield, Northamptonshire. *Quart. J. Geol. Soc., London* **106:** 1–36.

BIELECKA, W., 1960: Stratygrafia mikropaleontologiczna dolnego malmu okolic Chrzanowa. *Inst. Geol. Prace 33*: 1–155. (Micropaleontological stratigraphy of the Lower Malm in the vicinity of Chrzanóv).

BIZON, G., 1960: Révision de quelques espèces-types de Foraminifères du Lias du Basin Parisien de la collection Terquem. *Rev. Micropaléontol.* **3**(1): 3–18.

BJÆRKE, T., 1977: Mesozoic Palynology of Svalbard — II. Palynomorphs from the Mesozoic sequence of Kong Karls Land. *Norsk Polarinstitutt Årbok* 1976: 83–120.

BJÆRKE, T. & B. THUSU, 1976: Cretaceous Palynomorphs from Spitsbergen-banken, NW Barents Shelf. *Norsk Polarinstitutt Årbok* 1974: 258–262.

BROOKE, M. M. & W. K. BRAUN, 1972: *Biostratigraphy and microfaunas of the Jurassic system of Saskatchewan.* Report no. 161: 1–83.

BROUWER, J., 1969: Foraminiferal assemblages from the Lias of NW. Europe. *Ver. K. Ned. Akad. Wet., Afd. Natuurk.* **1**(25) No. 4. 48 pp.

BULYNNIKOVA, S. P., DAIN, L. G., KOSYREVA, V. F., KOMISSARENKO, V. K., LEVINA, V. I., & K. E. TYLKINA, 1972: Foraminifera of the Upper Jurassic deposits of western Siberia. **In:** DIAN, L. G. (Ed.) *All-Union Petroleum Scientific-Research Geological-Prospecting Inst. (VNIGRI), Trans. (Trudy)* **317.** 273 pp. (Russian).

CALLOMON, J. H., 1959: The ammonite Zones of the Middle Jurassic beds of East Greenland *Geol. Mag.* **96:** 505–513.

CHAMNEY, T. P., 1977: Foraminiferal morphogroup symbol for paleoenvironmental interpretation of drill cutting samples: Arctic America. Ist. Int. Symp. on Benthonic Foraminifera of Continental Margins. Part B. Paleoecology and Biostratigraphy. *MARITIME SEDIMENTS Spec. Pub.* **1:** 585–624.

CIFELLI, R., 1959: Bathonian foraminifera of England. *Bull. Mus. Comp. Zool. Cambridge* **121:** 265–368.

CORDEY, W. G., 1962: Foraminifera from the Oxford Clay of Staffin Bay, Isle of Skye, Scotland. *Senckenb. Lethaia* **43:** 375–409.

CUSHMAN, J. A., 1930: Note sur quelques foraminifères jurassiques d'Auberville (Calvados). *Soc. Linn. Normandie, Bull.* Ser. 8, **2:** 132–135.

CUSHMAN, J. A. & J. A. WATERS, 1927: Some arenaceous foraminifera from the Upper Cretaceous of Texas. *Cushman Lab. Foram. Res., Contr.* **2** (4): 81–85.

DIBNER, V. D., 1961: The stratigraphy of Upper Triassic and Jurassic deposits of the islands of the Barents-Kara Shelf and the mountains of Taimyr. Reprints of *Acad. Sci. USSR. Geology* **139** (4): 947–949.

EDWARDS, M., 1976: Gravel fraction on the Spitsbergen Bank, NW Barents Shelf. *Norges Geol. Unders.* **316:** 205–217.

EDWARDS, M., T. BJÆRKE, J. NAGY, T. S. WINSNES, & D. WORSLEY, 1979: Mesozoic Stratigraphy of Eastern Svalbard: a Discussion. *Geol. Mag.* **116:** 49–54.

ELLISON, S. P., Jr., 1951: Microfossils as environment indicators in marine shales. *Jour. Sedimentary Petrology* **21:** 214–255.

GIBSON, L. B., 1966: Some unifying characteristics of species diversity. *Cushman Found. Foram. Research Contr.* **17:** 117–124.

GORDON, W. A., 1970: Biogeography of Jurassic Foraminifera. *Geol. Soc. Am. Bull.* **81:** 1689–1704.

GÜMBEL, C. W. 1862: Die Streitberger Schlammlager und ihres Foraminiferen Einschlüsse. *Jb. Ver. Vaterländ Naturk. Württemberg* **18.**

IMLAY, R. W., 1953: Callovian (Jurassic) ammonites from the United States and Alaska. *U.S. Geol. Survey Prof. Paper* **249**-B: 41–108.

JONES, T. R. & W. K. PARKER, 1860: On the Rhizopodal fauna of the Mediterranean, compared with that of the Italian and some other Tertiary deposits. *Geol. Soc. London, Quart. Jour.* **16.**

KAPTARENKO-CHERNOUSOVA, O. K., 1959: Jurassic foraminifera from the Dnieper-Donets Basin. *Akad. Nauk Ukrain. RSR, Inst. Geol. Nauk, Ser. Strat. Pal. Trudi* **15:** 1–121. (Ukrainian).

KLUBOV, B. A., 1970: The Triassic and Jurassic deposits of Wilhelmøya. **In:** *Geology of Spitsbergen*, 1965, transl. J. E. BRADLEY (ed. W. B. HARLAND). Boston. Spa N.L.L. 1970: 182–192 (from the Russian ed. V. N. SOKOLOV, Leningrad 1965).

LOEBLICH, A. R. & H. TAPPAN, 1950a: North American Jurassic foraminifera: I. The type Redwater shale (Oxfordian) of South Dakota. *Journal Paleont.* **24:** 39–60.

LOEBLICH, A. R. & H. TAPPAN, 1950b: North American Jurassic foraminifera. II. Characteristic western interior Callovian species. *Washington Acad. Sci., Jour.* **40:** 5–19.

LOEBLICH, A. R. & H. TAPPAN, 1964: Sarcodina, chiefly "Thecamoebians" and Foraminiferida. **In:** MOORE, R. C., Ed., *Treatise on Invertebrate Paleontology*, Part C, Protista 2. I–II. Geol. Soc. Amer. and Univ. Kansas Press. 900 pp.

LOWMAN, S. W., 1949: Sedimentary Facies in the Gulf Coast. *Bull. Amer. Assoc. Petrol. Geol.* **33:** 1939–1997.

LUTZE, G. F., 1960: Zur Stratigraphie und Paläontologie des Callovien und Oxfordien in Nordwest-Deutschland. *Geol. Jahrb.* **77:** 391–532.

MACFADYEN, W. A., 1936: d'Orbigny's Lias foraminifera. *Roy. Micr. Soc. London, Jour.* ser. 3, **56.**

MELLO, J. F., 1971: Foraminifera from the Pierre Shale (Upper Cretaceous) at Red Bird, Wyoming. *Geol. Survey Prof. Paper* **393**-C: 1–54.

MONTAGU, G., 1808: *Supplement to Testacea Britannica.* 183 pp. S. Woolmer (Exeter, England).

MOORKENS, T. L., 1976: Palökologische Bedeutung einiger Vergesellschaftungen von sandschaligen Foraminiferen aus dem NW europäischen Alttertiär und ihre Beziehung zu Muttergesteinen. Sonderdruck aus dem COMPENDIUM 75/76. Erganzungsband der Zeitschrift *Erdöl und Kohle, Erdgas, Petrochemie*: 77–95.

MURRAY, J., 1973: *Distribution and ecology of living benthic foraminiferids.* Heinemann Educational Books, 48 Charles Street, London. 274 pp.

MYATLYUK, E. V., 1939: Foraminifera from the Jurassic of the Nordvik oil district. **In:** MUTAFI, N. N., and others, Geology and mineral resources of the Yenisei-Lena region, Part I. *Arctic Inst.* (*Komissiya po Severu*), *Irans.* **126.** 276 pp. (Russian).

— 1954: **In:** SHOKHINA, V. A., Foraminifera from the Jurassic and Cretaceous of Gorki Oblast. Yses. Nauchno-Issled. Geol.-Razved. Neft. Inst. (VNIGRI) (All-Union Scientific-Research Geological-Prospecting Petroleum Institute). *Pal. Sbornik* **1:** 99–117. (Russian).

NAGY, J., 1973: Fossilførende blokker av mesozoisk alder fra Svalbardbanken. *NTNF's Kontinentalsokkelprosjekt Publ.* **42:** 1–26.

NATHORST, A. G., 1901: Bidrag til Kung Karls Lands geologi. *Geol. Förh.* **23:** 341–378.

NORLING, E., 1972: Jurassic stratigraphy and foraminifera of Western Scania, Southern Sweden. *Sveriges Geol. Unders.* Ser. Ca, **47:** 1–120.

NØRVANG, A., 1957: The Foraminifera of the Lias Series in Jutland, Denmark, *Medd. Dansk Geol. Foren.* **13:** 1–135.

D'ORBIGNY, A. D., 1850: *Prodrome de paléontologie stratigraphique universelle des animaux mollusques et rayonnés.* Paris, V. Masson, 1.

PHLEGER, F. B. & W. R. WALTON, 1950: Ecology of march and bay foraminifera, Barnstab Mass. *Amer. Journ. Sci.* **248:** 274–294.

POKORNÝ, V., 1958: *Grundzüge der zoologischen Mikropaläontologie*, Band I. VEB Deutscher Verlag der Wissenschaften. 582 pp.

SCHWAGER, C., 1865: Beitrag zur Kenntniss der mikroskopischen Fauna jurassischer Schichten. *Ver. Vaterl. Naturk. Württemberg, Jahreshefte, Stuttgart, 21.*

SMITH, D. G., W. B. HARLAND, N. F. HUGHES & C. A. G. PICKTON, 1976: The geology of Kong Karls Land, Svalbard. *Geol. Mag.* **113:** 193–232.

SOUAYA, F. J., 1976: Foraminifera of Sun-Gulf-Global Linckens Island Well P-46, Arctic Archipelago, Canada. *Micropaleontology* **22**: 249–306.

TAPPAN, H., 1955: Foraminifera from the arctic slope of Alaska. Part 2, Jurassic foraminifera. *U.S. Geol. Survey, Prof. Paper* **236**-B: 21–90.

TERQUEM, O., 1862: Recherches sur les foraminifères du Lias; second mémoire. *Acad. Imp. Metz. mém.* année 42 (sér. 2, année 9): 1860–1861.

— 1863: Troisième mémoire sur les foraminifères du Lias des départements de la Moselle, de la Cote d'Or, du Rhône, de la Vienne et du Calvados. *Acad. Imp. Metz*, année 44 (sér. 2, année 11, pt. 2): 1862–1863.

— 1864: *Quatrième mémoires sur les foraminifères du Lias, comprenant les Polymorphines des départements de la Moselle, de la Cote d'Or et de l'Indre*. Metz, Lorette.

— 1886: Les foraminifères et les ostracodes du Fuller's earth des environs de Varsovie. *Soc. Géol. France, Mém.* sér. 3, 4: 1–112.

WALL, J. H., 1960: Jurassic Microfaunas from Saskatchewan. *Dept. Mineral Resources, Rept.* **53**: 1–229.

WALTON, W. R., 1955: Ecology of living benthonic foraminifera, Todos Santos Bay, Baja California. *Journal of Paleontology* **29**: 952–1018.

— 1964: Recent foraminiferal ecology and paleoecology. **In:** J. IMBRIE & N. NEWELL (Eds.) *Approaches to paleoecology*: 151–237. New York: John Wiley and Sons, Inc.

WIŚNIOWSKI, T., 1890: Mikrofauna ilów ornatowych okolicy Krakowa; Cześć I — Otwornice górnego Kellowayu w Grojcu (Microfauna of the Ornatus clay in the vicinity of Krakow; Part I — Foraminifera of the upper Callovian of Grojec) *Akad. Umiej. Krakowie, Wydz. Mat.-Przyr., Pamietnik* **17**: 181–242. (Polish).

Plates 1—6

PLATE 1

Figs. 1–3. *Ammodiscus cheradospirus* LOEBLICH & TAPPAN ..... (p. 75)
1–2: Side views of two megalospheric specimens (A37811 and A37812, respectively) from sample 50; × 23.
3: Side view of a microspheric specimen (A37813) from sample 51; × 23.

Figs. 4–5. *Haplophragmoides canui* CUSHMAN ..... (p. 76)
4: Umbilical side, 5: spiral side of a specimen (A37814) from sample 47; × 75.

Figs. 6–7. *Ammodiscus asper* (TERQUEM) ..... (p. 75)
Side views of two specimens (A37815 and A37816, respectively) from sample 26; × 23.

Figs. 8–10. *Ammodiscus limitatus* (TERQUEM) ..... (p. 75)
8–9: Side views of two specimens (A37817 and A37818, respectively) from sample 24; × 46.
10: Side view of a specimen (A37819) from sample 2; × 24.

Figs. 11–12. *Ammodiscus rugosus* (TERQUEM) ..... (p. 75)
Side views of two specimens (A37820 and A37821, respectively) from sample 21; × 46.

Fig. 13. *Psammosphaera ? metensis* (TERQUEM) ..... (p. 74)
Specimen (A37822) from sample 47; × 42.

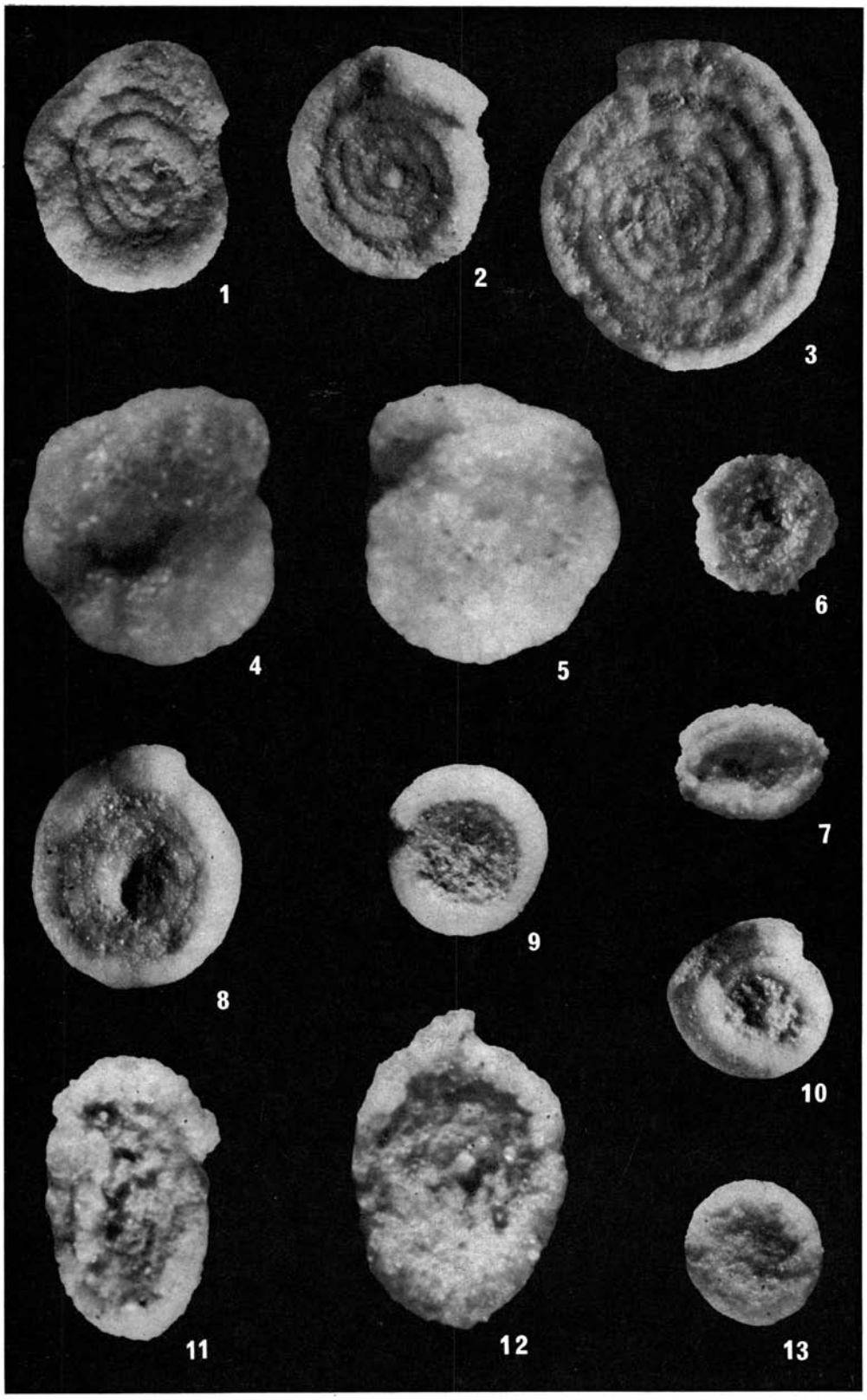
1
2
3
4
5
6
7
8
9
10
11
12
13

PLATE 2

Figs. 1–2. *Haplophragmoides canuiformis* DAIN ..... (p. 76)
Opposite sides of a specimen (A37823) from sample 47; × 62.

Figs. 3–6. *Haplophragmoides* aff. *excavatus* CUSHMAN & WATERS ..... (p. 76)
Opposite sides of two specimens (A37824 and A37825, respectively) from sample 41; × 62.

Figs. 7–9. *Recurvoides eotrochus* DAIN ..... (p. 77)
7: Spiral side, 8: edge view, 9: umbilical side of a specimen (A37826) from sample 47; × 74.

Figs. 10–11. *Recurvoides disputabilis* DAIN ..... (p. 77)
10: Spiral side, 11: umbilical side of a specimen (A37827) from sample 47; × 62.

Figs. 12–13. *Ammobaculites suprajurassicum* (SCHWAGER) ..... (p. 77)
Opposite sides of a specimen (A37828) from sample 41; × 71.

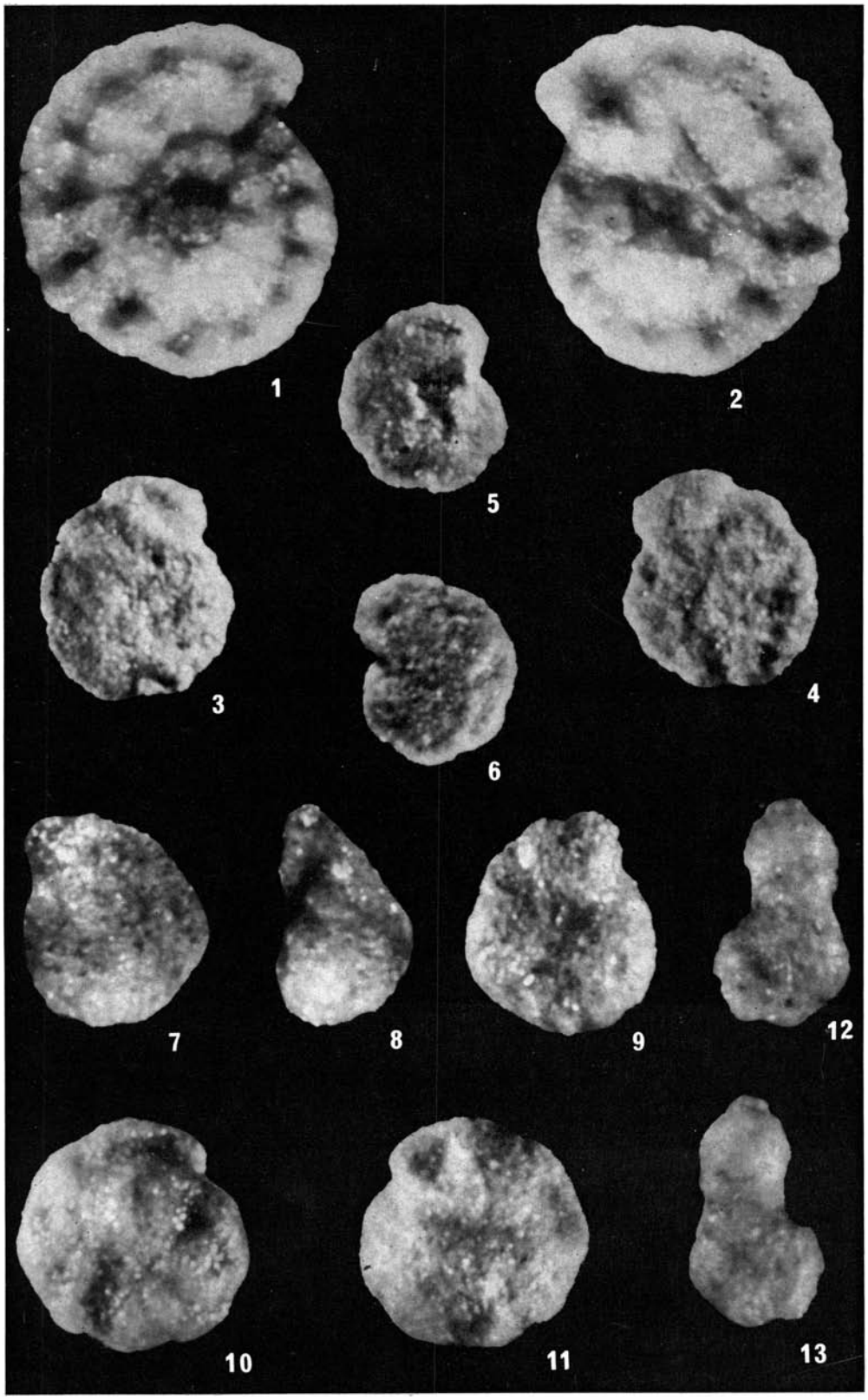
1
2
5
3
4
6
7
8
9
12
10
11
13

PLATE 3

Figs. 1–2. *Trochammina inflata* (MONTAGU) ..... (p. 78)
1: Spiral side, 2: umbilical side of a specimen (A37829) from sample 43; × 72.

Figs. 3–4. *Ammobaculites suprajurassicum* (SCHWAGER) ..... (p. 77)
Opposite sides of a specimen (A37830) from sample 41; × 72.

Figs. 5–7. *Recurvoides scherkalyensis* LEVINA ..... (p. 77)
5: Spiral side, 6: umbilical side, 7: apertural view of a specimen (A37831) from sample 47; × 72

Figs. 8–14. *Haplophragmoides barentsi* n.sp. ..... (p. 76)
8 and 10: Opposite sides, 9: apertural view of the holotype (A37832) from sample 41; × 69.
11: apertural view, 12–13: opposite sides of a specimen (A37833) from sample 41; × 76.
14: side view of a specimen (A37834) from sample 40; × 76.

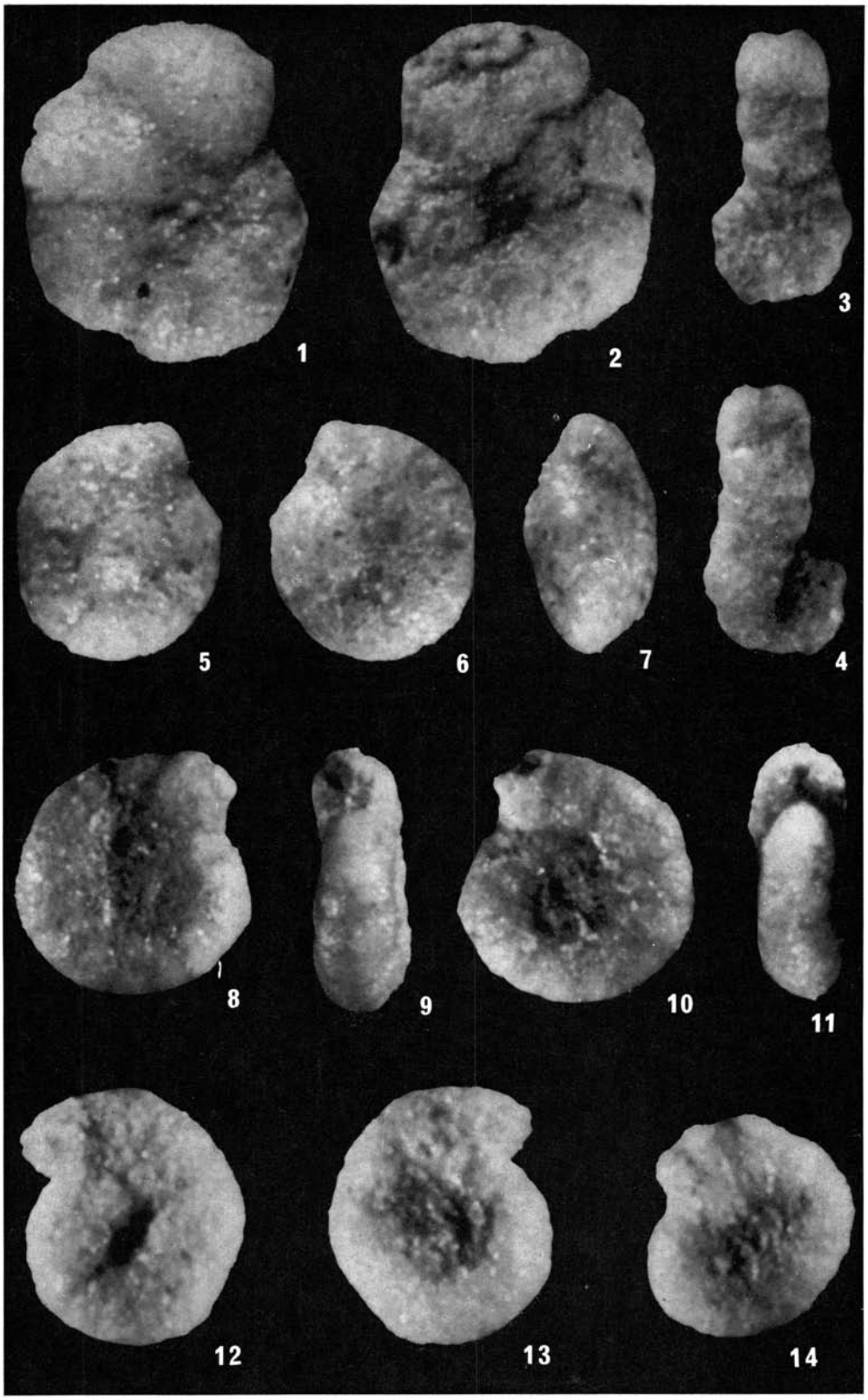
1
2
3
5
6
7
4
8
9
10
11
12
13
14

PLATE 4

Figs. 1–2. *Trochammina gryci* TAPPAN ..... (p. 77)
1: Umbilical side, 2: spiral side of a specimen (A37835) from sample 43; × 72.

Figs. 3–4. *Trochammina* cf. *septentrionalis* SCHAROVSKAJA ..... (p. 78)
3: Umbilical side, 4: spiral side of a specimen (A37836) from sample 43; × 31.

Figs. 5–6. *Trochammina squamataformis* KAPTARENKO-CHERNOUSOVA ..... (p. 78)
5: Umbilical side, 6: spiral side of a specimen (A37837) from sample 41; × 72.

Figs. 7–8. *Dentalina* aff. *primaeva* D'ORBIGNY ..... (p. 79)
Opposite sides of a specimen (A37838) from sample 48; × 70.

Figs. 9–12. *Marginulina* aff. *caelata* LOEBLICH & TAPPAN ..... (p. 79)
9: Side view, 10: apertural view, 11: coil side, 12: peripheral view of a specimen (A37839) from sample 48; × 71.

Figs. 13–14. *Ammobaculites* aff. *alaskaensis* TAPPAN ..... (p. 77)
Opposite sides of a specimen (A37840) from sample 38; × 72.

Figs. 15–16. *Astacolus cordiformis* (TERQUEM) ..... (p. 78)
15: Side view, 16: peripheral view of a specimen (A37841) from sample 48; × 72.

Figs. 17–19. *Lenticulina wisniowskii* (MYATLYUK) ..... (p. 79)
17–18: Opposite sides, 19: apertural view of a specimen (A37842) from sample 48; × 70.

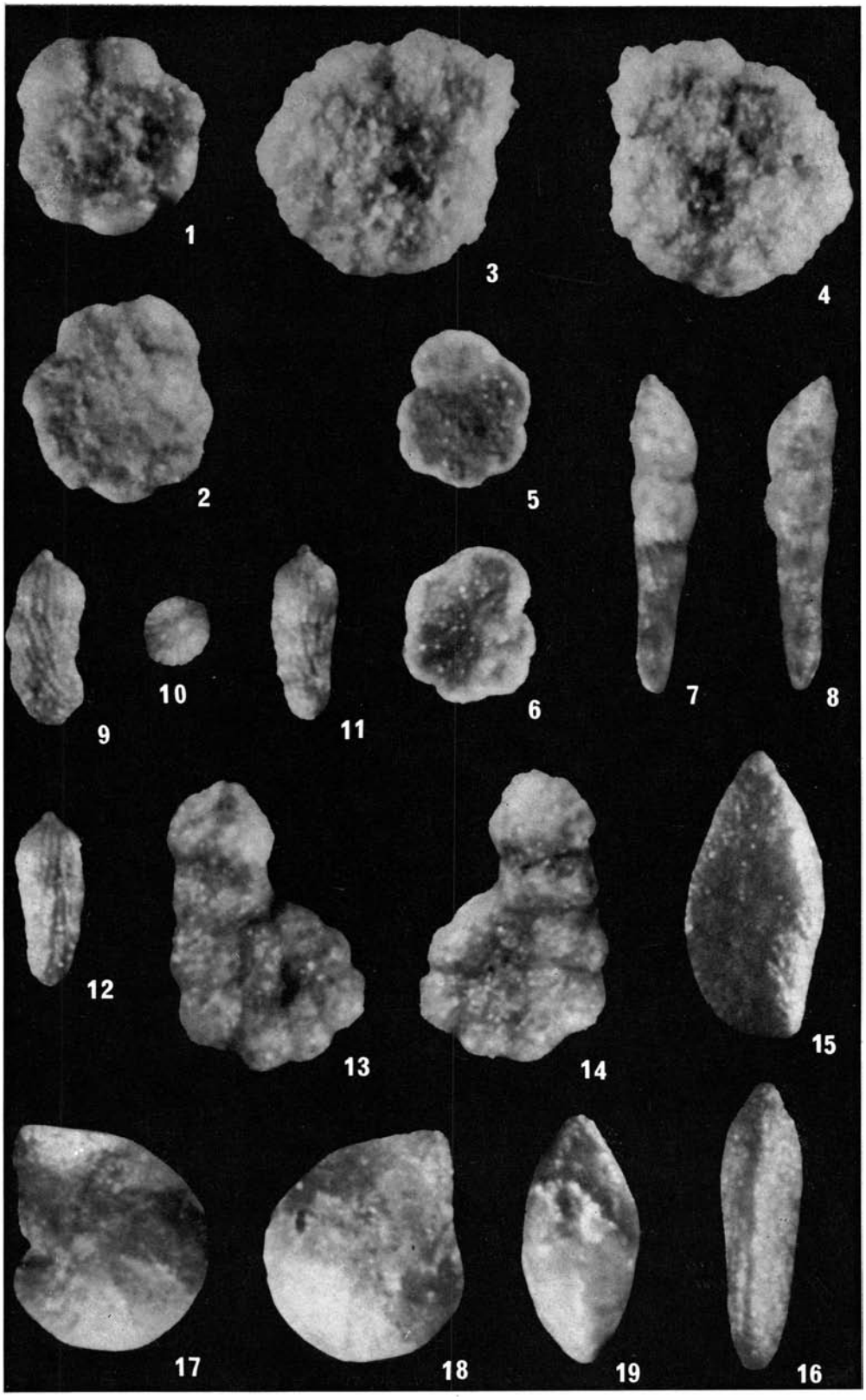
1
3
4
2
5
7
8
9
10
11
6
12
13
14
15
17
18
19
16

PLATE 5

Figs. 1–4. *Saracenaria oxfordiana* TAPPAN ..... (p. 79)
1–2: Opposite sides, 3: apertural view, 4: peripheral view of a specimen (A37843) from sample 48; × 71.

Figs. 5–8. *Vaginulinopsis ectypa* LOEBLICH & TAPPAN ..... (p. 79)
5–6: Opposite sides, 7: apertural view, 8: peripheral view of a specimen (A37844) from sample 48; × 69.

Figs. 9–12. *Astacolus pediacus* TAPPAN ..... (p. 78)
9–10: Opposite sides, 11: apertural view, 12: peripheral view of a specimen (A37845) from sample 48; × 71.

Figs. 13–16. *Lenticulina pseudocrassa* (MYATLYUK) ..... (p. 79)
13–14: Opposite sides, 15: apertural view, 16: peripheral view of a specimen (A37846) from sample 48; × 71.

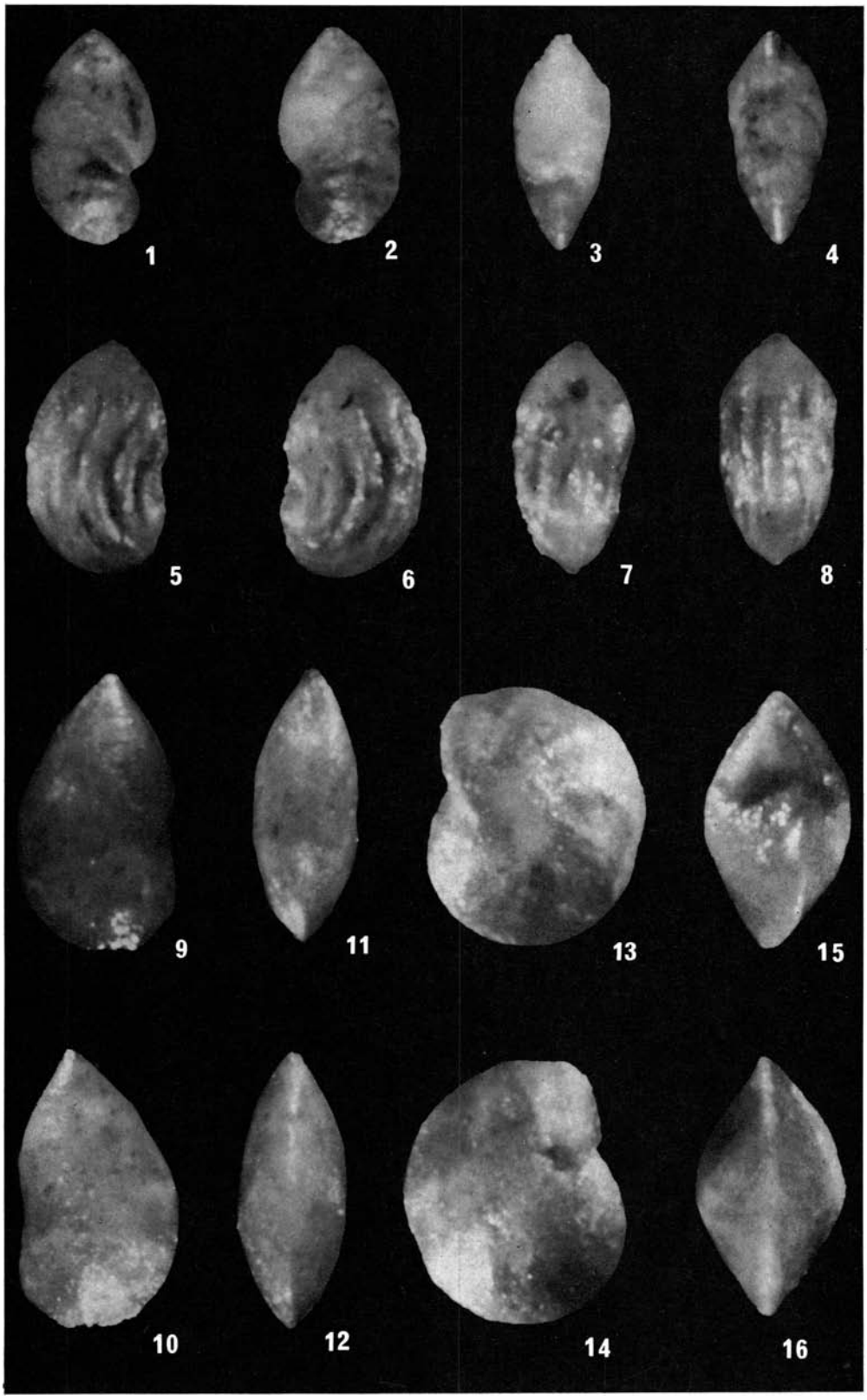
1
2
3
4
5
6
7
8
9
11
13
15
10
12
14
16

PLATE 6

Figs. 1–6. *Lingulina praenodulosa* (DAIN) ..... (p. 80)
1: Side view, 2: edge view, 3: apertural view of a megalospheric specimen (A37847) from sample 48; × 74.
4: Side view, 5: edge view, 6: apertural view of a microspheric specimen (A37848) from sample 48; × 69.

Fig. 7. *Trochammina sablei* TAPPAN ..... (p. 78)
Side view of a specimen (A37849) from sample 41; × 71.

Fig. 8. *Textularia jurassica* (GÜMBEL) ..... (p. 77)
Side view of a specimen (A37850) from sample 47; × 69.

Fig. 9. *Eoguttulina bilocularis* (TERQUEM) ..... (p. 80)
Side view of a specimen (A37851) from sample 48; × 70.

Figs. 10–11. *Lenticulina rovnini* (DAIN) ..... (p. 79)
10: Side view, 11: apertural view of a specimen (A37852) from sample 48; × 71.

Figs. 12–13. *Trochammina quinquelocularis* DAIN ..... (p. 78)
12: Umbilical side, 13: spiral side of a specimen (A37853) from sample 46; × 75.

Figs. 14–15. *Astacolus* aff. *quadricostatus* (TERQUEM) ..... (p. 79)
Opposite sides of a specimen (A37854) from sample 48; × 71.

Fig. 16. *Glomospirella* aff. *otorica* ROMANOVA ..... (p. 75)
Side view of a specimen (A37855) from sample 49; × 71.

Figs. 17–20. *Lenticulina involvens* (WISNIOWSKI) ..... (p. 79)
17–18: Opposite sides, 19: apertural view, 20: peripheral view of a specimen (A37856) from sample 48; × 71.

Figs. 21–23. *Astacolus ectypus* LOEBLICH & TAPPAN ..... (p. 78)
21: Side view, 22: apertural view, 23: peripheral view of a specimen (A37857) from sample 48; × 72.

Figs. 24–27. *Haplophragmoides kingakensis* TAPPAN ..... (p. 76)
24–25: Opposite sides, 26: apertural view of a specimen (A37858) from sample 41; × 74.
27: Side view of a specimen (A37859) from sample 41; × 71.

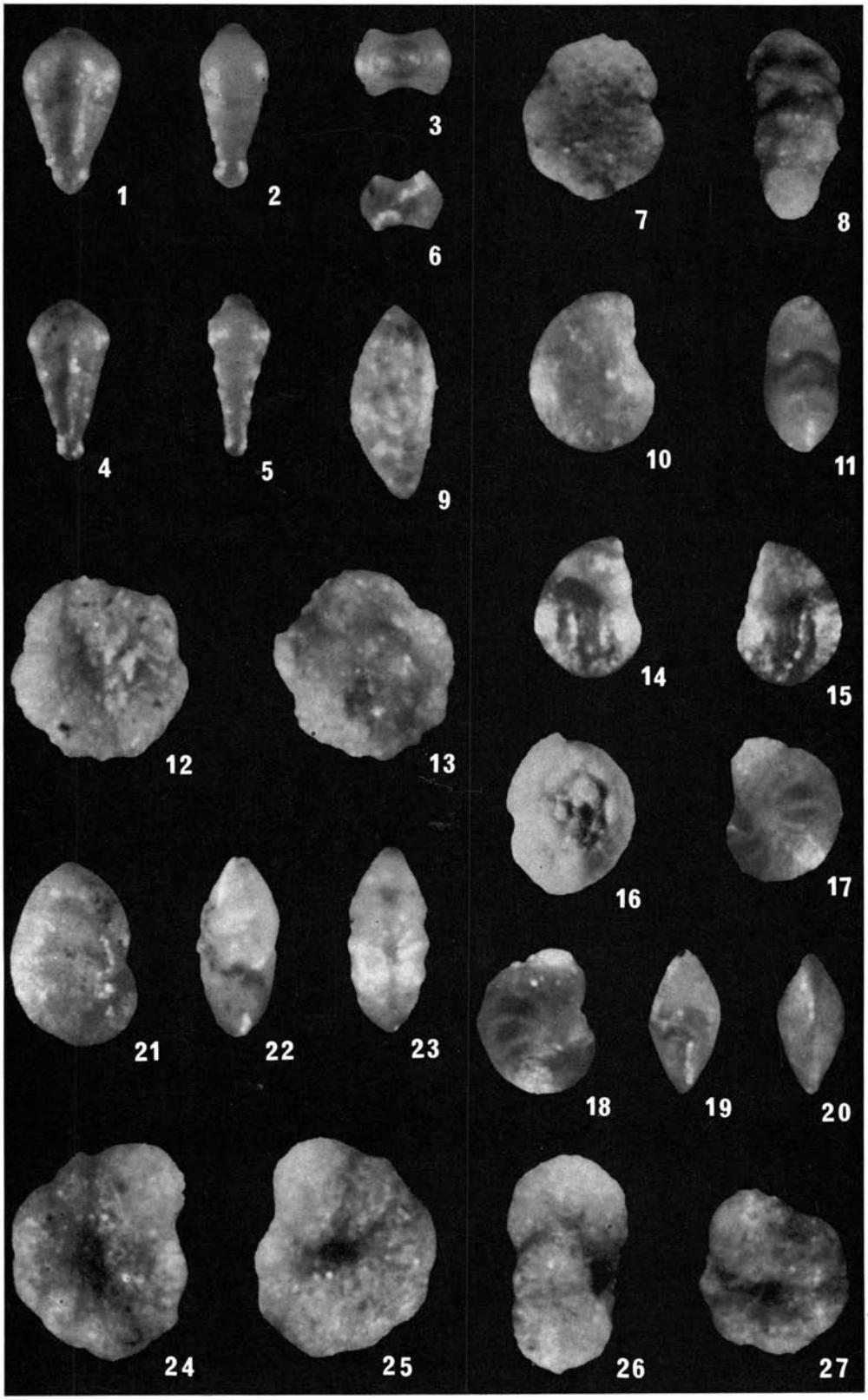
1
2
3
6
7
8
4
5
9
10
11
12
13
14
15
16
17
21
22
23
18
19
20
24
25
26
27

The sedimentology of the Janusfjellet Formation, Central Spitsbergen (Sassenfjorden and Agardhfjellet areas)

By Henning Dypvik[1]

Abstract

Detailed mineralogical and geochemical analyses of the Janusfjellet Formation have been carried out in order to provide more information concerning its depositional and diagenetic history.

The results have shown that the Upper Jurassic Agardhfjellet Member, deposited in an open shelf environment during a transgressive phase, is characterized by more stagnant conditions than the Lower Cretaceous Rurikfjellet Member. The Rurikfjellet Member, slightly enriched in volcanogenic components compared to the Agardhfjellet Member, displays regressive shelf sedimentation ending in prodeltaic to delta front depositional environments. Based on the sedimentpetrographical analyses, each member is divided into minor regressive and transgressive phases, probably reflecting tectonic activity or eustatic sea level variations.

Clay minerals, organic matter and iron oxides are the main cements in the shaly parts, while a more complex diagenetic history involving both quartz and carbonate cementation has taken place in the few silty/sandy units.

I. Introduction

The Janusfjellet Formation in the Sassenfjorden area outcrops mainly as a thick, rather monotonous shale sequence. Due to limited occurrences of sedimentary structures and few visible lithological variations, field studies offer little detailed sedimentological information. In order to provide a better understanding of the depositional processes and diagenetic development of the formation, mineralogical and geochemical analyses were carried out. In addition to the investigation presented here, palynological and micropaleontological studies of the Janusfjellet Formation are also currently being carried out (T. Bjærke and J. Nagy, Univ. of Oslo).

II. Geology

The Janusfjellet Formation, divided into the Agardhfjellet and Rurikfjellet Members (Parker 1967; Major & Nagy 1972), is a marine shale and siltstone sequence found throughout Spitsbergen occurring between the shales and

[1] Institutt for geologi, Universitetet i Oslo, Blindern, Oslo 3.

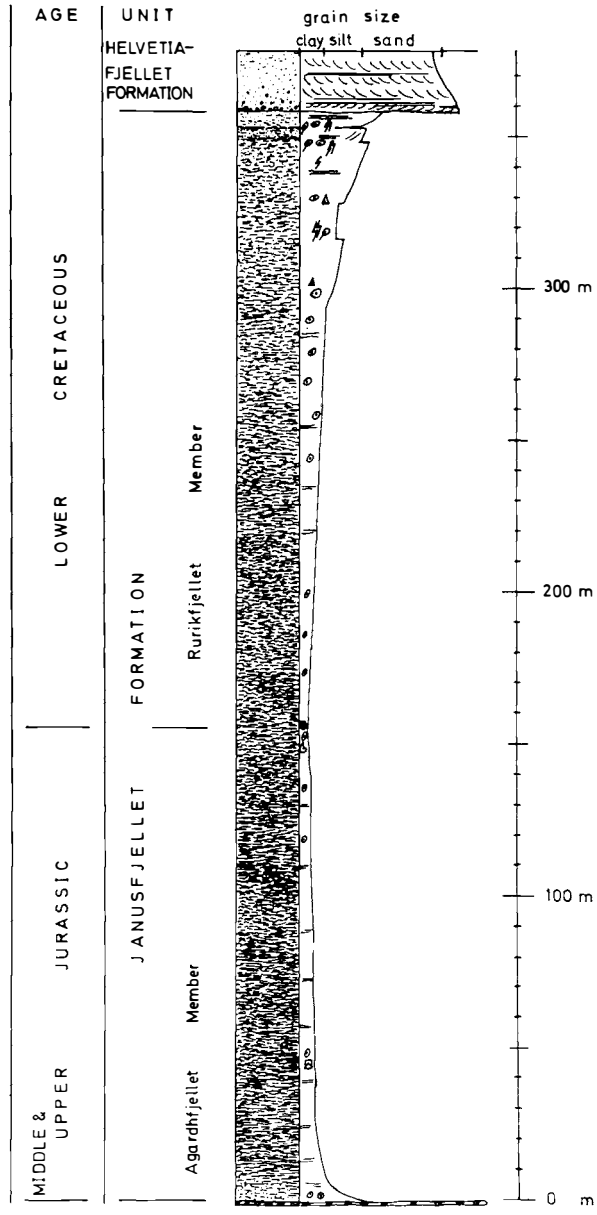

Fig. 1. *Lithological column for the Janusfjellet Formation, Isfjorden, Svalbard.*

sandstones of the underlying Kapp Toscana Group and the sandstones of the overlying Helvetiafjellet Formation (Fig. 1).

In central Spitsbergen the 400–600 m thick Janusfjellet Formation outcrops along the margins of the Tertiary basin (Fig. 2). After the deposition of the marginal marine Wilhelmøya Formation of the Kapp Toscana Group, which Bjærke & Dypvik (1977) showed to be present in the Isfjorden area, there was a break in sedimentation (Worsley 1973). After this break the Brentskardhaugen Bed (Parker 1967) was deposited, probably in the Bathonian/Bajocian (Birkenmajer 1972; Major & Nagy 1972; Parker 1966). The Brentskard-

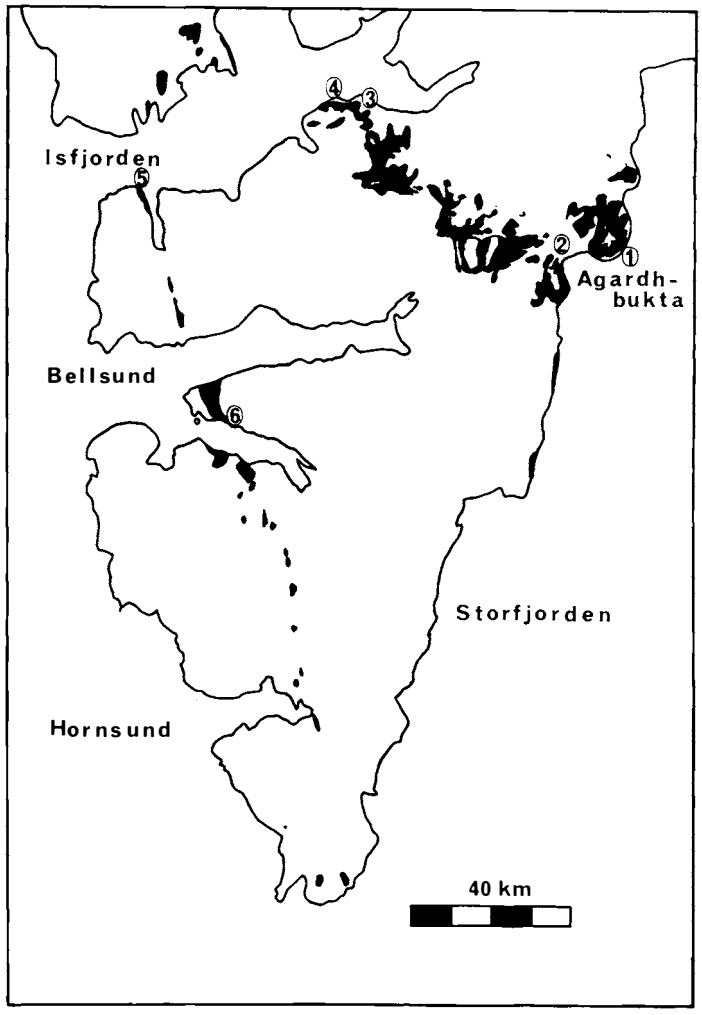

Fig. 2. *Outcrops of the Janusfjellet Formation in Spitsbergen, Svalbard. Localities studied in this paper: 1. Agardhfjellet, 3. Knorringfjellet, 4. Wimanfjellet.*

haugen Bed was overlain in the Callovian by marine clays, silts and sands of the Agardhfjellet Member. This marine depositional episode lasted to about Volgian times, when another break in sedimentation took place (ROZYCKI 1959; PARKER 1966; PČELINA 1970a & b) probably connected with folding, faulting and dolerite intrusion. GAYER et al. (1966) dated (K/Ar) the dolerites to be about 140 m.y. old, i.e. from the Jurassic/Cretaceous boundary.

The Agardhfjellet Member of central Spitsbergen consists mainly of shales and siltstones. The equivalent unit in Torell Land, the Ingebrigtsenbukta Series (ROZYCKI 1959) is similar. However, the hiatus in Torell Land spans the Upper Kimmeridgian–Lower Volgian (ROZYCKI 1959; FLOOD et al. 1971) and is overlain by a minor conglomerate horizon of Portlandian age. In the Isfjorden area PARKER (1967) and PČELINA (1970a) found a hiatus between the Volgian and Valanginian, so that Berriasian sediments are missing. In this

area renewed marine sedimentation (the Rurikfjellet Member) therefore started in the Valanginian and lasted throughout the Hauterivian after volcanic and tectonic activity (Bjærke 1978). In Torell Land the Tirolarpasset Series and the Ullaberget Series represent equivalent units (Rozycki 1959). While the Tirolarpasset Series consists of shales, sediments of the Ullaberget Series are more sandy and silty. In Isfjorden a similar sandy and silty development is found in the uppermost beds of the Rurikfjellet Member (Parker 1967; Pčelina 1970a). In Sørkapplandet the whole member consists of several coarsening upwards sequences with high amounts of sand- and siltstones deposited in coastal environments (Edwards 1976).

The Rurikfjellet Member shows a generally coarsening upwards development and is overlain by the Festningen Sandstone Member of the Helvetiafjellet Formation which was deposited in deltaic environments (Steel 1977).

The Janusfjellet Formation contains relatively rich faunas of belemnites, ammonites and bivalves; some plesiosaur remains also have been found (Rozycki 1959; Pčelina 1970a & b). The bivalve genus *Buchia* is particularly common throughout the unit (Major & Nagy 1972). Løfaldli & Thusu (1976) described several foraminifera from the formation, and suggested the Agardhfjellet Member to be a transgressive and the Rurikfjellet Member a regressive sequence. Palynomorphs found in the formation are of varying quality and preservation, but are best developed in the Rurikfjellet Member (Bjærke 1978). Bjærke also noted the decreasing abundance of marine palynomorphs towards the top of the Rurikfjellet Member, marking the unit's regressive development.

Several carbonate beds and nodules of varying composition have been described from the Janusfjellet Formation. Siderite is frequently found (Pčelina 1970a; Dypvik 1978) in the Callovian sediments, while dolomite is more common in the rest of the Agardhfjellet Member. Sideritic carbonates dominate the lower parts of the Rurikfjellet Member, while the more silty uppermost carbonate horizons are enriched in calcite.

Similar sedimentological developments are found in Upper Jurassic and Lower Cretaceous sediments elsewhere in the North Atlantic and Arctic areas, mainly reflecting the regional transgression which established seaways between Boreal and Tethyian areas (P. A. Ziegler 1975).

On Andøya (northern Norway) Oxfordian to Kimmeridgian sediments were deposited in a fining upwards sequence on a kaolinized basement (Dalland 1975; Dypvik 1979a). After a break in sedimentation, Valanginian to Hauterivian clays and silts were deposited in a second fining upwards sequence (Dalland 1975; Dypvik 1979a).

The continuous Upper Jurassic/Lower Cretaceous sequence of the central part of the Sverdrup Basin (northern Canada) is dominated by shales. More sporadic sandy sedimentation occurred in marginal areas (Plauchut 1971; Thorsteinson & Tozer 1970). Also here, a "continental blanket sandstone" similar to the Festningen Sandstone Member of Svalbard, overlies the marine shales. The palynology of the Sverdrup Basin is closely comparable to that of Spitsbergen (Johnson & Hills 1973; Bjærke pers. comm. 1978).

Both near and offshore marine clays and sands are found in East Greenland; in southern areas folding occurred in Rhyazanian times and overlying Cretaceous sediments were deposited in a synclinal structure (Birkelund 1975; Clemmensen & Surlyk 1976; Surlyk 1973; Surlyk 1975; Surlyk et al. 1973). In northern areas tilting of fault blocks in the Upper Jurassic/Lower Cretaceous resulted in Cretaceous sedimentation of resedimented material with varying marginal marine affinities (Surlyk 1975). Similar tilting of fault blocks is found in the northern North Sea (Hamar 1975).

In the North Sea the Upper Jurassic commenced with a marine transgression which connected the Boreal and Tethyian seas (Hallam 1971). This transgression started in the Callovian and terminated in a regressive phase towards the Jurassic/Cretaceous boundary (W. H. Ziegler 1975). Clays were deposited in the central basins, while sandy sediments were deposited in marginal parts and areas close to islands. After the Kimmerian movements, with their major phase in the middle Volgian, fine-grained sedimentation of clays continued in Cretaceous times. The Cretaceous shales are generally richer in carbonates than the Jurassic shales.

As this brief summary shows, marginal marine depositional environments existed in Svalbard and comparable areas during the Upper Jurassic and Lower Cretaceous. Lithological variations are mostly due to local palaeogeographical developments. In all areas several sedimentational breaks occur at this time,

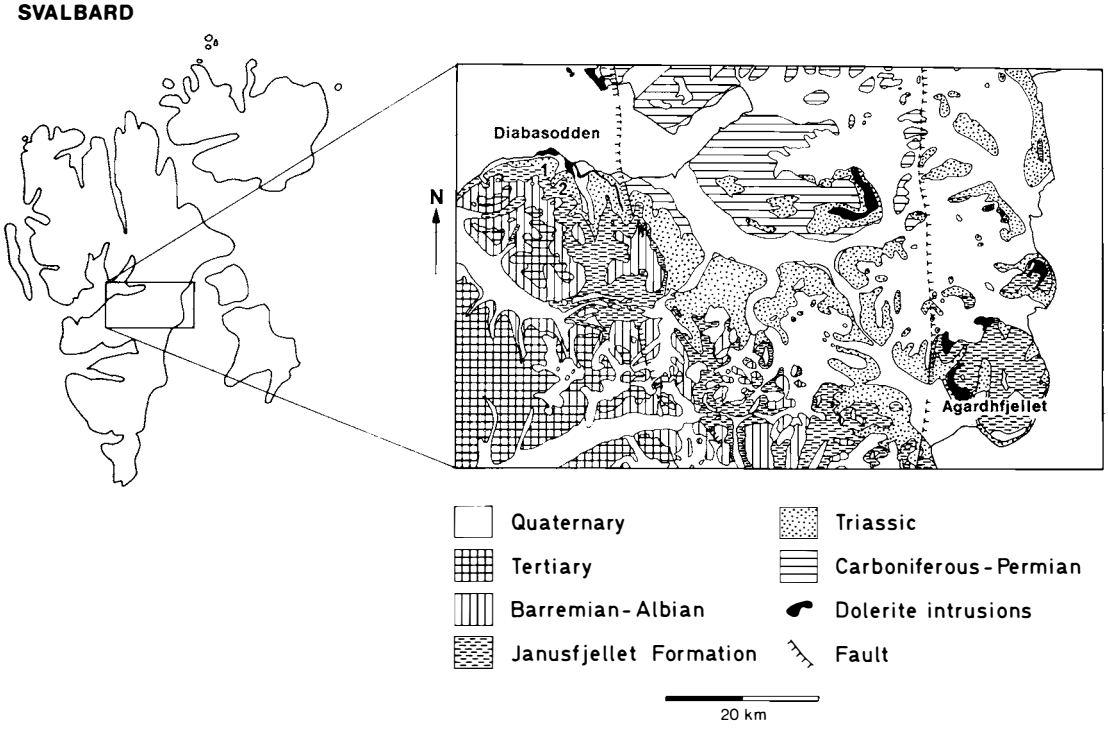

Fig. 3. *Geological map of the Isfjorden–Sassendalen area, Svalbard. Based on* Flood *et al. (1971). 1. Wimanfjellet, 2. Knorringfjellet.*

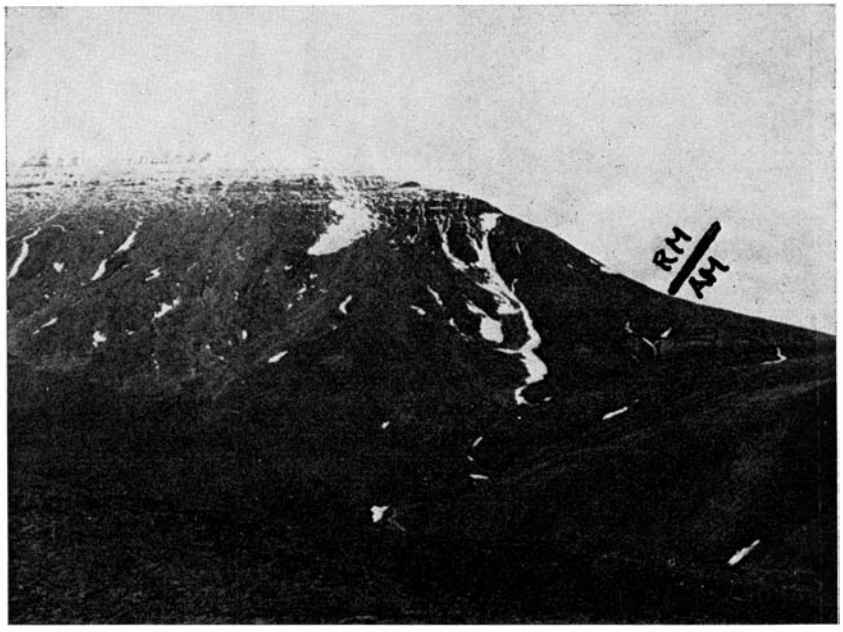

Fig. 4. *Janusfjellet Formation on Wimanfjellet, Svalbard. The upper Rurikfjellet Member is characterized by steeper slopes than the underlying Agardhfjellet Member.*

Photo: T. BJÆRKE

with major breaks concentrated at or around the Jurassic/Cretaceous boundary. These tectonic movements may be connected to the opening of the Amerasian basin and the eastward movements of the Kolymski area (HERRON et al. 1974).

Svalbard and Axel Heiberg Land (northern Canada) were probably separated in the early Tertiary, when spreading along the Nansen (Gakkel) ridge started (PITMAN & TALWANI 1972; HERRON et al. 1974; TALWANI & ELDHOLM 1977). According to TALWANI & ELDHOLM (1977) spreading started in the Svalbard–Greenland Sea about 38 m.y.a., while there have been transcurrent movements along the Greenland–Senja fracture zone from about 60 to 38 m.y.a. (HARLAND 1969; LOWELL 1972; TALWANI & ELDHOLM 1977).

III. Description of sections

The samples analysed were collected from three sections, at Agardhfjellet, Knorringfjellet and Wimanfjellet (Fig. 3). The Agardhfjellet section was sampled by Dr. M. B. EDWARDS (Continental Shelf Institute, IKU) the other two by Mr. T. BJÆRKE and the author.

All three sections (Fig. 2), show similar lithological developments. These will therefore be described generally below, and differences highlighted in the ensuing detailed descriptions.

The lower boundary of the Janusfjellet Formation is marked by the Brentskardhaugen Bed, while the top of the unit is overlain by the prominent Festningen Sandstone Member of the Helvetiafjellet Formation (Fig. 1). In the

field the transition between the Agardhfjellet and Rurikfjellet members is seen as a break in slope, the more resistant Rurikfjellet Member producing steeper slopes (Fig. 4). In the investigated areas a laterally persistent yellow weathering clay horizon is found between the members. Similar developments were described in the Agardhbukta area by PARKER (1967).

In the Knorringfjellet section the Agardhfjellet Member is about 75 m and the Rurikfjellet Member about 205 m thick. Equivalent thicknesses from the Wimanfjellet section are 155 m and 205 m, respectively. At Agardhfjellet the Agardhfjellet Member is 215–225 m and the Rurikfjellet Member about 190 m thick.

Above the Brentskardhaugen Bed, after a minor sequence of bituminous siltstones (about 2 m), dark shales are found continuously through the whole Agardhfjellet Member (Fig. 1). In their lower parts these shales have a darker colour than at higher stratigraphical levels. The shales are typical "paper shales". Some yellowish and reddish concretionary, often silty, carbonate units and beds are found dispersed throughout the sections (DYPVIK 1978). The dark paper shales of the Agardhfjellet Member terminate in thin yellowish clay beds (about 0.5 m). The overlying Rurikfjellet Member consists mainly of dark grey, prismatic fracturing shales with interbedded generally reddish carbonate horizons. The upper 40 to 60 m of the member show a more silty/sandy lithology. Silty, bituminous shales are found in the lower part of the uppermost beds. These grade up into regularly to irregularly laminated siltstones, terminating in the Helvetiafjellet Formation. The lower silty shales are highly bioturbated, while only minor bioturbation is found in the laminated beds. Plant remains are common in these beds. In the Wimanfjellet section few asymmetric ripples are seen.

Several ammonites, belemnites and bivalves have been found in the Knorringfjellet and Wimanfjellet sections and these will be further studied by Dr. J. NAGY (University of Oslo).

IV. Mineralogy and petrography

A. METHODS

i. Thin section analyses

Because of their low grade of cementation, the samples were impregnated with "Araldite" before thin sections were made. This method leaves structures and minerals unchanged, the "Araldite" only filling the pore space and cavities between different chips. Thin section analyses were made of 41 samples.

ii. Scanning electron microscopy (SEM)

Ten of the samples were prepared for SEM analyses. Fresh, broken chips of the samples were cemented with Ag glue to a holder and a thin, transparent Au-film was laid on the sample surface under vacuum. A Cambridge SEM instrument was used in the analyses, with technical assistance of Ms. E. BRÅTEN (University of Oslo).

iii. X-ray diffraction analyses (x-diff.)

Oriented and unoriented X-ray slides were prepared from rockpowder of all (154) collected samples. Oriented slides, (suspension slides; GIBBS 1965) were made for qualitative clay mineral determinations, and unoriented slides (vaseline slides; GIBBS 1965) for bulk analyses and semi-quantitative mineral estimates.

In the clay mineral determinations the following treatments were used:

1. Untreated
2. Glycolated
3. Heated to 300° C
4. Heated to 600° C

Kaolinite and chlorite relations were determined by slow scan analyses in the 3.50–3.60 Å area. Based on these results (interpreted according to BROWN 1961 and CARROL 1970) and the bulk analyses, the following minerals were found:

17Å (glyc.)	Smectite
14Å	Chlorite, smectite, vermiculite
10Å	Illite, glauconite
7.56 Å	Gypsum
7 Å	Kaolinite, chlorite
5.04 Å	Jarosite (Na)
4.26 Å	Quartz, gypsum
3.24 Å	Potash feldspar
3.18 Å	Plagioclase
3.03 Å	Calcite
2.89 Å	Dolomite
2.80 Å	Siderite
2.71 Å	Pyrite

In the semiquantitative determinations peak height multiplied by width at half height from X-ray diffractograms (unoriented) is supposed to be proportional to mineral content (NORRISH & TAYLOR 1962; DYPVIK 1977). For convenience and for presentation of the main mineralogical variations, the minerals have been grouped into five categories:

1) Clay minerals; 14Å + 10Å + 7Å
   Chlorite, smectite, vermiculite, illite, glauconite, kaolinite.
2) Quartz; 4.26Å
3) Feldspar; 3.24Å + 3.18Å
   Potash feldspar, Plagioclase
4) Autigenic minerals; 3.03Å + 2.89Å + 2.80Å + 2.71Å
   Calcite, dolomite, siderite, pyrite.
5) Secondary minerals; 7.56Å + 5.04Å
   Gypsum, jarosite.

iv. Microprobe analyses

These analyses were performed at the Central Institute of Industrial Research (SI, Oslo). The analyses were carried out on polished thin sections which were covered with a thin, transparent carbonfilm. An ARL-EMX instrument was used and the investigation was performed with the help of Dr. W. L. GRIFFIN (University of Oslo).

v. Grain size analyses

Three samples, WIM 5–76, WIM 26–76, and WIM 52–76, were disintegrated by ultrasonic treatment. Subsequently the samples were treated with Na-citrate–dithionite–bicarbonate solutions (MEHRA & JACKSON 1960) to remove Fe-compounds (cementing agents), and NaTPB solutions for dispersion of clay minerals (one of the cementing agents in several samples). Most of the samples were completely dispersed by these methods and grain size analyses were performed using settling tubes. Microscope examination of the different fractions showed sample WIM 26–76 to be poorly disintegrated in contrast to WIM 5–76 and WIM 52–76.

B. RESULTS AND EVALUATION OF MINERALOGICAL AND PETROLOGICAL ANALYSES

The upper 50–60 m of the Janusfjellet Formation on Wimanfjellet and Knorringfjellet consist mainly of siltstones and silty shales, while the lower 300 m of these sections are dominated by dense, impermeable shales. In thin section the mineralogy of the upper siltstones and the darker shales will be treated separately, before petrological variation throughout the Janusfjellet Formation is described.

i. Shales.

Description of minerals present.

The lower 300 m of the sections from Wimanfjellet and Knorringfjellet and the whole section from Agardhfjellet are made up of more or less silty, dense dark grey to black shales, with weathered coatings of reddish brown iron oxides.

X-ray diffraction analyses show these shales to consist of illite, kaolinite, mixed layered clay minerals of smectite/illite and probably some vermiculite. In addition, small amounts of quartz, feldspars, pyrite, siderite and dolomite have been detected. In a few samples the secondary weathering minerals jarosite and gypsum are seen in the X-ray diffractograms.

Generally, the shales in thin section are dark and dense because of dispersed organic debris and iron oxide coatings. In most of the samples, however, dispersed quartz grains (normally between 0.008–0.01 mm) are seen in varying amounts. Quartz grains up to 0.4 mm have been found. The quartz grains often have an undulating extinction and rather rugged outlines. Angular grains of plagioclase with An content about 20 (Michel Levy, X-ray diffraction) are found.

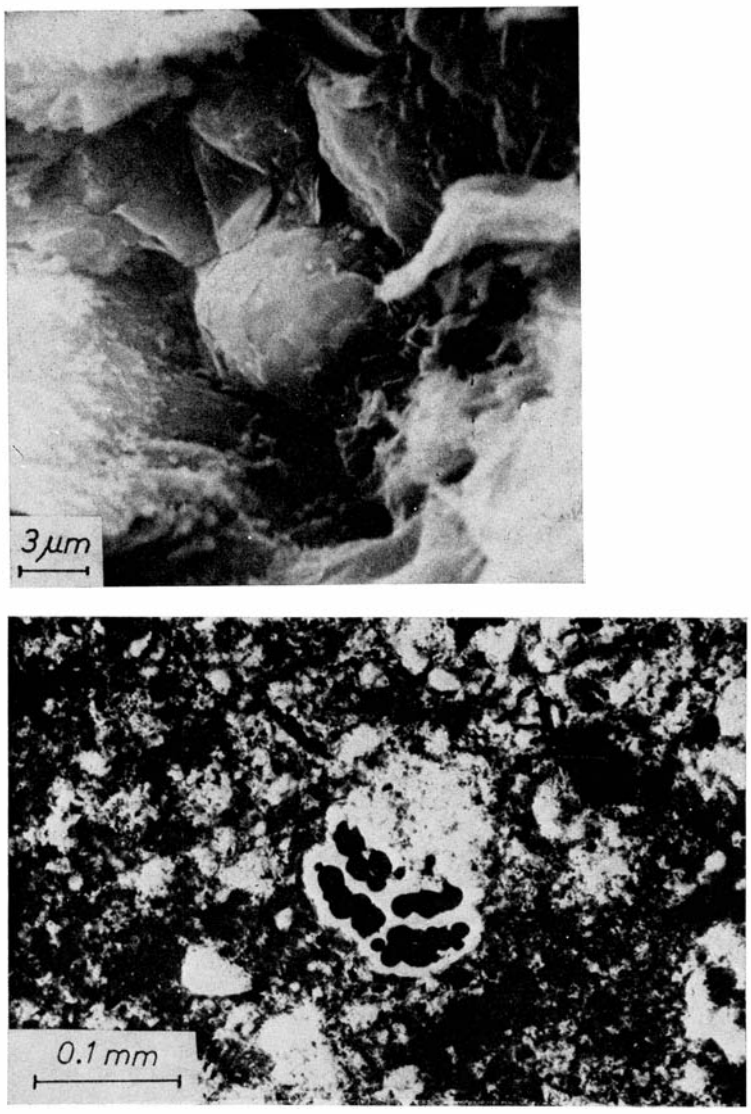

Fig. 5. *Scanning electron micrographs of framboidal pyrite, upper half. In the lower part of the figure thin section photo shows pyrite filling the test of a foraminifer.*

Laths of mica and grains of glauconite are seen in thin section in addition to siderite and (often framboidal) pyrite. Framboidal pyrite has been described in detail from Jurassic shales by ELVERHØI (1977). Agglutinating foraminifera have been found in some samples from the middle of the Janusfjellet Formation (Fig. 5). With NaTBP dissolution techniques they were separated and assigned to the agglutinated genus *Haplophragmoides*.

Description of mineral relations

In contrast to the overlying siltstones the shales do not show any extensive diagenetic growth of quartz or calcite. Only a few silty samples from the lowermost beds of the Agardhfjellet Member show minor secondary quartz over-

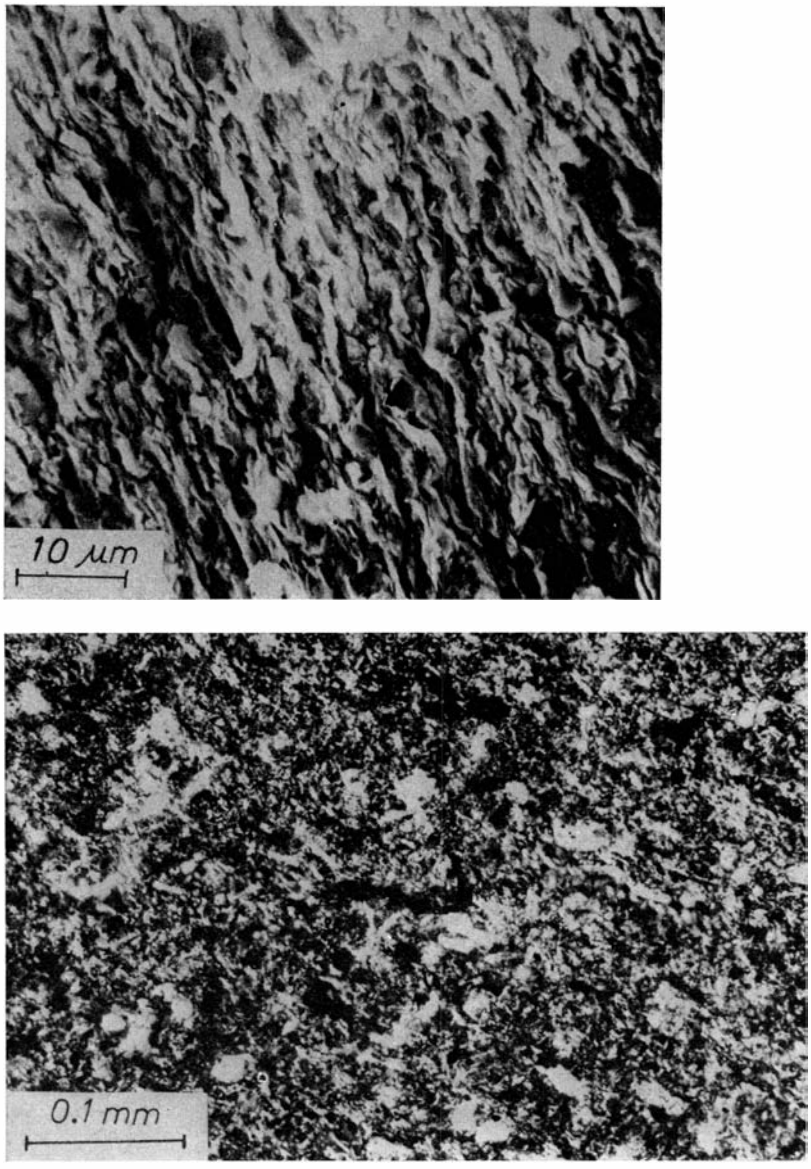

Fig. 6. *Parallel orientation of mica seen by scanning electron microscopy (upper half) and in thin section (lower half), Agardhfjellet Formation, Knorringfjellet.*

growth. Consequently quartz does not cement the shale to any major extent. Dissolution experiments with HCl (dissolving carbonate), H_2O_2 (dissolving organic material) and Na-citrate solutions (MEHRA & JACKSON 1960) (dissolving Fe-hydroxide coatings), indicate late diagenetic Fe-oxides/hydroxides to be an important cementing agent in the samples (DYPVIK 1980).

The glauconite grains and the pyrite have an early authigenic origin, while the iron oxide/hydroxide coatings were probably formed at a relatively late stage of diagenesis. Some of the iron oxides probably result from oxidation reactions of pyrite. K-fixation in the clay minerals during diagenesis resulted in

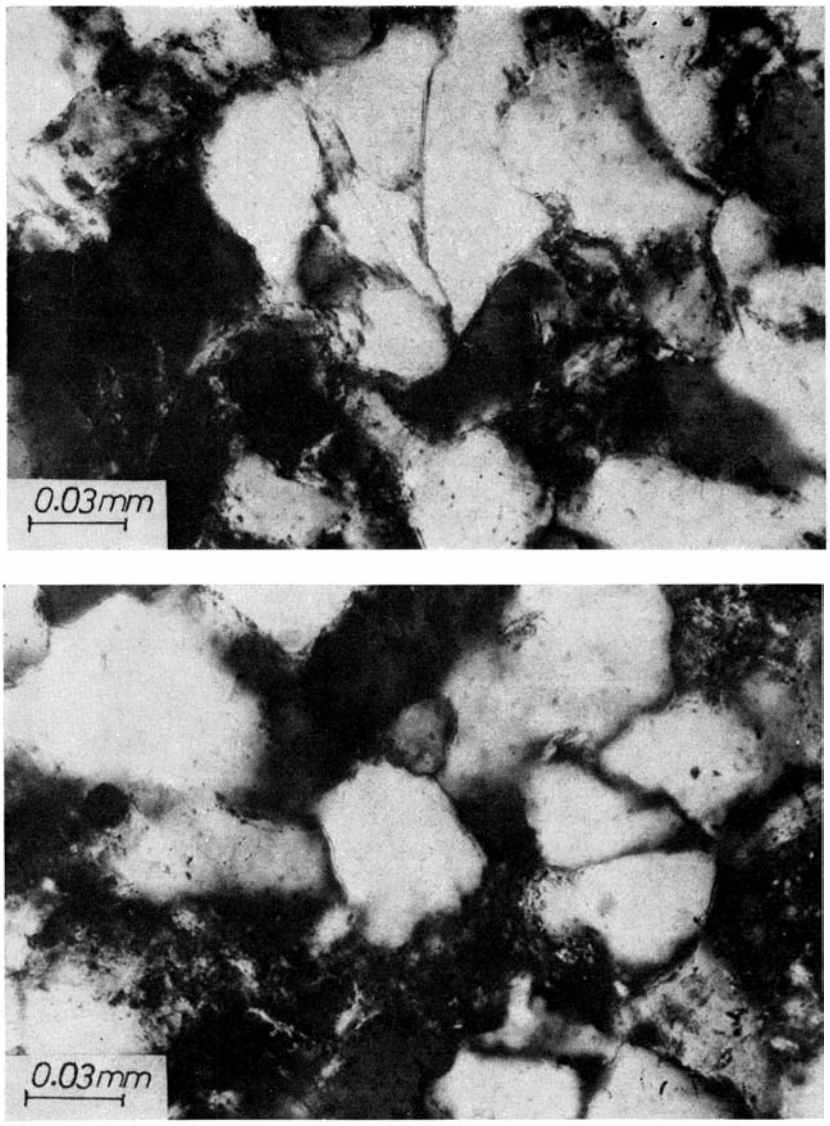

Fig. 7. *Photos of thin sections of silty sandstones from the Rurikfjellet Member, Wimanfjellet section.*

increasing amounts of illitic layers. Orientation of mica flakes perpendicular to the lamination indicates a possible diagenetic origin (Fig. 6) of some of the clay minerals. Grains of siderite present probably represent later sideritised calcite.

ii. Siltstones

Description of minerals present.

Thin section and X-ray diffraction analyses show the siltstones to consist mainly of quartz, feldspars and mica/illite with minor amounts of calcite, dolomite, pyrite, kaolinite and organic material. The siltstones generally have a mean grain size between 0.02 and 0.08 mm, although dispersed quartz grains

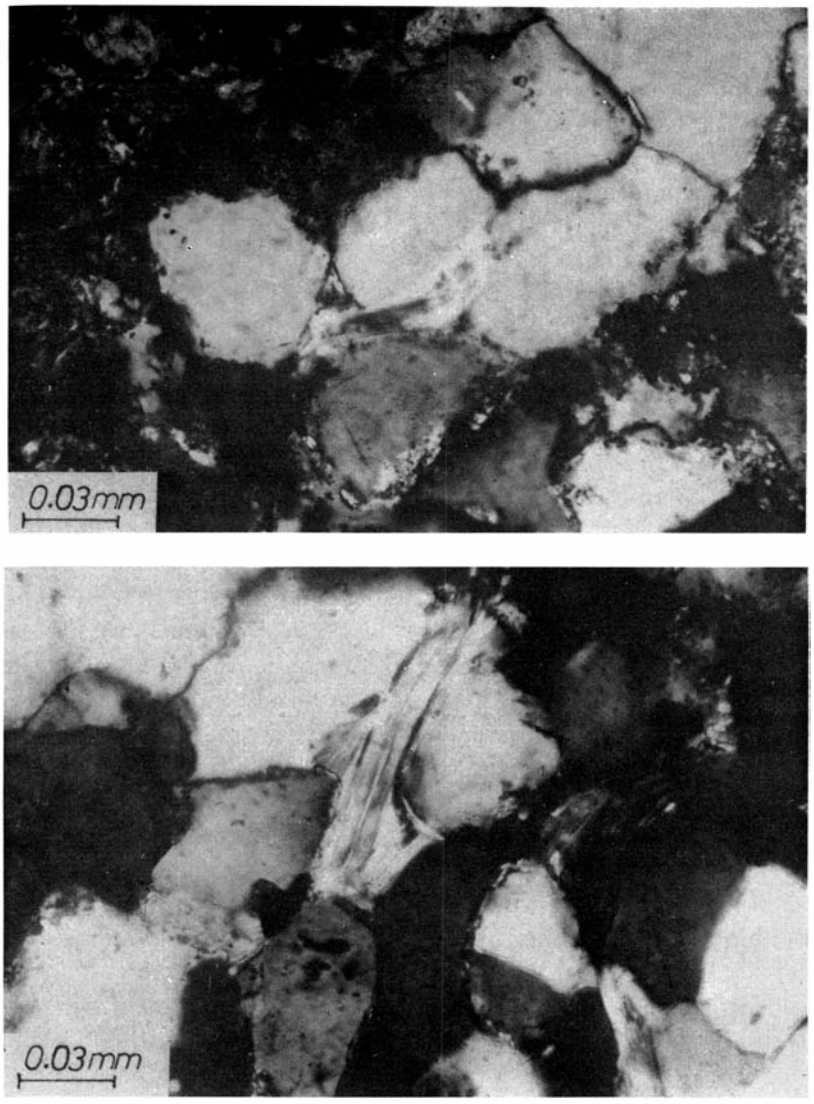

Fig. 8. *Photos of thin sections from the Rurikfjellet Member, Knorringfjellet, showing authigenic mica spreading out into porespace.*

up to 0.2 mm are found. The siltstones are usually well cemented (minor porosity) and often show parallel lamination. They may contain more than 95% quartz grains, and often show secondary quartz overgrowths defined by dust lines in thin section (Figs. 7 & 9) or by grains with euhedral form morphology. Such structures may be altered quickly during transportation and consequently indicate diagenetic growth. Neither the euhedral morphology nor the dust lines are seen where mica or feldspar grains cover the original quartz grains.

Several microprobe analyses and SEM analyses from the centres of quartz grains across the overgrowth zone to the centre of adjacent quartz grains show minor flakes of kaolinite to be present in the overgrowth zones of secondary

quartz (Figs. 10 & 11). The texture and occurrence of kaolinite may indicate diagenetic formation in the sediments prior to the secondary formation of quartz. Low K^+ activity resulted in kaolinite formation, instead of e.g. illite formation.

Several of the quartz rich siltstones (with minor feldspar content) are well sorted and probably had an original more or less grain supported structure. In addition to quartz grains with undulating extinction, feldspar grains with some overgrowth are also seen. The samples usually contain more plagioclase than potash feldspar. The potash feldspar often has a microcline structure, while the plagioclase has An 7–13/23–27 (Michel Levy and X-ray diffraction). In contrast, the An content in the plagioclase from the dolerites in Isfjorden was found to be 45–65.

In addition to sericitisation of plagioclase some mica and clay minerals have probably grown diagenetically in the sediment. Detrital mica flakes have been bent, folded and broken around detrital grains during compaction of the sediments (Figs. 8 and 9). Some possible authigenic mica is found surrounding secondary quartz (Fig. 8) and some (mica and kaolinite) spread in fans in original porespace, indicating a diagenetic formation or modification of original grains (Figs. 7 and 8).

Glauconite pebbles (illite/smectite mixed layered minerals) are also thought to have an early diagenetic origin. Today glauconite is often formed in shallow marine environments. During and after consolidation the glauconite may have been altered towards an illitic composition. Early diagenetic pyrite was formed together with glauconite. Such pyrite, often with a framboidal morphology (Fig. 5), is found in recent sediments together with glauconite in shallow marine environments (Porrenga 1967). However, there have probably been several generations of pyrite formation. With today's complicated texture formational mechanisms are difficult to explain in detail.

In addition to quartz, minor amounts of carbonates are found as cement in some of the siltstones (Fig. 8). In some samples minor carbonate grains are seen to grow between quartz grains, while sparry calcite in other samples completely fills the remaining porosity. Calcite and dolomitised calcite have etched some of the quartz grains and often show a rhombic form. Pore space previously filled by mica, however, contains no carbonate.

Description of mineral relations.

Most of the minerals in the analysed samples obviously have a detrital allogenic origin, but authigenic minerals and diagenetic growth on detrital minerals are also clearly observed.

Most of the quartz, feldspar and mica/illite are detrital, with typical marine, early diagenetic formation of pyrite and glauconite seen in the samples.

Quartz overgrowth marks a later diagenetic stage, but took place before diagenetic calcite and clay mineral formation. However, some secondary kaolinite formation happened immediately before or together with the secondary quartz overgrowth. Quartz overgrowths are found mainly on clean quartz grains with minor coatings of clay minerals. The quartz cement only partly filled the pore space. The minor diagenetic growth of mica, seen as fans

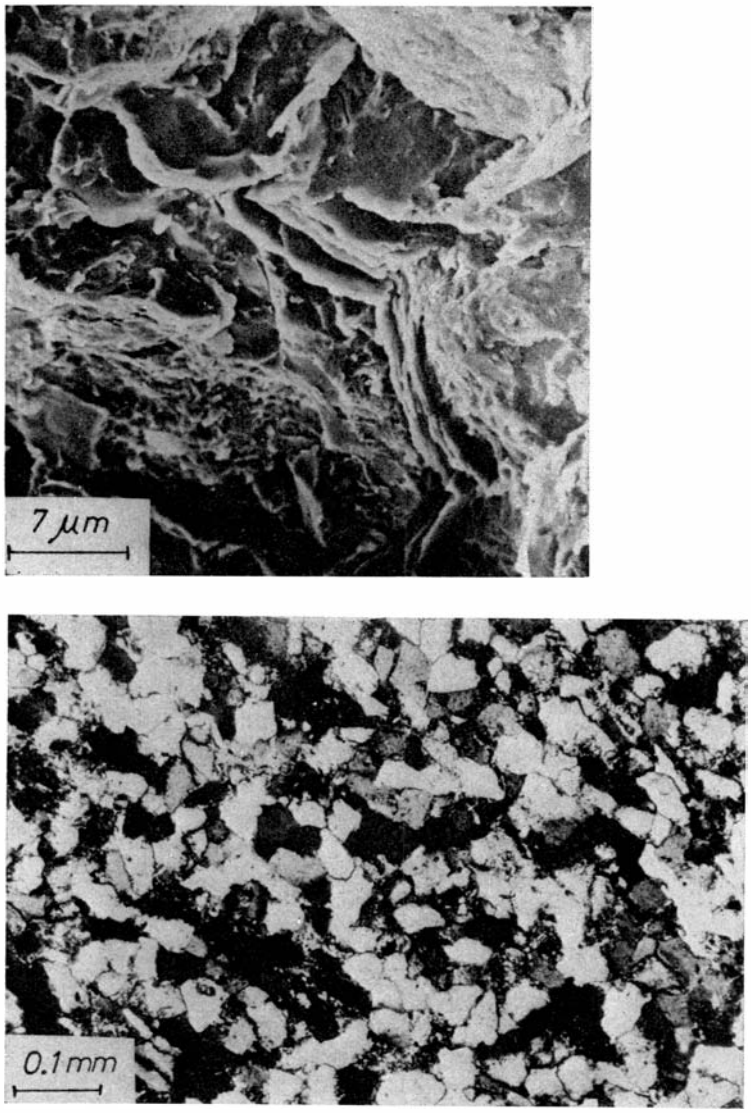

Fig. 9. *Scanning electron micrographs, upper half, and thin section photos of siltstones from Rurikfjellet Member, Wimanfjellet.*

developed at the ends of original clastic mica flakes is seen to overlap diagenetic quartz and is consequently of younger age.

In the samples containing carbonate, sparry and microsparitic calcite completely fill the remaining pore space after the quartz and mica growth. The calcite consequently represent the last major diagenetic episode.

On the surface of several samples a light redbrown to brown weathering coating is seen, indicating late oxidation of the sediments. This is probably the latest of the diagenetic reactions in these siltstones and reflects post-Cretaceous weathering. The surface oxidation is, however, less developed in these siltstones than in the underlying shales.

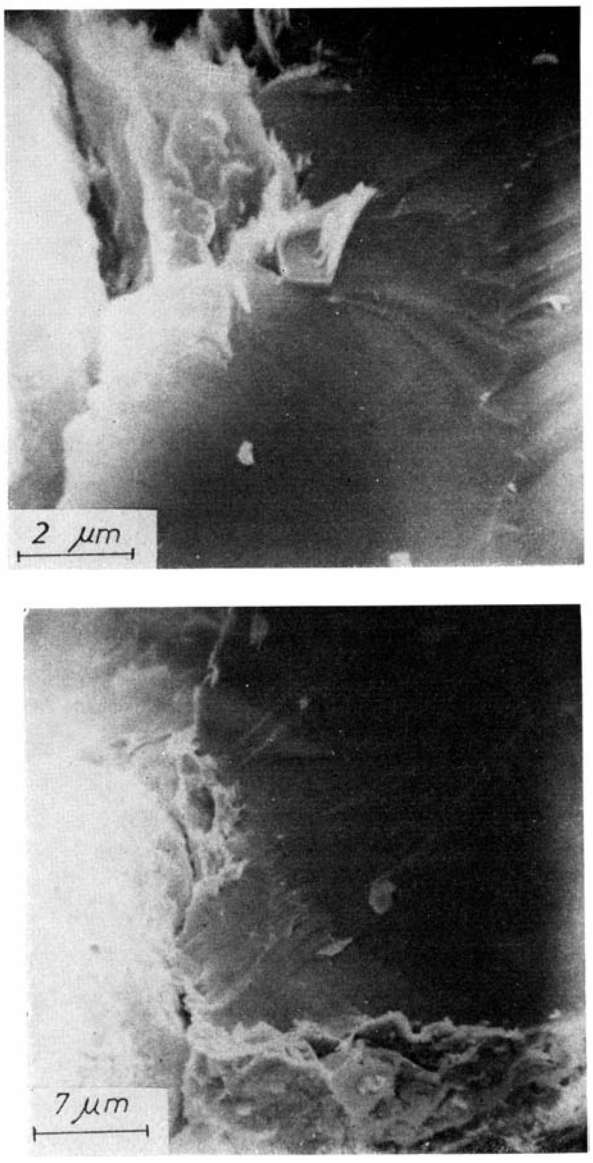

Fig. 10. *Authigenic clay minerals, probably kaolinite flakes, seen along quartz grains in scanning electron micrographs, Rurikfjellet Member, Knorringfjellet.*

iii. Grain size variation throughout the formation.

The ratio (sand+silt)/clay has been estimated in thin section. These estimates match the variations in mean grain size measured.

Similar grain size trends are seen in the three sections. Generally the Agardhfjellet Member shows a fining upwards grain size distribution, while the Rurikfjellet Member shows a coarsening upwards trend. The development in the Rurikfjellet Member is also seen mesoscopically in the sections on Knorringfjellet and Wimanfjellet. The largest grains present have also been measured,

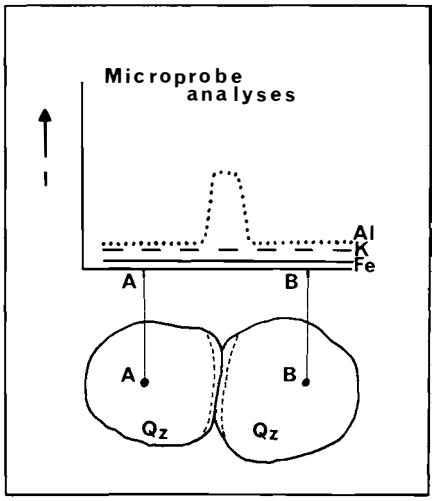

Fig. 11. *Microprobe analyses of elements along a path across contact between quartz grains. The analyses indicate occurrences of kaolinite, clay minerals enriched in Al and depleted in K and Fe.*

the largest grain sizes being found in the uppermost beds of the Agardhfjellet and Rurikfjellet Members.

As mentioned earlier, samples WIM 5–76 (upper part of Rurikfjellet Mb), WIM 26–76 (from upper part of Agardhfjellet Member) and WIM 52–76 (from lowermost part of Agardhfjellet Member) have been dispergated to obtain more accurate data on grain size variation. In sample WIM 5–76 about 80 weight % of total sample was found in the coarse silt/fine sand fraction, with a tail in the finer fractions. This tail is partly overestimated due to the dissolution techniques used. Sample WIM 5–76 seems to show an overall good sorting, probably reflecting reworking.

Sample WIM 26–76 was only poorly disintegrated by the methods used. Binocular studies of the different fractions separated from sample WIM 52–76, however, showed good disintegration. This sample, which contains much coarse silt, shows rather poor sorting, reflecting bioturbation and deposition in an open shelf environment.

iv. Mineralogical variation throughout the formation.

The general mineralogical development is similar in the three sections studied, as shown in Fig. 12. The semiquantitative amounts of clay minerals, quartz, feldspar, authigenic minerals (carbonates) and secondary minerals (gypsum and jarosite), calculated from X-ray diffractograms, have been plotted.

While only minor amounts of carbonates and secondary minerals occur in the top of the Rurikfjellet Member, varying and higher amounts of these minerals are found in the Agardhfjellet Member. The occurrence of secondary minerals points to zones of secondary oxidation, where organic matter and sulphides may have been oxidized. Shales from the Agardhfjellet Member are generally more oxidized than those of the Rurikfjellet Member. This may explain the

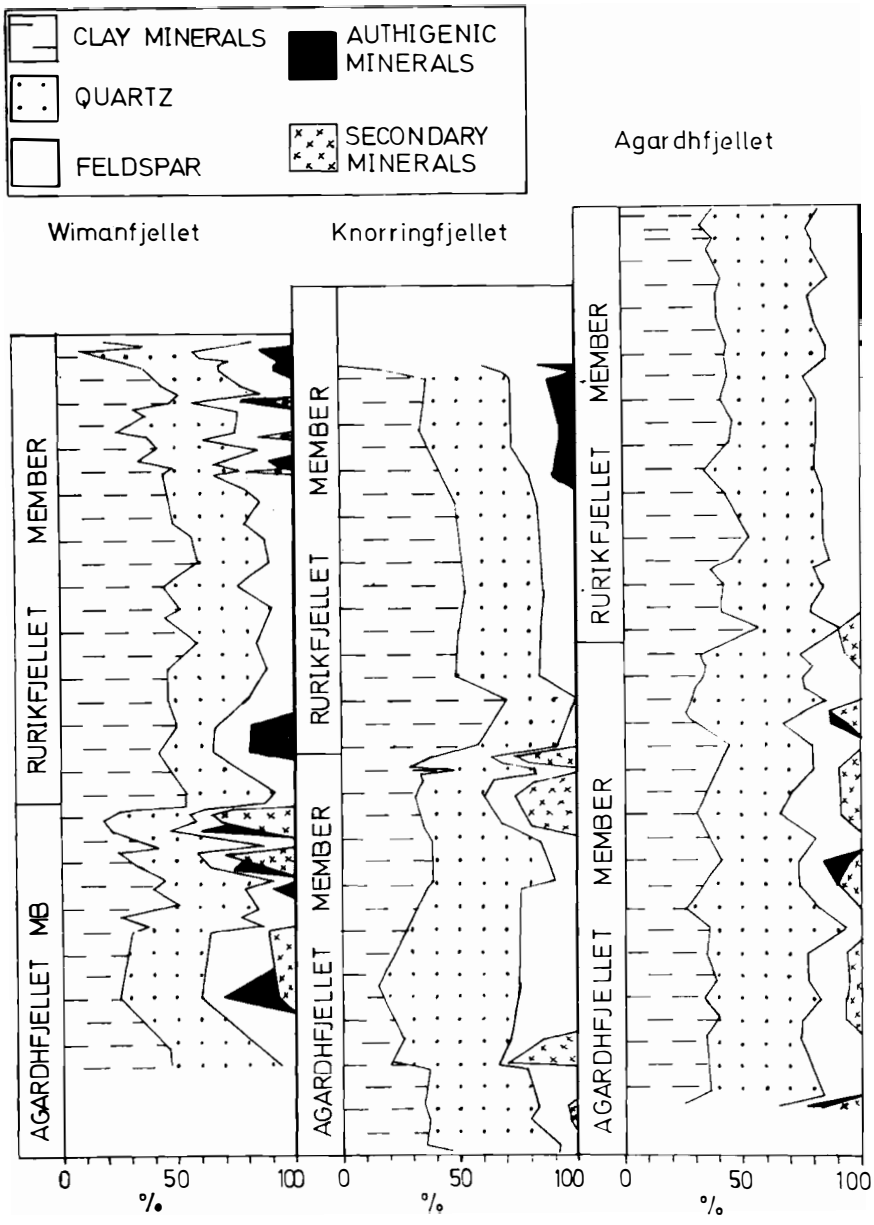

Fig. 12. *Stratigraphical variation in mineralogy in the Janusfjellet Formation, Svalbard. Authigenic minerals are calcite, dolomite, siderite, and pyrite, while secondary minerals are jarosite and gypsum.*

relatively poor preservation of palynomorphs in the Agardhfjellet Member as noted by Bjærke et al. (1976).

The content of clay minerals decreases upwards to the middle of the Agardhfjellet Member, and after a minor increase, decreases again towards the junction with the Rurikfjellet Member. In the Rurikfjellet Member the clay mineral content decreases slightly upwards. Other variations in the distribution of the

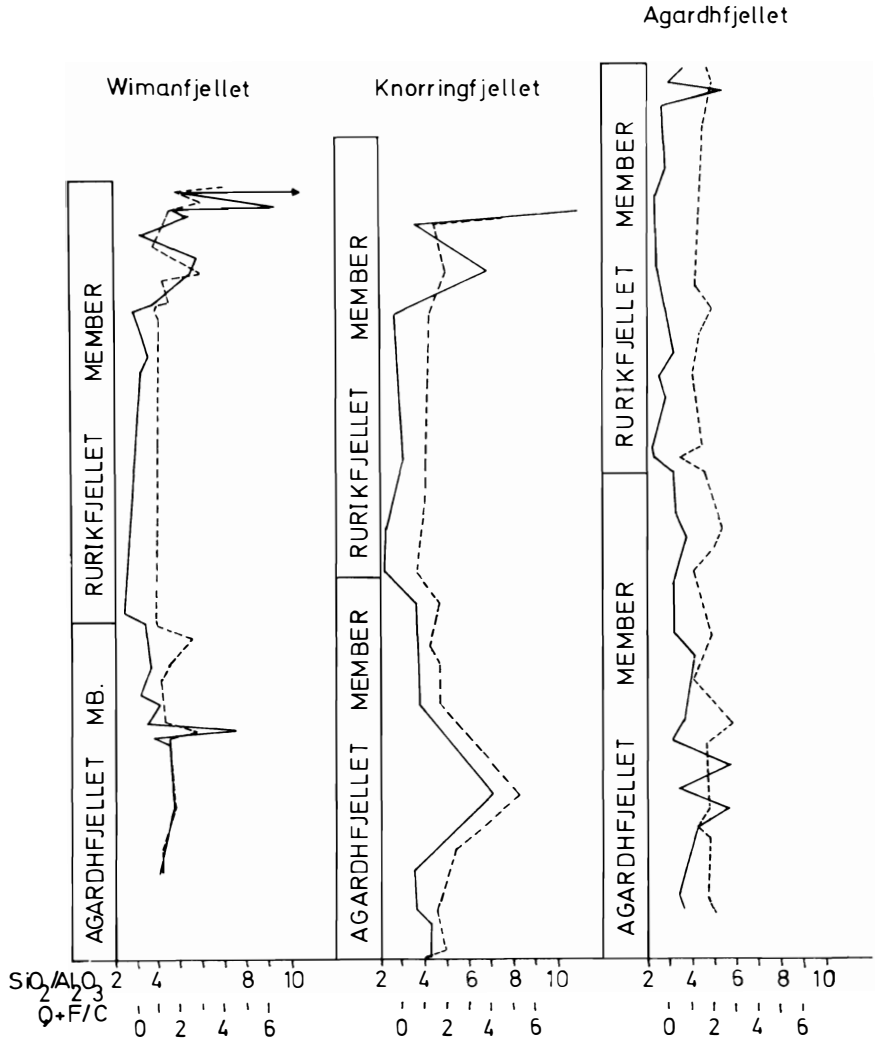

Fig. 13. *Stratigraphical variation in the SiO_2/Al_2O_3 ratio* (——) *and Quartz + Feldspar/Clay minerals ratios* ($Q + F/C$, – – – –), *Janusfjellet Formation, Svalbard.*

clastic minerals are, however, better displayed and more informatively studied by inspection of their mutual relations.

The estimated (quartz+feldspar)/clay mineral ratio reflects grain size variations in the samples, with highest ratios in the coarsest samples (Fig. 13). In the Agardhfjellet Member the ratio is varying, generally with an increasing ratio to the middle of the member, and above this an upwards decreasing trend is seen towards the Rurikfjellet Member. In the Rurikfjellet Member a general upwards increasing ratio (coarsening upwards) is seen in all the three sections.

Generally the quartz/feldspar ratio is higher in mature than in immature sediments, due to weathering of feldspar and resistance of quartz. Consequently analyses of this ratio may give information on the varying maturity

through the sections (BJØRLYKKE 1974). In the samples from the Janusfjellet Formation this ratio has been calculated from the X-ray diffractograms. In the Agardhfjellet Member the ratio decreases upwards in the Wimanfjellet and Agardhfjellet sections, while the development in the Knorringfjellet section is seen to be composed of several minor upwards decreasing patterns. In the Rurikfjellet Member a decreasing ratio upwards has also been established. In both members the sediments therefore generally suggest an upward decrease in maturity. On a more detailed scale, minor, more uncertain, fluctuations are found in these ratios.

Some major mineralogical and petrological trends may be outlined from the above ratios. Most of the shale samples from the Agardhfjellet Member contain more quartz and feldspar and are usually coarser grained and more mature than most of the Rurikfjellet Member (except for the upper 50–60 m of this Member).

Similar grain sizes are found in all three sections, but in the uppermost part of the Rurikfjellet Member the silty/sandy beds from Wimanfjellet and Knorringfjellet are coarser grained than similar beds from the Agardhfjellet section. Maturity indicia are also similar in the three sections. However, the Agardhfjellet Member from the Knorringfjellet section is apparently more mature than similar horizons in the other two sections.

V. Geochemistry

A. METHODS

After crushing in a steel disc mill, the 154 samples were prepared for different mineralogical and chemical analyses.

i. X-ray fluorescence (XRF) analyses

Melted, diluted (sample: $Li_2B_4O_3$, 1:9) pellets were used for major element analyses, while undiluted, pressed pellets were used for determinations of trace elements. The semiautomatic Siemens equipment used is situated at the Department of Geology, University of Oslo. Analyses were made with Cr- or Au tubes depending on the element to be determined (MÜLLER 1967). International standards were used for the main element analyses, while both additional and international standards were used in trace element analyses (FLANAGAN 1973). Precision, as standard deviation from the mean, was found to be:

TiO_2, Al_2O_3, Fe_2O_3, MnO, CaO, K_2O, Sr	± 1%
SiO_2, Na_2O, Cr, Ba	± 2%
MgO, P_2O_5	± 3%
Ni	± 4%
Co	±10%

ii. Instrumental neutron activation analyses (INAA).

The INAA analyses were made after irradiation for one hour in a JEEP-II reactor at IFA (Institute for Atomic Energy, Kjeller, Norway). After 2–3 days of cooling, La and Sm were determined, and after about 15–18 days, Sc, Cr, Co, Th, Cs, Eu, and Ce were determined. BCR-1 and G-2 standards were used, with values from GORDON et al. (1968), BRUNFELT & STEINNES (1971) and FLANAGAN (1973). KeV values from ADAMS & DAMS (1969) were used. 57 samples from the Agardhfjellet section were analysed for trace elements by INAA. Parallel analyses gave the following standard deviations:

Cr	± 2%
Th	± 5%
Co	±10%
Cs	±30%

iii. Combustion method for determination of C_{org}.

Due to the relatively minor carbonate content in the shales (not detected by X-ray diffraction and only minor amounts seen in thin section), crushed samples were analysed directly for organic carbon. A Leco Induction furnace system was used in the combustion method. Parallel analyses gave standard deviation of ±2%. Analyses of HCl soluble fraction from several samples from Knorringfjellet show carbonate contents below 8%. Variations in carbonate concentrations are relatively small in the clastic rocks and consequently have minor impact on the interpreted variations in organic carbon. Correct and actual organic carbon values seem to be about 10% lower than the values presented here.

B. RESULTS AND EVALUATION OF GEOCHEMICAL ANALYSIS

i. The SiO_2/Al_2O_3 ratio.

The ratio between SiO_2 and Al_2O_3 concentrations usually reflects grain size variations in marginal marine sediments. The SiO_2 concentrations are supposed mainly to represent quartz, which are enriched in the coarser fractions, and Al_2O_3 variations reflect the different amounts of fine grained clay minerals (PETTIJOHN 1957; BJØRLYKKE 1974.)

The grain size interpretation of the ratio may be disturbed by the occurrences of fine grained quartz, coarser grains of feldspar which contain some Al, coarse grained mica, etc.

In the three sections analysed, the SiO_2/Al_2O_3 ratio decreases upwards in the Agardhfjellet Member and increases upwards in the Rurikfjellet Member (Fig. 13).

The chemically interpreted grain size variations, with a shift in pattern at the boundary between the two members, are also seen in the petrological and mineralogical analyses. The SiO_2/Al_2O_3 ratio, therefore, in this case seems to be a reasonable grain size parameter.

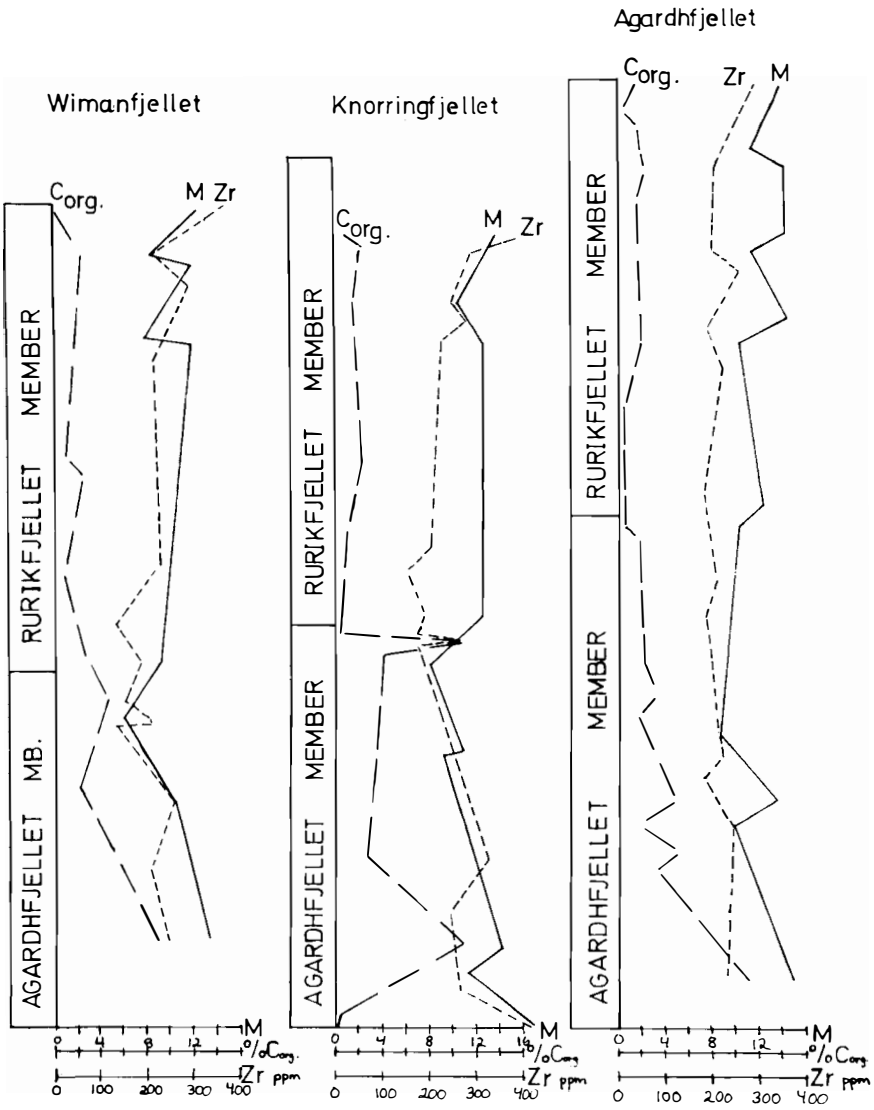

Fig. 14. *Stratigraphical variation in the M-ratio* = $(Al_2O_3 + K_2O/MgO + Na_2O)$ *and* $C_{org.}$ *and Zr concentrations in the Janusfjellet Formation, Svalbard.*

ii. The $\dfrac{Al_2O_3 + K_2O}{MgO + Na_2O} = M$ *ratio.*

The $Al_2O_3 + K_2O/MgO + Na_2O$ = M ratio may generally express the ratio between relatively stable minerals (mica, potash feldspar (Al, K), etc.) compared to often unstable minerals such as ferromagnesian minerals (chlorite) and sodium rich plagioclase (Mg, Na). An increasing M ratio may consequently be interpreted as showing increasing maturity (Bjørlykke 1974).

Generally the M ratio shows an upwards decreasing trend in the Agardhfjellet Member and upwards increasing to constant development in the Rurikfjellet Member (Fig. 14). However, the decreasing trend of the Agardh-

fjellet Member stops about 2 m below the junction between the two members. From there on an increasing trend of M ratio starts developing. Such maturity evolution may reflect winnowing of sediments connected with the hiatus at the Jurassic/Cretaceous transition.

Accordingly these results indicate decreasing maturity upwards in the Agardhfjellet Member and weakly increasing to stable maturity throughout the Rurikfjellet Member. Lateral variations indicate equivalent beds from Wimanfjellet and Agardhfjellet to be less mature (lower M ratios) than those from Knorringfjellet; however, the samples from Wimanfjellet are always the least mature.

iii. The K_2O/Na_2O ratio

This ratio may also be used as a maturity indicator on the supposition that the K_2O content mainly reflects potash feldspar and phyllosilicates, and Na_2O content mainly reflects plagioclase. Since potash feldspar is normally the most resistant feldspar (MILLOT 1970) high K_2O/Na_2O ratios would indicate more altered, mature sediments than lower ratios. Variations in contents of mica (K_2O), clay minerals (K_2O, Na_2O) may, however, complicate such an interpretation.

The generally upwards decreasing ratio in the Agardhfjellet Member and the upwards increasing and later decreasing ratios in the Rurikfjellet Member partly match the results of the M analyses. The M-ratio indicates relative constant maturity in the upper part of the Rurikfjellet Member, while the K_2O/Na_2O ratio indicates decreasing maturity. This discrepancy may have several explanations, but the increasing grain sizes make an upwards decreasing maturity development most probable.

Comparison of similar beds from the three sections studied, show the highest values on Knorringfjellet, intermediate values on Wimanfjellet, and the lowest ratios in the Agardhfjellet section. Consequently both the K_2O/Na_2O and the M ratio show the shales in the Knorringfjellet to be most mature, while there are discrepancies in the relationships between the Agardhfjellet and the Wimanfjellet sections.

iv. Other main elements (Fe_2O_3, P_2O_5, MnO)

The contents of Fe_2O_3 and TiO_2 in the Rurikfjellet Member are generally higher than in the underlying Agardhfjellet Member. Minor MnO enrichments in the lowermost beds of the Rurikfjellet Member and small P_2O_5 enrichments in the top of the Agardhfjellet Member are found in all three sections. Both MnO and P_2O_5 concentrations are rather similar in the sections sampled. Since enrichment of P_2O_5 generally characterizes minor clastic sedimentation (MCKELVEY 1957; D'ANGLEJAN 1967), the P_2O_5 enrichment in the top of the Agardhfjellet Member probably indicates a break in clastic sedimentation. As Mn often precipitates as oxides and is immobile in oxidizing environments (CARVAJAL & LANDERGREN 1969; YAALON et al. 1974; SUMMERHAYES & WILLIS 1975), MnO enrichment in the Rurikfjellet Member indicates more oxidizing conditions.

v. Organic carbon ($C_{org.}$)

The lowermost beds of the Agardhfjellet Member contain 1.5–2% $C_{org.}$ (Fig. 14). At 40–50 m above the base of the Agardhfjellet member the rocks are, however, heavily enriched in $C_{org.}$ (10–12%). From that level and towards the top of the member the concentrations decrease to about 1.5–2%. In the Knorringfjellet section some beds just beneath the Agardhfjellet/Rurikfjellet boundary also contain 10–20% $C_{org.}$ The Rurikfjellet Member from the three sections shows a rather constant content of $C_{org.}$ between 0.5 and 2%. Consequently, the average organic content of the Agardhfjellet Member is higher than that of the Rurikfjellet Member. The decreasing $C_{org.}$ content in the Agardhfjellet Member probably reflects the transgressive development, while the regressive development, with increasing influx of terrestrial material (BJÆRKE 1978) in the Rurikfjellet Member does not seem to be reflected in the $C_{org.}$ variations.

vi. Sulphur (S)

Higher sulphur contents are generally found in the Agardhfjellet Member than in the Rurikfjellet Member. Varying distributions occur in the Agardhfjellet Member, while weak upwards increasing concentrations are observed in the Rurikfjellet Member. S mainly occurs in pyrite in the shales from the Janusfjellet Formation, with only minor amounts in secondary formed gypsym and jarosite. Sulphur and organic carbon enrichment in the Agardhfjellet Member compared to the Rurikfjellet Member, may indicate more reducing conditions during the deposition of the Agardhfjellet Member.

vii. Zirconium (Zr)

The Agardhfjellet Member displays an upwards decreasing concentration of Zr, while there are increasing concentrations in the Rurikfjellet Member (Fig. 14). These variations are similar to those of the sand and silt distributions and therefore probably indicate Zr to be associated with those fractions, probably in zircon and other heavy minerals.

BOWEN (1966) and BOSTRÖM et al. (1974) show only minor amounts of Zr to be enriched in biological matter, and confirm the general occurrence of Zr in clastic minerals, especially zircon (DESBOROUGH et al. 1976). Enrichments of Zr in the Janusfjellet Formation may therefore reflect a more mature composition of the sediments of this unit than seen in average shales.

viii. Titanium, Scandium and Thorium (TiO_2, Sc, and Th).

TiO_2, Sc, and Th show upwards increasing trends in the Agardhfjellet Member and upwards decreasing trends in the Rurikfjellet Member of Agardhfjellet (Fig. 15). It is difficult to determine whether these elements occur in heavy minerals or whether they are adsorbed to clay minerals or organic material. The results of DYPVIK (1980) make the first suggestion most probable.

DYPVIK (1980) showed that about 100% of Ti is bound in the finegrained

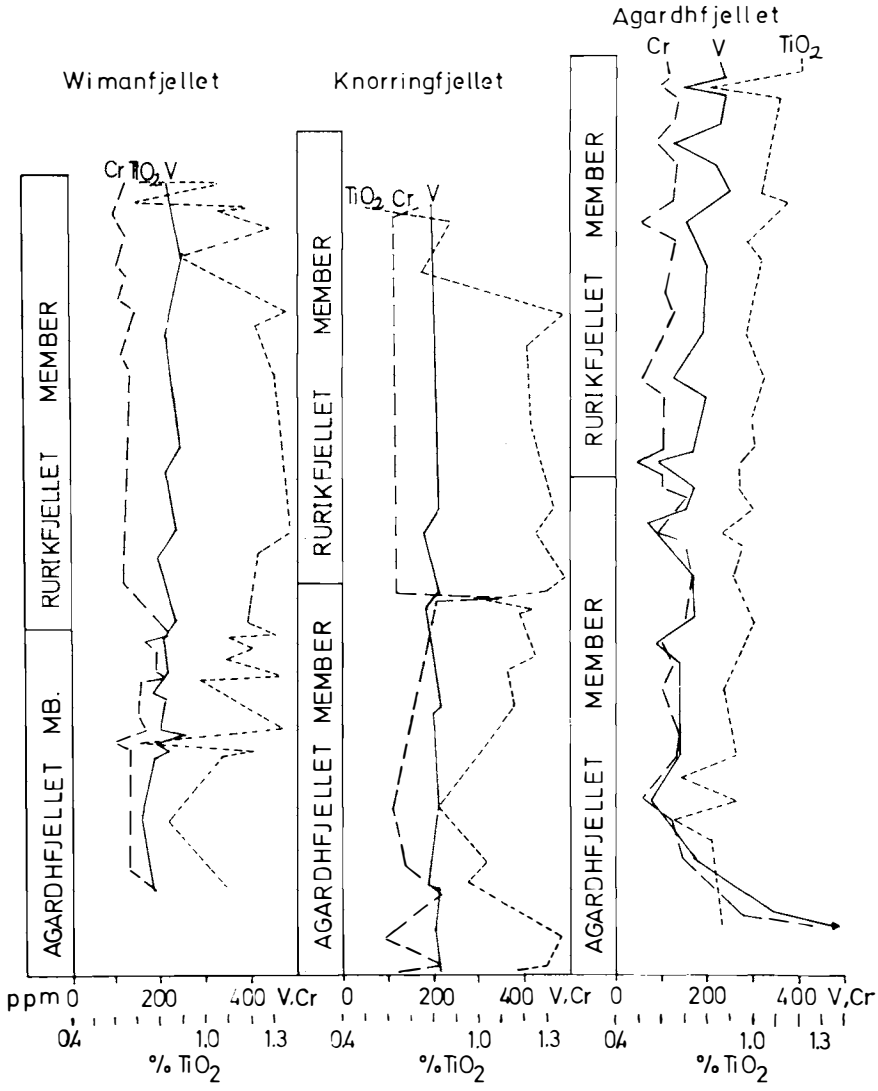

Fig. 15. *Stratigraphical variation in the Cr, TiO_2, and V concentrations of the Janusfjellet Formation, Svalbard.*

clastic fraction, in contrast to Zr which is bound in the coarser clastic fractions. Analyses of the Zr/TiO_2 will consequently give information concerning grain size distributions, with higher values in coarser than in finer grained material. Variations in this ratio in the Janusfjellet Formation confirm the grain size trends suggested above.

Sc, Ti, and Th are found to be relatively immobile in depositional environments and during weathering (Frondel 1970; Logomerac 1969; McNeal & Rose 1974; Yaalon et al. 1974; Dypvik 1977) and are associated to the detrital fraction. The association between these elements and the detrital clay fraction in the Janusfjellet Formation consequently matches these results.

ix. Vanadium and Chromium (V, Cr).

Vanadium concentrations increase weakly upwards in both members in the three sections, while the Cr contents vary (Fig. 15). The Agardhfjellet Member, however, shows constantly higher Cr contents than the Rurikfjellet Member, and there is a significant break in Cr content between the two members. The Cr content of the Agardhfjellet Member first decreases and then increases towards the top of the member. In the Rurikfjellet Member the Cr concentrations show a slight increase upwards.

Vanadium is usually associated with the detrital, volcanic or biogenic constituents of recent marine and older sediments (Vine & Tourtelot 1969; Boström & Fisher 1971; Cosgrove 1973; Bjørlykke 1974; Boström et al. 1974; Desborough et al. 1976; Dypvik 1977). Vine & Tourtelot (1969; 1970) and Bjørlykke (1974) found V in black shales to be associated with organic and detrital material, while Cr is usually bound in the clastic fraction (Bjørlykke 1974; Chester et al. 1976; Dypvik 1977; Parekh et al. 1977). In some cases, however, Cr has been found to be associated with the organic material of black shales (Vine & Tourtelot 1969, 1970; Mothersill 1975). Reinson (1975) interpreted Cr as precipitated as hydroxides from the water column in reducing, estuarine environments.

The relatively high Cr contents of the Agardhfjellet Member may partly be due to hydroxide precipitation in a reducing environment, while V enrichments in the Rurikfjellet Member may be due to the influx of volcanic debris. Dypvik (1980), however, found that about 90% of Cr was bound in clastic minerals.

x. Nickel and Cobalt (Ni, Co)

Generally Ni and Co contents are higher in the Rurikfjellet Member than in the Agardhfjellet Member (Fig. 16). The Ni content decreases through the Agardhfjellet Member, and varies slightly with no observable trend in the Rurikfjellet Member. The Co concentrations increase slightly upwards in the Agardhfjellet Member, while only minor variations are seen in the Rurikfjellet Member.

Most Co and Ni in the suspension load of the Amazon and Yukon rivers is associated with oxide coatings (Gibbs 1977); ferromanganoan sediments from the Bauer Deep (east Pacific) are enriched in Ni and Co due to adsorption (Sayles et al. 1975). Krishnaswami (1976) showed about 80% of Co and Ni in Pacific pelagic clays to occur in the authigenic fraction, while Reinson (1975) found Ni in the clastic fraction and Co (because of oxidation) associated with Mn in estuarine muds from Australia. Ni and Co are usually associated with silicates and sulphides; Co (because of $Co^{2+} \rightarrow Co^{3+}$ oxidation) may, however, also be enriched in Fe–Mn oxides (Carvajal & Landergren 1969; Burns 1976). Both Ni and Co have been found to be rather immobile during weathering of Israeli basalts (Yaalon et al. 1974). Basaltic rocks and the Jurassic dolerites of Spitsbergen are usually enriched in Ni and Co compared to "average shale" contents of 70 and 20 ppm, respectively (Taylor 1965).

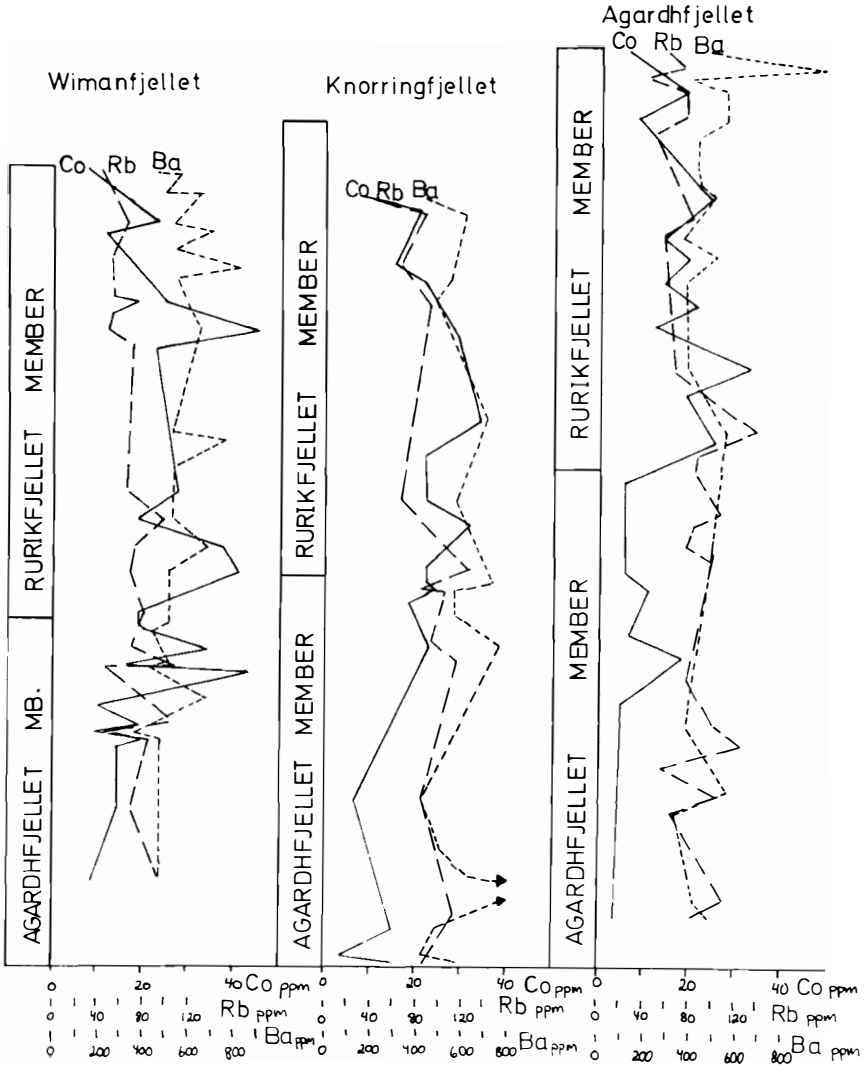

Fig. 16. *Stratigraphical variation in the Co, Rb, and Ba concentrations of the Janusfjellet Formation, Svalbard.*

About 70–80% of Co and Ni in the samples is bound in secondary oxides with minor amounts of Ni in organic material or adsorbed positions (Dypvik 1980). Only a minor amount of Ni and Co is associated with the clastic fraction. Therefore the variations found rather reflect secondary weathering than original variation of e.g. redox potential.

xi. Barium and Strontium (Ba, Sr).

Barium concentrations increase slightly upwards in the Agardhfjellet Member, while relatively constant contents are seen in the Rurikfjellet Member (Fig. 16). Strontium concentrations are, however, almost constant in both members in all three sections.

In silicate minerals Sr and Ba often occur in micas and feldspar. However, Ba may be precipitated as baryte in SO_4^{2-}-enriched environments, while Sr may be enriched in carbonates. In addition BOSTRÖM (1970) mentions that enrichment of Ba may be caused by submarine volcanism and BOSTRÖM et al. (1973a) associated Ba enrichments with biological activity. YAALON et al. (1974) showed both Ba and Sr to be removed by weathering of Israeli basalts. VINE & TOURTELOT (1969) found Ba associated with organic matter and the clastic fraction of black shales. Sr was found in carbonates and clastic minerals in these shales.

Both Ba and Sr are mainly found in clastic minerals (probably feldspar) in the Janusfjellet Formation (DYPVIK 1980). Their distributions consequently indicate relatively constant feldspar contents in the analysed samples. The formation of concretionary carbonate horizons has not produced any secondary enrichment of Sr.

xii. Rubidium and Caesium (Rb, Cs).

Rb and Cs are found in feldspar and mica in sediments (HEIER & ADAMS 1974); both elements are, however, concentrated during weathering, probably due to rapid readsorption after liberation (HORSTMAN 1957; HEIER & ADAMS 1964).

Varying Rb concentrations have been detected in the Agardhfjellet Member (Fig. 16), while concentrations in the Rurikfjellet Member are constant to decreasing. In the Knorringfjellet and Wimanfjellet sections the Rb content of the Agardhfjellet Member is higher than that of the Rurikfjellet Member. Similar Rb contents are found in both members in the Agardhfjellet section. Cs contents also show constant distributions throughout this section. Rb displays a distribution proportional to that of quartz and feldspar and inversly proportional to that of the 7Å/10Å ratio. This indicates Rb to be associated with feldspar and clastic 10Å minerals.

VI. Discussion

A. STRATIGRAPHICAL VARIATIONS IN SEDIMENTOLOGY

It is possible to separate the Agardhfjellet and Rurikfjellet Members into several minor sequences here informally termed "zones" (Fig. 17) on the basis of their composition. The lower 40 m of the Agardhfjellet Member (only systematically sampled in the Knorringfjellet section) shows a slight coarsening upwards trend, increasing $C_{org.}$ content, and decreasing maturity. This development (zone 1) reflects a slight regression and probably decreasing distance to the source area. The zone, which is probably of Callovian to Oxfordian age, is also characterized by red sideritic carbonate beds, iron probably being supplied as colloids from adjacent land areas (DYPVIK 1978). Zone 2, which is about 70 m thick, shows similar, relatively constant grain sizes in all three sections. This indicates rather stable sedimentation. The $C_{org.}$ content and maturity index decrease in the uppermost beds and these are also characterized

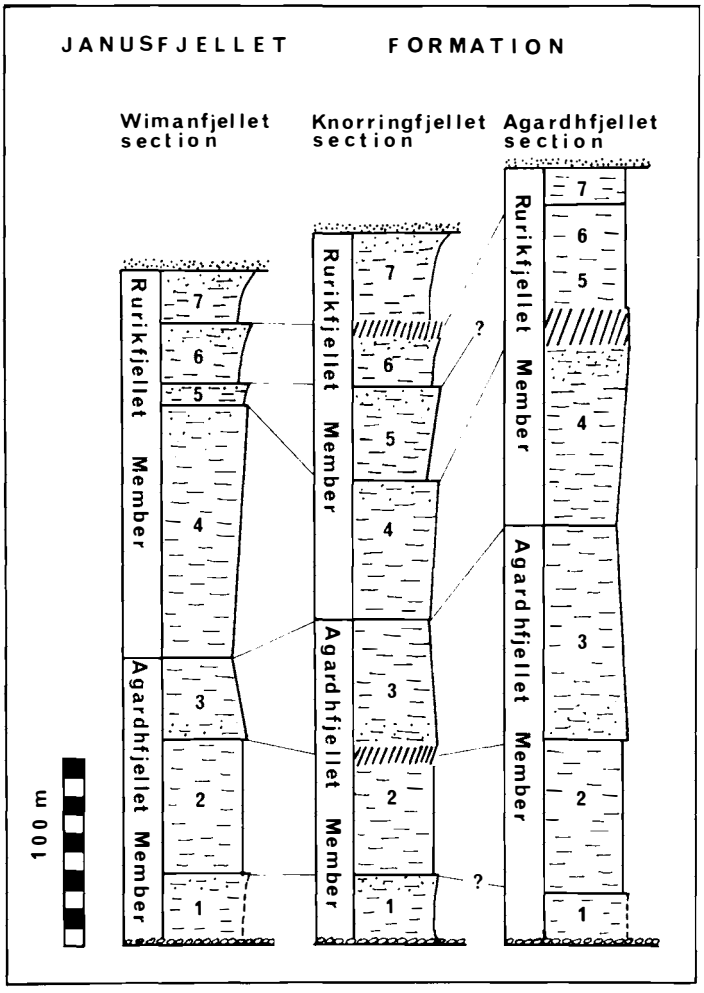

Fig. 17. *Summary section showing petrographical variation through the Janusfjellet Formation, Svalbard. Zone-division numbers are referred to in the text.*

by extremely high Ni/Co ratios. These phenomena indicate a stop in the regression with less weathering in the source area; this is also suggested by minor occurrences of sideritic carbonates. The most mature and organic rich sediments from this zone are found in the Knorringfjellet section. Dorag dolomitisation (Badiozamani 1973) of carbonates may have taken place under the relatively shallow water conditions represented by zone 2, which corresponds to the dolomitic carbonate unit C of Dypvik (1978). Clastic grains in the carbonate beds of zones 1 and 2 also show an increasing grain size upwards.

Zone 3 represents the upper part of the Agardhfjellet Member and is thickest in the Agardhfjellet section and thinnest in the Wimanfjellet section. This zone is characterized by shales with upwards decreasing grain size and maturity, and increasing content of organic carbon, interbedded sandstones also occur. The grain sizes are similar in all three sections studied, while the most mature and organic rich sediments are found in Knorringfjellet section. The grain size

variations indicate similar transgressive developments in all three sections in this zone. The high $C_{org.}$ contents, grain size distributions and maturity variations at the top of this zone in the Wimanfjellet section may weakly indicate that reworking and erosion are the cause of variation in thickness between the sections, rather than subsidence or sedimentary facies variations. These differences are, however, only minor and the more likely differential subsidence is therefore thought to be the *most* important factor producing thickness variations.

The transgression which started in zone 3, continued up to the Jurassic/Cretaceous boundary, where there probably was a break in sedimentation, and minor erosion and reworking. In the Agardhfjellet section the transgressive development continued to about 260 m above base (also noted by LÖFALDLI & THUSU 1976).

There are significant breaks in several of the distributions studied at the boundary between zones 3 and 4, i.e. between the Agardhfjellet and Rurikfjellet Members. The boundary in the Agardhfjellet section may be placed at a horizon 244 m above the Brentskardhaugen Bed on the basis of mineralogical and geochemical similarity with the other two sections.

The base of zone 4, is marked by the deposition of mature, organic rich material with high Cr/V ratios; the zone shows upwards coarsening grain sizes, decreasing maturity and increasing contents of organic material. This indicates after initial transgression, a development towards more proximal sediments with an increasing influx of terrestrial organic debris (BJÆRKE 1978). Zone 4 probably corresponds to the Valanginian (BJÆRKE 1978) and shows similar thickness and grain size distributions in all three sections.

Zones 5 and 6 are combined on Agardhfjellet, but are separated in the other two sections, on the basis of grain size variations. Zone 5 shows a similar coarsening upward sequence to that seen in zone 4, and only Ni/Co ratios are different from the underlying zone. Coarsest grain sizes are found in the Wimanfjellet section, and finest in the Agardhfjellet section in these zones, which according to BJÆRKE (1978) are of Hauterivian age. Zone 7 is characterized by coarsest sediments in the Knorringfjellet and shows two strongly upwards coarsening sequences with increasing maturity and $C_{org.}$ content, probably reflecting deposition of prodeltaic or deltafront sediments. These grain size variations and distributions indicate the Wimanfjellet and Knorringfjellet sections to be more proximal than the Agardhfjellet section.

Zones 3, 4, and 5 correspond to unit B of DYPVIK (1978) with sideritic carbonate beds and dolomites, while zones 6 and 7 are characterized by calcitic and dolomitic beds (unit A of DYPVIK (1978)). This indicates sediments from zones 3, 4, and 5 to be more slowly deposited with more highly weathered products than sediments from 6 and 7.

Grain size developments in all sections are similar and it is reasonable to conclude that both source areas and the depositional environments were also rather similar.

The average composition of shales in the Janusfjellet Formation shows several similarities to the "average black shales" of VINE & TOURTELOT (1970) and the "average shale" of TAYLOR (1965) (Table 1).

B. DEPOSITIONAL ENVIRONMENTS

The Agardhfjellet Member shows a transgressive fining upwards sequence and the Rurikfjellet Member a general regressive coarsening upwards sequence in the three sections studied. These developments are poorly seen in the field and are mainly established by several chemical and mineralogical analyses (thin section, SiO_2/Al_2O_3, quartz + feldspar/clay minerals ratios). The uppermost beds (about 50 m) of the Rurikfjellet Member of the Knorringfjellet and Wimanfjellet sections contain several bioturbated and laminated silty/sandy beds.

Moore & Scruton (1957) and Coleman & Cagliano (1965) described regularly laminated silt beds close to the delta front, passing distally into finer grained and bioturbated beds in Mississippi deltaic environments. They claim such regular laminated prodelta slope beds to be deposited rapidly by unidirectional currents of varying intensities and loads. Moore & Scruton (1957) claimed that only minor bioturbation occurs because of rapid deposition. In the Fraser Delta (British Columbia) Matthews & Shepard (1962) also noted decreasing sand content with increasing distance from delta. Allen (1965) also found laminated silt, clay and sand in the upper part of the prodelta slope and lower part of delta front environments and also decreasing grain size seawards, in the Niger delta. Allen (1965) noted a high degree of bioturbation in the open shelf area, distal to the delta. Van Straaten (1959) and Oomkens (1967) noted similar developments in the Rhone delta. Thus, both constructive (Mississippi) and destructive (Niger, Rhone) deltaic build-ups (Fisher et al. 1974) may show the same sedimentological characteristics as the upper part of the Rurikfjellet Member. However, the conclusions of Fisher et al. (1974) make a constructive delta model most probable as laminated prodeltaic slope sediments seem more common in such environments. The lack of bar sands, which often occur in destructive deltas, may also suggest a constructive deltaic origin. A fluvial-dominated delta origin has also been suggested by Steel et al. (1978).

Bioturbated shales occurring below the laminated silt and shale probably represent open shelf environments as described by Van Straaten (1959), Allen (1965), and Fisher et al. (1974).

The Rurikfjellet Member is therefore marked by a regressive development from open shelf clay sedimentation to bioturbated silty clays from the distal parts of prodeltaic environments. These beds are finally overlain by laminated silts, representing upper prodelta slope to lower delta front deposits. This regressive development is also recorded in the palynological distributions where increasing terrestrial and decreasing marine floras are seen upwards in the Rurikfjellet Member (Bjærke 1978). The prodelta slope sediments of the Rurikfjellet Member may be the precursors of the deltaic environments of the overlying Helvetiafjellet Formation (Steel 1977; Steel et al. 1978).

According to Dypvik (1978) the Janusfjellet Formation contains several minor hiatus or stillstands in clastic sedimentation, often represented by carbonate horizons, in addition to the possible greater hiatus between the two members at the Jurassic/Cretaceous transition. Discontinuous deposition may

reflect local isostatic movements resulting from tectonic activity such as movements of fault blocks.

Grain size distributions are rather similar in equivalent beds from the three sections analysed, indicating only minor differences in sedimentary environments between the sections. Maturity indexes, such as the M and K_2O/Na_2O ratios, indicate beds from Knorringfjellet to be more mature than equivalent beds from Wimanfjellet and Agardhfjellet. Between the sections of Wimanfjellet and Agardhfjellet more confusing and complicated relations exist. Generally, however, the maturity relations may indicate the Knorringfjellet section to be originally situated further from source areas than the other two sections.

The presence of post Upper Jurassic–pre Lower Cretaceous movements along the Flowerdalen fault zone, where the Triassic Botneheia Formation is unconformably overlain by Valangian shales of the Rurikfjellet Member (PARKER 1966), seem only to have had local sedimentological effects. None of the sedimentological analyses from Wimanfjellet or Knorringfjellet (only some kilometres away) seem to show any clearcut evidence of direct influence from the tectonically generated highs in that area. Neither does the Agardhfjellet section show any notable impact of the tectonic movements along the Agardhbukta fault zone at the same time. At Wimanfjellet, Knorringfjellet and Agardhfjellet there is a break in sedimentation at the Jurassic–Cretacous boundary, but no sedimentological response to the nearby tectonically active high has been observed in the two areas (Sassenfjorden, Agardhfjellet).

In all sections there is upwards decreasing maturity in the Agardhfjellet Member and varying maturity values in the Rurikfjellet Member. Decreasing maturity upwards in Agardhfjellet Member may reflect lower rates of weathering than erosion during the transgressive development, while the maturity variations during the regressive Rurikfjellet Member are difficult to interpret.

The Agardhfjellet Member displays high contents of S and $C_{org.}$, especially 40 to 50 m above the base of the member (6–12 %$C_{org.}$). This may indicate the Agardhfjellet Member to be deposited under less oxidising conditions than the Rurikfjellet Member. The marginal marine and deltaic affinities of the Rurikfjellet Member make such a relation reasonable. The S and $C_{org.}$ concentrations in the Agardhfjellet Member show a varying upwards decreasing trend, while concentrations increase upwards in the Rurikfjellet Member. These variations reflect the transgressive (Agfj.Mb) and regressive (Rufj.Mb) developments already mentioned. In the Janusfjellet Formation DYPVIK (1978) showed that Ni and Co are mainly bound in secondary minerals, such as weathering products with iron oxides. Variations in the present Ni/Co ratio are therefore controlled by later secondary weathering reactions and not by primary Eh variations. The generally higher Fe, Ni and Co concentrations in the Rurikfjellet Member compared to the Agardhfjellet Member may indicate higher contents of volcanic (Fe, Ni and Co rich) debris in this unit. DYPVIK (1978) observed similar element enrichments in the associated carbonate beds. Crude estimates based on the Fe and Co distributions in dolerites (DYPVIK 1979b) and shales from the Agardhfjellet Member, indicate 10–30 % of Fe and

Co in the Rurikfjellet Member to be derived from a dolerite-like source. The Rurikfjellet Member of Knorringfjellet and Agardhfjellet is relatively richer in volcanic material than the Wimanfjellet section. This may suggest an easterly source for the volcanic debris in these sediments.

The shaly sediments of the Janusfjellet Formation are found to be cemented by clay minerals, organic matter and secondary oxides/hydroxides of Fe and Mn. In the silt/sandstones and the more silty shales from the top of the Rurikfjellet Member, quartz is the major cementing agent. Clay minerals, quartz and minor amounts of calcite surrounding kaolinite grains are the only cements detected from the uppermost beds of the Rurikfjellet Member. These sediments were deposited in prodelta slope/delta front environments, and early diagenetic quartz overgrowths and cements may have formed in the mixing zone between fresh and marine waters (Fisher et al. 1974).

VII. Conclusion

The Agardhfjellet Member mainly represents open shelf depositional environments, succeeding the shallow marine Brentskardhaugen Bed. Initial transgression was followed by a minor regressive development in Callovian to Oxfordian times when continually less mature sediments were deposited. After a period of steady sedimentation, a transgressive phase marks the top of the Agardhfjellet Member (probably of Volgian age). After a stillstand or break in sedimentation at the Jurassic/Cretaceous boundary, the deposition of the Rurikfjellet Member started in the Valanginian, with an initial transgression followed by a regressive development. In the uppermost parts of this mainly regressive member, highly bioturbated, silty muds succeeded the open shelf development. This Hauterivian regression is seen by deposition of silt- and sandstones of prodelta slope to delta front environments at the top of the Rurikfjellet Member. The overlying Helvetiafjellet Formation represents the main deltaic development in the area, and may probably be of constructive delta affinity.

The Flowerdalen and Agardhbukta fault zones had no visible impact on the sedimentological evolution of the studied sections. These fault zones are, however, probably only part of a larger regional tectonic pattern, which resulted in the development of several highs and basins in this Jurassic/Cretaceous epicontinental sea. Such tectonic movements (of minor dimension) close to the studied sections, may be the explanation for the transgressive and regressive developments which disrupted rather stable shelf sedimentation through Jurassic and Cretaceous times.

The Rurikfjellet Member is generally enriched in volcanic debris compared to the Agardhfjellet Member. The Agardhfjellet Member was, however, deposited under more stagnant conditions, characterized by higher concentrations of organic carbon and sulphur.

The Agardhfjellet and Knorringfjellet sections seem to contain more volcanic debris than the Wimanfjellet section, while the Knorringfjellet section seems to contain the most mature sediments.

Periods of minor clastic deposition throughout the formation are indicated by carbonate horizons, which have a diagenetic mineralogy, reflecting the varying supply of weathering material. Generally varying subsidence in the different areas resulted in different sediment thicknesses, and erosion and reworking had only a minor impact. Most subsidence took place in the eastern areas (the Agardhfjellet area).

The Janusfjellet Formation consists of shales which are weakly cemented by iron oxides and organic matter. Only minor diagenetic processes have been observed, but the occurrence of early diagenetic glauconite and framboidal pyrite has been established in these shales. Siltstones and silty shales occurring at the top of the formation show a more complex diagenetic history. In addition to early diagenetic glauconite formation, quartz cement was also precipitated relatively early, probably as a result of pH variation in the mixing zone between fresh and marine waters. Some minor amounts of kaolinite were probably formed before or about this time. After quartz cementation and confined kaolinite growth, minor amounts of carbonates filled most of the remaining pore space. The calcite was probably derived from dissolved skeletal fragments at a later stage of burial. Some minor diagenetic formation of mica may, however, have taken place before calcite cementation.

Part of the Janusfjellet Formation seems to have suffered weathering and oxidation, which has led to the formation of jarosite and gypsum.

Such secondary oxides are common in the Agardhfjellet Member and these explain the poor preservation of palynomorphs in this member.

Except for the extremely organic rich shales from the middle and the top of the Agardhfjellet Member, the shales of the Janusfjellet Formation are on average very similar in composition to black shales from other areas of the world.

Acknowledgements

This project is a part of the project: "Paleontological and sedimentological investigations on Svalbard" led by Dr. D. Worsley, University of Oslo. The programme is supported by NAVF (D.40.38–8), NTNF (B1810.6790), Statoil, and Norsk Polarinstitutt.

Thanks are extended to Mr. T. Bjærke for several discussions and valuable field cooperation, to Dr. M. B. Edwards for collecting the samples from Agardhfjellet, and to Dr. A. O. Brunfelt, Ms. E. Bråten and Dr. W. L. Griffin for laboratory guidance. Ms. B. Bue, Prof. K. Bjørlykke, Mr. H. G. Rueslåtten, and Dr. D. Worsley kindly commented on drafts of the manuscript.

References

Adams, F. & R. Dams, 1969: A compilation of precisely determined gamma-transition energies of radionuclides produced by reactor irradiation. *J. of Radioanalytical Chemistry* **3**: 99–125.

Allen, J. R. L., 1965: Late Quaternary Niger Delta, and adjacent areas; sedimentary environments and lithofacies. *Am. Assoc. Petr. Geol Bull.* **49**: 547–600.

Badiozamani, K., 1973: The Dorag dolomitization model – application to the Middle Ordovician of Wisconsin. *Journ. Sed. Pet.* **43**: 965–984.

BIRKELUND, T., 1975: A review of the Jurassic of East Greenland. *JNNS Symposium Proceed.*: 6–1 — 6–27. Stavanger 1975, NPF.

BIRKENMAJER, K. 1972: Megaripples and phosphorite pebbles in the Rhaeto-Liassic beds south of Van Keulenfjorden. Spitsbergen. *Norsk Polarinst. Årbok* 1970: 117–127.

BJØRLYKKE, K., 1974: Depositional History and Geochemical Composition of Lower Paleozoic Epicontinental Sediments from the Oslo Region. *Norges Geol. Unders.* **305**: 1–81.

BJÆRKE, T., 1978: Mesozoic Palynology of Svalbard III. Dinoflagellates from the Rurikfjellet Member, Janusfjellet Formation (Lower Cretaceous) of Spitsbergen. *Palinologia, nun. extraord.* **1**: 69–93.

BJÆRKE, T. & H. DYPVIK, 1977: Sedimentological and palynological studies of Upper Triassic–Lower Jurassic sediments in Sassenfjorden, Spitsbergen. *Norsk Polarinst. Årbok* 1976: 131–150.

BJÆRKE, T., M. B. EDWARDS & B. THUSU, 1976: Cretaceous Palynomorphs from Spitsbergenbanken, NW Barents Shelf. *Norsk Polarinst. Årbok* 1974: 258–262.

BOSTRØM, K., 1970: Submarine Volcanism as a source for iron. *Earth Planet. Sci. Lett.* **9**: 348–354.

BOSTRØM, K. & D. E. FISHER, 1971: Volcanogenic uranium, vanadium and iron in Indian Ocean Sediments. *Earth Planet. Sci. Lett.* **11**: 95–98.

BOSTRØM, K., O. JOENSUU, & I. BROHM, 1974: Plankton: Its chemical composition and its significance as a source of pelagic sediments. *Chem. Geol.* **14**: 255–271.

BOSTRØM, K., O. JOENSUU, C. MOORE, B. BOSTRØM, M. DALZIEL, & A. HOROWITZ, 1973: Geochemistry of barium in pelagic sediments. *Lithos* **6**: 159–174.

BOSTRØM, K., T. KRAEMER, & S. GARTNER, 1973: Provenance and Accumulation rates of opaline silica, Al, Ti, Fe, Mn, Cu, Ni, & Co in Pacific Pelagic Sediments. *Chem. Geol.* **11**: 123–148.

BOWEN, H. J. M., 1966: *Trace Elements in Biochemistry.* Academic Press, London 1966: 241 pp.

BROWN, G., 1961: *The X-ray identification of clay minerals.* Min. Soc., London 1961. 544 pp.

BRUNFELT, A. O. & E. STEINNES, 1971: Instrumental Activation Analysis of silicate rocks with epithermal neutrons. *Anal. Chim. Acta* **48**: 13–24.

BURNS, R. G., 1976: The uptake of cobalt into ferromanganese nodules, soils and synthetic manganese (IV) oxides. *Geoch. Cosm. Acta* **40**: 95–102.

CARROL, D., 1970: Clay Minerals: A Guide to Their X-ray Identification. *Geol. Soc. Am. Spec. Paper* **126**. 80 pp.

CARVAJAL, M. C. & S. LANDERGREN, 1969: Marine sedimentation processes. The interrelationship of manganese, cobalt and nickel. *Stockh. Contrib. Geol.* **18**: 99–122.

CHESTER, R., S. R. ASTON, & D. BRUTY, 1976: The trace-element partition geochemistry in an ancient deep-sea sediment core from the Bermuda Rise. *Mar. Geol.* **21**: 271–288.

CLEMMENSEN, L., & F. SURLYK, 1976: Upper Jurassic coal-bearing shoreline deposits, Hochstetter Forland, East Greenland. *Sedim. Geol.* **15**: 192–211.

COLEMAN, J. M. & S. M. CAGLIANO, 1965: Sedimentary Structures: Mississippi River deltaic plain. In: G. V. Middleton (ed.): Primary sedimentary structures and their hydrodynamic interpretation. *Soc. Econ. Pal. Min., Spec. Paper* **12**: 133–148.

COSGROVE, M. E., 1973: The geochemistry and mineralogy of the Permian red beds of southwest England. *Chem. Geol.* **11**: 31–47.

DALLAND, A., 1975: The Mesozoic Rocks of Andøy, Northern Norway. *Norges Geol. Unders.* **316**: 271–287.

D'ANGLEJAN, B. F., 1967: Origin of marine phosphorites off Baja California, Mexico. *Marine Geol.* **5**: 15–40.

DESBOROUGH, G. A., J. K. PITMAN, & C. HUFFMAN Jr., 1976: Concentration and mineralogical residence of elements in rich oil shales of the Green River Formation, Piceance Creek Basin, Colorado, and the Uinta Basin, Utah — A preliminary report. *Chem. Geol.* **17**: 13–26.

DYPVIK, H., 1977: Mineralogical and geochemical studies of Lower Palaeozoic rocks from the Trondheim and Oslo regions, Norway. *Norsk Geol. Tidsskr.* **57**: 205–241.

DYPVIK, H., 1978: Origin of carbonate in marine shales of the Janusfjellet Formation, Svalbard. *Norsk Polarinst. Årbok* 1977: 101–110.

— 1979a: Mineralogy and geochemistry of the Mesozoic sediments of Andøya, Northern Norway. *Sedim. Geol.* **24**: 45–67.

— 1979b: Major and minor element chemistry of Triassic black shales near a dolerite intrusion at Sassenfjorden, Spitsbergen. *Chem. Geol.* **25**: 53–65.

— 1980: Geochemical studies of sedimentary constituents in Mesozoic shales from Svalbard. *Norsk Polarinst. Skrifter* Nr 172: 135–143 (this volume).

EDWARDS, M. B., 1976: Depositional environments in Lower Cretaceous regressive sediments, Kikutodden, Sørkapp Land, Svalbard. *Norsk Polarinst. Årbok* 1974: 35–50.

ELVERHØI, A., 1977: Origin of framboidal pyrite in clayey sediments and in Jurassic black shale in the north-western part of the Barents Sea. *Sedimentology* **24**: 591–595.

FISHER, W. L., L. F. BROWN JR., A. J. SCOTT, & J. H. MCGOWEN, 1974: *Delta Systems in the Exploration for Oil and Gas*. The Univ. of Texas, Austin, Texas, 1969. 77 pp.

FLANAGAN, F. J., 1973: 972 values for international geochemical reference samples. *Geoch. Cosmo. Acta* **37**: 1189–1200.

FLOOD, B., J. NAGY, & T. S. WINSNES, 1971: Geological map, Svalbard 1:500 000, Sheet 1G Spitsbergen Southern Part. *Norsk Polarinst. Skrifter* Nr. 154A.

FRONDEL, C., 1970: Scandium. **In**: K. H. WEDEPOHL (ed.), *Handbook of Geochemistry. II–2, 21–1 – 21–0–1.* Springer Verlag.

GAYER, P. A., D. G. GEE, W. B. HARLAND, J. A. MILLER, H. R. SPALL, R. H. ALLIS, & T. S. WINSNES, 1966: Radiometric age determinations of rocks from Spitsbergen. *Norsk Polarinst. Skrifter* Nr. 137.

GIBBS, R. J., 1965: Error due to segregation in quantitative clay mineral X-ray diffraction mounting techniques. *Am. Mineralogist* **50**: 741–751.

— 1977: Transport phases of transition metals in the Amazon and Yukon Rivers. *Geol. Soc. Am. Bull.* **88**: 829–843.

GORDON, G. E., K. RANDLE, G. G. GOLES, J. B. CORLISS, M. H. BEESION, & S. S. OXLEY, 1968: Instrumental activation analysis of standard rocks with high-resolution γ-ray detectors. *Geoch. Cosmo. Acta* **32**: 369–396.

HALLAM, A., 1971: Mesozoic Geology and the opening of the North Atlantic. *Journ. of Geol.* **79**: 129–157.

HAMAR, G., 1975: A Jurassic structure complex in northern North Sea. *JNNSS Symposium Proceed.* 17–1 – 17–18. Stavanger 1975. NPF.

HARLAND, W. B., 1969: Contribution of Spitsbergen to understanding of tectonic evolution of North Atlantic region. **In**: M. HAY (ed.): North Atlantic-Geology and Continental drift, *Am. Assoc. Petr. Geol., Mem.* **12**: 817–851.

HEIER, K. S. & J. A. S. ADAMS, 1964: The Geochemistry of the Alkali Metals. **In**: L. H. AHRENS (ed.). *Physics and Chemistry of the Earth 5*: 253–381. Pergamon Press, 1964.

HERRON, E. M., J. F. DEWEY, & W. C. PITMAN III, 1974: Plate Tectonics Model for the Evolution of the Arctic. *Geology* Aug. 1974: 377–380.

HORSTMAN, E. L., 1957: The Distribution of Li, Rb & Cs in igneous and sedimentary rocks. *Geoch. Cosmo. Acta* **12**: 1–28.

JOHNSON, C. D. & L. V. HILLS, 1973: Microplankton zones of the Savik Formation (Jurassic), Axel Heiberg and Ellesmere Islands, District of Franklin. *Bull. Can. Pet. Geology* **21**: 178–218.

KRISHNASWAMI, S., 1976: Authigenic transition elements in Pacific pelagic clays. *Geoch. Cosmo. Acta* **40**: 425–434.

LOGOMERAC, V. G., 1969: The distribution of rare earths and other minor elements in Surinam bauxite and laterite and the red mud obtained from them. *Proceed. of the J. Guiana Geol. Conf.* 1968: 155–162.

LOWELL, J. D., 1972: Spitsbergen Tertiary orogenic belt and the Spitsbergen Fracture Zone. *Geol. Soc. Am. Bull.* **83**: 3091–3101.

LØFALDLI, M. & B. THUSU, 1976: Microfossils from the Janusfjellet Subgroup (Jurassic–Lower Cretaceous) at Agardhfjellet and Keilhaufjellet, Spitsbergen. *Norsk Polarinst. Årbok* 1975: 69–77.

MAJOR, H. & J. NAGY, 1972: Geology of the Adventdalen map area. *Norsk Polarinst. Skrifter* Nr. 138. 58 pp.

MATTHEWS, W. H. & F. P. SHEPARD, 1962: Sedimentation of Fraser Delta, British Columbia. *Am. Assoc. Petr. Geol. Bull.* **46**: 1416–1443.

MCKELVEY, V. E., 1967: Phosphate deposits. *U.S. Geol. Surv. Prof. Paper* 1252–D. 21 pp.

MCNEAL, J. M. & A. W. ROSE, 1974: The geochemistry of mercury in sedimentary rocks and soils in Pennsylvania. *Geoch. Cosmo. Acta* **38**: 1759–1784.

MEHRA, O. P. & M. L. JACKSON, 1960: Iron oxide removal from soils and clays by a dithionite-citrate system buffered with sodium bicarbonate. *Clays and clay minerals* **7**: 317–327.

MILLOT, G., 1970: *Geology of clays*. Springer Verlag, Heidelberg, 1970. 429 pp.

MOORE, D. G. & P. L. SCRUTON, 1957: Minor internal structures of some recent unconsolidated sediments. *Am. Ass. Petr. Geol. Bull.* **47**: 2723–2751.

MOTHERSILL, J. S., 1975: Lake Chad: Geochemistry and sedimentary aspects of a shallow polymictic lake. *Am. Assoc. Petr. Geol. Bull.* **41**: 2723–2751.

MÜLLER, R. O., 1967: *Spektrochemische Analysen mit Röntgen fluoreszenz*. R. Oldenbourg, München-Wien, 1967. 315 pp.

NORRISH, K. & R. M. TAYLOR, 1962: Quantitative analyses by X-ray diffraction. *Clay Min. Bull.* **5**: 98–104.

OOMKENS, E., 1967: Depositional sequences and sand distribution in a deltaic complex. *Geol. en Mijnbouw* **46**: 265–278.

PAREKH, P. P., P. MØLLER, P. DULSKI, & W. M. BAUSCH, 1977: Distribution of trace elements between carbonate and non-carbonate phases of limestone. *Earth Planet. Sci. Lett.* **34**: 39–50.

PARKER, J. R., 1966: Folding, faulting and dolerite intrusions in the Mesozoic rocks of the fault zone of central Spitsbergen. *Norsk Polarinst. Årbok* 1964: 47–55.

— 1967: The Jurassic and Cretaceous Sequence in Spitsbergen. *Geol. Mag.* **104**: 487–505.

PČELINA, T. M., 1970: Stratigraphy and composition of the Mesozoic deposits in central Vestspitsbergen. **In**: W. B. HARLAND (ed.): *Geology of Spitsbergen, 1965 1–*: 131–154. Nat. Lending Lib. for Sci. and Tecn., England.

— 1970b: Mesozoic deposits around Van Keulenfjorden Vestspitsbergen. **In**: W. B. HARLAND (ed.): *Geology of Spitsbergen, 1965. 1*: 155–181. Nat. Lending Lib. for Sci. and Tecn., England.

PETTIJOHN, F. J., 1957: *Sedimentary Rocks. Sec. ed.* Harper, New York. 718 pp.

PITMAN, W. C. & M. TALWANI, 1972: Sea-floor spreading in the North Atlantic. *Geol. Soc. Am. Bull.* **83**: 619–646.

PLAUCHUT, B. P., 1971: Geology of the Sverdrup Basin. *Bull. Can. Petr. Geol.* 1971: 659–679.

PORRENGA, D. H., 1967: Glauconite and Chamosite as depth indicators in the marine environment. *Mar. Geol.* **5**: 495–501.

REINSON, G. E., 1975: Geochemistry of muds from a shallow restricted estuary, Australia. *Mar. Geol.* **19**: 297–314.

ROZYCKI, S. Z., 1959: Geology of the north-western part of Torell Land, Vestspitsbergen. *Studia geol. polon.* **2**: 1–98.

SAYLES, F. L. T., L. KU, & P. C. BOWERK, 1975: Chemistry of ferromanganoan sediment of the Bauer Deep. *Geoy. Soc. Am. Bull.* **86**: 1423–1431.

SMOOT, T. W., 1960: Clay mineralogy of pre-Pennsylvanian sandstones and shales of the Illinois Basin, Part III. Clay minerals of various facies of some Chester formations. *Ill. State Geol. Surv.* **293**: 1–19.

STEEL, R. J., 1977: Observations on some Cretaceous and Tertiary sandstone bodies in Nordenskiøld Land Svalbard. *Norsk Polarinst. Årbok* 1976: 43–68.

STEEL, R. J., J. GJELBERG, & G. HAARR, 1978: Helvetiafjellet Formation (Barremian) at Festningen, Spitsbergen – a field guide. *Norsk Polarinst. Årbok* 1977: 111–128.

VAN STRAATEN, L. M. J. U., 1959: Minor structures of some recent littoral and neritic sediments. *Geol. en Mijnbouw.* **21**: 197–216.

SUMMERHAYES, C. P. & J. P. WILLIS, 1975: Geochemistry of Manganese deposits in relation to environment on the sea floor around southern Africa. *Mar. geol.* **18**: 159–173.

SURLYK, F., 1973: The Jurassic-Cretaceous boundary in Jameson Land, East Greenland. **In**: R. CASEY & P. F. RAWSON (eds): *The Boreal Lower Cretaceous, Geological Journ. Spec. Issue* **5**: 81–100.

— 1975: Block faulting and associated marine sedimentation at the Jurassic–Cretaceous Boundary, East Greenland. *JNNSS NPF Symp. Proceed. Stavanger 1975: 7/1 – 7–31.*

SURLYK, F., J. H. CALLOMON, R. G. BROMLEY, & T. BIRKELUND, 1973: Stratigraphy of the Jurassic–Lower Cretaceous sediments of Jameson Land and Scoresby Land, East Greenland. *Grøn. Geol. Unders. Bull.* **105**. 76 pp.

TALWANI, M. & O. ELDHOLM, 1977: Evolution of the Norwegian–Greenland Sea. *Geol. Soc. Am. Bull.* **88**: 969–999.

TAYLOR, S. R., 1965: The application of trace element data to problems in petrology. **In**: L. A. AHRENS, F. PRESS, S. K. RUNCORN, & C. UREY (eds): *Physics and Chemistry of the Earth.* Oxford, Pergamon Press **6**: 133–214.

THORSTEINSSON, R., & E. T. TOZER, 1970: Geology of the Arctic Archipelago. **In**: R. J. DOUGLAS (ed.): Geology and Economica Minerals of Canada. *Geol. Surv. Can. Econ. Geology Rept.* **1**: 548–590.

VINE, J. D. & E. B. TOURTELOT, 1969: Geochemical Investigations of some Black Shales and Associated Rocks. *U.S. Geol. Surv. Bull.* **1314-A**. 43 pp.

VINE, J. D. & E. B. TOURTELOT, 1970: Geochemistry of Black Shale Deposits – A summary Report. *Econ. Geol.* **65**: 253–272.

WORSLEY, D., 1973: The Wilhelmøya Formation – a new lithostratigraphical unit from the Mesozoic of eastern Svalbard. *Norsk Polarinst. Årbok* 1971: 7–16.

YAALON, D. H., I. BRENNER, & H. KOYUMDJISKY, 1974: Weathering and mobility sequence of minor elements on a basaltic pedomorphic surface, Galilee, Israel. *Geoderma* **12**: 233–244.

ZIEGLER, P. A., 1975: The Geological Evolution of the North Sea Area in the Tectonic Framework of North Western Europe. *Norges Geol. Unders.* **316**: 1–27.

ZIEGLER, W. H., 1975: Outline of the geological history of the North Sea. **In**: A. W. WOODLAND (ed.): *Petroleum and the Continental Shelf of North-West Europe.* **1**: 165–187.

Table 1.

The average concentration of some elements in shales of Janusfjellet Formation compared to average black shales (VINE & TOURTELOT *1970*) *and the average shale of* TAYLOR (*1965*).

Element	*Average Jan. Fj. Fm Shale*	*Avrg. Black Shale*	*Avrg. Shale*
Corg.	2.6 %	3.2 %	n.a.
Zr	227 ppm	70 ppm	160 ppm
TiO_2	1.11 %	0.2 %	n.a.
Sc	15.5 ppm	10 ppm	15 ppm
Th	12 ppm	n.a.	12 ppm
V	199 ppm	150 ppm	130 ppm
Cr	137 ppm	100 ppm	100 ppm
Ni	69 ppm	50 ppm	70 ppm
Co	17 ppm	10 ppm	20 ppm
Ba	532 ppm	300 ppm	700 ppm
Sr	140 ppm	200 ppm	300 ppm

n.a. = Not available Vine & Tourtelot (1970) Taylor (1965)

Geochemical studies of sedimentary constituents in Mesozoic shales from Svalbard

By Henning Dypvik[1]

Abstract

Eight samples of Jurassic and lower Cretaceous black shales from Svalbard have been disintegrated and chemically analysed for major and trace elements. All the studied elements are mainly bound in clastic silicates. Fe, Mn, Co, Ni, and partly Zn and Mo are also present in secondary oxide rims in the sediments, while some Na, Cu, Ni, Mo, and Zn are associated with organic material. Generally minor amounts of Mo, Cu, Ba, and Na are found in adsorbed positions.

Introduction

Due to the heterogeneous composition of sediments, bulk geochemical analyses may often be rather difficult to interpret. The present investigation was designed to provide more information on the chemical position of the different constituents in shales.

Eight samples of black shales from the Janusfjellet Formation (Upper Jurassic–Lower Cretaceous), Svalbard, four from Agardhfjellet and four from Knorringfjellet were analysed (see Fig. 3 of Dypvik 1980, p. 101 this volume). The same samples have been studied sedimentologically, mineralogically, geochemically and palynologically (Bjærke et al. 1976; Bjærke 1978; Dypvik 1980; Edwards 1976).

Geology

The Middle and Upper Jurassic to Lower Cretaceous Janusfjellet Formation (Parker 1967) consists mainly of marine black shales (see Fig. 1 of Dypvik 1980, p. 98, this volume). In the studied areas the formation is separated into two members; the Jurassic Agardhfjellet Member was deposited as a fining upwards shale sequence, and after a break in sedimentation, the coarsening upwards sediments of the Rurikfjellet Member were deposited. The Rurikfjellet Member terminates in the Helvetiafjellet Formation which is thought to be of Barremian age (Major & Nagy 1972).

The analysed samples which consist of badly sorted clay and silt material, show only minor mineralogical variations. The main constituents are quartz,

[1] Institutt for geologi, Universitetet i Oslo, Blindern, Oslo 3.

feldspar, mixed layered clay minerals, illite, kaolinite, with additional minor amounts of organic carbon, secondary iron oxides, and in some samples minor amounts of pyrite. Carbonates have not been found in these samples (thin section, X-ray diffraction). Only minor diagenetic alterations are observed in thin section.

Methods

NH_4Ac/HAc treatment

This treatment (modified from JACKSON 1958) is performed to remove adsorbed ions from the shales. NH_4^+ is thought to replace elements in adsorbed positions on the clay minerals (CHAPMAN 1965). The solutions are, however, weakly acid, and consequently carbonates may be dissolved by this treatment.

Na – citrate treatment

By Na-citrate treatment (MEHRA & JACKSON 1960) ferric iron is reduced to ferrous iron and consequently rims of secondary iron/manganese oxides/hydroxides are dissolved. These Na-citrate solutions are acid and may therefore dissolve available carbonates and sulfates.

H_2O_2 – treatment

H_2O_2 treatment of sediments removes organic material. Kerogen and bitumenous material are dissolved by oxidation, and sulfides will also be dissolved (FARMER & MITCHELL 1963). The H_2O_2 dissolution technique is modified from PRESTLEY et al. (1972).

The chemical treatments were done in two systematically different ways; one by performing a continuous sequence of analyses on the same sample, the other by performing each analytical treatment on a different subsample.

Continuous analyses

Rock powder of the samples was first treated with NH_4Ac/HAc buffer solution. The resulting solutions were removed for atomic absorption (AA) analysis, while the solid residues were treated with Na-citrate solutions. After citrate solution, the effluents were analysed for main and trace elements, while the solid residues were treated with H_2O_2 solutions. The resulting solutions were analysed by AA.

Separate analyses

Three different splits, 2 to 4 g of rock powder, of each sample were treated with NH_4Ac/HAc – buffer, Na-citrate and H_2O_2 solutions separately. The resulting solutions and solid residues were separated and chemical analyses were executed on the extracted solutions. By this treatment it is possible to obtain excessive concentrations of the different constituents. For example, Na-citrate and H_2O_2 treatment may also release some adsorbed ions resulting in too high values in the extracts analysed.

The chemical composition of the following fractions was determined by atomic absorption analysis of the solutions obtained by the different chemical treatments:

A) Adsorbed ions (NH_4Ac/HAc – treatment)
B) Ions mainly in secondary Fe – and Mn minerals (Na – citrate treatment)
C) Ions mainly associated with organic material (H_2O_2 – treatment)

The acid solutions probably dissolve minor, undetectable amounts of carbonates which may have been present. Total concentration of the bulk samples minus concentrations in fractions A, B, and C above, are considered to represent mainly silicates, most of which are clastic in origin.

Chemical analyses

The major and trace elements in the bulk samples were analysed by X-ray fluorescence, (XRF), while main and trace elements in solutions (effluents) and Cu, Zn, and Mo for bulk samples were determined by atomic absorption (AA). Standard deviation was generally from 1 to 6%, while XRF analyses of Co gave 10% and AA-analyses of Ba 14%.

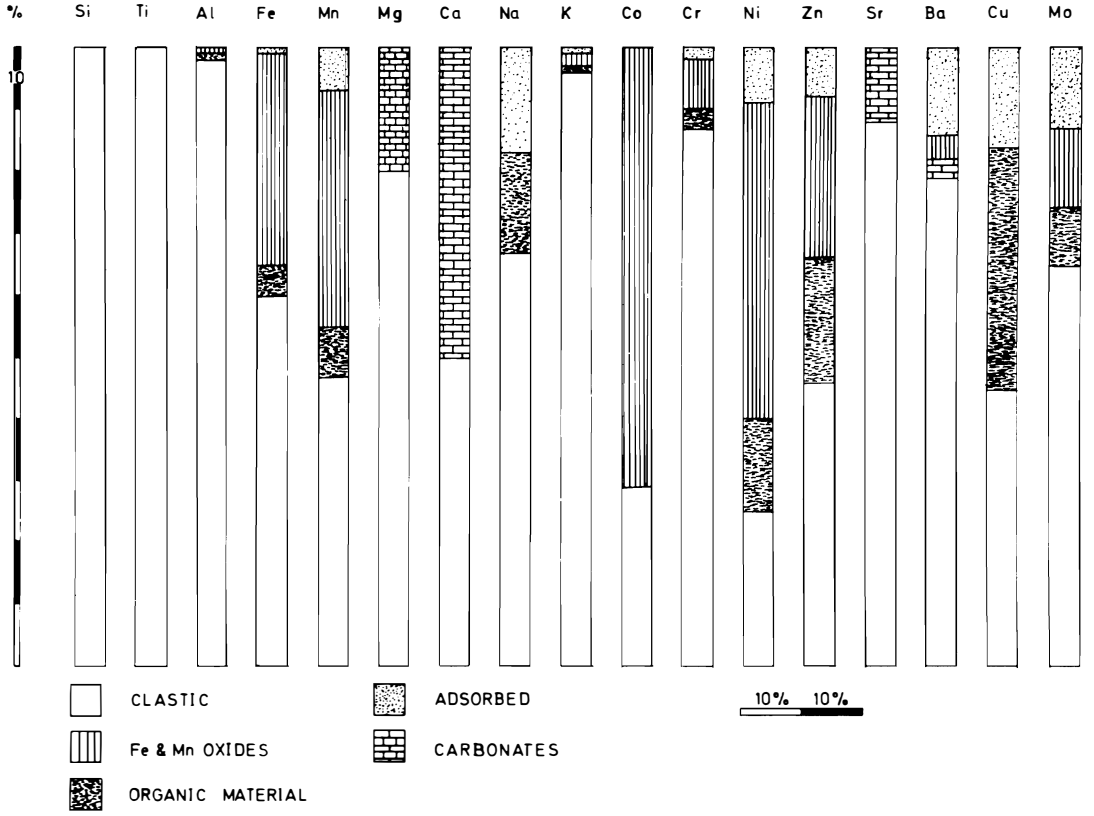

Fig. 1. *Distribution of elements in different parts of the sediments. The figure is based on average values calculated from Tables 1 and 2. For each element the whole column represents 100 %.*

Results

The NH_4Ac/HAc buffer treatment generally removes little material (Fig. 1, Tables 1 and 2). Enrichments of Ca, Sr, and Mg in the extracts from both areas may indicate dissolution of small undetectable amounts of carbonates which may be present (<5%). The low concentrations found in this exchange treatment with NH_4^+, are probably due to firm ion fixation. During diagenesis adsorbed ions may have entered several minerals, formed new ones or been firmly bound to clay minerals. In the fraction dissolved with this treatment 0–55% of total (in the sediment) Na, 0–20% of total Ba, Zn, and Mo, and 0–35% of total Cu are found. Only minor amounts of Mn, Fe, K, and Cr were detected.

Also the Na-citrate solutions dissolve some carbonates, and enrichments of Ca and Sr are seen in solutions extracted. Samples which are treated with NH_4Ac/HAc buffer solution before Na-citrate treatment, do not display such signs of carbonate dissolution, as carbonates were already partially dissolved. Both continuous and separate treatments with Na-citrate solutions result in similar enrichments of some elements in the effluents. About 15–65% of total Fe, 5–75% of total Mn, 15–100% of total Co, 15–95% of total Ni, and 0–100% of total Zn are found in the solutions extracted. Minor amounts of Cr, Ba, and Mo are also detected. The H_2O_2 treatment displayed minor amounts of dissolved elements in that fraction. Somewhat higher concentrations of Na, Cu, and Zn were dissolved by continuous treatment. This may be due to the fact that the organic material is partly rimmed by secondary iron minerals which delay H_2O_2-dissolution. Concerning the other elements both treatments gave similar results. To block secondary ionic exchanges by H_2O_2 dissolution, vacant positions on clay minerals were blocked by Al^{3+} addition. In this way, ions newly liberated by dissolution would not be quickly readsorbed by clay minerals. The results of these analyses were not very different from treatments without Al^{3+} rich solutions. In the H_2O_2 soluble fraction 0–75% of total Cu, 0–40% of total Ni and Zn, 0–30% of total Mo, and 0–50% of total Na were found.

Discussion and conclusion

These analyses show that different elements are often bound to certain minerals and several sedimentary fractions. Fig. 1 shows the average quantities of the different elements which are found in the different fractions based on the analyses presented:

A) Adsorbed ions

B) Mainly Fe/Mn oxides/hydroxides

C) Organic material (kerogen, bitumen, sulfides)

D) Clastic fraction (mainly clastic silicates)

E) Estimated acid soluble (carbonates).

Table 1.

Major element concentrations of diffent fractions from samples S5 150–152, S5 236–238, S5 311–313, and S5 395–397 from Agardhfjellet section and samples KF 6A–76, KF 13–76, KF 24–76, and KF 37–76 from Knorringfjellet section. Values in ppm if nothing else noted. For each sample first bulk analysis, then A-adsorbed fraction, B-Na-citrate soluble fraction, and C-elements mainly associated the organic material, are given. n.d. means not detected, while – means not analysed. Bulk analyses by X-ray fluorescence and analyses of fractions A, B, and C by atomic absorption.

SAMPLE	SiO_2	TiO_2	Al_2O_3	Fe_2O_3	*MnO*	*MgO*	*CaO*	Na_2O	K_2O
Agardhfjellet section.									
S5 150–152	61.6%	0.87%	15.6%	5.9%	200	1.56%	0.97%	0.77%	3.48%
A	82	14	270	413	40	2600	4425	35	364
B	602	11	874	8221	98	829	1163	—	173
C	37	n.d.	756	10830	62	3150	4967	276	452
S5 235–238	59.7%	0.98%	18.6%	5.2%	90	1.52%	0.07%	0.54%	3.79%
A	94	n.d.	274	425	9	207	203	32	313
B	1137	21	1476	14297	19	135	136	—	151
C	32	22	680	4504	15	240	325	209	319
S5 311–313	57.8%	0.97%	18.4%	7.1%	230	1.38%	0.18–	0.85%	3.31%
A	145	n.d.	705	262	18	276	593	29	429
B	1110	21	3070	15191	122	218	341	—	158
C	n.d.	6	1445	2681	21	290	420	88	542
S5 395–397	53.3%	1.06%	20.8%	8.3%	160	1.29%	0.09%	0.46%	3.36%
A	107	n.d.	951	469	6	238	131	30	395
B	1056	24	3118	24662	35	176	114	—	136
C	182	24	1748	3932	9	390	378	317	494
Knorringfjellet section.									
KF 6A–76	74.3%	0.74%	11.2%	4.3%	200	0.81%	0.79%	0.57%	2.89%
A	581	n.d.	280	148	13	819	4891	473	416
B	2159	n.d.	1130	27252	135	496	314	—	450
C	187	13	279	876	2	91	245	1685	81
KF 13–76	50.9%	1.25%	22.2%	9.0%	450	2.06%	0.94%	0.11%	3.93%
A	735	n.d.	366	214	258	2280	4198	438	678
B	1280	n.d.	727	25059	2594	851	568	—	575
C	802	n.d.	675	593	32	116	206	3134	211
KF 24–76	62.9%	1.16%	16.5%	3.8%	200	1.43%	0.17%	0.38%	3.52%
A	438	n.d.	410	689	4	120	1433	974	581
B	1771	n.d.	612	13897	5	18	30	—	1301
C	449	13	331	357	2	66	164	3976	166
KF 37–76	65.7%	1.18%	16.2%	4.6%	100	0.97%	0.40%	0.15%	2.98%
A	443	n.d.	428	296	n.d.	129	1359	847	507
B	2326	n.d.	1562	23633	33	36	n.d.	n.d.	1415
C	535	4	482	200	n.d.	68	119	2359	196

Table 2.

Trace element concentrations of different fractions from samples S5 150–152, S5 236–238, S5 311–313, and S5 395–397 from Agardhfjellet section and samples KF 6A–76, KF 13–76, KF 24–76, and KF 37–76 from Knorringfjellet section. Values in ppm. For each sample first bulk analysis, then A-adsorbed fraction, B-Na-citrate soluble fraction, and C-elements mainly associated the organic material are given. n.d. means not detected, while – means not analysed. Bulk analyses by X-ray fluorescence and analyses of fractions A, B, and C by atomic absorption.

SAMPLE	*Co*	*Cr*	*Cu*	*Mo*	*Ni*	*Sr*	*Zn*	*Ba*
Agardhfjellet section.								
S5 150–152	13	105	—	—	77	113	216	430
A	3	3	4	34	14	12	16	—
B	12	11	5	n.d.	35	24	13	—
C	6	2	23	n.d.	26	25	40	—
S5 236–238	5	155	—	—	45	105	38	440
A	1	2	20	8	4	4	11	—
B	15	14	12	n.d.	25	23	11	—
C	2	2	25	2	10	4	17	—
S5 311–313	12	116	—	—	73	89	85	395
A	2	2	7	16	7	7	4	—
B	24	26	21	n.d.	40	11	19	—
C	2	n.d.	25	2	11	20	16	—
S5 395–397	15	88	—	—	56	28	70	430
A	2	2	6	5	5	4	4	—
B	23	125	8	n.d.	52	10	18	—
C	6	5	10	4	13	4	10	—
Knorringfjellet section.								
KF 6A–76	15	101	n.d.	n.d.	49	205	2500	575
A	n.d.	1	n.d.	2	2	40	1	54
B	9	7	n.d.	n.d.	24	15	19	11
C	n.d.	9	9	2	4	4	20	n.d.
KF 13–76	32	113	73	14	88	205	320	656
A	n.d.	2	3	3	3	63	2	144
B	5	n.d.	n.d.	n.d.	15	10	7	21
C	n.d.	1	10	n.d.	n.d.	2	4	n.d.
KF 24–76	11	166	15	11	25	194	22	731
A	n.d.	2	4	2	3	8	3	90
B	4	4	n.d.	4	11	32	22	50
C	n.d.	4	11	3	3	3	9	n.d.
KF 37–76	15	125	9	14	46	158	85	580
A	n.d.	3	3	2	3	4	3	71
B	10	4	n.d.	2	22	22	18	22
C	n.d.	3	6	1	3	2	14	n.d.

In recent marine sediments Bostrøm et al. (1973) found especially Ti and Al to be related to the detrital fraction. The same relation is observed here, where more than 95% of Si, Ti, Al, and K are in the clastic fraction (quartz, feldspar, mica, some heavy minerals). In the sediments Ti, Al, and K are mutually well correlated (Dypvik 1980). The Mg and Ca distributions are controlled by variations in carbonates (calcite and dolomite) and clastic minerals such as feldspars and mafic minerals. In other more carbonate rich shales the carbonate content will dominate the Ca and Mg distributions even more. Fe and Mn are bound mainly in secondary oxides and ferromagnesian minerals and small amounts occur in adsorption positions, organic material and sulfides. On the average about 40 to 50% of Fe and Mn are in secondary oxides/hydroxides (the cementing agent in several samples), while somewhat larger amounts are in the clastic fraction. More than 50% of total Na occurs in the clastic fraction, while in two samples from Knorringfjellet more than 50% of Na is found in adsorbed positions or in organic matter. This probably reflects higher concentrations of smectite or mixed layered clay minerals.

The trace element variations mostly reflect those of the clastic minerals with the exception of, however, Co and Ni. Up to 100% of these elements are found in the secondary Fe/Mn oxide fraction with the small remaining parts in the clastic fraction, in adsorbed position, in organic material or sulfides. Co and Ni are often found enriched in Fe/Mn oxide minerals, where, however, Co is more quickly adsorbed than Ni (Carvajal & Landergren 1969). According to Burns (1976) and van der Weijden (1976), Co together with Ni, Cu, and Zn may be adsorbed on surfaces of such oxides/hydroxides. In contrast to Cu, Ni, and Zn, Co^{2+} may be oxidized to Co^{3+}, which may be precipitated as $Co(OH)_3$ or exchange Mn^{4+}. This last mechanism may be the reason why almost no Co is found in adsorbed positions, while some Ni, Zn, and Cu are found in such exchangeable positions. Because of such secondary alterations the variations in the Ni/Co ratio of bulk samples are difficult to interpret. Original environment dependent variations may be altered by diagenetic, secondary oxidation reactions which formed the Fe and Mn oxides/hydroxides.

Cr, Ba, and Sr are mainly bound in clastic minerals, but minor amounts of Cr are found in secondary oxides, some amounts of Sr in carbonates and some Ba in adsorbed positions. Ba and Sr are probably found in feldspar and mica, substituting Ca and K, while Cr may be associated with heavy minerals.

About half of Zn, Cu, and Mo are bound in clastic grains, Cu in addition is found in adsorbed positions, organic material and sufides. Zn is also found in Fe and Mn oxides, organic material, and sulfides. Minor amounts of Mo are found in adsorbed positions, Fe-Mn oxides and organic material and sulfides. Zn, Cu, and Mo are usually found together in sediments enriched in sulfides and organic material from reducing environments (Gross 1967; Bertine & Turekian 1973; Reinson 1975), and some Mo enrichments are also found in iron oxides/hydroxides as described by Cronan (1969) and Bertine & Turekian (1973). The well known Mo, Cu, Zn, and Ni correlation is partly observed here.

A comparison between samples from the Agardhfjellet and Knorringfjellet

sections indicates that the samples from the Agardhfjellet section contain more secondary oxides than those from Knorringfjellet. With respect to other geochemical variations the samples from the two localities seem to be rather similar.

This paper demonstrates that the distribution of major and trace elements in different fractions of a sediment may be rather complex. The results also indicate that results of geochemical analyses have to be studied in the light of mineralogical variations and that even in clays extensive secondary oxidation may take place.

Acknowledgements

Field work was carried out during the summer of 1976 and supported by the Norwegian Petroleum Directorate, the Norwegian Polar Research Institute, the Norwegian Research Council for Science and Humanities (NAVF), and the Norwegian Council for Scientific and Industrial Research (NTNF). Thanks are due to Dr. D. Worsley, leader of the expedition, and to Dr. M. Edwards (IKU – Continental Shelf Institute, Trondheim) who collected the samples from the Agardhfjellet section. The samples from the Knorringfjellet section were collected by cand. real. T. Bjærke and the author. Dr. K. Bjørlykke, Dr. M. Edwards, Dr. E. Roaldset, cand. real. B. Bue, cand. real. H. Rueslåtten, and cand. real. J. Vollset kindly read the manuscript and gave helpful comments.

References

Bertine, K. K. & K. K. Turekian, 1973: Molybdenum in marine deposits. *Geoch. Cosmoc. Acta* **37**: 1415–1434.

Bjærke, T., 1978: Mesozoic Palynology of Svalbard III. Dinoflagellates from the Rurikfjellet Member, Janusfjellet Formation (Lower Cretaceous) of Spitsbergen. (in prep.).

Bjærke, T., M. B. Edwards, & B. Thusu, 1976: Microplankton from the Janusfjellet Subgroup (Jurassic–Lower Cretaceous) at Agardhfjellet Spitsbergen. A preliminary report. *Norsk Polarinst. Årbok* 1974: 63–68.

Bostrøm, K., T. Kraemer, & S. Gartner, 1973: Provenance and accumulation rates of opaline silica, Al, Ti, Fe, Mn, Cu, Ni and Co in Pacific pelagic sediments. *Chem. Geol.* **11**: 123–148.

Burns, R. G., 1976: The uptake of cobalt into ferromanganese nodules, soils and synthetic manganese (IV) oxides. *Geoch. Cosmoc. Acta* **40**: 95–102.

Carvajal, M. C. & S. Landergren, 1969: Marine sedimentation processes. The interrelationships of manganese, cobalt and nickel. *Stockh. Contrib. Geol.* **18**: 99–122.

Chapman, H. D., 1965: Cation-Exchange Capacity. **In**: C. A. Black (ed.): Methods of soil analyses. Part 2, Chemical and Microbiological Properties. *Am. Soc. of Agronomy Inc., Madison*, 1965: 891–904.

Cronan, D. S., 1969: Average abundances of Mn, Fe, Ni, Co, Cu, Pb, Mo, Cr, Ti and P in Pacific pelagic Clays. *Geoch. Cosmoc. Acta* **33**: 1562–1566.

Dypvik, H., 1980: The sedimentology of the Janusfjellet Formation, Central Spitsbergen (Sassenfjorden and Agardhfjellet areas). *Norsk Polarinstitutt Skrifter* Nr. 172: 97–134 (this vol.).

Edwards, M. B., 1976: Depositional environments in Lower Cretaceous regressive sediments, Kikutodden, Sørkapp Land, Svalbard. *Norsk Polarinst. Årbok* 1974: 35–50.

FARMER, V. C. & D. B. MITCHELL, 1963: Occurrence of oxalates in soil clays following hydrogen peroxide treatment. *Soil Sci.* **96**: 221–229.

FLOOD, B., J. NAGY, & T. S. WINSNES, 1971: Geological map Svalbard 1:500 000 Sheet 1G, Spitsbergen, southern part. *Norsk Polarinst. Skrifter* Nr. 154A. Map.

GROSS, M. G., 1967: Concentration of minor elements in diatomaceous sediments of a stagnant fjord. **In**: G. H. LAUFF (Ed.), Estuaries. *A.A.A.S. Publ.* **83**: 273–282.

JACKSON, M. L., 1958: *Soil chemical analysis*. Englewood Cliffs, N. J. Prentice Hall. 498 pp.

MAJOR, H. & J. NAGY, 1972: Geology of the Adventdalen map area. *Norsk Polarinst. Skrifter* Nr. 138. 58 pp.

MEHRA, O. P. & M. L. JACKSON, 1960: Iron oxide removal from soils and clays in a dithionite-citrate system buffered with sodium bicarbonate. *Clays and Clay Min.* **7**: 317–327.

PARKER, J. R., 1967: The Jurassic and Cretaceous Sequence in Spitsbergen. *Geol. Mag.* **104**: 487–505.

PRESTLEY, B. Y., Y. KOLODNY, A. NISSENBAUM, & I. R. KAPLAN, 1972: Early diagenesis in a reducing fjord, Saanich Inlet, British Columbia. II. Trace element distribution in interstitial water and sediment. *Geoch. Cosmoc. Acta* **36**: 1073–1090.

REINSON, G. E., 1975: Geochemistry of muds from a shallow restricted estuary, Australia. *Marine Geol.* **19**: 297–314.

VAN DER WEIJDEN, C. H., 1976: Some geochemical controls of Ni and Co concentrations in marine ferromanganese deposits. *Chem. Geol.* **18**: 65–80.

Mesozoic Palynology of Svalbard V. Dinoflagellates from the Agardhfjellet Member (Middle and Upper Jurassic) in Spitsbergen

By Tor Bjærke[1]

Abstract

Four sections through the 150 to 250 m thick Agardhfjellet Member (?Upper Bathonian–Callovian to Lower Volgian) have been investigated palynologically. Preservation was generally poor and workable assemblages were restricted to the lower and upper parts of the unit. Assemblages from the middle part of the unit show extremely poor preservation probably due to biological degradation.

Three assemblage zones have been defined on the basis of dinoflagellate assemblages. Zone 1, covering the lowermost few metres, is characterized by *Nannoceratopsis pellucida*, *Tubotuberella eisenackii*, *Gonyaulacysta jurassica* var. *longicornis*, *Pareodinia evittii*, *Tapeinosphaeridium pericompsum* and other species of *Pareodinia*, *Ellipsoidictyum*, *Pluriarvalium*, and *Ctenidodinium*. This interval is dated as Upper Bathonian or Lower Callovian on the basis of ammonites.

Zone 2, covering a 20 to 40 m interval immediately above Zone 1, is characterized by *Acanthaulax senta*, *Lithodinia jurassica*, *Tubotuberella dangeardii*, *Stephanelytron redcliffense*, and *Wanaea* sp. The age of this interval is Middle or Upper Callovian.

From the uppermost 20 to 40 m of the Agardhfjellet Member (Lower Volgian) *Paragonyaulacysta capillosa* and rare *Horologinella spinosigibberosa* indicate similarity with an assemblage described from the Upper Jurassic of Arctic Canada.

The dinoflagellate assemblages recorded from the Agardhfjellet Member in Spitsbergen compare with assemblages of similar age from Europe, East Greenland, and Arctic Canada.

Introduction

This paper is the fifth in a series of papers presenting the results of palynological investigations in the Mesozoic sequence of Svalbard. Previous papers have dealt with the Upper Triassic, Lower Jurassic and Lower Cretaceous part of the sequence (Bjærke & Manum 1977; Bjærke 1977; Bjærke 1978; Bjærke, in press). Jurassic dinoflagellate assemblages were reported from Kong Karls Land in Bjærke (1977). The present paper deals with the Middle and Upper Jurassic Agardhfjellet Member of the Janusfjellet Formation. It is the first palynological study of this interval in Spitsbergen.

[1] Institutt for geologi, Universitetet i Oslo, Blindern, Oslo 3.

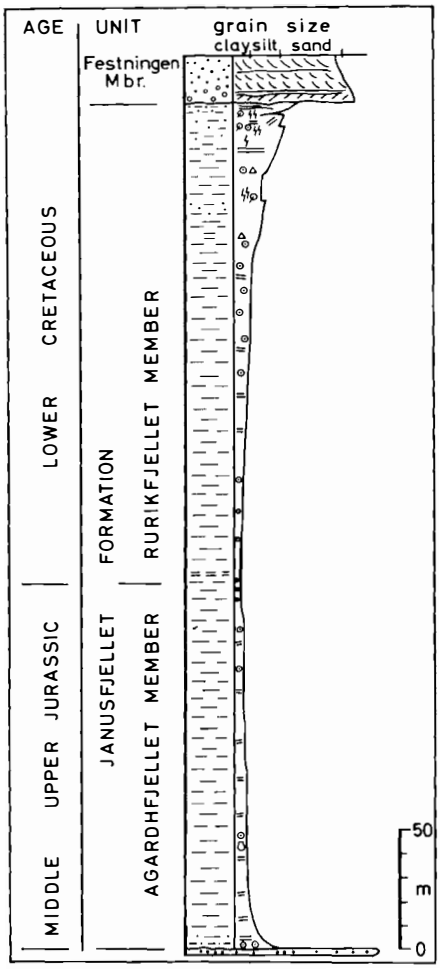

Fig. 1. *Lithological column through the Janusfjellet Formation (Agardhfjellet and Rurikfjellet Members) at Wimanfjellet (locality 2, Fig. 2). (From* Dypvik *1978.)*

The Agardhfjellet Member forms the Jurassic part of the Janusfjellet Formation (Fig. 1). It is a 150 to 250 m thick shale sequence with red and yellow weathering carbonate lenses. The lower few metres present a more silty development than the rest of this monotoneous unit (Parker 1967; Dypvik 1978).

Six ammonite zones have been recognized within the Agardhfjellet Member (Parker 1967). The *Kepplerites* fauna is found a few metres above the base indicating an Upper Bathonian or Lower Callovian age. The *Cadoceras-Longaeviceras* fauna of Upper Callovian age is found 50 to 60 m above the base, while the Oxfordian is represented by both the *Cardioceras* of Lower and *Amoeboceras nigrum* of Upper Oxfordian age. The Lower Oxfordian fauna has been recorded from 73 m above the base of Agardhfjellet Member at Keilhaufjellet, southern Spitsbergen.

The *Amoeboceras-Rasenia* fauna is widely distributed and shows the presence

of the Kimmeridgian stage. Approximately 20 to 40 m below the top of the unit abundant *Dorsoplanites* spp. of the *dorsoplanus*-zone are found, representing the Lower Volgian. The Upper Volgian has not been identified in Svalbard and is probably missing.

In Spitsbergen the Agardhfjellet Member crops out along the margins of the Spitsbergen Trough and in a few outliers to the east (Fig. 2). Along the western margin it is heavily folded within the Tertiary deformation zone, to the east and northeast it is dipping gently towards the central part of the Spitsbergen Trough affected only by block faulting and slight deformation along fault zones. This tectonic episode occurred at the end of the Jurassic and the absence of Upper Volgian sediments in the area is probably due to this tectonic activity. Subsequent erosion removed the Agardhfjellet Member locally (PARKER 1966; BJÆRKE 1978).

Material

Four sections through the Agardhfjellet Member have been studied. Location of sampled sections and the stratigraphical distribution of the samples are given in Figs. 2 and 3. At Wimanfjellet, Knorringfjellet and Klementievfjellet bedding is almost horizontal and tectonically undisturbed, while the section at Festningen is situated within the Tertiary zone of deformation. Here the shales acted as decollement horizons and the sequence may contain repetitions.

Of the 76 samples studied, only about 20 yielded workable assemblages. Productivity was generally high but preservation was poor through most of the sequence. Especially in the middle part of the unit palynomorphs show extremely poor preservation making identification impossible in most cases. Only the dinoflagellate *Sirmiodinium grossi* could be recognized through most of the sequence.

The workable assemblages were all from the lowermost 20 to 50 m and from the uppermost 20 to 40 m in all four sections, the most diverse and well preserved being from the lower part.

Variation in petrographical composition of carbonate lenses occurring in the Janusfjellet Formation at Wimanfjellet and Knorringfjellet suggests a subdivision of the sequence (DYPVIK 1978). PARKER (1967) pointed out the stratigraphical significance of changes in colour on weathered surfaces of calcareous siltstone lenses through the Agardhfjellet Member. Poor preservation of palynomorphs is observed within intervals where the carbonate lenses show a high content of calcite and dolomite, weathering yellow, whereas fair to well preserved assemblages are restricted to intervals with a high siderite content in the siltstone lenses resulting in a brownish to red colour on weathered surfaces. This applies to Agardhfjellet as well as the overlying Rurikfjellet Member and shows that preservation is controlled by facies, depending on biological and possibly chemical conditions in the sediment.

Results

The dinoflagellate species recorded from the Agardhfjellet Member are listed below. Morphological and taxonomic comments are included for some of the species. In addition to the species mentioned the assemblages include rare and poorly preserved species which because of their preservation are omitted from consideration. Therefore, the species listed cannot be regarded as an exhaustive account of the Middle and Upper Jurassic dinoflagellate cysts in the area. More favourable facies of equivalent units are likely to produce more diverse assemblages. For the same reason quantitative data have not been considered.

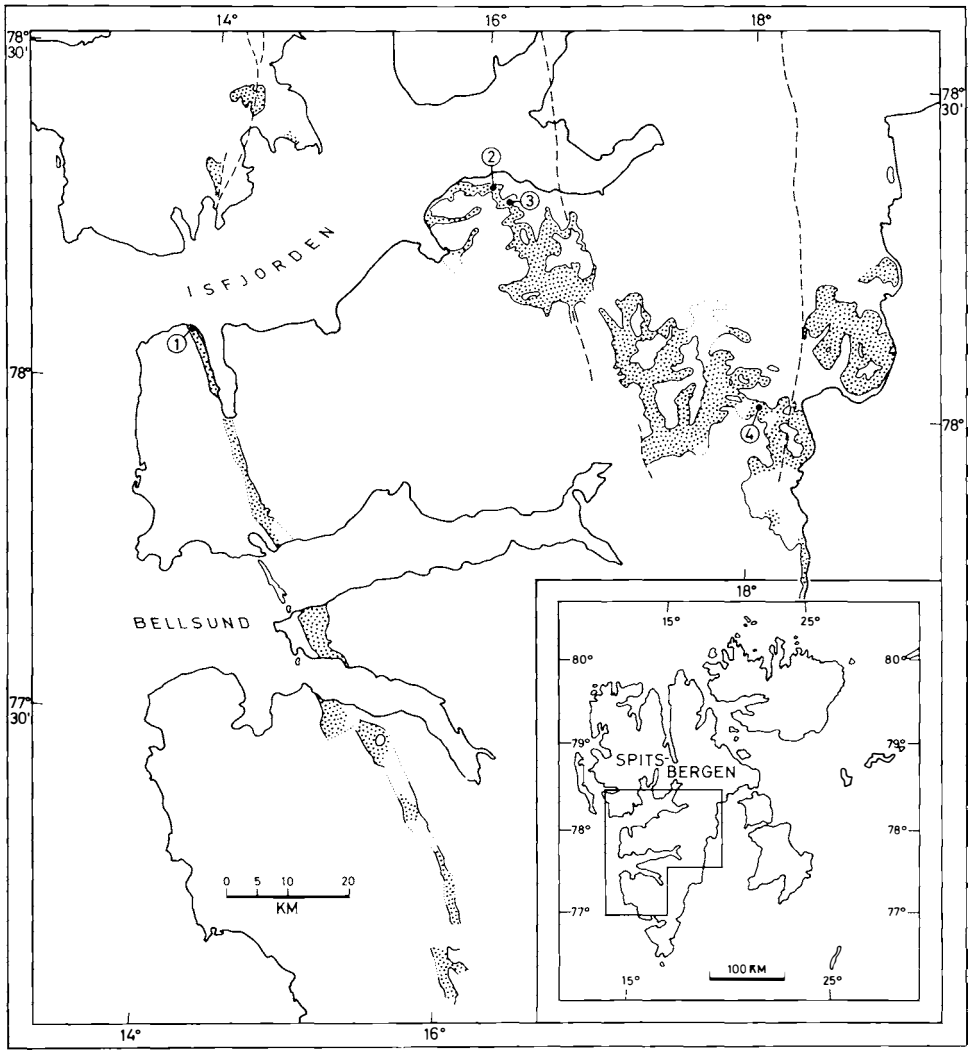

Fig. 2. *Distribution of the Janusfjellet Formation in Central Spitsbergen (dotted areas). Location of sections studied: 1) Festningen, 2) Wimanfjellet, 3) Knorringfjellet, and 4) Klementievfjellet. (From* Flood *et al. 1971.)*

The remarks given on the morphology of some of the species are only intended to provide information in addition to the illustrations found in Plates 1–5.

Numbers in brackets following each species refer to species numbers in the range chart (Fig. 3). For references to authors of taxa not given in this paper, see Stover & Evitt 1978.

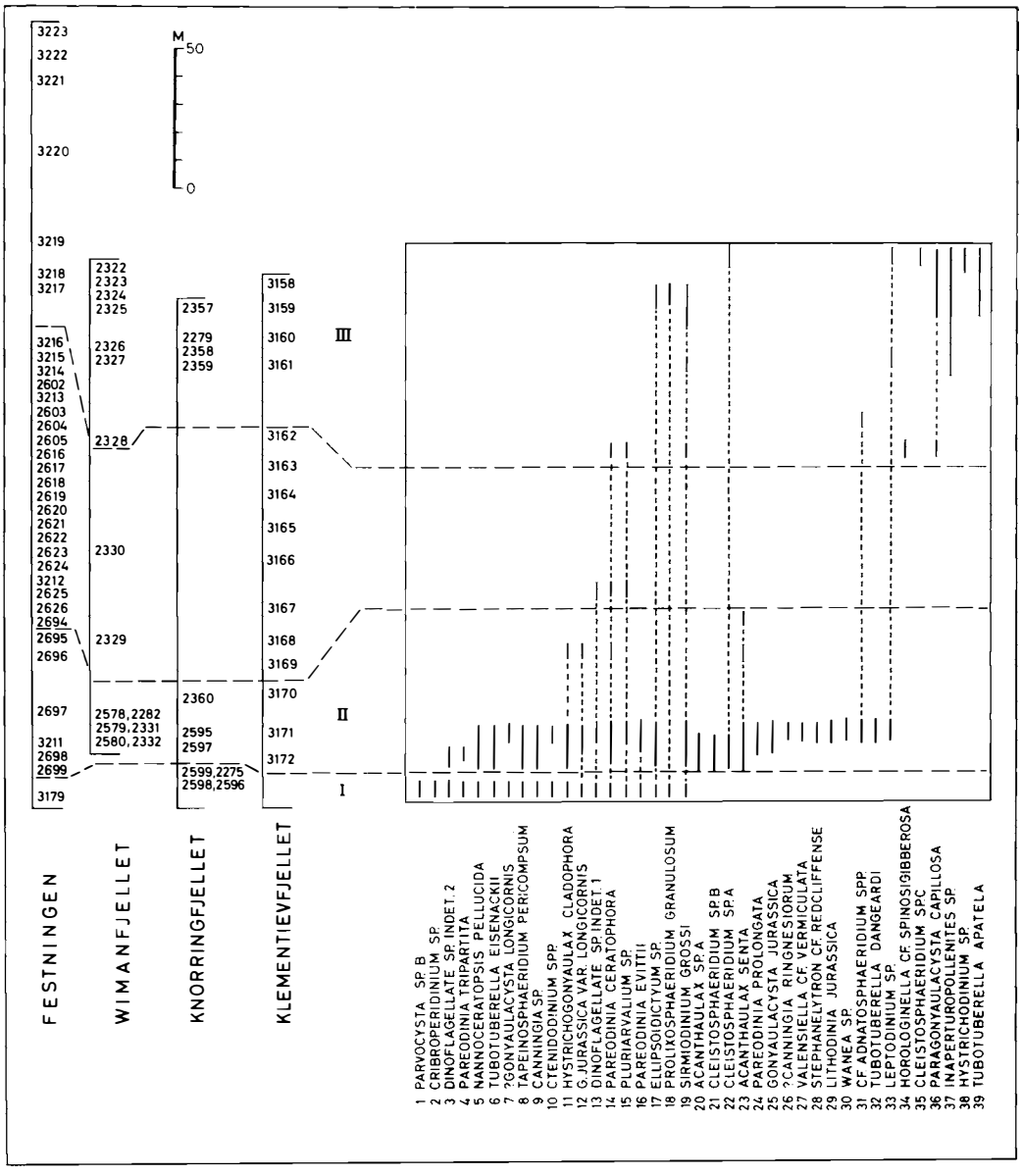

Fig. 3. *Range chart for selected palynomorph species and the stratigraphical position of samples studied.*

ALPHABETICAL LIST OF DINOFLAGELLATE CYST SPECIES RECORDED FROM THE AGARDHFJELLET MEMBER.

Acanthaulax senta DRUGG 1978

(23) Pl. 3, Figs. 1–4.

This species is locally common. The observed specimens agree in all respects with the original description. *A. senta* is here regarded as conspecific with *Acanthaulax* sp. 1 of JOHNSON & HILLS 1973. As also noted by JOHNSON and HILLS this species resembles "*Gonyaulacysta*" *scarboroughensis* SARJEANT 1964. However, the original description and illustration of that species is inadequate and a restudy of the type material is needed before synonymy can be verified. Specimens of *Gonyaulacysta areolata* SARJEANT 1961 (SARJEANT 1961, Pl. 13, Fig. 13 (holotype) and SARJEANT 1960, Pl. 13, Fig. 1) and of cf. *Paleohystrichophora spinosissima* (DEFLANDRE) SARJEANT (SARJEANT 1960, Pl. 12, Fig. 5) also appear to be closely related to *A. senta*.

Acanthaulax sp. A

(20) Pl. 3, Figs. 7, 8

Subspherical cysts with a short, blunt apical horn. Surface densely covered by short, simple spines. Archeopyle precingular, paratabulation otherwise not evident.

cf. *Adnatosphaeridium* spp.

(31) Pl. 3, Fig. 9

Rare specimens showing branched processes appearing to be arranged in groups with distally connecting trabeculae have been recorded. They are here grouped together as cf. *A.* spp.

?*Canningia ringnesii* MANUM and COOKSON 1964

(26) Pl. 1, Fig. 5

Canningia spp.

(9) Pl. 1, Figs. 1, 6

Spherical cysts densely ornamented with low conical and rounded verrucae. Archeopyle apical, representing several paraplates. Paratabulation otherwise not evident.

Cleistosphaeridium sp. A

(22)

Small, spherical cysts bearing numerous simple spines. Archeopyle apical, paratabulation not evident.

Cleistosphaeridium sp. B

(21) Pl. 1, Fig. 4

Spherical or slightly elongated cysts with numerous bifurcating spines, approximately $\frac{1}{2}$ diameter long. Archeopyle formed by the loss of several apical paraplates.

Cleistosphaeridium sp. C

(35)

Subspherical cysts covered by numerous simple spines, $\frac{1}{2}$ to 1 diameter long, thickened at terminations. Archeopyle apical, paracingulum indicated by linear organization of spines in equatorial area.

Cribroperidinium sp.

(2)

Cysts with a short apical horn. Paracingulum indicated by a shallow equatorial groove, surface except for paracingulum covered by low warts. Archeopyle precingular, formed by the loss of a large, mid-dorsal paraplate. Paratabulation except for archeopyle not evident.

Ctenidodinium spp.

(10) Pl. 2, Figs. 8, 9, 11, 12

Fragments of specimens belonging to this genus occur in several assemblages. Variations in the development of crests indicate that more than one species are represented. The material does not allow a more detailed identification.

Dinoflagellate sp. indet. 1
(13) Pl. 2, Figs. 6, 7
Cavate cysts with a prominent apical horn formed by the extension of ectophragm, the endophragm protruding partly into the horn. Cyst outline elongated, antapical area broadly rounded. Endocoel restricted equatorially. A characteristic reticulate pattern is evident, probably resulting from ornamentation on the inner surface of ectophragm. Outer surface smooth. Paratabulation indicated by low crests, arheopyle intercalary 3 I.

Dinoflagellate sp. indet. 2
Pl. 5, Figs. 1, 2, 4, 5
Small, spherical dinoflagellate cysts with a smooth surface. Faint parasutures seen but paratabulation extremely difficult to work out because the delicate cyst wall is readily folded and parasutures often fade. Archeopyle formed by the loss of apical and possibly precingular paraplates.
This species occurs in masses in some assemblages within Zone 3.

Ellipsoidictyum sp.
(17) Pl. 1, Fig. 2

Gonyaulacysta jurassica (Deflandre) Norris and Sarjeant 1965
(25)

Gonyaulacysta jurassica var. *longicornis* (Deflandre) Gitmez 1970
(12) Pl. 2, Figs. 4, 5
The species *G. jurassica* var *brevis* Johnson & Hills 1973 is here regarded as a junior synonym of *G. jurassica* var. *longicornis*.

?Gonyaulacysta longicornis (Downie) Sarjeant 1969
(7)

Horologinella spinosigibberosa Brideaux and Fisher 1976
(34) Pl. 5. Figs. 3, 6, 7

Hystrichodinium sp.
(38)
A few poorly preserved specimens referable to *Hystrichodinium* have been recorded. Similar specimens were illustrated by Ioannides et al. 1976 from the Kimmeridgian (Pl. 3, Fig. 11).

Hystrichogonyaulax cladophora (Deflandre) Stover and Evitt 1978
(11) Pl. 4, Fig. 3

Hystrichogonyaulax spp.
Pl. 4, Figs. 13, 14

Kalyptea diceras Cookson and Eisenack 1960
Pl. 2, Fig. 1
This species occurs rarely within Zone 2.

Leptodinium sp. A
(33)
This form was illustrated in Bjærke (1977) (Pl. 8, Figs. 7, 8) from Kong Karls Land.

Lithodinia jurassica (Eisenack) Gocht 1975
(29) Pl. 4, Figs. 1, 2

Lithodinia cf. *valensi* Sarjeant 1966
Pl. 4, Fig. 15

Nannoceratopsis pellucida Deflandre 1938
(5) Pl. 1, Figs. 17–18, Pl. 2, Figs. 2, 3

Paragonyaulacysta capillosa (Brideaux and Fisher) Stover and Evitt 1978
(36) Pl. 5, Figs. 8, 9, 11–13

Pareodinia ceratophora Deflandre 1947
(14)

Pareodinia evittii (Pocock) Wiggins 1975
(16) Pl. 1, Figs. 12–14, 16
P. evittii is separated from *P. tripartita* mainly by ornamentation. Both show the three opercular pieces partly or completely detached.

Pareodinia prolongata Sarjeant 1959
(24)

Pareodinia tripartita Johnson and Hills 1973
(4) Pl. 1, Figs. 11, 15

Parvocysta sp. B. Bjærke (in press)
(1)
This species was first reported from the Middle Jurassic of Kong Karls Land (Bjærke 1977, Pl. 10, Fig. 5) and later described from the phosphorite pebbles of the Brentskardhaugen Bed at Knorringfjellet, central Spitsbergen. It has also been recorded from the Passet Member on Kong Karls Land. The occurrence of *P.* sp. B. in the Bathonian–Callovian is considered to be a result of reworking.

Pluriarvalium sp.
(15)

Prolixosphaeridium granulosum (Sarjeant) Davey et al. 1969
(18) Pl. 1, Fig. 10

Sirmiodinium grossi Alberti 1961
(19) Pl. 4, Figs. 10, 11

Stephanelytron redcliffense (Sarjeant) Stover, Sarjeant and Drugg 1977
(28) Pl. 4, Figs. 4, 5

Tapeinosphaeridium pericompsum Ioannides et al. 1976
(8) Pl. 1, Figs. 3, 9
Two varieties of the species seem to be represented in the present material. Some assemblages within Zone 1 are dominated by rather large specimens of *T. pericompsum* (Pl. 1, Fig. 3). The problem of synonymy between *Tapeinosphaeridium* and *Chyrtroeisphaeridia* is not yet settled. If the genus *Chytroeisphaeridia* is emended to include cysts with a precingular archeopyle, *Tapeinosphaeridium* becomes a junior synonum of that genus. The specimens here referred to *Tapeinosphaeridium* clearly posess a precingular archeopyle. A precingular archeopyle is also present in specimens from the Middle Jurassic of Kong Karls Land referred to *Chytr. chytroeides* Sarjeant 1962 reported by Bjærke 1977 (Pl. 7, Figs. 3, 5, 6).

Tapeinosphaeridium sp. A
Pl. 1, Fig. 7
A species of *Tapeinosphaeridium* showing a small, typically angular precingular archeopyle. Surface smooth.

Tapeinosphaeridium sp. B
Pl. 1, Fig. 8
A species of *Tapeinosphaeridium* characterized by a slighly elongated outline and an apical protrusion. A large precingular archeopyle present, surface smooth.

Tubotuberella apatela (Cookson and Eisenack) Ioannides et al. 1976
(39) Pl. 5, Fig. 10

Tubotuberella eisenackii (Deflandre) Stover and Evitt 1978
(6) Pl. 4, Fig. 8

Tubotuberella eisenackii subsp. *oligodentatum* (Cookson and Eisenack) Stover and Evitt 1978
Pl. 3, Figs. 5, 6

Tubotuberella dangeardii (Sarjeant) Stover and Evitt 1978
(32) Pl. 4, Fig. 9

Valensiella cf. *vermiculata* Gocht 1970
(27)

Wanaea sp.
(30) Pl. 4, Fig. 7

STRATIGRAPHICAL ZONATION

The ranges given in Fig. 3 suggest a subdivision of the Agardhfjellet Member into three assemblage zones. Zone 1, covering the lower few metres at Knorringfjellet and Festningen, is characterized by *Nannoceratopsis pellucida* (rare-common), *Tubotuberella eisenackii* (rare), *Tapeinosphaeridium pericompsum* (common), *Gonyaulacysta jurassica* var. *longicornis* (rare-common), *Pareodinia evittii* (rare) and species of the generae *Pareodinia*, *Ellipsoidictyum*, *Pluriarvalium* and *Ctenidodinium*. Zone 2 covers a 20 to 40 m thick interval immediately above Zone 1. It is characterized by *Acanthaulax senta* (common), *Stephanelytron redcliffense* (rare), *Lithodinia jurassica* (rare), *Tubotuberella dangeardii* (rare), *Wanaea* sp. (rare), and some other species (see Fig. 3). The species found in Zone 1 range into Zone 2 with a few exceptions, *N. pellucida* now becoming rare.

Zone 3 covers the uppermost 20 to 40 m of the unit and it is characterized by *Paragonyaulacysta capillosa* (rare to common), *Tubotuberella apatela* (rare), a species of *Inaperturopollintes* which occurs in masses in some of the assemblages and Dinoflagellate sp. indet. 2, also dominating in some assemblages. *Horologinella spinosigibberosa* is recorded from the lower part of this interval at Wimanfjellet.

Discussion

The sections studied here have not been directly related to ammonite zones. However, using data given by PARKER (1967), Zones 1 and 2 obviously occur below the *Cadoceras-Longaeviceras*-fauna of Upper Callovian age. This fauna is found in the upper part of an interval with red weathering siderite siltstone lenses (see PARKER 1967, Fig. 6). Zones 1 and 2 are found within this interval. The age of Zone 1 is regarded as uppermost Bathonian or Lower Callovian, Zone 2 being of Middle or Upper Callovian age.

Zone 3 occurs within the *dorsoplanus* zone and it is of Lower Volgian age. The lower part of this zone may, however, extend downwards into beds of uppermost Kimmeridigian age.

In Kong Karls Land dinoflagellate assemblages recorded from 220–230 m a.s.l. at Hårfagrehaugen, Kongsøya, may be correlated with Zone 1 (association D, BJÆRKE 1977). The age of this horizon was regarded as Callovian and it was found 5 to 10 m above the supposed base of the Janusfjellet Formation at this locality.

Association E recorded from Svenskøya, Kong Karls Land (BJÆRKE 1977), was regarded as Oxfordian in age and the absence of *Nannoceratopsis pellucida* and *Acanthaulax senta* further supports that it is younger than Zone 2 of Middle or Upper Callovian age and probably not older than Middle Oxfordian.

In Arctic Canada a dinoflagellate zonation of the Savik Formation (Toarcian-Kimmeridgian) was established by JOHNSON & HILLS (1973). A dinoflagellate assemblage including several of the stratigraphically important species that characterize Zone 2 in Spitsbergen, was recorded from a narrow

interval near the top of the Lower Savik Member, between 1185 and 1195 feet above the base of the Savik Formation. Within this interval *N. pellucida* is present in association with *Acanthaulax senta* (al. *A.* sp. 1), *Gonyaulacysta jurassica* var. *longicornis* (al. *G. jurassica* var. *brevis*), *Wanaea digitata*, *Tubotuberella eisenackii* (al. *Endoscrinium eisenacki*), and *Stephanelytron redcliffense*. This interval is found approximately 10 m above the Upper *Cadoceras*-bed of Lower Callovian age.

The assemblage defining Zone 1 finds no direct counterpart in the sequence described by JOHNSON & HILLS, but it may be referred to the lower or middle part of their *Nannoceratopsis pellucida*-range zone. Here *Tubotuberella eisenackii* and several species of *Pareodinia* are found in association with *N. pellucida*. The age of this zone in Arctic Canada is Upper Bathonian and Lower Callovian.

The species *Paragonyaulacysta capillosa* and *Horologinella spinosigibberosa* of Zone 3 are components of the *borealis*-assemblage described by BRIDEAUX & FISHER (1976) from Arctic Canada. This assemblage was recorded from beds ranging in age from Upper Oxfordian to the Berriasian. The more restricted range of these species in Spitsbergen is determined by facies. A more accurate correlation with sections in other areas on the basis of this poor assemblage, is not possible.

Two Jurassic dinoflagellate assemblages were described from East Greenland by SARJEANT (1972). They included *Gonyaulacysta jurassica*, *G. jurassica* var. *longicornis*, *Hystrichogonyaulax cladophora* (al. *Gonyaulacysta cladophora*), *Tubotuberella eisenackii* (al. *Gonyaulacysta eisenacki*), *Tubotuberella dangeardii* (al. *Psaligonyaulax apatela*) in association with species of *Tapeinosphaeridium* (al. *Chytroeisphaeridia*), *Canningia* (al. *Tenua*), and *Pareodinia*. The youngest assemblage, probably of Callovian age, also included *Acanthaulax* spp. (cf. *A. senta* al. *A. scarboroughensis*), *Nannoceratopsis pellucida*, *Tubotuberella eisenackii* var. *oligodentatum* (al. *Gonyaulacysta eisenacki* var. *oligodentata*), *Wanaea digitata*, and *Prolixosphaeridium* sp. (al. *P.* aff. *deirense*). This assemblage compares closely with those of Zone 2 in Spitsbergen. A Middle Callovian age was suggested by SARJEANT (1972, p. 59) for this assemblage.

Although *N. pellucida* is absent from the oldest assemblage described by SARJEANT, it may be referred to the more broadly defined *N. pellucida*-range zone of Middle Bathonian to Lower Callovian age. This also agrees in several respects with Zone 1 as defined here.

The dinoflagellate assemblages of Zone 1 and 2 are essentially similar to assemblages from the Callovian and lowermost Oxfordian in western Europe (cp. DEFLANDRE 1938; SARJEANT 1962, 1965, 1968; RILEY & SARJEANT 1972). The Middle Callovian assemblage described by MUIR & SARJEANT (1978) from the Langdale Beds of Yorkshire shows several species in common with assemblages from Zone 2, but lacks the characteristic *Acanthaulax* species. This may indicate that Zone 2 is slightly younger than the Middle Callovian.

Conclusions

1) The Agardhfjellet Member is generally producing poorly preserved palynomorph assemblages. Workable assemblages including stratigraphically important species of dinoflagellate cysts have been recorded from the lower 50 m and upper 40 m of the unit.

2) Quality of preservation is correlated with changes in sediment composition, showing that it is controlled by primary conditions in the sediment.

3) Three assemblage zones based on dinoflagellate assemblages have been defined; Zone 1 and 2, covering the lower 20 to 50 m, are of ?Upper Bathonian–Callovian age, Zone 3, covering the upper 20 to 40 m, is of Lower Volgian age.

4) The dinoflagellate assemblages described here from the Agardhfjellet Member in Spitsbergen are comparable to assemblages of similar age from Arctic Canada, East Greenland, and Europe.

5) The appearance of the assemblages characteristic of Zone 2 during the Callovian seems to represent a distinctive change in assemblage of considerable stratigraphical importance all over the North Atlantic and Arctic area. This change in assemblage allows correlation of the lower part of the Agardhfjellet Member with the uppermost part of the Lower Savik Member, Savik Formation, in Arctic Canada.

Acknowledgements

This study forms part of a research project financially supported by the Royal Norwegian Council for Scientific and Industrial Research (NTNF). The author is pleased to thank Dr. Svein B. Manum, Institute of Geology, University of Oslo, who initiated and leads the project. The field work was carried out during expeditions organized by the "Svalbard Group", University of Oslo, lead by Dr. David Worsley. The sections at Wimanfjellet and Knorringfjellet were sampled by Cand. real. Henning Dypvik and the author in 1976. The section at Festningen was sampled by Sven A. Bäckström in 1977 and additional material from this section as well as the material from Klementievfjellet was collected by H. Dypvik in 1978. Norsk Polarinstitutt, Sysselmannen for Svalbard, Statoil A/S, and the Norwegian Council for Science and Humanities (NAVF) offered logistic and financial support towards field work. Mrs. Leena Klaveness carefully processed the samples.

References

(Full references to dinoflagellate cyst species listed in Table 1 are to be found in STOVER & EVITT 1978).

BJÆRKE, T., 1977: Mesozoic Palynology of Svalbard II. Palynomorphs from the Mesozoic sequence of Kong Karls Land. *Norsk Polarinst. Årbok* 1976: 83–120, Pls. 1–10.

— 1978: Mesozoic Palynology of Svalbard III. Dinoglagellates from the Rurikfjellet Member, Janusfjellet Formation (Lower Cretaceous) of Spitsbergen. *Palinologia*, num. extraord. 1, Leon 1978: 69–93. Pls. 1–7.

— in press: Mesozoic Palynology of Svalbard IV. Toarcian dinoflagellates from Spitsbergen. *Palynology* **4** (in press).

BJÆRKE, T. and S. B. MANUM, 1977: Mesozoic Palynology of Svalbard I. The Rhaetian of Hopen, with a preliminary report on the Rhaetian and Jurassic of Kong Karls Land. *Norsk Polarinst. Skrifter* Nr. 165. 1–48 pp. 9 Pls.

BRIDEAUX, W. W. and M. J. FISHER, 1976: Upper Jurassic–Lower Cretaceous dinoflagellate assemblages from Arctic Canada. *Geol. Surv. Can. Bull.* **259**. 53 pp. 7 Pls.

DEFLANDRE, G., 1938: Microplancton des mers jurassiques conserves dans les marnes de Villers-sur-Mer (Calvados). Etude liminaire considerationes generales. *Trav. Stat. zool. Wimereux* **13**: 147–200. Pls. 5–11.

DODEKOVA, L., 1975: New Upper Bathonian dinoflagellate cysts from northeastern Bulgaria. *Bulg. Acad. Sci., Paleontol., Stratigr., Lithol.* **2**: 17–34.

DRUGG, W. S., 1978: Some Jurassic dinoflagellate cysts from England, France and Germany. *Palaeontographica* (B) **168**: 61–79. 8 Pls.

DYPVIK, H., 1978: Origin of carbonate in marine shales of the Janusfjellet Formation, Svalbard. *Norsk Polarinst. Årbok* 1977: 101–110.

JOHNSON, C. D. and L. V. HILLS, 1973: Microplankton zones of the Savik Formation (Jurassic), Axel Heiberg and Ellesmere Islands, District of Franklin. *Bull. Can. Petr. Geol.* **21** (2): 178–218. 3 Pls.

MUIR, M. D. and W. A. S. SARJEANT 1978: The palynology of the Langdale Beds (Middle Jurassic) of Yorkshire and its stratigraphical implications. *Rev. Paleobot. Palynol.* **25**: 193–239.

PARKER, J. R., 1966: Folding, faulting and dolerite intrusions in the Mesozoic rocks of the fault zone of central Spitsbergen. *Norsk Polarinst. Årbok* 1964: 47–55.

— 1967: The Jurassic and Cretaceous sequence in Spitsbergen. *Geol. Mag.* **104**: 487–505.

RILEY, L. A. and W. A. S. SARJEANT, 1972: Survey of the stratigraphical distribution of dinoflagellates, acritarchs and tasmanitids in the Jurassic. *Geophytology* **2** (1): 1–40.

SARJEANT, W. A. S., 1960: Microplankton from the Corallian Rocks of Yorkshire. *Proc. Yorkshire Geol. Soc.* **32** (4): 389–408. Pls. 12–14.

— 1961: Microplankton from the Kellaways Rock and Oxford Clay of Yorkshire. *Palaeontology* **4** (1): 90–118. 3 Pls.

— 1962: Microplankton from the Ampthill Clay of Melton, south Yorkshire. *Palaeontology* **5** (3): 478–497. 2 Pls.

— 1965: Microplankton from the Callovian (S. calloviense Zone) of Normandy. *Rev. Micropal.* **8**: 175–184.

— 1968: Microplankton from the Upper Callovian and Lower Oxfordian of Normandy. *Rev. Micropal.* **10**: 221–242.

— 1972: Dinoflagellate cysts and acritarchs from the Upper Vardeklöft Formation (Jurassic) of Jameson Land, East Greenland. *Meddel. Grönland* **195**: 1–69. Pls. 1–9.

STOVER, L. E. and W. R. EVITT, 1978: Analyses of Pre-Pleistocene organicwalled Dinoflagellates. *Stanford Univ. Publ. Geol. Sci.* XV. 300 pp.

Plates 1–5

All specimens figured at magnification X600. Location of specimens given by sample No., slide No., and mechanical stage coordinates referring to Leitz Dialux 820292 belonging to Institute of Geology, University of Oslo.

PLATE 1

Fig. 1. *Canningia* sp., 3171/7:44.3–101.4
Fig. 2. *Ellipsoidictyum* sp., 3171/7:31.7–104.9
Fig. 3. *Tapeinosphaeridium pericompsum* Ioannides et al. 1976, 3179/10:30.2–105.2
Fig. 4. *Cleistosphaeridium* sp. B, 3171/5:29.1–108.7
Fig. 5. *?Canningia ringnesii* Manum and Cookson 1964, 3171/8:34.5–103.4
Fig. 6. *Canningia* sp., 3179/3:35.2–105.5
Fig. 7. *Tapeinosphaeridium* sp. A, 3179/4:44.4–102.1
Fig. 8. *Tapeinosphaeridium* sp. B, 3171/3:40.1–102.3
Fig. 9. *Tapeinosphaeridium pericompsum* Ioannides et al. 1976, 3171/5:33.7–91.2
Fig. 10. *Prolixosphaeridium granulosum* (Sarjeant) Davey et al. 1969, 3171/2:32.0–107.2
Fig. 11. *Pareodinia tripartita* Johnson and Hills 1973, 3171/1:36.7–102.5
Fig. 12. *Pareodinia evittii* (Pocock) Wiggins 1975, 3171/1:34.2–103.8
Fig. 13. *Pareodinia evittii* (Pocock) Wiggins 1975, 2275/3:41.2–96.7
Fig. 14. *Pareodinia evittii* (Pocock) Wiggins 1975, 3171/7:40.0–101.7
Fig. 15. *Pareodinia tripartita* Johnson and Hills 1973, 3171/6:38.4–97.9
Fig. 16. *Pareodinia evittii* (Pocock) Wiggins 1975, 3171/7:42.4–101.0
Fig. 17. *Nannoceratopsis pellucida* Deflandre 1938, 3179/3:37.2–107.2
Fig. 18. *N. pellucida* Deflandre 1938, 3179/3:39.5–105.5
Fig. 19. *N. pellucida* Deflandre 1938, 3179/1:38.3–93.4

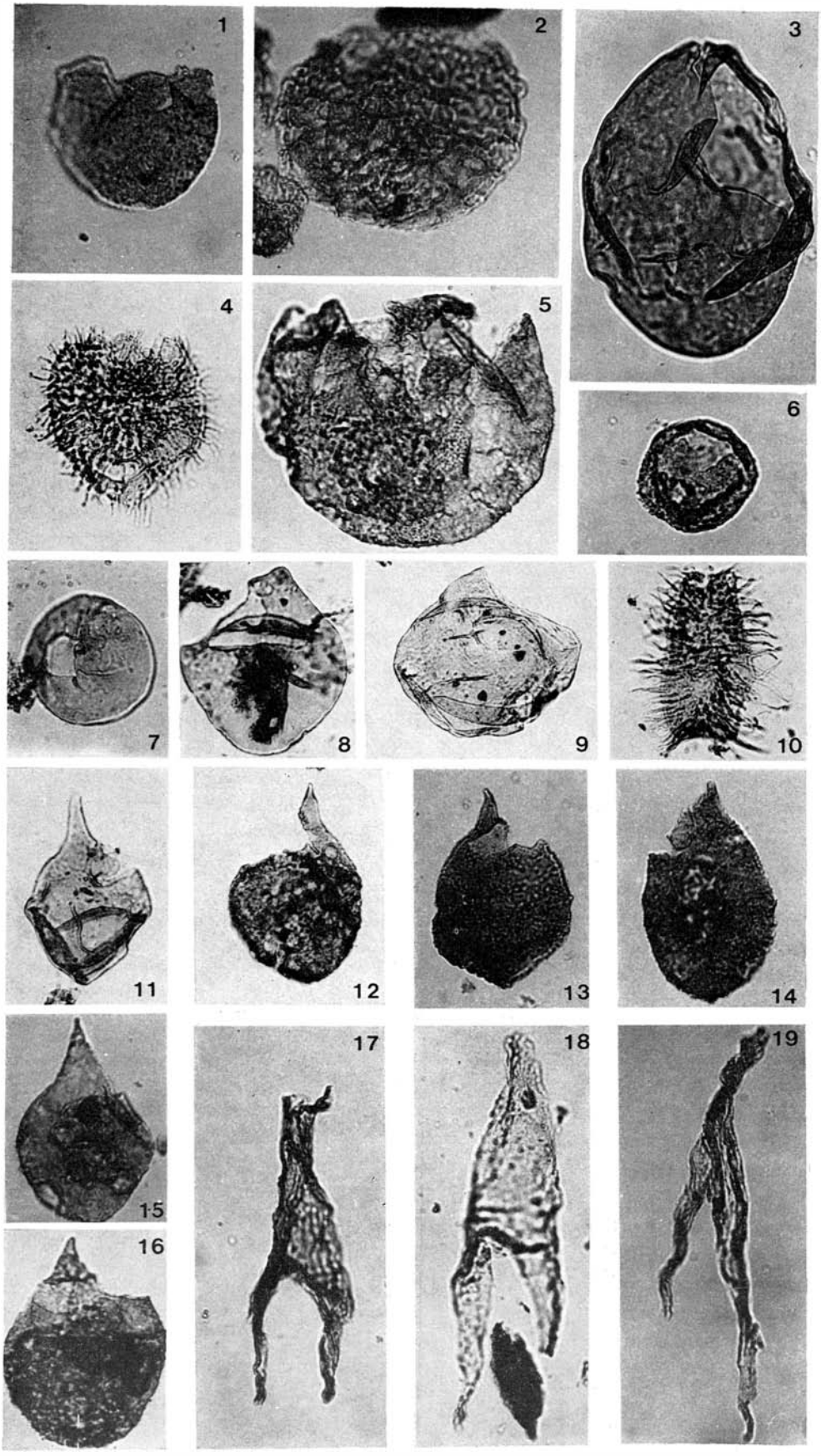
1
2
3
4
5
6
7
8
9
10
11
12
13
14
15
16
17
18
19

PLATE 2

Fig. 1. *Kalyptea diceras* Cookson and Eisenack 1960, 3171/7:30.3–97.9
Fig. 2. *Nannoceratopsis pellucida* Deflandre 1938, 3179/2:37.3–98.1
Fig. 3. *Nannoceratopsis pellucida* Deflandre 1938, 3179/1:33.2–93.3
Fig. 4. *Gonyaulacysta jurassica* var. *longicornis* (Defl.) Gitmez 1970, 3171/7:43.3–99.8
Fig. 5. *G. jurassica* var. *longicornis* (Defl.) Gitmez 1970, 3171/4:32.8–105.2
Fig. 6. Dinoflagellate sp. indet. 1, 3179/1:30.9–104.1
Fig. 7. Dinoflagellate sp. indet. 1, 3179/7:31.0–98.4
Fig. 8. *Ctenidodinium* sp., 3179/8:51.6–112.7
Fig. 9. *Ctenidodinium* sp., 3179/3:38.5–94.9
Fig. 10. *Gonyaulacysta* sp., 3179/3:40.7–106.2
Fig. 11. *Ctenidodinium* sp., 3171/7:42.1–101.4
Fig. 12. *Ctenidodinium* sp., 3171/3:36.0–101.8

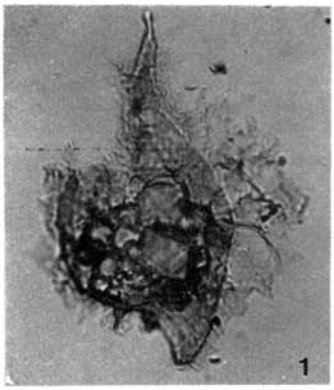
1


2

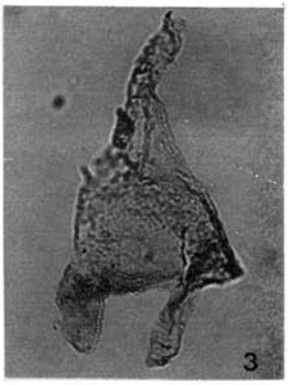
3

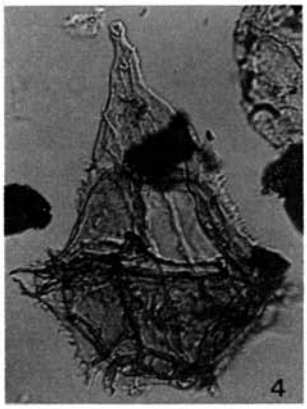
4

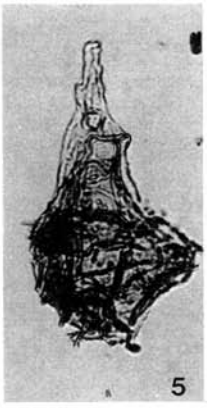
5

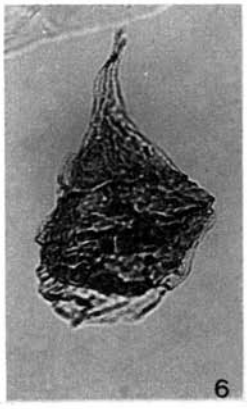
6


7

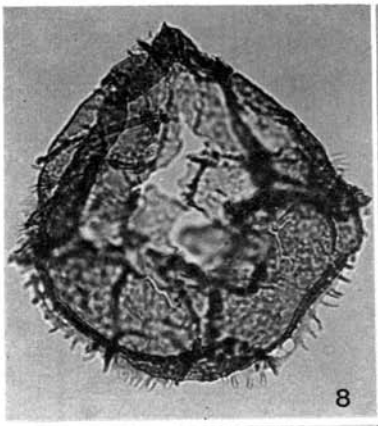
8

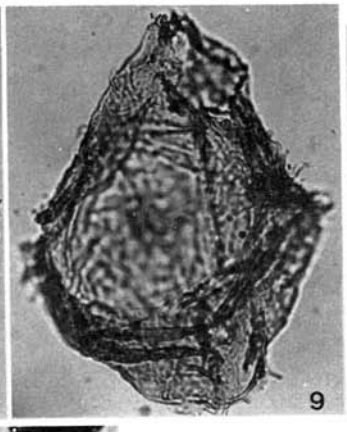
9


10

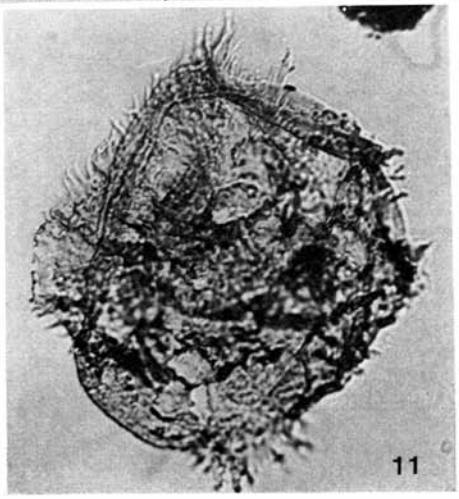
11

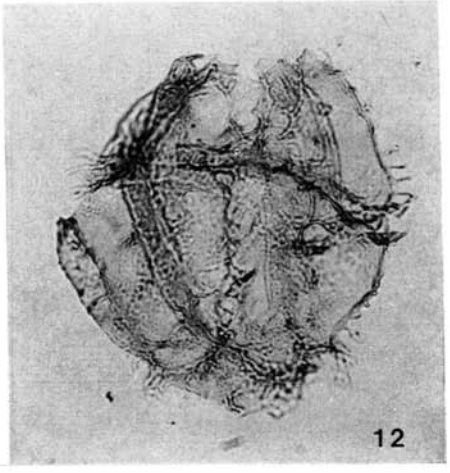
12

PLATE 3

Fig. 1. *Acanthaulax senta* DRUGG 1978, 3171/7:43.5–102.6
Fig. 2. *A. senta* DRUGG 1978, 3171/6:38.2–102.6
Fig. 3. *A. senta* DRUGG 1978, 3171/4:37.4–106.6
Fig. 4. *A. senta* DRUGG 1978, 3171/2:38.3–105.5
Figs. 5,6. *Tubotuberella eisenackii* subsp. *oligodentatum* (COOKSON and EISENACK) STOVER and EVITT 1978, 3171/7:36.9–98.8
Fig. 7. *Acanthaulax* sp. A, 2580/2:41.5–97.4
Fig. 8. *Acanthaulax* sp. A, 3171/1:38.5–99.9
Fig. 9. cf. *Adnatosphaeridium* sp., 3171/5:35.6–106.7

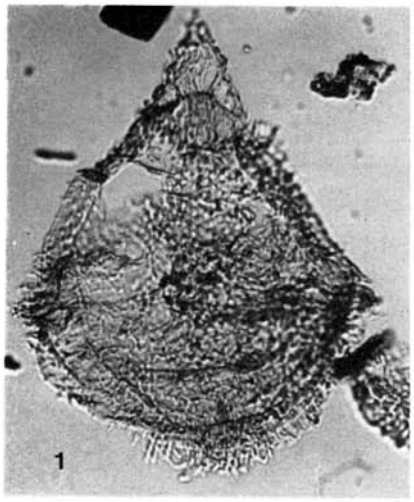
1

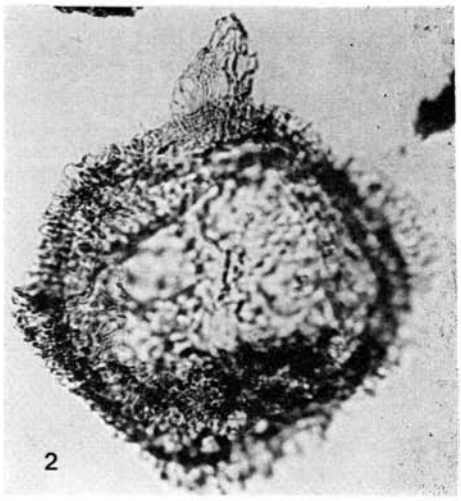
2

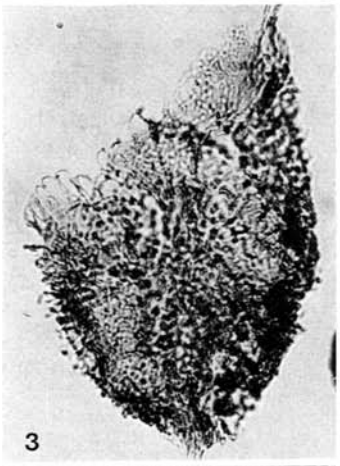
3

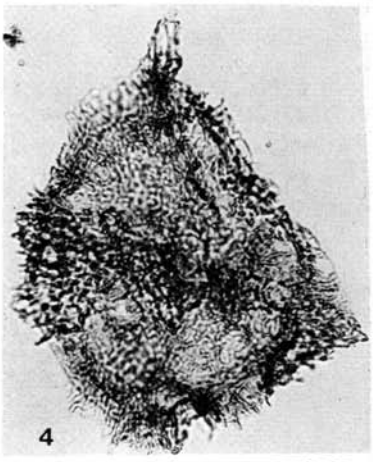
4

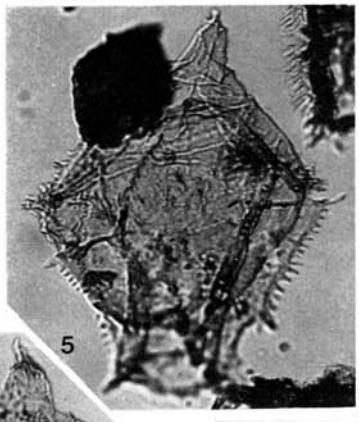
5

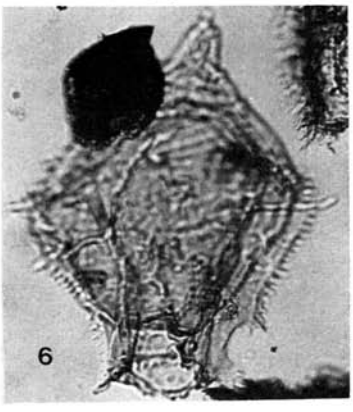
6

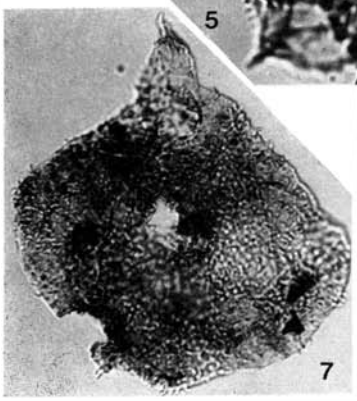
7

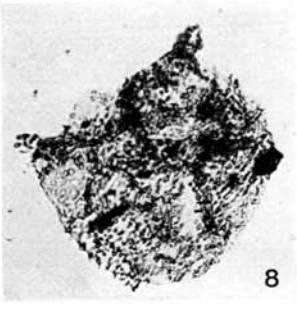
8

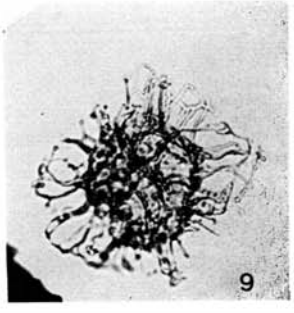
9

PLATE 4

Fig. 1. *Lithodinia jurassica* (Eisenack) Gocht 1975, 3171/1:36.8–102.2
Fig. 2. *L. jurassica* (Eis.) Gocht 1975, 3171/2:32.6–108.2
Fig. 3. *Hystrichogonyaulax cladophora* (Defl.) Stover and Evitt 1978, 3179/7:50.3–100.2
Fig. 4. *Stephanelytron redcliffense* (Sarjeant) Stover, Sarjeant and Drugg 1977, 3171/5: 43.5–105.4
Fig. 5. *S. redcliffense* (Sarj.) Stover et al. 1977, 3171/5:35.3–107.8
Fig. 6. *Gonyaulacysta* sp., 3171/5:33.3–107.0
Fig. 7. *Wanaea* sp., 3171/8:34.5–106.3
Fig. 8. *Tubotuberella eisenackii* (Defl.) Stover and Evitt 1978, 3171/5:29.8–106.9
Fig. 9. *Tubotuberella dangeardii* (Sarjeant) Stover and Evitt 1978, 3171/8:38.4–97.8
Fig. 10. *Sirmiodinium grossi* Alberti 1960, 2275/4:37.4–96.4
Fig. 11. *S. grossi* Alberti 1960, 3171/1:34.4–103.1
Fig. 12. *Lithodinia* sp., 3171/5:35.9–98.1
Fig. 13. *Hystrichogonyaulax* sp., 3171/3:32.8–105.6
Fig. 14. *Hystrichogonyaulax* sp., 3171/6:36.0–100.7
Fig. 15. *Lithodinia* cf. *valensi* Sarjeant 1966, 3171/2:32.2–100.4

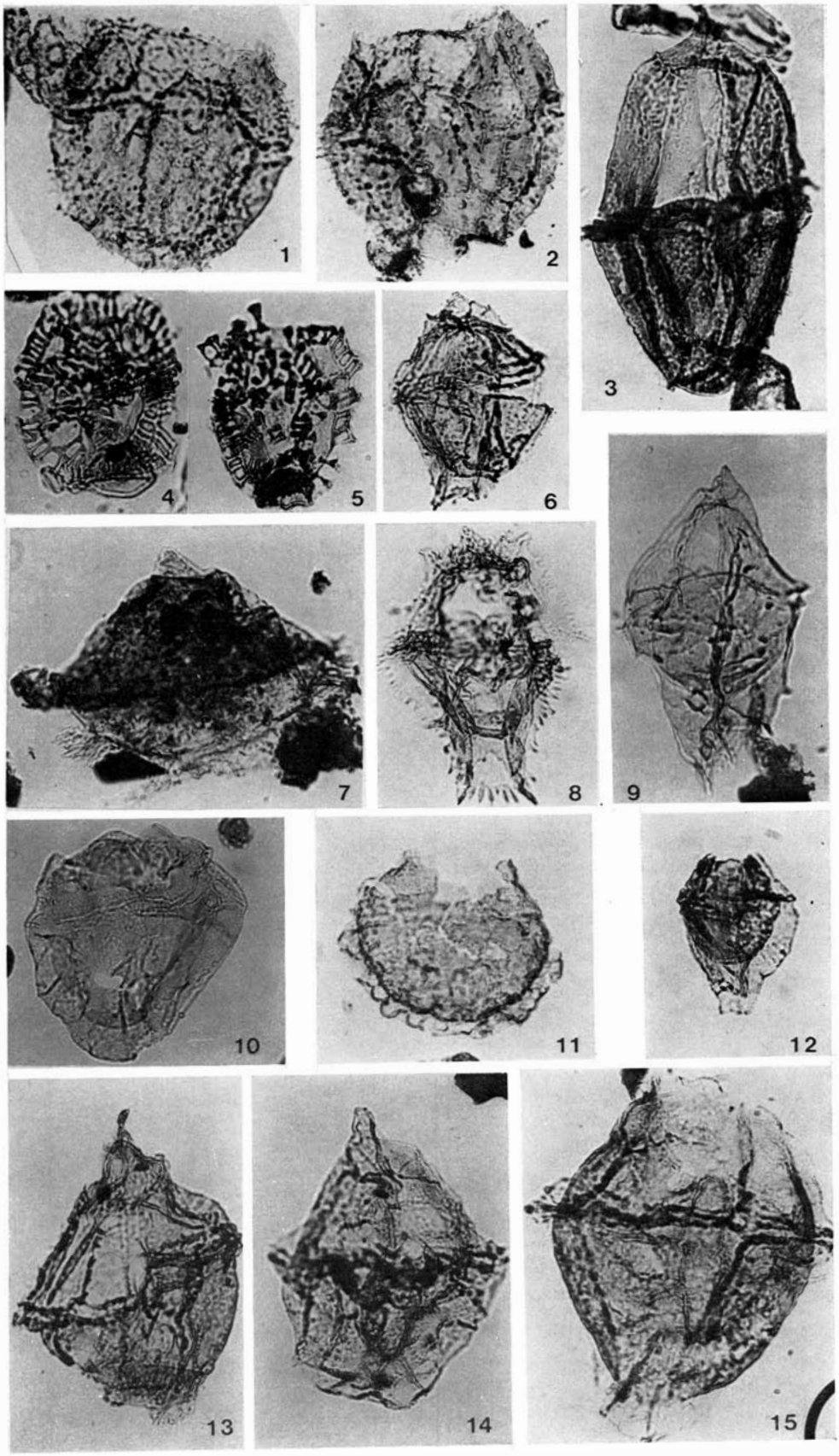
1
2
3
4
5
6
7
8
9
10
11
12
13
14
15

PLATE 5

Fig. 1. Dinoflagellate sp. indet. 2, 2357/2(50μ):40.5–99.0
Fig. 2. Dinoflagellate sp. indet. 2, 2357/1(50μ):42.0–102.0
Fig. 3. *Horologinella spinosigibberosa* BRIDEAUX and FISHER 1976
Fig. 4. Dinoflagellate sp. indet. 2, 2357/3 ox:44.2–100.2
Fig. 5. Dinoflagellate sp. indet. 2, 2357/3 ox:47.3–99.4
Fig. 6. *H. spinosigibberosa* BRIDEAUX and FISHER 1976, 2328/2:34.5–108.2
Fig. 7. *H. spinosigibberosa* BRIDEAUX and FISHER 1976, 2328/2:34.5–101.2
Figs. 8,13 *Paragonyaulacysta capillosa* BRIDEAUX and FISHER 1976, 3222/2:35.1–97.2
Figs. 8,13 *Paragonyaulacysta capilosa* BRIDEAUX and FISHER 1976, 3222/2:35.1–97.2
Fig. 9. *P. capillosa* BRIDEAUX and FISHER 1976, 2324/2:34.7–97.2
Fig. 10. *Tubotuberella apatela* (COOKSON and EISENACK) IOANNIDES et al. 1976, 2357/2 (50μ): 42.2—101.7
Fig. 11. *P. capillosa* BRIDEAUX and FISHER 1976, 2324/2:34.8–99.9
Fig. 12. *P. capillosa* BRIDEAUX and FISHER 1976, 2328/2:43.1–100.7

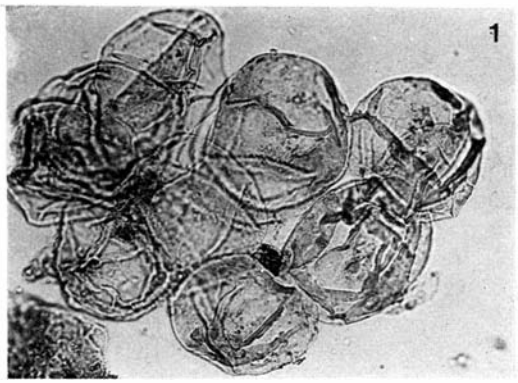
1

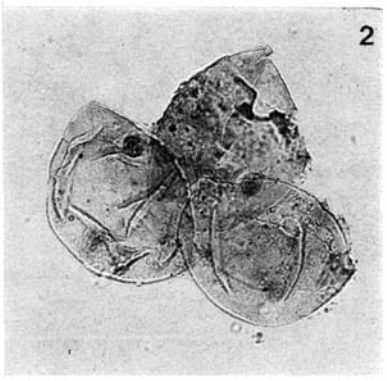
2

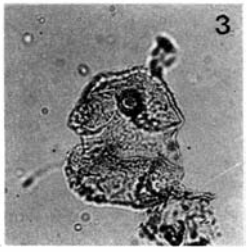
3

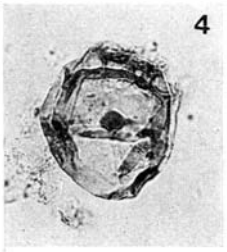
4

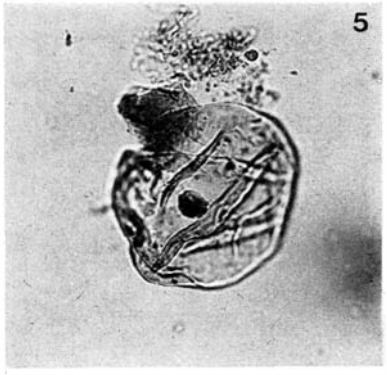
5

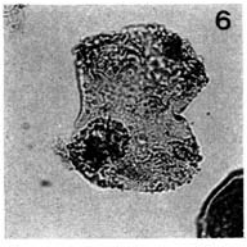
6


7

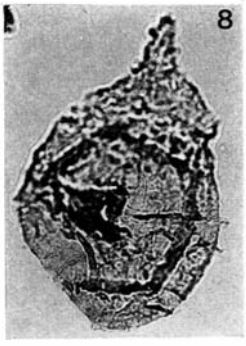
8

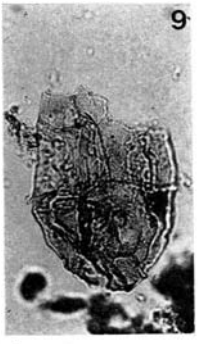
9

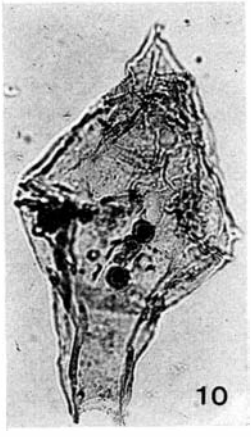
10

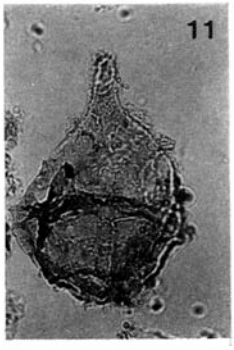
11

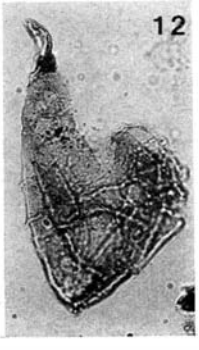
12

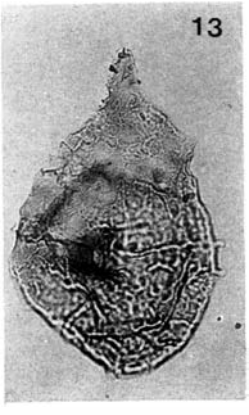
13

Petrography and mineralogy of phosphatic sediments, Svalbard

By A. M. EL-KAMMAR[1] and E. NYSÆTHER[2]

Abstract

Nodular phosphates have been recorded in shallow marine and deltaic Triassic and Jurassic sediments in Svalbard. The phosphate material is mostly of collophane nature, and has a composition between carbonate and fluor apatites. Its associated mineral assemblage includes quartz, feldspars, dolomite, calcite, pyrite, hematite-"limonite", glauconite, clays, carbonaceous matter, tourmaline, altered amphiboles, and zircon, in decreasing order of relative abundance. The sediments were cemented by calcite, which was dolomitized and later calcitized at a late diagenetic stage. Pyrite was introduced after the calcite cementation and before the dolomitization.

Introduction

Phosphate nodules, coprolites, bone debris, etc., have been encountered and sampled from the Sassendalen Group and Kapp Toscana Formation of the Triassic system and the Brentskardhaugen Bed of the Jurassic system. The investigated area includes the Sergeijevfjellet, Lidfjellet, Liddalen, Plogknatten, and Karentoppen sections along the west coast of Sørkapp Land, Spitsbergen. The sections were investigated and sampled by one of the authors (E. NYSÆTHER) in 1977 when he was a member of the Statoil Expedition to Svalbard. The stratigraphy and lithology of the sections investigated will form the basis of a separate paper by NYSÆTHER (in preparation). A map of the studied area is presented in Fig. 1.

The following are short notes on the general lithology of the sampled formations:

Sassendalen Group.

BUCHAN et al. (1965) divided the Sassendalen Group into three lithological units, from base upwards, the Vardebukta, Sticky Keep, and Botneheia Formations.

[1] Geology Department, Faculty of Science, Cairo University, Giza, Egypt.
[2] Geologisk Institutt, avd. A, Universitetet i Bergen, 5014 Bergen, Norway.

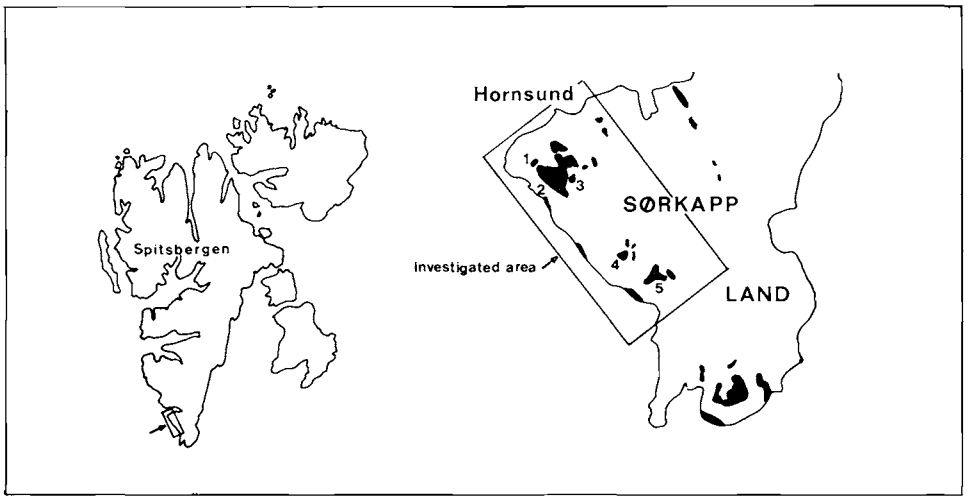

Fig. 1. *Distribution of Triassic sediments in Sørkapp Land, southern Spitsbergen. 1: Sergeijevfjellet, 2: Lidfjellet, 3: Liddalen, 4: Plogknatten, 5: Karentoppen.*

Since it has been impossible to discriminate between the two lowermost formations in the investigated area on lithological grounds, they are treated as a single unit. Apart from a locally developed thin conglomerate and sandstone sequence at the base, the rocks are organized into a generally upward-coarsing sequence from shales to medium grained sandstones. The upper part of the sequence has been deposited in a deltaic environment. Phosphate nodules have been found at many levels throughout the sequence.

The Botneheia Formation has a fairly uniform development in Svalbard. Normally it consists of dark silty marine shale with varying amounts of phosphate nodules at certain levels. In the investigated area the formation is somewhat more sandy than normal.

Kapp Toscana Formation.

The Kapp Toscana Formation consists in the lower part of black marine shales, interbedded with a few sandstone and siltstone layers. The upper half of the formation is typically sandy with only minor amounts of shale and siltstone, deposited in a continental to marginal marine environment. Phosphate material has been found only in the uppermost part of the formation.

Brentskardhaugen Bed (The Lias Conglomerate).

This conspicuous rock unit is widespread in Svalbard and forms the transition from the sandy Triassic-(?) Early Jurassic sequence below to the black Jurassic shale above. It is composed of dominantly phosphate nodules, with a varying amount of chert and quartz granules in a sandy matrix. Within the phosphate nodules are often found ammonites of Toarcian age (S. A. Backstrøm pers. comm.).

Experimental procedures

Bulk and separated phosphate samples were analyzed by the X-ray powder diffraction method, using Philips instrument. The working conditions were: Cu-K radiation, Ni-filter, 38 kV, 18mA, sensitivity 2×10^2 cps, and scanning rate 1°/sec. The samples were prepared by extracting bones and coprolites which were then crushed and purified. A scanning electron microscope of the JSM-35, JEDOL type was used in the study.

Petrography

Highly reworked phosphatic material occurs frequently (but at certain levels) in the sedimentary succession (c. 250 m thick) of the Vardebukta/Sticky Keep, Botneheia, and Kapp Toscana Formations of the Triassic system and the Brentskardhaugen Bed of the Jurassic system, on the west coast of Sørkapp Land. It is less abundant in the shale zones of the Kapp Toscana Formation. It is most abundant and displays a very heterogranular, or even conglomeratic aspect, at the top of the succession (the Brentskardhaugen Bed) in Karentoppen and Lidfjellet.

1. THE PHOSPHATIC MATERIALS

Different forms of phosphatic material have been recorded in the studied sediments: nodules, coprolites, organic fragments, and grains, in a decreasing order of abundance.

The nodules are up to 10 cm in diameter, always well to very well rounded,

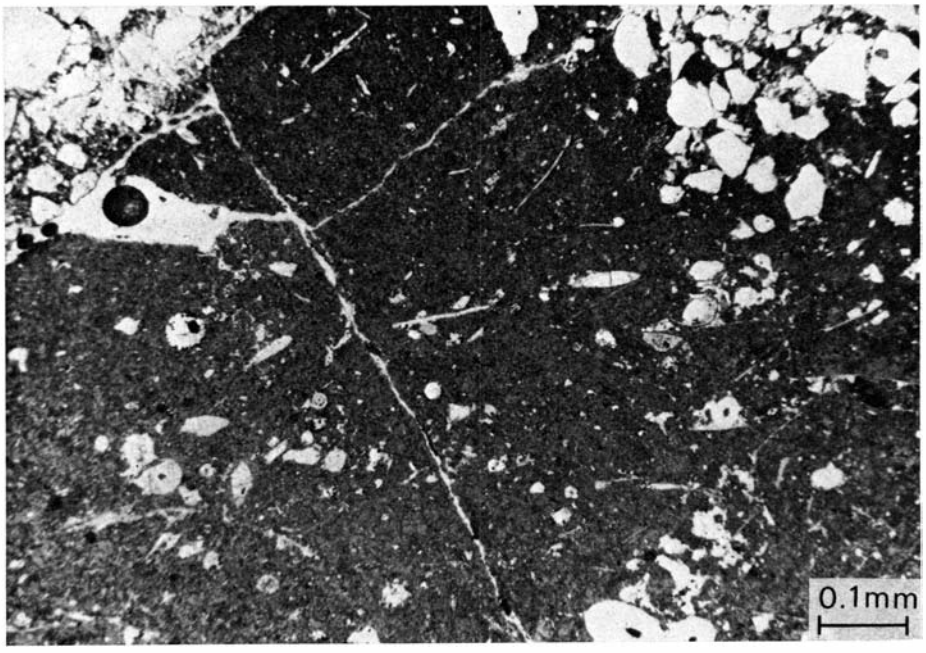

Fig. 2. *Reworked coprolite enclosing detrital quartz, feldspar, and small biologic debris.* (Polarized light.)

and spherical in shape. They show clear evidence of having been associated with strong reworking, as they embed very well sorted detrital grains of quartz, feldspars, smaller phosphate coprolites and grains, glauconite, and opaque minerals. The size of such embedded grains ranges between 0.08 and 0.3 mm in diameter. The collophanic material of the nodules acts as cement for the detrital admixtures and the outer rim of the nodules is often rich in clay minerals.

Coprolites are composed of accumulations of the remnants of micro-organisms, packed together in irregular-shaped bodies of about 2 mm in average diameter. They contain a considerable amount of detrital grains (Fig. 2).

The organic debris is usually highly fragmented and ill-defined, although it has been possible to recognize some vertebrate bones and fish-scales, spines and teeth. The coarsest bone fragment recorded was about 12 cm long and 1.5 cm wide, but smaller fragments ($<$2 mm) are most common. The internal micro-structure of the organic debris is always obscured by intensive impregnation of pyrite and ferruginous materials, rendering them an apparently amorphous habit. Sometimes, the microstructure is highlighted when inclusions and impregnations are concentrated along canals and fibration directions.

Collophane grains are not very common. They are very well rounded and contain, in many cases, a detrital nucleus. The collophane pellets are ovoidal and also very rich in detrital inclusions (Fig. 3). No oolites or even pseudo-oolites have been observed in any of the investigated sediments.

Similar to other sedimentary phosphates (El-Kammar 1974), the Svalbard nodular phosphates are petrographically composed of two apatite types: the apparently amorphous and the weakly birefringent variants. The former is known as collophane (McConnell 1973) and comprises about 80% of the phosphate material under consideration. The weakly birefringent apatite variant makes up most of the biologic debris and part of the coprolites.

The tricalcium phosphate content of the biologic debris is estimated to be about 77%, decreasing to 25% in the case of nodules. This is, of course, because of the detrital admixture of the nodules.

The phosphatic materials have reacted readily with the cementing carbonates. Partial, and sometimes complete replacement by calcite has been observed, especially for the smaller sized particles.

The phosphatic materials display different colours, varying from yellowish-brown to black, and are rarely colourless. This colouration is greatly dependent on the type and amount of the impregnating material. Pyrite and carbonaceous matter give the phosphates black shades, while the weathered free surfaces exhibit a yellow-brown colouration, due to "limonite"-hematite impregnation.

2. THE ASSOCIATED MINERALS

The main minerals associated with the phosphates are quartz, feldspars, calcite, and dolomite, besides a subordinate mineral assemblage, including pyrite, hematite-"limonite", glauconite, clay minerals and carbonaceous

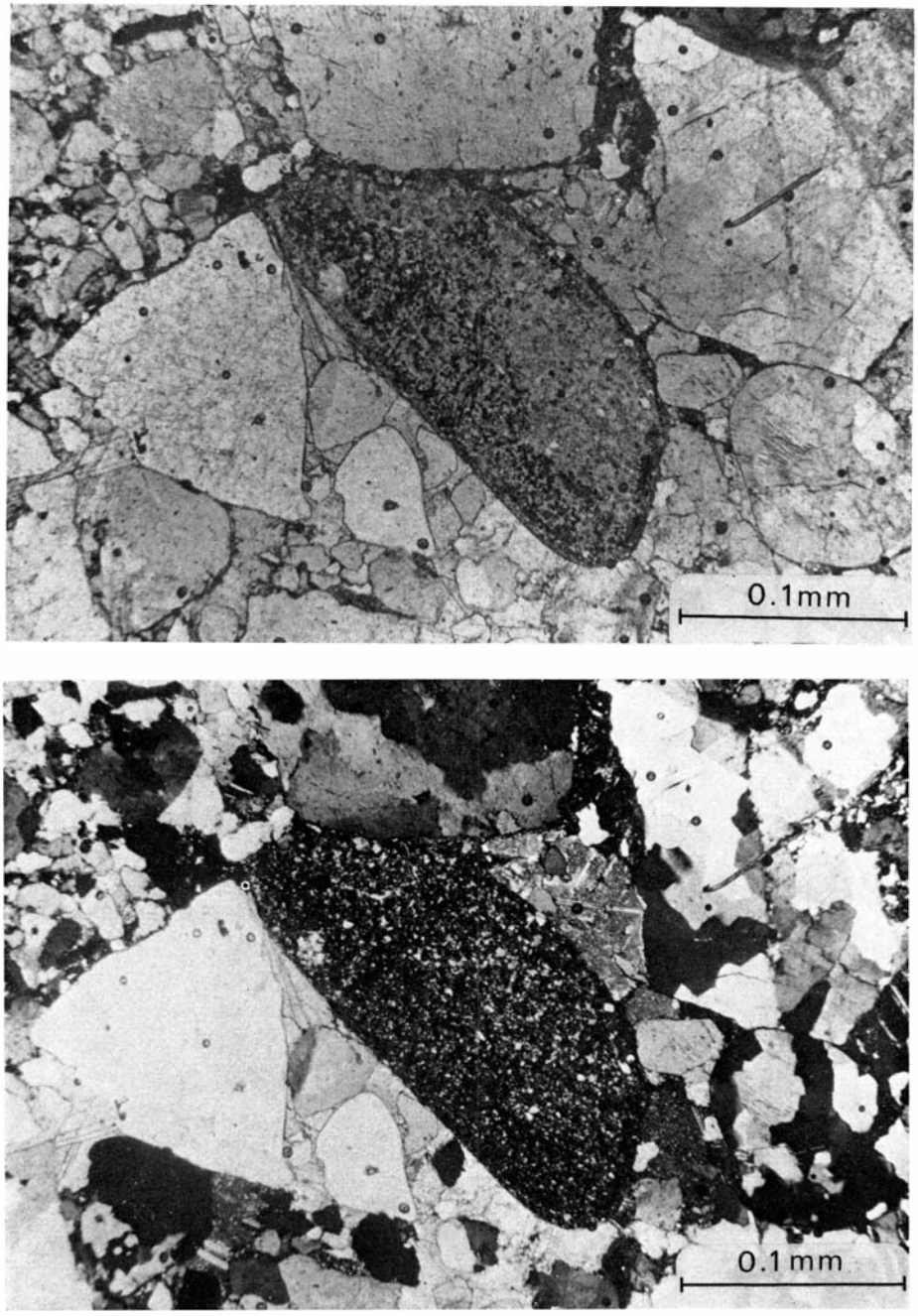

Fig. 3. *Photomicrograph showing a collophanic pellet, embedded with unequigranular clastics (mainly quartz and feldspar). The rock is cemented by microsparite. Notice that the pellet contains considerable inclusions of fine detrital quartz.* (Above: polarized light; below: crossed nicols.)

matter. Detrital grains of tourmaline, altered amphiboles and zircon are rarely observed. The following is a short account on the petrography of the main minerals as well as some of the subordinate ones.

(1) Quartz and feldspar

The studied rocks are principally composed of detrital unequigranular medium to very coarse quartz grains with small amounts of feldspars. The latter are usually unaltered orthoclase and some plagioclase. The quartz and feldspar grains are subangular to subrounded and are commonly corroded by the carbonate cement. The rocks contain also some coarse chert fragments, composed of microcrystalline, mosaic quartz.

(2) Dolomite

Dolomite, mainly of ferroan type, is the late diagenetic constituent of many of the studied samples and act as cement together with partly dolomitized calcite. The dolomite is usually idiotopic with inequigranular fabric. The common diagonal diameter ranges between 0.15 and 0.2 mm.

The dolomite rhombs are dispersed without grain contacts, and display different types of zoning, frequently with cloudy centres (Fig. 4). The latter is found to be aggregates of fine opaque inclusions of pyrite, due to an accumulation of ferruginous materials in thread-like form along the cleavage planes. This agrees fairly well with the argument put forward by KATZ (1971).

The ferroan dolomite is less stable than the nonferroan type (AL-HASHIMI & HEMINGWAY 1973) and is therefore later replaced by calcite. The replaced dolomite rhombs show hypidiotopic and xenotopic textures (see Fig. 4). The calcitization of dolomite (SCHOLLE 1971) or what is called the dedolomitization by some authors (e.g. BRAUN & FRIEDMANN 1970; BLATT et al. 1972), is a very

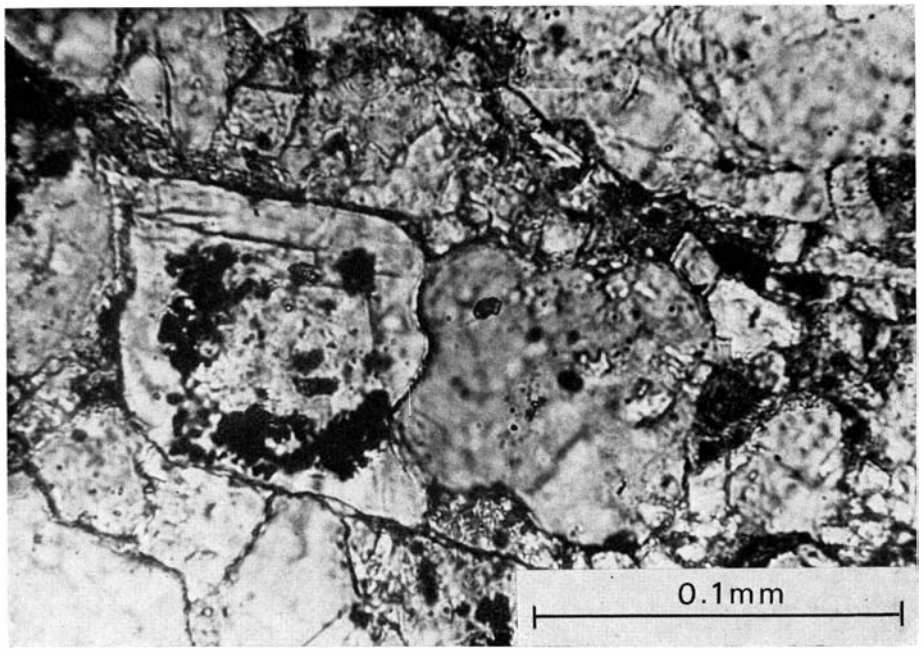

Fig. 4. *Hypidiotopic, partially calcitized dolomite with pyrite inclusions.* (Polarized light.)

late diagenetic process, and it indicates a percolation of Ca-rich solutions in the sediments.

The distribution pattern of dolomitization and calcitization of dolomite is very irregular in the studied Triassic sediments.

(3) Calcite

Calcite occurs as: (a) coarse mollusca shell fragments which show a cryptocrystalline habit and which were reworked with the phosphate nodules on the sea bottom, and (b) an authigenic microsparite to sparite cement. Pseudospar is found to crown poikilite and replace many of the rock constituents.

(4) Other minerals

The studied sedimentary rocks are, in places, strongly pyritized with the pyrite occurring as thin intersected veinlets, filling cracks and fractures, and disseminated within the whole constituents. The pyritization took place late diagenetically (after the calcite cementation) and has then been followed by oxidation (at the free surface) and production of "limonite"-hematite.

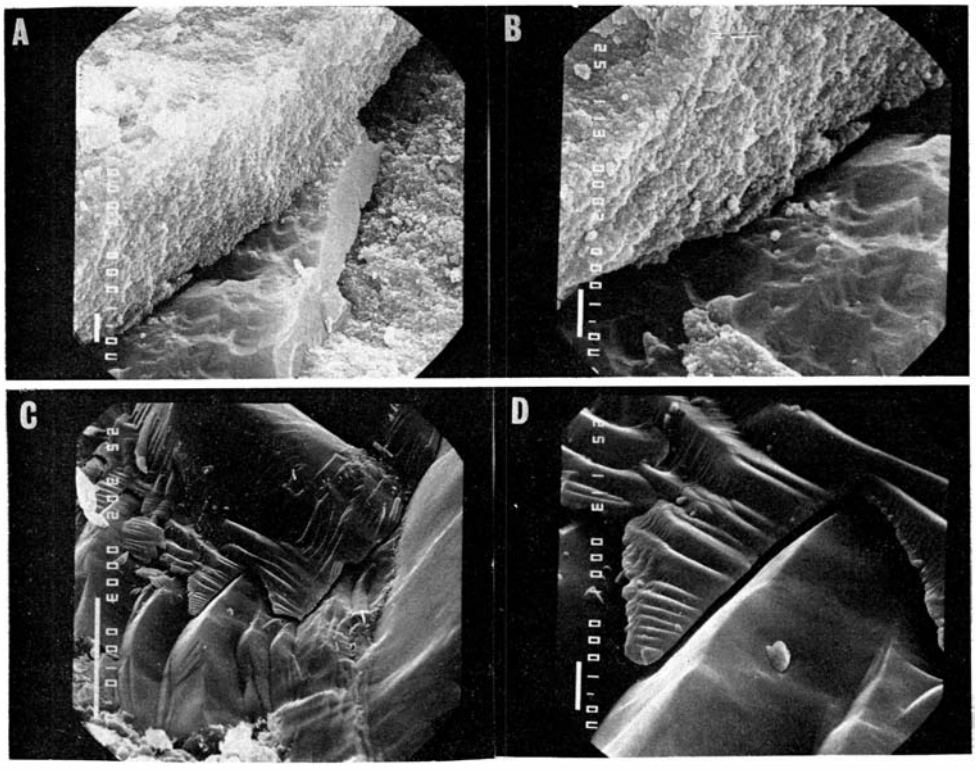

Fig. 5. *Photographs A (× 6000) and B (× 11,000) show two fibers of a bone fragment. The fibers are composed of anhedral crystal aggregates of apatite (A). Authigenic calcite (C) is filling the void space between the fibers. Photographs C (× 3000) and D (× 11,000) show the interaction between quartz (below) and authigenic calcite (above). Notice the aggradational crystallization of calcite at the contact boundary.*

Glauconite is a minor constituent and it occurs only as very well rounded ovoidal fine grains. It is also sometimes oxidized into celadonite.

Black carbonaceous matter predominates in biologic remains and in some coprolites. It has a characteristic dendritic shape.

Mineralogy

Electron microscopy has shown that both the apparently amorphous and the weakly birefringent bones are actually composed of microcrystallites (Fig. 5, A and B). The interstitial space between the bone fibers is filled with secondary calcite. As mentioned above, the strong impregnation is most probably responsible for the amorphous appearance of the apatite.

The X-ray powder diffraction analysis supports the above interpretation, as collophanic coprolites and bones produce clear diffraction patterns.

In general, the X-ray diffraction analyses of selected coprolites and bones (Fig. 6), as well as bulk samples (Fig. 7) reveal the following facts:

1. The two petrographic variants (i.e. collophane and the weakly birefringent apatite) gave identical diffraction patterns. This suggests that the crystal structure of the apatite is independent of its petrographic form.
2. The prominent diffraction spacing obtained for the analysed apatite: 2.81, 2.79, 2.70, and 2.63 Å, coincides with the corresponding spacing of francolite (GRUNER & MCCONNELL 1937), which is a carbonate-fluorapatite, but also with carbonate apatite (MCCONNELL 1960), and fluorapatite (MCCONNELL 1973).
   The electron microprobe study of the same apatite (Part II) showed that this apatite is a solid solution of carbonate and fluorapatite.
3. In general, the apatite forms are carriers of foreign material like clay minerals, quartz, and feldspar. The picked phosphate forms contain more clays, compared to the corresponding bulk samples. The clay minerals identified are kaolinite, illite, and probably mixed layered montmorillonite-chlorite. Such association of phosphates and clays can be considered as evidence for the mixing of uncongelated apatite with clay on the sea floor.
4. Coprolites contain more quartz and feldspars compared to bones. The solutions which caused calcitization and dolomitization of the rocks, were also acting inside the coprolites and bones.
5. The bulk samples (see Fig. 7) are essentially composed of quartz, apatite, calcite, dolomite and feldspar, besides minor pyrite and kaolinite. Fig. 5 (C and D) shows the interaction between quartz and the calcite cement.

The abundance of Ca-bearing minerals has been petrochemically calculated for some samples (Table 1). The calculations are based on the assumption that Ca is participating in three forms: apatite, calcite, and dolomite. The obtained data confirm the results of the X-ray diffraction and the petrographic composition.

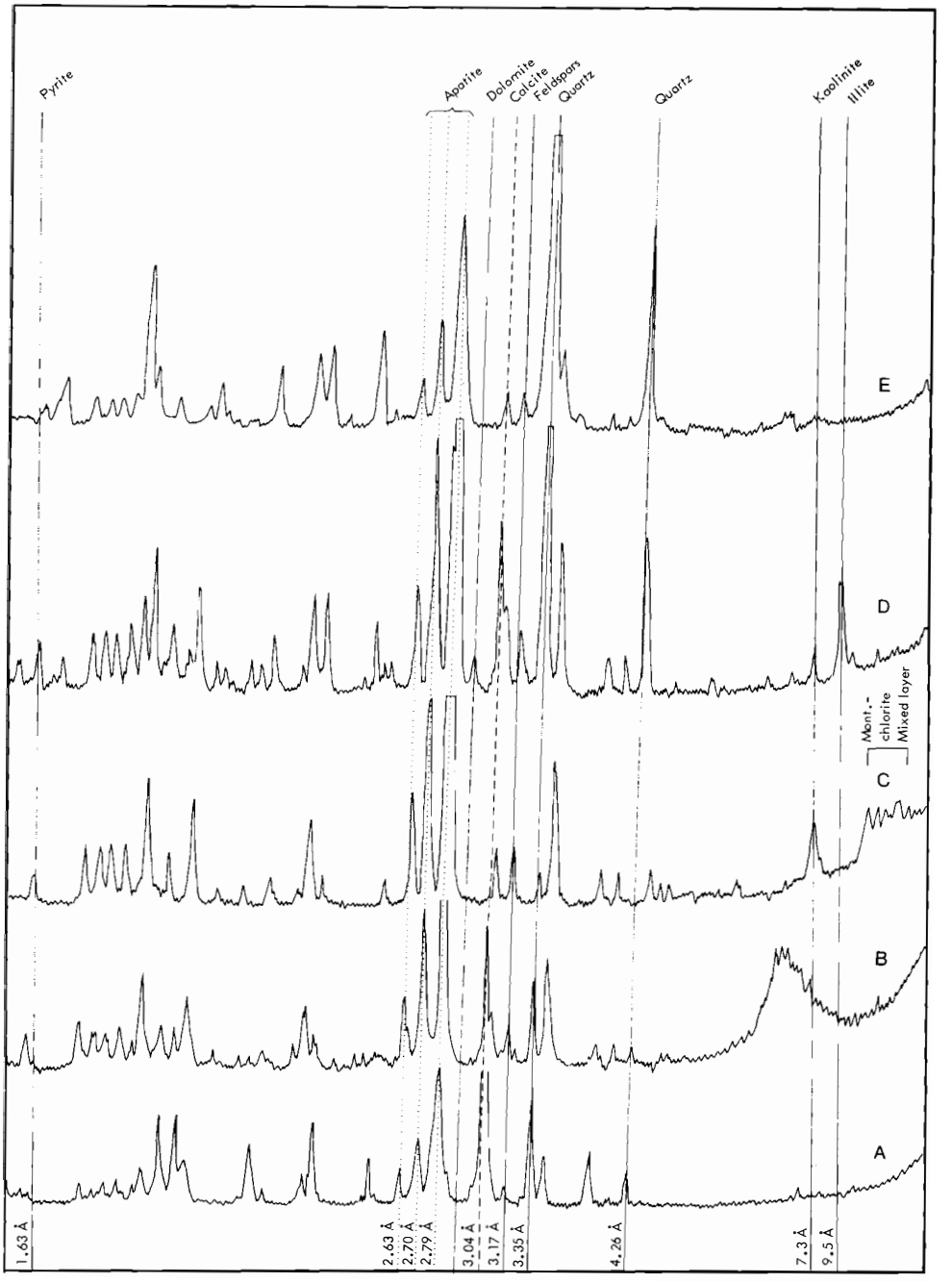

Fig. 6. *X-ray powder diffraction diagrams of bones and coprolites. Picked from phosphatic rocks from Svalbard.*

Legend: A, B, and C are bones separated from samples No. LN-25, LN-61, and LN-Lias, respectively, while D and E are coprolites separated from samples PK-35 and Lias conglomerate, respectively.

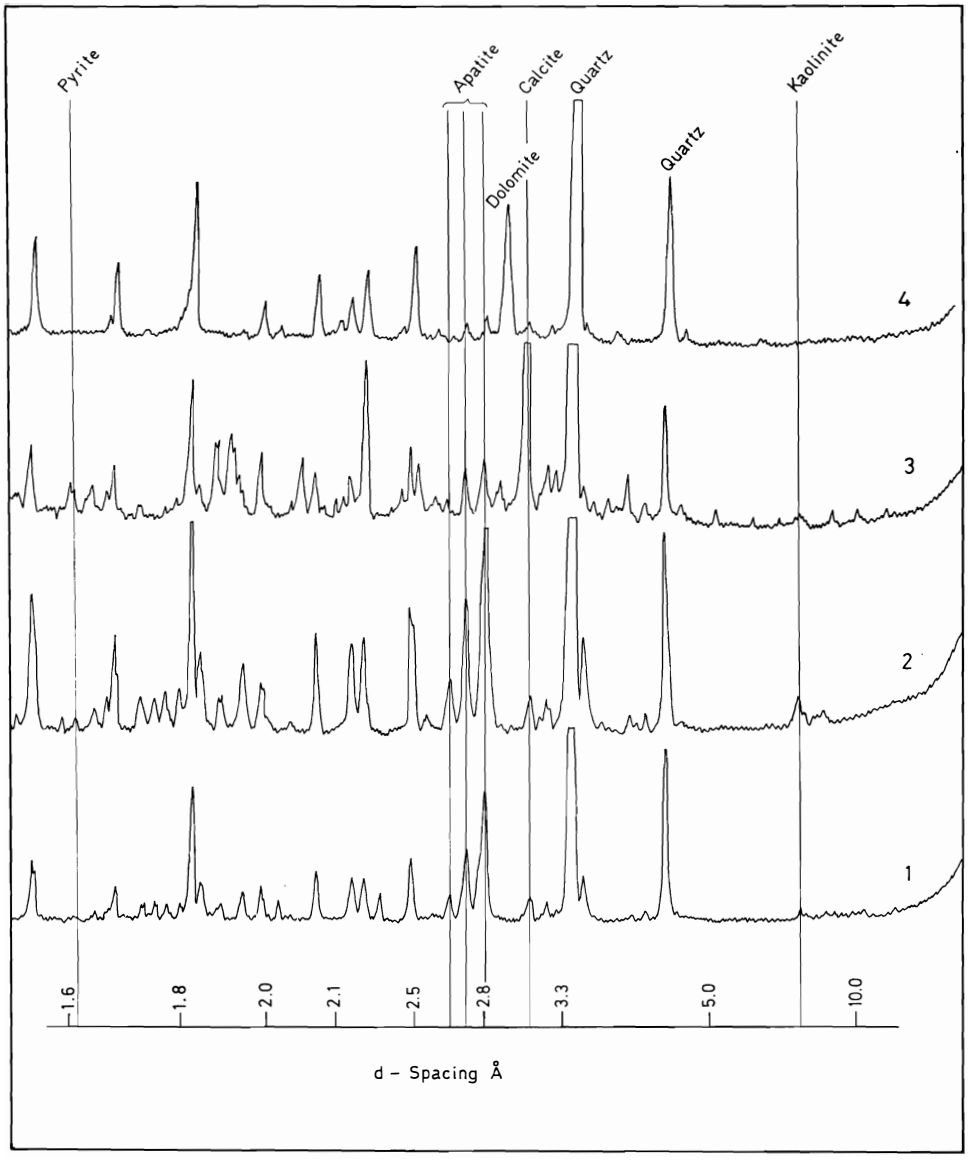

Fig. 7. *X-ray powder diffraction diagrams of phosphatic sediments from Svalbard.*

Legend: 1 = Lias conglomerate of Karentoppen.
2 = Lias conglomerate of Lidfjellet.
3 = Sample PK-7.
4 = Sample LD-12.

Table 1.

Petrochemical calculations of the Ca-bearing minerals.

Formation	Brentskardhaugen Bed		Botneheia Fm.		Vardebukta/Sticky Keep Fm.							
Samples → Minerals % ↓	Lidfj.	Karent.	LD_{12}	LD_{15}	PK_7	PK_{31}	LD_{45}	LD_{46}	LD_{61}	LN_{23}	LN_{24}	LN_{25}
Apatite	24.66	23.81	6.19	8.44	11.89	6.22	13.21	10.99	4.85	4.19	8.06	4.27
Dolomite	1.10	0.41	15.51	0.73	10.66	—	5.17	10.80	2.10	—	—	3.75
Calcite	4.68	3.25	—	5.59	14.81	13.35	22.24	8.80	8.69	3.48	4.50	6.57

Notes on genesis and diagenesis

The phosphate material in the surveyed rocks is found in two different depositional environments:

1. in a shallow marine-shelf environment where phosphatic pebbles occur disseminated in shales or siltstones, or are concentrated together with quartz granules and marine fossils on the disconformity at the base of the Brentskardhaugen Bed; and
2. in a deltaic environment where pebbles are found in sandstones of the upper shoreface-beach subenvironment or in siltstones-sandstones of lagoonal-bay origin.

The origin of the pebbles in category 1 can probably best be explained by reference to the classical upwelling theory, first formulated by KAZAKOV (1937). Seawater is normally nearly saturated with phosphate except in the uppermost 50 m of the ocean. The solubility is temperature dependent, however, and cold water may contain more phosphate than warm water. If cold phosphate enriched water from deep oceanic basins is brought to the surface by upwelling currents along a shoaling bottom, the simultaneous increasing temperature and pH and decreasing partial pressure of CO_2 may cause chemical precipitation of the phosphate.

The precipitation will normally take place in the sea bottom between 50 m and 200 m's water depth. Above this zone most of the remaining phosphate in the water will rapidly be assimilated by phytoplankton, so if and when the water reaches the nearshore environment, it is undersaturated and nearly depleted of phosphorous.

In the Brentskardhaugen Bed, the relatively high phosphate concentration in the deposit is probably the result of a low rate of clastic sedimentation together with reworking of the material by currents and waves in a shelf environment. In the Botneheia Formation such enrichment has not taken place and these deposits are consequently of a lower grade, even though the amount of nodules in the sequence is important.

The upwelling theory, however, probably does not give a plausible explanation for the occurrence of phosphate material in the deltaic deposits of the Vardebukta/Sticky Keep Formation. Here, pebbles are found in sediments that only to a limited degree can have been exposed to the marine waters from the outer shelf area. It also seems highly unlikely that the pebbles should have been transported shorewards from the shelf and mingled with sediments containing reptile bones in a nearshore-bay environment.

PEVEAR (1966) has put forward an interesting hypothesis for the origin of Tertiary phosphates found in similar environments on the Atlantic coastal plain of the United States. He theorizes that the phosphates have been formed by replacement of lime mud in estuaries which had a high content of phosphorous due to an important organic productivity.

A similar process may have been responsible for the formation of phosphate pebbles in the Vardebukta/Sticky Keep Formation. The deltaic environment including bays, lagoons, and estuaries, was probably the site of extensive life as indicated by the frequent discovery of reptile and fish remains in the sediments. No pure limestones have been found in the sequence, but the sandstones are often nearly completely cemented by calcite (or dolomite). Since most pebbles have a high sand content, it is possible that these in fact are remnants of phosphate cemented sandstones that were later broken up, reworked and resedimented in the form of phosphatic pebbles. Phosphate must have replaced the calcite in the sediment before it was broken up, which calls for a very early calcite cementation of the rocks.

The sediments were affected by diagenetic processes that took place in the following order:

Early:
1. Cementation by microsparry to sparry calcite.
2. In reducing environments, pyrite was introduced to the sediments by solutions potentially rich in sulfides (BERNER 1971).
3. Mg-rich solutions caused partial dolomitization of the cementing calcite. The process took place in an acidic environment (BLATT et al. 1972).

Late:
4. Ca-rich solution caused partial calcitization of the dolomite (i.e-dedolomitization), and oxidized a part of the pyrite into "limonite"-hematite.

Summary and conclusions

The studied nodular phosphates of the Triassic and Jurassic systems of Svalbard are low grade, where the tricalcium phosphate occurs as coarse nodules, organic and inorganic coprolites, grains, and biologic debris. These phosphate forms are usually well rounded and highly reworked. They predominate at the top of the succession, which is represented by the Brentskardhaugen Bed of the Jurassic.

The apparently isotropic apatite (collophane) comprises about 80 per cent by volume of the phosphate material under consideration. The main minerals

associating phosphates are quartz, feldspars, calcite, and dolomite. The latter is of the ferroan type, and it is calcitized in many cases. The subordinate minerals are pyrite, hematite-"limonite", glauconite, clay minerals, and carbonaceous matter. The rare minerals are tourmaline, altered amphiboles, and zircon.

The scanning electronmicroscope and X-ray diffraction studies showed that collophane is not an isotropic mineral, and that it is composed of microcrystallites. The studied apatite has a solid solution between carbonate and fluor apatites.

The formation of the studied nodular phosphate is attributed to two different depositional environments, shallow marine and deltaic. The sediments were diagenetically cemented by calcite, which was dolomitized at the late diagenetic stage. Pyrite was introduced to the sediments after the calcite cementation and before dolomitization.

Acknowledgements

The writers are grateful to Statoil for granting permission to publish this paper, which to a great extent is based upon information collected on their behalf. The authors would also like to thank Dr. R. Steel for his improving of the English manuscript.

References

Al-Hashimi, W. S. & J. E. Hemingway, 1973: Recent dedolomitization and the origin of the rusty crusts of Northumberland. *Jour. Sed. Petrology* **43**: 82–91.

Berner, R. A., 1971: *Principles of Chemical Sedimentology*. McGraw-Hill Book Company, New York, Düsseldorf, London. 240 pp.

Blatt, H., G. Middleton, and R. Murray, 1972: *Origin of Sedimentary Rocks*. Prentice-Hall, Inc., Englewood Cliffs, New Jersey. 634 pp.

Braun, M. and G. M. Friedman, 1970: Dedolomitization fabric in peels: A possible clue to unconformity surfaces. *Jour. Sed. Petrology* **40**: 417–419.

Buchan, S. H. et al., 1965: The Triassic Stratigraphy of Svalbard. *Norsk Polarinstitutt Skrifter* Nr. 135.

El-Kammar, A. M., 1974: *Comparative mineralogical and geochemical studies on the Egyptian Phosphorites*. Ph.D. Thesis, Cairo University, Faculty of Science, Egypt.

Gruner, J. W. and D. McConnell, 1937: The problem of the carbonate apatites. The structure of francolite. *Zeits. Kristallogr.* **97A**: 208–215.

Katz, A., 1971: Zoned dolomite. *Jour. Geology* **79**: 38–51.

Kazakov, A. V., 1937: The phosphorite facies and the genesis of phosphorites. Pp. 95–113 **in**: Geological investigations of agricultural ores, USSR. *Leningrad Sci. Inst. Fertilizers and Insecto-Fungicides Trans.* (*USSR*) No. 142.

McConnell, D., 1960: The crystal chemistry of dahllite. *Amer. Mineral* **45**: 209–216.

— 1973: *Apatite, its crystal chemistry, mineralogy, utilization, and geologic and biologic occurrences*. Springer Verlag, Wien, New York. 111 pp.

Pevear, D. R., 1966: The estuarine formation of United States. *Econ. Geol.* **61**: 251–256.

Scholle, P., 1971: Diagenesis of deep-water carbonate turbidites, Upper Cretaceous Monte Antola Flysch, Northern Apennines, Italy. *Jour. Sed. Petrology* **41**: 233–250 pp.

A.S JOHN GRIEG